Integrating observations and models to understand ecophysiological controls on terrestrial water-carbon coupling

Dissertation

(kumulativ)

zur Erlangung des akademischen Grades doctor rerum naturalium

(Dr. rer. nat.)

vorgelegt dem Rat der Chemisch-Geowissenschaftlichen Fakultät der Friedrich-Schiller-Universität Jena

von M.Sc. Jürgen Knauer

geboren am 30. November 1989 in Eggenfelden

Gutachter:

1. . . . .

2. . . . .

Tag der Verteidigung: . . . .

Contents

List of Figures

VIII

List of Tables

List of Symbols and Abbreviations

Units are reported in the text because they may differ across chapters

A	available energy
A_c	carboxylation-limited net photosynthesis
A_j	RuBP regeneration-limited net photosynthesis
A_n	net photosynthesis
A_p	TPU-limited net photosynthesis
$B^{-1} = B_h^{-1}$	inverse Stanton number
B_s^{-1}	inverse Stanton number for bare soil surface
C_d	foliage drag coefficient
$C_s = C_0$	(ecosystem) surface CO_2 concentration
C_t	heat transfer coefficient of the leaf
D_a	atmospheric vapor pressure deficit
D_l	leaf characteristic dimension
$D_s = D_0$	(ecosystem) surface vapor pressure deficit
G	ground heat flux
G_{am}	aerodynamic conductance to momentum transfer
$G_a = G_{ah}$	aerodynamic conductance to heat transfer
$G_b = G_{bh}$	(ecosystem) boundary layer conductance to heat transfer
G_c	canopy conductance to water vapor
G_r	longwave radiative transfer conductance
G_{sc}	surface conductance to CO_2
$G_s = G_{sw}$	surface conductance to water vapor
H	sensible heat flux
H_a	activation energy
H_d	deactivation energy
J	electron transport rate
J_{max}	maximum electron transport rate
K_c	Michaelis-Menten constant for CO_2
K_o	Michaelis-Menten constant for O_2
L	Monin-Obukhov length
N	number of leaf sides participating in heat transfer
N	leaf nitrogen content
O_i	intercellular O_2 concentration
R	universal gas constant
R_{am}	aerodynamic resistance to momentum transfer
$R_a = R_{ah}$	aerodynamic resistance to heat transfer

$R_{\mathbf{b}} = R_{\mathbf{bh}}$	(ecosystem) boundary layer resistance to heat transfer
$R_{\mathbf{d}}$	leaf respiration in darkness
$R_{\mathbf{eco}}$	ecosystem respiration
$R_{\mathbf{l}}$	leaf respiration in daylight
$R_{\mathbf{n}}$	net radiation
$R_{\mathbf{p}}$	photorespiration
S	(ecosystem) energy storage flux
$S_{\mathbf{p}}$	biochemical energy
T	transpiration
$T_{\mathbf{a}}$	air temperature
$T_{\mathbf{l}}$	leaf temperature
$T_{\mathbf{ref}}$	reference temperature
$T_{\mathbf{r}}$	radiometric surface temperature
$T_{\mathbf{s}} = T_{\mathbf{0}}$	(ecosystem) surface temperature
$V_{\mathbf{cmax}}$	maximum carboxylation rate
$V_{\mathbf{c}}$	carboxylation
$V_{\mathbf{pmax}}$	maximum PEP-carboxylation rate
Δ	isotopic discrimination
ΔS	entropy term
Γ_*	photorespiratory CO_2 compensation point
Ω	aerodynamic vegetation-atmosphere decoupling factor
Θ	soil moisture content
Θ	curvature parameter in the light response curve
$\Theta_{\mathbf{crit}}$	critical soil moisture content
$\Theta_{\mathbf{wilt}}$	wilting point
α	Priestley-Taylor constant
α	initial slope of the light response curve
β	water stress factor
ϵ	emissivity
η	ratio of g_0 to $g_{\mathbf{s}}$
γ	psychrometric constant
λE	latent heat flux
$\lambda E_{\mathbf{eq}}$	equilibrium latent heat flux
$\lambda E_{\mathbf{imp}}$	imposed latent heat flux
$\lambda E_{\mathbf{pot}}$	potential latent heat flux
ϕ	ratio of evaporation to evapotranspiration
$\psi_{\mathbf{h}}$	integrated form of the stability correction function for heat
$\psi_{\mathbf{m}}$	integrated form of the stability correction function for momentum
ρ	air density
σ	Stefan-Boltzmann constant
$\mathbf{LW}_{\downarrow}$	longwave incoming radiation

$LW_\uparrow$	longwave outgoing radiation
Pr	Prandtl number
Re	Reynolds number for bare soil
Re_h	Reynolds number
$SW_\downarrow$	shortwave incoming radiation
$SW_\uparrow$	shortwave outgoing radiation
Sc	Schmidt number
rH	relative humidity
ξ	stomatal sensitivity factor
ζ	atmospheric stability parameter
b	parameter describing the reference G_s at a VPD of 1kPa
$c_{a,base}$	baseline CO_2 concentration
c_a	atmospheric CO_2 concentration
c_c	chloroplastic CO_2 concentration
c_i	intercellular CO_2 concentration
c_m	CO_2 concentration in the mesophyll cytosol (C4 plants)
c_s	(leaf) surface CO_2 concentration
c_p	heat capacity of dry air
d	displacement height
e_{sat}	saturation vapor pressure
$e_s = e_0$	(ecosystem) surface vapor pressure
f_c	fractional canopy cover
f_{min}	minimum fraction of g_m
g_0	minimum stomatal conductance parameter
g_1	stomatal slope parameter
g_b	(leaf) boundary layer conductance
g_m	mesophyll conductance
g_s	stomatal conductance
$g_{m,max25}$	maximum g_m at 25°C
h_s	roughness length of bare soil
k	von Kármán constant
m	parameter describing sensitivity of G_s to D_s
p	atmospheric pressure
q	specific humidity
q_b	water stress shape factor for biochemistry
q_m	water stress shape factor for g_m
q_s	water stress shape factor for g_s
r_m	mesophyll resistance
r_s	stomatal resistance
s	slope of the saturation vapor pressure curve
u	horizontal wind speed

u_*	friction velocity
v	kinematic viscosity of air
w	leaf width
z_{0h}	roughness length for heat
z_{0m}	roughness length for momentum
z_h	canopy height
z_r	reference height
aPPFD = APPFD	absorbed photosynthetic photon flux density
C3C	C3 crops
C3G	C3 herbs and grasses
C4C	C4 crops
C4G	C4 herbs and grasses
CDIAC	Carbon Dioxide Information Analysis Center
DBF	deciduous broadleaf trees
DNF	deciduous needle-leaf trees
DOY	day of year
DSH	deciduous shrubs
EB	energy balance
EBF	evergreen broadleaf trees/shrubs
EBR	energy balance ratio
EC	eddy covariance
ENF	evergreen needle-leaf trees
ET	evapotranspiration
EUE	energy use efficiency
FACE	free-air CO_2 enrichment
GPP	gross primary productivity
GRDC	Global Runoff Data Centre
HD	hydrological discharge
HYDE	History Database of the Global Environment
ISIMIP	Inter-Sectoral Impact Model Intercomparison Project
IWUE	inherent water-use efficiency
iWUE	intrinsic water-use efficiency
JSBACH	Jena Scheme of Biosphere-Atmosphere Coupling in Hamburg
LAI	leaf area index
LSM	land surface model
LUE	light use efficiency
MAP	mean annual precipitation
MAT	mean annual temperature
MPI	Max Planck Institute
NBP	net biome productivity
NEE	net ecosystem exchange

OLS	ordinary least-squares
PEP	phosphoenolpyruvate
PFT	plant functional type
PM	Penman-Monteith
PPFD	photosynthetic photon flux density
ppm	parts per million
PSII	photosystem II
RCP	representative concentration pathway
RMA	reduced major axis
RSH	raingreen shrubs
RuBP	ribulose 1,5-bisphosphate
SD	standard deviation
SE	CO_2-sensitive stomatal model version (chapter 2)
SER	standard error of the regression
SLA	specific leaf area
ST	standard stomatal model version (chapter 2)
TDF	tropical deciduous trees
TPU	triose phosphate utilization
TRF	tropical evergreen trees
USO	unified stomatal model
uWUE	underlying water-use efficiency
VPD	vapor pressure deficit
WUE	water-use efficiency

Acknowledgements

Summary

Background: Vegetation exerts a major control on the simultaneous exchange of water and carbon between the land surface and the atmosphere, a process which has important implications for the surface energy balance and global climate. Understanding the eco-physiological mechanisms underlying the coupling of water and carbon fluxes is therefore crucial for predicting the response of the terrestrial biosphere to, and its feedbacks on, global climate change. Process-based models, which represent key physiological processes at leaf level and their implications for water, carbon, and energy exchanges at larger scales (land surface models, LSMs) are invaluable tools to cope with this challenge. However, LSMs are only useful if they are combined with observations, which are needed to parameterize, constrain, and evaluate model formulations in an adequate manner. Nowadays, a wide range of observations related to water-carbon coupling are available and include leaf gas exchange measurements, ^{13}C discrimination, eddy covariance (EC) data, as well as large-scale observations such as continental discharge or atmospheric CO_2 records. These datasets provide information on the behavior of vegetation gas exchange at different spatial scales and with a different temporal integration, thus their inter-comparison, but also the derivation of physiologically meaningful signals from these observations, is not always straightforward. For example, observations at ecosystem level can in most cases not directly be related to the underlying physiological processes, and as a consequence, not directly be used to inform models which require information at leaf-level. An additional challenge is that missing or inadequate model formulations may lead to biased predictions as well as to an incorrect interpretation of data on water-carbon fluxes or their coupling. The common misconception of an infinite leaf internal conductance to CO_2 transfer (mesophyll conductance, g_m) for instance is known to misrepresent the photosynthetic sensitivity to atmospheric CO_2 concentrations and to bias inferred water-use efficiency (WUE) trends from ^{13}C discrimination data. Hence, both the correct interpretation of data and the adequate representation of associated processes in models are essential prerequisites for understanding the present and future behavior of water-carbon coupling and its role in the climate system.

Research objectives and methods: The overarching research objective of this thesis is to improve our understanding of how observations related to vegetation water and carbon exchange should be interpreted and how they can be used for modeling purposes. The thesis is composed of four main chapters (chapters 2 - 5). The research objectives of chapter 2 are twofold: the first aim is to investigate the large-scale implications of a strong trend in inherent WUE (IWUE), as has recently been found with EC data in temperate and boreal forests (Keenan et al., 2013). This is achieved by forcing the observed trend in the LSM JSBACH by simulating an increased CO_2 sensitivity of stomatal conductance, and by confronting the simulated continental discharge, evapotranspiration, and the seasonal CO_2 exchange with the respective observations or observation-based data products. The

second aim of this chapter is to explore the relationship between an observed IWUE response at ecosystem-level and the associated physiological behavior (in particular the ratio of intercellular to atmospheric CO_2 concentration, c_i/c_a) at leaf level; an analysis which investigates the effects of scale-dependent factors on leaf- and ecosystem-level trends of WUE. In the third chapter, a key physiological parameter characterizing intrinsic WUE (G_1) is derived from EC data at six contrasting forest sites and compared to leaf-level estimates of g_1 at the same location. The analysis aims to assess both qualitatively and quantitatively the effects of six mechanisms (non-transpirational water fluxes, aerodynamic conductance, meteorological deviations between measurement height and canopy surface, energy balance non-closure, net ecosystem exchange partitioning, and physiological within-canopy gradient) on the observed discrepancies between leaf- and ecosystem-level estimates of G_1. A data-oriented, "big-leaf" approach is used in combination with various data processing and modeling approaches. Chapter 4 presents a software package that aims to provide consistent and reproducible calculation routines to derive G_1 and other physiological as well as biometeorological variables from EC data. The metrics are calculated for both single- and two-level EC sites. Chapter 5 investigates the effects of an explicit representation of g_m with respect to present and future simulations (RCP scenarios from 2070-2099) of photosynthesis and transpiration at leaf, ecosystem and global scales. An extensive database of leaf-level measurements of g_m is compiled and used to parameterize the model. A parameter adjustment method is presented which ensures a consistent conversion from an implicit (infinite g_m) to an explicit g_m model formulation. In addition, the potential role of environmental factors (intercellular CO_2 concentration and light), whose effects on g_m are not yet resolved, are tested at the large scale.

Key results: Observed, large-scale trends from 1992-2010 in continental discharge, evapotranspiration, and the seasonal amplitude of atmospheric CO_2 do not agree with the JSBACH simulations in which the stomatal sensitivity to CO_2 concentration is increased in order to reproduce the IWUE trend as observed by Keenan et al. (2013) ($\approx 2.3\% \ \mathrm{yr}^{-1}$), whereas these data agree with standard simulations that simulate a physiological response as expected from theory and as found in leaf-level data. It is further shown that a IWUE trend of that magnitude would require a strong physiological response that is associated with decreasing c_i, whereas the large-scale observations are consistent with a constant c_i/c_a over time. The detailed analysis at selected EC sites (chapter 3) revealed that of all confounding factors investigated, the energy balance non-closure caused the highest uncertainties in the derivation of the G_1 parameter, in particular if the non-closure is caused by an underestimated latent heat flux. Other factors like aerodynamic conductance, non-transpirational water fluxes, or meteorological deviations between the canopy surface and the measurement height do in most cases not critically confound the bulk canopy estimates of G_1 if simple measures (e.g. use of additional simple models, application of basic data filtering) are taken to minimize their effects. Chapter 4 further shows that the 'big-leaf' analysis can be successfully applied to both single- and two-level EC sites to character-

ize a wide range of ecophysiological and biometeorological ecosystem properties. Chapter 5 demonstrates that the explicit consideration of g_m in the Farquhar et al. (1980) photosynthesis model leads to altered photosynthetic sensitivities to environmental factors, foremost temperature and CO_2 concentration. In particular, the analysis reveals that the g_m-explicit model predicts a significantly higher photosynthetic CO_2 sensitivity in regions that are characterized by cold temperatures and vegetation with low g_m. Consequently, considerable effects were found in the boreal forests, which showed an increase in gross primary productivity (GPP) of 15-25% when g_m is considered explicitly, whereas the tropics did not show significant changes between the implicit and explicit model versions. Similar spatial patterns are found for transpiration, but with a lower magnitude. Globally, the model simulations (RCP 8.5 scenario from 2070-2099) suggest moderate increases in projected GPP of 3.6 - 6.6 Pg C yr^{-1}.

Main conclusions: The clear disagreement of large-scale observations and simulations of the dynamics of water and carbon fluxes is a clear indication that the IWUE trend in the magnitude as found by Keenan et al. (2013) is not a large-scale phenomenon, but potentially a sampling bias in space and time. Reproducing the strong trend in the model further revealed that changes in IWUE of that magnitude would be clearly detectable in continental signals related to large-scale water and carbon fluxes. Another important conclusion is that scale-dependent factors must be taken into account in order to infer correct changes in leaf physiology from observed trends in WUE at larger scales or vice versa, to correctly up-scale the consequences of leaf physiological changes to ecosystem and larger scales. The ecophysiological interpretation of EC data is compromised in particular by factors that are often overlooked such as the energy balance non-closure, or aerodynamic decoupling. It is crucial to adequately consider, and if possible, correct the confounding effects of these factors if EC data are interpreted in an ecophysiological context. In addition, it is shown that a wide range of bulk biometeorological variables derived from EC data such as temperature and atmospheric moisture at the canopy surface, aerodynamic decoupling, or the ecosystem light response, can characterize the physiological and physical processes underlying the measured fluxes, and therefore significantly facilitate the interpretation of EC data. The incorporation of g_m into LSMs changes the simulated dynamics of photosynthesis, in particular its response to CO_2 concentration and temperature. The ability of next generation LSMs to adequately represent both the magnitude and the dynamics of g_m will be relevant for predicting the CO_2 fertilization effect in the extratropical northern hemisphere. A better understanding of g_m further allows to employ a more comprehensive carbon isotope discrimination model, which will help to better constrain the current and future behavior of vegetation gas exchange.

Zusammenfassung

wissenschaftlicher Hintergrund: Die Vegetation kontrolliert maßgeblich den gleichzeitigen Austausch von Kohlenstoff und Wasser zwischen der Landoberfläche und der Atmosphäre, welcher erhebliche Auswirkungen auf die Energiebilanz der Landoberfläche und auf das globale Klima hat. Ein tiefgreifendes Verständnis über die ökophysiologischen Mechanismen, welche den gekoppelten Wasser- und Kohlenstoffflüssen zu Grunde liegen, ist deswegen wichtig um die Reaktion der terrestrischen Biosphäre auf den globalen Klimawandel, sowie entsprechende Rückkopplungen vorhersagen zu können. Prozessbasierte Modelle, welche grundlegende physiologische Prozesse auf Blattebene sowie deren Effekte auf den großflächigen Kohlenstoff-, Wasser-, und Energieaustausch abbilden (Landoberflächenmodelle, LSMs), sind wertvolle Mittel um diese Herausforderung zu bewältigen. LSMs können jedoch nur dann sinnvoll eingesetzt werden, wenn sie mit Beobachtungen kombiniert werden, welche für die Parametrisierung und Evaluierung von Modellen herangezogen werden müssen. Mittlerweile gibt es eine Vielzahl von Beobachtungen welche im Zusammenhang mit gekoppelten Kohlenstoff- und Wasserflüssen stehen: Gasaustauschmessungen auf Blattebene, ^{13}C Kohlenstoffisotope, Eddy-Kovarianz (EC) Daten, sowie Beobachtungen auf größerer Skala wie kontinentale Abflussmessungen oder Messreihen der atmosphärischen CO_2 Konzentration. Diese Daten beinhalten Informationen über den Gasaustausch der Vegetation auf unterschiedlichen räumlichen Skalen sowie mit unterschiedlicher zeitlicher Integration, was den Vergleich dieser Datensätze untereinander, als auch die Ableitung physiologischer Signale von diesen Daten erschwert. So können zum Beispiel Messungen auf Ökosystemebene in den meisten Fällen nicht direkt auf die zugrundeliegenden physiologischen Prozesse zurückgeführt werden, wodurch sie auch nicht für die Parametrisierung von Modellen verwendet werden können, die Informationen auf Blattebene benötigen. Eine weitere Schwierigkeit besteht darin, dass fehlende oder inadäquate Modellformulierungen zu systematisch falschen Modellvorhersagen sowie zu einer falschen Interpretation von Daten führen, welche im Zusammenhang mit Wasser- und Kohlenstoffflüssen sowie deren Kopplung stehen. Die weit verbreitete, aber falsche Annahme einer unendlich großen blattinternen CO_2 Leitfähigkeit (Mesophyll-Leitfähigkeit, g_m) zum Beispiel führt zu einer falschen CO_2-Sensitivität der Photosynthese, sowie zu einer systematisch falschen Abschätzung der Wassernutzungseffizienz von ^{13}C Diskriminierungsdaten. Sowohl die richtige Interpretation von Beobachtungsdaten als auch eine adäquate Darstellung der entsprechenden Prozesse in Modellen sind wichtige Voraussetzungen, um die heutige und die zukünftige Funktionsweise des Gasaustausches von Pflanzen sowie dessen Rolle im Klimasystem zu verstehen.

Forschungsziele und Methoden: Das übergreifende Forschungsziel dieser Arbeit besteht darin, ein verbessertes Verständnis zu entwickeln wie Daten, welche im Zusammenhang mit dem Austausch von Wasser und Kohlenstoff der Vegetation stehen, zu interpretieren sind und wie sie für Modellierungszwecke verwendet werden können. Diese Arbeit besteht aus

vier Hauptkapiteln (Kapitel 2 - 5). Das erste Kapitel verfolgt zwei wesentliche Forschungsziele: das erste Ziel besteht darin, die großflächigen Effekte eines starken Trends in der inhärenten Wassernutzungseffizienz (IWUE), welcher kürzlich in EC Daten in temperaten und borealen Wäldern gefunden wurde (Keenan et al., 2013), zu untersuchen. Dies wird dadurch bewerkstelligt, indem der beobachtete Trend im LSM JSBACH reproduziert wird, was durch eine Erhöhung der simulierten stomatären CO_2-Sensitivität geschieht, und anschließend die modellierten kontinentalen Abflüsse, Evapotranspiration, und der Jahresgang der CO_2 Amplitude in der Atmosphäre mit den entsprechenden Beobachtungen bzw. mit beobachtungsbasierten Datenprodukten verglichen werden. Das zweite Forschungsziel dieses Kapitels besteht darin, den Zusammenhang zwischen den beobachteten WUE Trends auf Ökosystemebene und das zugrundeliegende, physiologische Verhalten, vor allem das Verhältnis von interzellulärer zu atmosphärischer CO_2 Konzentration, c_i/c_a) zu ergründen. In dieser Analyse werden skalenabhängige Effekte von verschiedenen Faktoren auf die WUE Trends auf Blatt- und Ökosystemebene untersucht. Im dritten Kapitel wird ein bedeutender physiologischer Parameter (G_1), welcher ein Maß für die intrinsische WUE ist, für sechs verschiedene Waldstandorte abgeleitet und mit den Werten auf Blattebene (g_1), welche am gleichen Standort geschätzt wurden, verglichen. Diese Analyse zielt darauf ab, den Einfluss von sechs verschiedenen Mechanismen (nicht-transpirative Wasserflüsse, aerodynamische Leitfähigkeit, meteorologische Unterschiede zwischen Messhöhe und Kronendach, Nicht-Schließung der Energiebilanz, Aufteilung des Nettoökosystemaustausches, physiologische Gradienten innerhalb der Vegetation) auf die beobachtete Diskrepanz zwischen den Parameterschätzungen auf Blatt- und Ökosystemebene qualitativ und quantitativ zu untersuchen. Für diese Analyse wird ein datenorientierter, sogenannter "big-leaf" Ansatz in Kombination mit verschiedenen Datenprozessierungsmethoden und Modellierungsansätzen verwendet. In Kapitel 4 wird ein Software-Packet vorgestellt, welches eine konsistente und reproduzierbare Ableitung von G_1 und anderen physiologischen sowie biometeorologischen Kenngrößen von EC Daten ermöglicht. Beispielberechnungen werden für EC Stationen gemacht, welche auf einer und auf zwei Messhöhen messen. In Kapitel 5 wird untersucht, welche Effekte eine explizite Berücksichtigung von g_m auf Simulationen der Photosynthese und der Transpiration auf Blatt-, Ökosystem- und globaler Ebene hat. Eine umfassende Datenbank von g_m Messungen wird angelegt um das Modell zu parametrisieren, und eine Methode wird vorgestellt, welche nützlich ist um Modelle konsistent von einer gm-impliziten zu einer gm-expliziten Version umzustellen. Darüber hinaus wird die potentielle Rolle von Umweltfaktoren, deren Einfluss auf g_m noch nicht abschließend geklärt ist, auf großer Skala untersucht.

Hauptergebnisse: Beobachtete Trends des kontinentalen Abflusses, der Evapotranspiration, und der Amplitude des Jahresgangs von CO_2 von 1992-2010 sind nicht vereinbar mit den JSBACH Simulationen, in denen die stomatäre CO_2-Sensitivität erhöht wurde um den IWUE Trend, wie er von Keenan et al. (2013) gefunden wurde ($\approx 2.3\%$ Jahr^{-1}), im Modell zu reproduzieren. Die Daten stimmen jedoch mit den Standardsimulationen

überein, die eine physiologische Antwort in dem Maße simulieren, welcher im Einklang mit theoretischen Darstellungen und den Ergebnissen von Daten auf Blattebene stehen. Des Weiteren wird gezeigt, dass ein IWUE Trend in dieser Größenordnung nur mit einer starken physiologischen Reaktion, welche mit einer Reduzierung der interzellulären CO_2 Konzentration einhergeht, erklärt werden könnte. Im Gegensatz dazu sind die großskaligen Beobachtungen konsistent mit einem konstanten c_i/c_a. Die detaillierten Analysen an ausgewählten EC Messstationen (Kapitel 3) zeigen, dass von allen analysierten Störfaktoren, welche die Ableitung des G_1 Parameters beeinflussen, die Nicht-Schließung der Energiebilanz mit der größten Unsicherheit verbunden ist, insbesondere dann, wenn diese mit einer Unterschätzung des latenten Wärmeflusses einhergeht. Andere Faktoren wie der Einfluss der aerodynamischen Leitfähigkeit oder nicht-transpirative Wasserflüsse führen in den meisten Fällen nicht zu einer kritischen Fehlabschätzung des G_1 Parameters, vorausgesetzt dass einfach durchzuführende Maßnahmen getroffen werden (z.B. einfache zusätzliche Modellberechnungen, Einsatz von geeigneten Datenfiltern), welche den Einfluss dieser Faktoren auf ein Minimum beschränken. Kapitel 4 zeigt zudem, dass der "big-leaf" Ansatz erfolgreich angewendet werden kann um eine Vielzahl von ökophysiologischen und biometeorologischen Eigenschaften von Ökosystemen zu berechnen, was unabhängig davon funktioniert, ob das EC System auf einer oder auf zwei Höhen misst. In Kapitel 5 wird gezeigt, dass eine explizite Berücksichtigung von g_m zu veränderten Sensitivitäten hinsichtlich verschiedener Umweltfaktoren, vor allem Temperatur und CO_2 Konzentration, führt. Die Analyse zeigt auch, dass das g_m-implizite Modell eine deutlich höhere CO_2-Sensitivität vor allem in solchen Regionen simuliert, welche durch kalte Temperaturen und Vegetation mit niedriger g_m charakterisiert sind. Dies hat insbesondere in den borealen Nadelwäldern beträchtliche Auswirkungen. In diesen Gebieten erhöht sich die simulierte Bruttoprimärproduktion (GPP) um 15%-25% wenn g_m explizit berücksichtigt wird, wohingegen es keine signifikanten Änderungen in den tropischen Regionen gibt. Modellierte Transpirationsraten zeigen ähnliche räumliche Muster, aber geringere absolute Änderungen als GPP. Simulationen mit dem RCP8.5 Szenario für die Jahre 2070-2099 zeigen moderate Erhöhungen in der Höhe von 3.6 - 6.6 Pg C Jahr^{-1}.

Schlussfolgerungen: Die deutliche Diskrepanz zwischen den großskaligen Beobachtungen und den entsprechenden Simulationen von Wasser- und Kohlenstoffflüssen sind klare Anzeichen dafür, dass der beobachtete IWUE Trend in der Größenordnung wie er von Keenan et al. (2013) beobachtet wurde, nicht auf großer Skala existiert, sondern wahrscheinlich durch eine nicht-repräsentative Auswahl von Messstationen zustande gekommen ist. Die Simulation des Trends im Modell konnte des Weiteren aufdecken, dass sich ein IWUE Trend in dieser Größenordnung klar in Beobachtungen auf kontinentaler Skala, welche im Zusammenhang mit Wasser- und Kohlenstoffflüssen stehen, widerspiegeln würde. Eine weitere wichtige Schlussfolgerung ist, dass die Effekte von skalenabhängigen Faktoren in weitergehenden Analysen berücksichtigt werden müssen, um sowohl WUE Trends hinsichtlich dem physiologischen Verhalten auf Blattebene interpretieren zu können, als auch

um die Auswirkungen von physiologischen Änderungen auf Blattebene auf Ökosystem- und größerer Skala abschätzen zu können. Die ökophysiologische Interpretation von EC Daten ist vor allem durch solche Störfaktoren gefährdet, die oft nicht hinreichend berücksichtigt werden, wobei vor allem die Nicht-Schließung der Energiebilanz relevant ist. Für die ökophysiologische Interpretation von EC Daten ist es jedoch von enormer Wichtigkeit, dass alle vorhandenen Störfaktoren adäquat berücksichtigt, und wenn möglich, deren Einflüsse auf die physiologische Zielvariable minimiert werden. Darüber hinaus konnte gezeigt werden, dass biometeorologische Variablen, welche von EC Daten abgeleitet werden können (z.B. Temperatur und Luftfeuchte an der Bestandsoberfläche, die aerodynamische Entkopplung zwischen der Vegetationsbedeckung und der Atmosphäre, oder die Lichtantwort des Ökosystems) prinzipiell dazu geeignet sind die zugrundeliegenden physiologischen und physikalischen Prozesse zu charakterisieren und damit die Interpretation von EC Daten erheblich zu vereinfachen. Die Berücksichtigung von g_m in LSMs führt zu veränderten Dynamiken der Photosynthese und verändert vor allen Dingen deren CO_2- und Temperaturantwort. Die Fähigkeit zukünftiger LSMs sowohl die absoluten Werte als auch die zeitlichen Veränderungen von g_m adäquat darstellen zu können ist wichtig um den CO_2-Düngungseffekt der außertropischen Nordhalbkugel richtig abschätzen zu können. Ein verbessertes Verständnis von g_m ermöglicht überdies die Anwendung eines umfassenderen Diskriminierungsmodells, welches eine verbesserte Quantifizierung von Veränderungen im Verhalten des Gasaustausches der Vegetation ermöglicht.

List of publications and manuscripts

The following publications and manuscripts are part of this cumulative PhD thesis:

Chapter 2: Knauer, J., Zaehle, S., Reichstein, M., Medlyn, B.E., Forkel, M., Hagemann, S., and Werner, C. (2017). The response of ecosystem water-use efficiency to rising atmospheric CO_2 concentrations: sensitivity and large-scale biogeochemical implications. *New Phytologist* 213, 1654-1666, doi: 10.1111/nph.14288.

Chapter 3: Knauer, J., Zaehle, S., Medlyn, B. E., Reichstein, M., Williams, C. A., Migliavacca, M., De Kauwe, M. G., Werner, C., Keitel, C., Kolari, P., Limousin, J-M., Linderson, M-L. (2018). Towards physiologically meaningful water-use efficiency estimates from eddy covariance data. *Global Change Biology* 24, 694-710, doi: 10.1111/gcb.13893.

Chapter 4: Knauer, J., El-Madany, T.S., Zaehle, S., Migliavacca, M. (2018). Bigleaf – An R package for the calculation of physical and physiological ecosystem properties from eddy covariance data. *PLoS ONE* 13, e0201114, doi:10.1371/journal.pone.0201114.

Chapter 5: Knauer, J., Zaehle, S., De Kauwe, M.G., Bahar, N.H.A., Evans, J.R., Medlyn, B.E., Reichstein, M., Werner, C. Effects of mesophyll conductance on vegetation responses to elevated CO_2 concentrations in a land surface model. Submitted to *Global Change Biology* on 07 September 2018.

The publications and manuscripts listed above were copy-edited to obtain a harmonized style and format. This includes numbering of chapters, figures, tables, and equations, as well as the layout of tables. The citation style was harmonized and all references were combined to one single list. The content of these chapters, including text, figures, and tables fully agree with the original publications or manuscripts.

The following publications were authored or co-authored during the doctoral studies and are closely related to the work presented in this PhD thesis:

Knauer, J., Werner, C., and Zaehle, S. (2015). Evaluating stomatal models and their atmospheric drought response in a land surface scheme: A multibiome analysis. *Journal of Geophysical Research: Biogeosciences* 120, 1894-1911, doi:10.1002/2015JG003114

De Kauwe, M. G., Medlyn, B. E., Knauer, J., and Williams, C. A. (2017). Ideas and perspectives: how coupled is the vegetation to the boundary layer? *Biogeosciences* 14, 4435-4453, doi:10.5194/bg-14-4435-2017

Medlyn, B. E., De Kauwe, M. G., Lin, Y.-S., Knauer, J., Duursma, R. A., Williams, C. A., Arneth, A., Clement, R., Isaac, P., Limousin, J.-M., et al. (2017). How do leaf and ecosystem measures of water-use efficiency compare? *New Phytologist* 216, 758-770, doi:10.1111/nph.14626

Wutzler, T., Lucas-Moffat, A., Migliavacca, M., Knauer, J., Sickel, K., Sigut, L., Menzer, O., and Reichstein, M. (2018). Basic and extensible post-processing of eddy covariance flux data with REddyProc. *Biogeosciences* 15, 5015-5030, doi:10.5194/bg-15-5015-2018

1 Introduction

1.1 Role of vegetation in the Earth system

When the first general circulation models (GCMs) appeared in the late 1960s, all they represented was a purely physical description of the exchange of energy between the land surface - reduced to a simple "bucket" - and the atmosphere (Sellers et al., 1997). Vegetation appeared in the second generation of GCMs, but its role was still reduced to its effects on the land surface energy and water balance. It was not until the third generation of GCMs in the mid 1990s that both the biophysical and the biogeochemical role of vegetation in the Earth system was fully acknowledged (Sellers et al., 1997). It was then also primarily with the help of these third-generation models that the prominent role of vegetation in the climate system (see Fig. 1.1) could be understood and its effects quantified (Bonan, 2008).

Vegetation exerts significant biophysical controls on the land surface. The presence of vegetation on land generally increases surface roughness, which increases the transfer of momentum and the efficiency of latent and sensible heat transfer between the land surface and the atmosphere (Dorman and Sellers, 1989). The effects of increased surface roughness as a consequence of vegetation cover is strong enough to significantly affect low-level wind fields as well as atmospheric circulation and precipitation patterns (Sud et al., 1988). Vegetation also significantly affect the albedo (i.e. the fraction of incoming radiation that is reflected back to space) of the land surface and thus the amount of energy available for surface heat fluxes (Lyons, 2002). Vegetation further plays a major role in the terrestrial hydrological cycle. More than half of the global land-atmosphere water flux (Evapotranspiration; ET) is actively controlled by plants (transpiration, the water flux passing through plants) (Schlesinger and Jasechko, 2014). However, also the non-biological part of ET (evaporation) is significantly modulated by vegetation. Plant canopies are able to intercept large parts of precipitation (Grelle et al., 1997; Benyon and Doody, 2015), and this short-term storage of surface water is readily evaporated back to the atmosphere and not available for increasing soil moisture and surface runoff (Fisher et al., 2014). These hydrological processes are important for the dynamics of the surface energy balance, in particular the partitioning of the available energy into sensible and latent heat (Kleidon et al., 2000; Bonan, 2008). Vegetation is further a major component of the global carbon cycle as it largely controls the uptake of carbon dioxide (CO_2) by the land surface. This uptake is large enough to reduce the atmospheric CO_2 concentration by several ppm in the summer months (Keeling, 1960; Randerson et al., 1997). The majority of this carbon is respired back to the atmosphere over different timescales, but some parts are stored in different plant organs or in the soil. The ability of the terrestrial biosphere to act as a carbon sink makes it an important regulating factor for global climate (Cox et al., 2000; Friedlingstein et al., 2014). However, vegetation does not only affect climate, but is in turn also affected by changes in climate, which invokes complex biosphere-atmosphere feedbacks. For example, plants respond to rising atmospheric CO_2 concentrations by increasing photosynthesis,

which acts as a negative feedback to increasing CO_2 concentration.

The three components described above (surface energy, hydrology, and the carbon cycle) are intimately linked, and in particular the link between these major components of the climate system is significantly affected by vegetation. The role of vegetation in the coupling of the water and the carbon cycle, as well as its regulating role on climate may best be demonstrated by the function of stomata, tiny pores on the leaf surface which control the majority of the water loss, but also the carbon uptake, of plants. The role of stomata in the climate system is indeed considerable. Of particular importance is the so-called "physiological forcing", which describes the effects of stomatal closure in response to rising atmospheric CO_2 concentrations. Modeling studies have shown that CO_2-induced stomatal closure has similar effects on climate than the well known effects of "radiative forcing" as caused by the emission of greenhouse gases (Sellers et al., 1986), or that large-scale stomatal closure significantly affects surface hydrology by reducing ET, increasing soil moisture and consequently increasing continental discharge (Gedney et al., 2006; Betts et al., 2007; Cao et al., 2010), which again feedbacks on land surface temperature, and surface energy fluxes (Boucher et al., 2009).
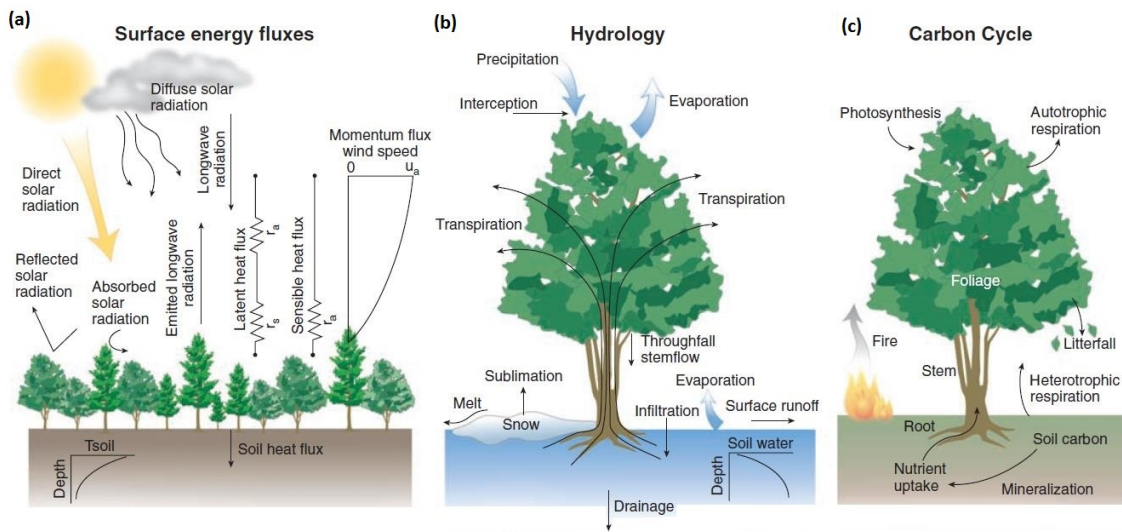
Fig. 1.1. Illustration of key processes considered in state-of-the-art LSMs related to (a) surface energy fluxes, (b) surface hydrology, and (c) the carbon cycle. Taken from Bonan (2008).

The development of GCMs did not end with the third generation, but they continuously evolved into what is now known as Earth system models (ESMs) (Bonan and Doney, 2018), which represent various climate-relevant processes on land, in the ocean, and in the atmosphere as well as their interactions. The land part of ESMs, land surface models (LSMs), consider the basic biochemical and biogeophysical principles summarized above, but are also becoming increasingly complex in order to adequately present ongoing anthropogenic perturbations of the climate system such as rising CO_2 concentrations and associated increasing temperatures and atmospheric water demands (Cook et al., 2014), changes in nutrient availability through nutrient deposition and fertilization (Zaehle and

Friend, 2010; Wieder et al., 2015), land use and land cover change (Brovkin et al., 2004; Pongratz et al., 2010), as well as disturbances and associated large-scale vegetation dynamics (Bonan et al., 2003). All of these ongoing changes interact with plant physiology and consequently, a sound process understanding of the physiological basis of water-carbon coupling and an adequate representation in LSMs is a prerequisite to understand complex feedbacks with, and future trajectories of, the Earth system in times of global change.

1.2 Water-carbon coupling in land surface models

This section provides a basic overview of the representation of plant physiological processes in LSMs, with a focus on those processes that are relevant for water-carbon coupling. The work presented in this thesis was performed using the LSM JSBACH (Raddatz et al., 2007; Reick et al., 2013), which is the land component of the MPI Earth system model (Giorgetta et al., 2013). However, the basic formulations presented here are similar in most state-of-the-art LSMs (Rogers et al., 2017).

The principle of the biological components of LSMs is to model physiological processes in dependence on environmental factors at leaf level and subsequently scale the simulated leaf-level fluxes up to the canopy and larger (regional to global) spatial scales. Vegetation in LSMs is usually discretized into plant functional types (PFTs), which describe similar plant phenotypes, and which have specific biochemical (e.g. photosynthetic capacity), biophysical (e.g. albedo, vegetation height), and phenological (e.g. max. LAI) attributes. Notwithstanding such PFT-specific attributes (i.e. parameters), leaf-level processes are calculated in the same manner for all PFTs of the same photosynthetic pathway. Note that formulations provided here are for C3 plants only. The respective C4 model formulations can be found in von Caemmerer (e.g. 2000).

Photosynthesis is mostly calculated using the biochemical model developed by Farquhar et al. (1980) or variants thereof (e.g. Kull and Kruijt, 1998). This model describes net photosynthesis (or net assimilation, A_n) as the lesser of two rates, the carboxylation-limited photosynthesis rate (A_c), and ribulose 1,5-bisphosphate (RuBP) regeneration-limited photosynthesis rate (A_j):

$$A_n = \min(A_c, A_j) \tag{1.1}$$

where

$$A_n = \frac{(c_i - \Gamma_*)V_{cmax}}{c_i + K_c(1 + o_i/K_o)} - R_l \tag{1.2}$$

and

$$A_j = \frac{(c_i - \Gamma_*)J/4}{c_i + 2\Gamma_*} - R_l \tag{1.3}$$

c_i is the intercellular CO_2 concentration, Γ_* is the photorespiratory CO_2 compensation point, V_{cmax} is the maximum carboxylation rate, K_c and K_o are the Michaelis-Menten

constants for CO_2 and O_2, respectively, o_i is the intercellular O_2 concentration, J is the electron transport rate, and R_l is leaf day respiration. Occasionally, the photosynthesis rate limited by triose phosphate utilization (TPU) (A_p) is considered as a third limiting factor in Eq. 1.1 (Harley and Sharkey, 1991; Lombardozzi et al., 2018). Stomatal conductance (g_s, Fig. 1.2) is mostly simulated by semi-empirical formulations, of which the Ball-Berry model (Ball et al., 1987) is the most established one:

$$g_s = g_0 + g_1 \frac{A_n rH}{c_a} \tag{1.4}$$

where g_0 is the minimum g_s in the absence of light, g_1 is a parameter describing the sensitivity of A_n to g_s, rH is relative humidity at the leaf surface, and c_a is atmospheric CO_2 concentration. Eq. 1.4 clearly demonstrates the close coupling between A_n and g_s. This close relationship has a long-standing observational basis (Wong et al., 1979), and the Ball-Berry model has given accurate predictions under varying environmental conditions (Buckley and Mott, 2013), including sub-ambient and elevated CO_2 concentrations (Franks et al., 2013). In the last three decades, the Ball-Berry model has been repeatedly modified (Leuning, 1995; Medlyn et al., 2011), but all approaches currently employed in LSMs are based on the close correlation between A_n and g_s (see Sato et al., 2015, for an overview), and predict similar behavior at leaf and ecosystem level (Knauer et al., 2015; Franks et al., 2018). While a multitude of other stomatal models, including more mechanistic ones, exist (Damour et al., 2010), the poor process understanding and the difficulty involved in up-scaling these alternative models to larger scales has precluded their widespread use in LSMs (Berry et al., 2010).

A_n and g_s determine the ratio of intercellular to ambient CO_2 concentration (c_i/c_a), an important set point integrating the behavior of plant gas exchange (Ehleringer and Cerling, 1995). c_i/c_a is closely related to two other central physiological quantities: the stomatal slope parameter g_1 of the Ball-Berry model (Eq. 1.4) or related formulations (Leuning, 1995; Medlyn et al., 2011), and the intrinsic WUE (iWUE = A_n/g_s). The relationship between c_i/c_a and iWUE can be readily shown by re-arranging Fick's first law ($A_n = g_s(c_a - c_i)$):

$$\text{iWUE} = \frac{A_n}{g_s} = c_a \left(1 - \frac{c_i}{c_a} \right) / 1.6 \tag{1.5}$$

By combining Fick's first law and the Ball-Berry model (Eq. 1.4), it can be shown that g_1 and c_i/c_a are closely related and expected to change only with atmospheric humidity:

$$\frac{c_i}{c_a} = 1 - \frac{1.6}{g_1 \, rH} \tag{1.6}$$

where the factor 1.6 accounts for the differences in g_s for water vapor and CO_2 due to the different diffusivities of the two gases. Note that vapor pressure deficit (VPD) is likely to represent a better control on leaf gas exchange (Aphalo and Jarvis, 1991), which does however, not invalidate Eq. 1.6). Compared to other leaf gas exchange variables, c_i/c_a, as

well as g_1 and iWUE are remarkably constant in the absence of water stress (Ehleringer and Cerling, 1995; Prentice et al., 2014), and studies found no indication that g_1 changes with increasing CO_2 concentrations (i.e. there are currently no indications for acclimation of g_1 (Medlyn et al., 2001)). However, they do show important variations across plant types and species (Ball et al., 1987; Lin et al., 2015).

c_i is the CO_2 concentration in the substomatal cavities, and therefore not the CO_2 concentration that is available for photosynthesis, which is the chloroplastic CO_2 concentration (c_c). The difference between c_i and c_c, the CO_2 concentration drawdown from the substomatal cavity to the chloroplasts, depends on the internal conductance to CO_2 transfer, the mesophyll conductance (g_m; Fig. 1.2). Currently, g_m is not explicitly considered in most state-of-the-art LSMs. Instead, parameters describing the photosynthetic capacity (V_{cmax25} and J_{max25} in Eqs. 1.2 and 1.3, respectively) implicitly account for the effects of g_m on plant photosynthesis (e.g. Warren, 2008; Sun et al., 2014b). Note that in case of an explicit representation of g_m, c_i in Eqs. 1.2 and 1.3 is replaced by c_c, but also all other parameters need to be adjusted. However, the compensation of the infinite g_m in models does not fully account for its effects on photosynthesis, and first modeling exercises have shown substantial implications of g_m on global carbon fluxes (Sun et al., 2014b). Although g_m does not affect leaf-level water fluxes directly (Fig. 1.2), it is expected to change also transpiration due to the fact that any changes in A_n also affect g_s and thus transpiration (Eq. 1.4).

State-of-the-art LSMs generally calculate the physiological quantities at leaf-level, and upscale them to the canopy level by integration over the leaf area index (LAI) of the canopy. This up-scaling takes within-canopy variations of light, leaf nitrogen content, and eventually other leaf properties into account. The resulting canopy-level fluxes are subsequently averaged over the PFTs present in the respective grid cell and continental or global flux fields can be obtained. The described processes in this section are affected by various environmental factors, in particular by meteorological variables (temperature, radiation, VPD, etc.), soil moisture availability, and atmospheric transfer coefficients (i.e. aerodynamic conductance). Logically, models also simulate all relevant feedbacks between plant physiology and other state variables (e.g. soil moisture affects g_s and transpiration, which again affect soil moisture). See e.g. Pitman (2003) for a general description of LSMs, and Schulz et al. (2001) or Roeckner et al. (2003) for a description of the physical basis of JSBACH.

1.3 Ecophysiological observations of water-carbon coupling

Process-based formulations as employed in LSMs (see above) need to be parameterized and the results of model simulations need to be evaluated. For both of these steps, observations are needed. The parameterization of models with measurements ensures that models represent processes as observed in the real world, and model evaluation serves to test whether models are able to adequately predict the observed outcome. The ability of
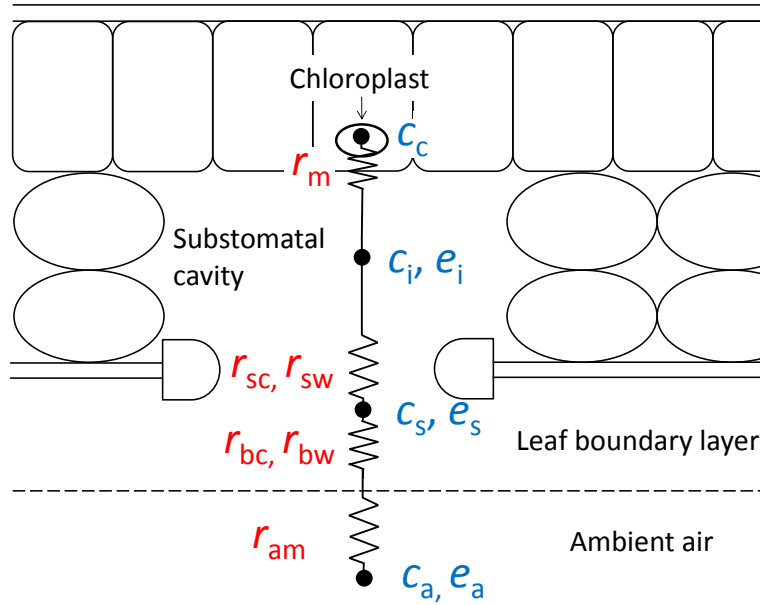
Fig. 1.2. Schematic illustration of the diffusion pathways of CO_2 into the leaf and water vapor out of the leaf. Blue symbols denote partial pressures of CO_2 (c) and water vapor (e), respectively. Subscripts denote the following: a = ambient, s = leaf surface, i = intercellular, c = chloroplastic. Red symbols denote resistances: r_{am} = aerodynamic resistance to momentum transfer, r_{bc} = leaf boundary layer resistance to CO_2 transfer, r_{bw} = leaf boundary layer resistance to water vapor transfer, r_{sc} = stomatal resistance to CO_2, r_{sc} = stomatal resistance to water vapor, r_m = mesophyll resistance to CO_2 transfer. Redrawn from Wohlfahrt et al. (2012).

models to reproduce patterns and dynamics of real-world phenomena gives confidence in the models, and further allows to extrapolate to conditions that have not yet been observed (e.g. elevated CO_2 concentrations) or to test hypothetical scenarios (e.g. land-use change, change in stomatal functioning) that help in understanding of how the Earth system works, and how it might respond to natural or anthropogenic perturbations.

Current ecophysiological observations are gathered at multiple spatial and temporal scales, using a wide variety of techniques. In the following, an overview over relevant data sources, including their advantages and potential pitfalls, is given. The focus will be on measurements which are used in this thesis or that can potentially be used for future work related to this thesis. Other measurement techniques such as chlorophyll fluorescence (Maxwell and Johnson, 2000) at leaf level, or remote sensing applications (e.g. Guanter et al., 2014; Frankenberg et al., 2014) at regional and continental scales are relevant and increasingly important data sources for modeling water-carbon coupling. However, describing these additional methods in further detail is not within the scope of this thesis.

1.3.1 Leaf gas exchange measurements

Leaf gas exchange is long-standing measurement technique, which has contributed significantly to the understanding of leaf-atmosphere interactions (Lange et al., 1971; Wong et al., 1979; von Caemmerer and Farquhar, 1981; Long et al., 1996). Gas (CO_2 and H_2O)

exchange at leaf level is commonly performed using portable devices, in which usually a single leaf is measured in a cuvette under controlled environmental conditions. Fluxes in and out of the leaf are determined based on the applied airflow and the concentration changes of the constituent of interest inside the cuvette. From the net fluxes of carbon dioxide and water vapor, g_s and c_i can be determined from first order principles as detailed in (e.g. von Caemmerer and Farquhar, 1981). Beyond that, the method allows the derivation of key biochemical parameters such as V_{cmax} and J_{max} from measured A_n at different CO_2 concentrations (i.e. $A_n - c_i$ curves), which may directly be used for the parameterization of photosynthesis models (e.g. Franks et al., 2018). By relating A_n to g_s and by accounting for the effects of CO_2 concentration and relative humidity or VPD, key stomatal parameters (g_1 and g_0, see e.g. Eq. 1.4) can be readily determined from these measurements (Ball et al., 1987; Lin et al., 2015; Wolz et al., 2017). State-of-the-art measurement devices allow strict control over conditions in the leaf cuvette (e.g. temperature, light, humidity, or CO_2 concentration), and a constant ventilation prevents the formation of a significant laminar leaf boundary layer. Hence, the measured leaf can be considered as aerodynamically fully coupled to the airflow in the cuvette, which has the advantage that no significant temperature or humidity gradients form above the leaf (i.e. the actual conditions at the leaf surface are close to those set by the device). Therefore, the advantages of leaf gas exchange measurements are their clear interpretability with respect to the physiological response of leaves to environmental conditions. Inevitable disadvantages of the method comprise the limited spatial and temporal coverage of the measurements, and partly the long time investment required to construct $A_n - c_i$ curves. In addition, technical challenges such as leaks or edge effects have to be taken care of (Long and Bernacchi, 2003). Nevertheless, the compilation of multiple gas exchange measurements provide the basis for the parameterization of coupled stomatal-photosynthesis models in past and current LSMs (Sellers et al., 1997; Lin et al., 2015).

1.3.2 Carbon isotope discrimination

A second major ecophysiological data source are ^{13}C isotopes. The isotopic composition ($\delta^{13}C$) of carbon molecules can be measured in various plant parts such as bulk leaf material (Diefendorf et al., 2010), leaf starch and soluble sugars (Brugnoli et al., 1988), or alpha-cellulose of tree rings (Feng, 1999; McCarroll and Loader, 2004; Frank et al., 2015)) using mass spectrometry of pre-processed (e.g. grinded and combusted) samples of the respective plant tissue (Boettger et al., 2007). If $\delta^{13}C$ of both the plant tissue and the atmosphere is known, the photosynthetic discrimination against ^{13}C by plants (Δ) can be calculated. In contrast to $\delta^{13}C$, Δ is independent of external factors such as atmospheric $\delta^{13}C$ and can therefore be more directly attributed to biological processes (Farquhar et al., 1989). In order to be able to relate Δ to c_i/c_a and to other basic physiological quantities such as iWUE, a photosynthetic discrimination model has to be applied. These models all consider additive fractionation factors weighted by the respective CO_2 concentration

difference (Farquhar et al., 1989), but differ with respect to what fractionation steps are included (see Ubierna and Farquhar (2014) for an overview, more details are provided in 6.3). Problematic in that respect is that the derived magnitude and dynamics (e.g. long term trends) of physiological variables depend on the kind of discrimination model used. Most relevant in that respect are the effects of the fractionation associated with CO_2 diffusion through the leaf mesophyll, which depends on the CO_2 concentration drawdown from c_i to c_c, and thus on g_m (Seibt et al., 2008; Ubierna and Farquhar, 2014). g_m is mostly ignored in models of $\Delta^{13}C$ photosynthetic discrimination due to its poor scientific understanding, however its effects on the interpretation of Δ have been estimated to be substantial (Seibt et al., 2008; Keeling et al., 2017).

Carbon isotope data are representative for the entire period in which the sampled tissue was physiologically active, thus they provide a temporally integrated, and therefore representative characterization of plant gas exchange (Diefendorf et al., 2010). In case of isotope data extracted from tree rings this time integration allows for the construction of multi-decadal time series (e.g. Feng, 1999). However, the meteorological conditions associated with the sampled isotope data (e.g. VPD), are usually not directly measured but have to be approximated by e.g. gridded climatological datasets (Frank et al., 2015; Medlyn et al., 2017), which may hamper the derivation of physiological variables from ^{13}C isotopes as well as their comparison to other data sources (Medlyn et al., 2017).

1.3.3 Eddy covariance measurements

The eddy covariance (EC) method provides direct, unobtrusive, continuous, and long-term measurements of mass and energy exchange between an entire ecosystem and the atmosphere (Baldocchi et al., 2001). The measurement of net fluxes is based on the covariance between fluctuations in the vertical wind speed and the concentration of the scalar of interest. The method makes a range of assumptions, for example that density fluctuations of the air are negligible, or that vertical air flow (advection) is zero (Foken and Wichura, 1996). Thus, the method only gives reliable flux measurements when these assumptions are met. Nighttime data, for example, are often not clearly interpretable due to stable atmospheric conditions, and relevant fluxes happening during these time periods (e.g. condensation) may not be measured by EC systems (Fisher et al., 2007). The method is further only applicable at sites that allow the above-mentioned assumptions to be fulfilled, i.e. sites characterized by horizontal and homogenous terrain. Unfulfilled assumptions, but also technical errors cause missing or unreliable data in EC time series. Hence, extensive data pre-processing (Foken and Wichura, 1996) and post-processing (u_*-filtering, gap-filling (Papale et al., 2006; Wutzler et al., 2018)) is required to obtain reliable time-aggregated (hourly or half-hourly) flux estimates.

The EC technique can only measure net fluxes of CO_2, H_2O and other trace gases, and modeling approaches have to be used to derive gross fluxes. Historically, most effort has been put into the separation of net CO_2 fluxes (NEE) into its components gross primary

productivity (GPP) and ecosystem respiration (R_{eco}) (Reichstein et al., 2005; Lasslop et al., 2010). The partitioning of net H_2O fluxes into transpiration and evaporation has recently received increasing attention (Zhou et al., 2016; Berkelhammer et al., 2016; Rigden et al., 2018b), but a standard approach has not yet been identified. The partitioning of measured net fluxes into its component fluxes is an important data processing step in ecosystem research because the derived gross fluxes provide a much stronger insight into the underlying processes compared to net fluxes. For example, the separation of the measured ET into transpiration and evaporation would allow to directly assess the degree of vegetation control on ecosystem water loss. A subsequent analysis step consists of the derivation of relevant ecophysiological variables (or parameters) like canopy conductance G_c or G_1 from the measured (or partitioned) fluxes, as has been attempted several times previously (Wolf et al., 2006; Groenendijk et al., 2011). While the methodology of these approaches is in generally well developed, the associated uncertainties, as well as the reliability of the derived parameters for modeling purposes are not sufficiently addressed.

A merit of EC measurements is that they are accompanied by many relevant meteorological measurements, and in many cases also by ancillary data (e.g. LAI, leaf nitrogen, species distribution), which are highly valuable for the interpretation of EC flux measurements. The EC method also suffers from challenges. Besides the above-mentioned fact that under certain conditions, EC data are not reliable, a further problem of EC measurements is that the energy balance is under most circumstances not closed (e.g. Wilson et al., 2002a). Nevertheless, EC data have contributed more than any other dataset to the understanding of land-atmosphere exchange at ecosystem level (Law et al., 2002; Ciais et al., 2005b; Baldocchi, 2008; Teuling et al., 2010; Williams et al., 2012).

1.3.4 Large-scale observations

In addition to observations of WUE at leaf and ecosystem level, several data products can be useful in characterizing water-carbon coupling at larger spatial scales (e.g. region to globe). These data do not allow to draw direct conclusions on the dynamics of WUE, however, they may be useful for constraining its components (i.e. water and carbon fluxes). Large-scale observations integrate the effects of various environmental processes and meteorological drivers, and are thus not suitable to detect changes in individual processes. For example, a decrease in river discharge cannot be directly attributed to stomatal closure, but may as well be the consequence of other factors happening at the same time, e.g. a decrease in precipitation or changes in vegetation cover. However, conclusions at process-level are possible when these observations are combined with process-based models, with which the sensitivity of changes in individual processes on the simulated, large-scale water and carbon exchanges can be assessed. Hence, LSMs can be used to simulate the effects of a change in a certain process on the large-scale fluxes, which can be directly compared to the respective observations. In this way, the effects of stomatal closure on continental discharge can be estimated, provided that all other relevant processes are also considered in

the model. Large-scale observations or observation-based products relevant to this thesis are:

- **Continental discharge**: River discharge is measured at most major rivers, and fairly complete time series exist for the last decades (see e.g. Dai et al., 2009). Discharge measurements are integrative of all hydrological processes happening in the watershed (i.e. ET, water storage, runoff), including climatic factors, human activities (e.g. land use change, irrigation) and changes in plant physiology (Gerten et al., 2008).

- **Diagnostic ET products**: In contrast to discharge, ET cannot be directly measured at larger scales. Regional or continental estimates are usually based on meteorological data as well as basic land surface properties and require the use of modeling approaches. A common approach is based on the Penman-Monteith equation using satellite-derived input data (e.g. Sheffield et al., 2010).

- **Atmospheric CO_2 records**: The atmospheric background concentration of CO_2 is routinely and accurately measured at several remote stations distributed around the globe (e.g. Rödenbeck, 2005). These stations are usually representative of large regions (e.g. measurements at Mauna Loa, Hawaii, 20°N, are affected by sources throughout the northern hemisphere Randerson et al., 1997). Of ecological significance are in particular the seasonal amplitude of CO_2, and its interannual variation, which are strongly related to vegetation activity (see e.g. Graven et al., 2013; Forkel et al., 2016; Zeng et al., 2014, for further details). These measurement stations commonly also provide measurements of the ^{13}C isotope. These observations are promising for future research because they provide additional insights into the processes involved in land-atmosphere carbon exchange (see section 6.3).

1.3.5 Ecophysiological metrics across scales

Some complication arises due to the fact that ecophysiological vegetation properties such as WUE can be calculated from different data sources which represent a different spatial and/or temporal integration. Likewise, often different metrics are used to describe a similar property or ecophysiological concept. This issue may best be demonstrated for WUE metrics (Fig. 1.3), but applies to other ecophysiological properties (e.g. c_i/c_a, photosynthetic capacity) in a similar manner. Fig. 1.3 gives an overview of WUE metrics commonly reported at leaf and ecosystem level. WUE metrics calculated at ecosystem level are spatially more representative, but are also associated with more confounding factors that need to be considered and that reduce their interpretability compared to leaf-level metrics (arrow from left to right). To account for these confounding factors (e.g. the effects of meteorological conditions), more detailed metrics (e.g. iWUE, g_1; arrow from top to bottom) can be calculated at both leaf and ecosystem level. These metrics are better comparable across environmental conditions and locations, but are still more difficult to

interpret at ecosystem level than at leaf level because of stronger effects of confounding factors at larger scales. Hence, there is an unavoidable tradeoff between interpretability and representativeness of ecophysiological observations at different scales. Note that this interpretability-representativeness tradeoff as shown for the spatial scale in Fig. 1.3 (leaf vs. ecosystem) also applies to the temporal scale in a similar manner (instantaneous measurements vs. temporally integrated metrics).
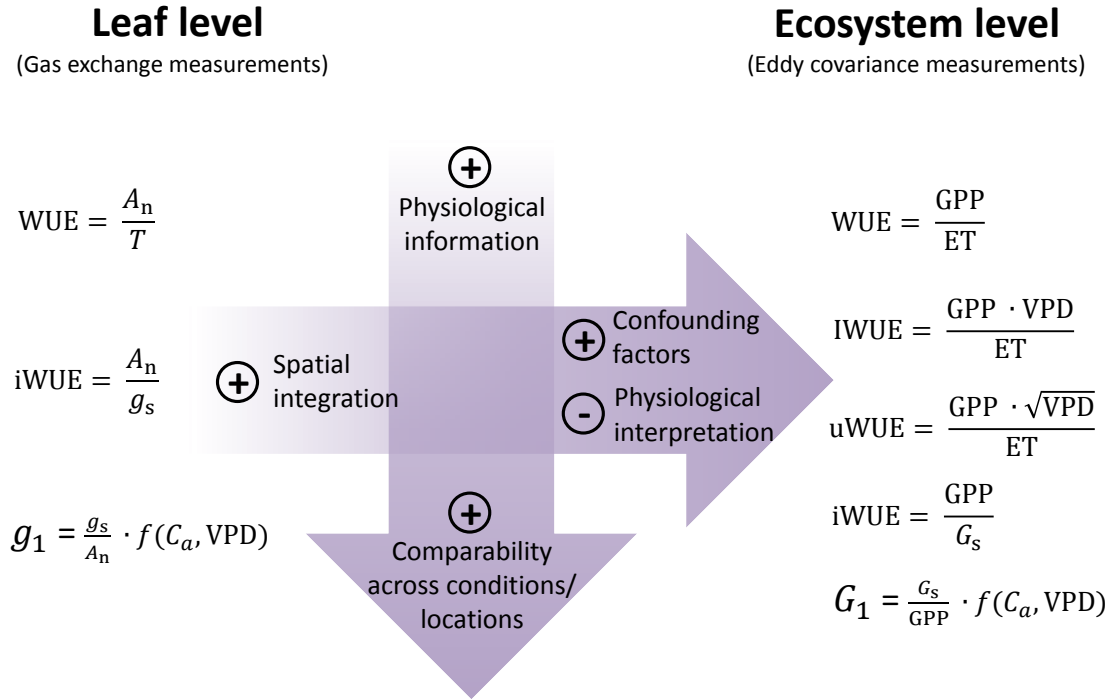
Fig. 1.3. Illustration of different WUE metrics at leaf and ecosystem level. WUE = water-use efficiency, iWUE = intrinsic water-use efficiency (Osmond et al., 1980), IWUE = inherent water-use efficiency (Beer et al., 2009), uWUE = underlying water-use efficiency (Zhou et al., 2014), g_1 / G_1 = stomatal slope parameter, A_n = net photosynthesis, T = Transpiration, g_s = stomatal conductance, C_a = atmospheric CO_2 concentration, VPD = vapor pressure deficit, GPP = gross primary productivity, ET = evapotranspiration, G_s = surface conductance.

As demonstrated in Fig. 1.3, the same ecophysiological metrics can be obtained from different data sources differing in their spatio-temporal extent. However, when these metrics are compared to each other, as has been done by e.g. Medlyn et al. (2017) for the g_1 parameter, considerable discrepancies were identified which could not be conclusively attributed to a single cause. The presence of such discrepancies among different observations suggests that beyond the characterization of uncertainties in the data (e.g. identification and and quantification of random and systematic errors), also conceptual considerations must be made. In general, two overarching questions can be formulated: first, *how do metrics that are derived from observations at different scales have to be interpreted in a given (in this case physiological) context?*; and second, *how should these observations be used to inform models?* These key questions appear in different contexts throughout this

thesis, and some aspects are answered in the following chapters, but they are of general importance for future ecophysiological research that integrates observations and models.

1.4   Aims and structure of the thesis

This thesis intends to explore the potential of observations related to water-carbon coupling at different spatio-temporal scales for constraining and improving the ability of process-based models to predict water-carbon coupling under current and anticipated future conditions. This work aims to give answers to the following research questions:

1. Is the recent, strong increase in ecosystem-level WUE as measured by the EC technique in accordance with large-scale observations or observation-based products of continental discharge, evapotranspiration, and the seasonal amplitude of atmospheric CO_2 (chapter 2)?

2. What is the physiological interpretation, in particular the implied c_i/c_a, of observed trends in ecosystem-level WUE (chapter 2)?

3. What are the most important confounding factors and the main sources of uncertainty in the derivation of physiological properties from EC data and how should these confounding factors and uncertainties be addressed in future research (chapter 3)?

4. How can g_m be incorporated in existing LSMs without introducing artifacts, how does g_m change simulations of photosynthesis and WUE and what effects does it have on future projections of GPP and transpiration (chapter 5)?

The main part of this thesis is composed of published or submitted manuscripts as presented in chapters 2-5.

In **chapter 2**, the trend in IWUE as recently observed across temperate and boreal ecosystems with the EC method (Keenan et al., 2013) is forced in the LSM JSBACH, and the large-scale biogeochemical implications of such a potential trend are investigated. This chapter further investigates how the interpretation of trends in WUE differs across scales and across metrics.

Chapter 3 deals with the derivation of the g_1 parameter from eddy covariance measurement sites using a parsimonious, data-driven approach. The focus of this chapter lies on the characterization and quantification of methodological and observational uncertainties, which confound the derivation of g_1 from EC data and potentially compromise their interpretation. This study further addresses the question of how far and under what circumstances these uncertainties need to be considered in future studies.

Chapter 4 presents a software package that can be used to calculate ecophysiological and biometeorological ecosystem properties from EC data and concurrent meteorological measurements in a consistent and reproducible manner. The chapter presents the basic theory and extends on possible applications of the derived quantities for both single- and double-sensor (e.g. whole ecosystem and understory) sites and discusses the potential as well as the limitations of the applied "big-leaf" approach.

Chapter 5 deals with the effects of g_m on future simulations of water and carbon fluxes in the land surface model JSBACH. This chapter details the implementation and the required adjustments of the model and investigates the implications of an explicit representation of g_m for carbon and water fluxes at the leaf to the global scale.

Chapter 6 summarizes the previous chapters and gives an outlook of potential future research applications which were motivated by the results of this thesis.

2 Large-scale implications of increasing WUE

This chapter is a copy-edited version of the following published article:

[1] Department of Biogeochemical Integration, Max Planck Institute for Biogeochemistry, 07745 Jena, Germany;

[2] International Max Planck Research School for Global Biogeochemical Cycles (IMPRS-gBGC), 07745 Jena, Germany;

[3] Michael-Stifel-Center Jena for Data-Driven and Simulation Science, 07745 Jena, Germany;

[4] Hawkesbury Institute for the Environment, Western Sydney University, Richmond, NSW 2753, Australia;

[5] Remote Sensing Research Group, Department of Geodesy and Geoinformation, Technische Universität Wien, 1040 Vienna, Austria;

[6] Max Planck Institute for Meteorology, 20146 Hamburg, Germany;

[7] Department of Ecosystem Physiology, University of Freiburg, 79085 Freiburg, Germany

Summary

Ecosystem water-use efficiency (WUE) is an important metric linking the global land carbon and water cycles. Eddy covariance-based estimates of WUE in temperate/boreal forests have recently been found to show a strong and unexpected increase over the 1992–2010 period, which has been attributed to the effects of rising atmospheric CO$_2$ concentrations on plant physiology. To test this hypothesis, we forced the observed trend in the process-based land surface model JSBACH by increasing the sensitivity of stomatal conductance (g_s) to atmospheric CO$_2$ concentration. We compared the simulated continental discharge, evapotranspiration (ET), and the seasonal CO$_2$ exchange with observations across the extratropical northern hemisphere. The increased simulated WUE led to substantial changes in surface hydrology at the continental scale, including a significant decrease in ET and a significant increase in continental runoff, both of which are inconsistent with large-scale observations. The simulated seasonal amplitude of atmospheric CO$_2$ decreased over time, in contrast to the observed upward trend across ground-based measurement sites. Our results provide strong indications that the recent, large-scale WUE trend is considerably smaller than that estimated for these forest ecosystems. They emphasize the decreasing CO$_2$ sensitivity of WUE with increasing scale, which affects the physiological interpretation of changes in ecosystem WUE.

2.1 Introduction

The ongoing rise in atmospheric CO_2 concentration (c_a) affects gas exchange between the vegetation and the atmosphere. Plants respond directly to rising ca through increased net carbon assimilation (A_n) and reduced stomatal conductance (g_s) (Morison, 1987; Field et al., 1995; Ainsworth and Rogers, 2007). These fundamental physiological responses lead to increased intrinsic water-use efficiency (iWUE $= A_n/g_s$) and reduced transpiration (T) at the leaf level, with potential implications for the terrestrial hydrological cycle and global climate (Sellers et al., 1996; Betts et al., 2007; Doutriaux-Boucher et al., 2009; Andrews et al., 2011). Current theory predicts a moderate decrease in g_s as CO_2 concentrations rise, which results in an approximately proportional increase of iWUE with c_a, and a constant ratio of intercellular (c_i) to ambient CO_2 concentrations (c_i/c_a) (Ball et al., 1987; Leuning, 1995; Katul et al., 2010; Medlyn et al., 2011).

These theoretical considerations are strongly supported by multiple lines of experimental and observational evidence at the leaf, plant, and stand level. Reconstructed long-term records of c_i using tree-ring carbon isotope ($\delta^{13}C$) measurements suggest a moderate increase in iWUE of 20.5% from the 1960s to the early 2000s with a consistent response among climate zones and biomes (Peñuelas et al., 2011). The same method applied to temperate and boreal forests over the 20th century has similarly shown an approximately proportional increase of iWUE and c_a (Feng, 1999; Saurer et al., 2014; Frank et al., 2015), with some sites showing a weakened iWUE response to c_a towards the end of the 20th century (Waterhouse et al., 2004; Gagen et al., 2011). Exposing plants to elevated CO_2 concentrations yields similar physiological responses. Results from three free-air CO_2 enrichment (FACE) experiments demonstrated that C3 plants growing in CO_2-enriched air (ambient CO_2 + 200 ppm; c. 50% increase in c_a) showed concurrent significant reductions in g_s and increases in photosynthesis, which resulted in an increase of 68% in iWUE, and an unchanged c_i/c_a (Ainsworth and Long, 2005).

Intrinsic WUE is an important metric at leaf level, characterizing plant physiological properties irrespective of atmospheric water demand (Ehleringer et al., 1993). At the ecosystem level, WUE can be approximated by the ratio of gross primary production (GPP) to evapotranspiration (ET) under conditions of low nonbiotic components of the evaporation flux, such as soil or interception evaporation. As ecosystem WUE is strongly modulated by climatic factors, in particular vapor pressure deficit (VPD), an 'inherent' WUE metric (IWUE $=$ (GPP $\cdot$ VPD)/ET) was defined to facilitate the comparison of ecosystems with different atmospheric demand and to provide an approximation of iWUE at the ecosystem level (Beer et al., 2009). IWUE, as all other WUE metrics at the ecosystem level, is subject to environmental feedbacks, which tend to strengthen as scale is increased (Field et al., 1995; Wilson et al., 1999). In particular, the partial decoupling of canopies from the atmosphere makes stand transpiration become increasingly insensitive to changes in canopy conductance (G_c) (Jarvis and McNaughton, 1986), and a given decrease in (G_c) has been shown to translate into a weaker response of transpiration, even in relatively well

coupled forests (e.g. Wullschleger et al., 2002). Elevated c_a further has structural effects on plant canopies through increasing leaf area index (LAI) (Norby and Zak, 2011), which has been surmised to reduce or even offset the physiological effects of c_a on vegetation water use (Piao et al., 2007; Gerten et al., 2008). Consequently, transpiration and WUE at the ecosystem level are less responsive to changes in c_a than their leaf-level equivalents (Wilson et al., 1999; Wullschleger et al., 2002; De Kauwe et al., 2013).

Notwithstanding these expectations, a recent analysis of eddy covariance data from 21 flux tower sites across temperate and boreal forests from 1992 to 2010 (Keenan et al., 2013, henceforth 'K13') showed a strong increase in ecosystem IWUE. This study attributed the trend in IWUE to vegetation responses to rising atmospheric CO_2 concentrations, but the observed increase was substantially stronger than predicted by current theory and found by previous empirical evidence. The hypothesis put forward was that plant gas exchange is regulated in a way to keep c_i constant despite continuously increasing c_a, which suggests that the most likely underlying physiological mechanism for the IWUE trend is a strong decrease in G_c as c_a rises. This finding challenges our capability to project vegetation responses to, and its feedbacks on, future climate and environmental change.

If such a strong physiological response occurred at the continental scale, it would entail significant impacts on hydrological and biotic processes on the land surface, especially when considering the fact that 55–67% of annual land water loss in temperate and boreal forests consists of transpiration (Schlesinger and Jasechko, 2014), that is, water that enters the atmosphere through stomata. Though changes in the regional water cycle and energy budget are hard to directly link to the physiological CO_2 effect experimentally, modeling studies using terrestrial biosphere models have demonstrated that land surface processes are sensitive to changes in G_c. Simulations showed that a CO_2-induced reduction in G_c triggers a reduction in ET, and consequently increases soil moisture, and continental runoff (Gedney et al., 2006; Betts et al., 2007; Cao et al., 2010), as well as sensible heat flux and land surface temperature (Boucher et al., 2009; Andrews et al., 2011). Owing to the tight coupling of G_c and canopy photosynthesis, substantial large-scale changes in G_c are also likely to affect GPP and net biome productivity (NBP) at the regional to global scale, ecological processes which affect the concentration of atmospheric CO_2 and its seasonal amplitude (Randerson et al., 1997; Forkel et al., 2016).

Here we tested the plausibility of the strong increase in ecosystem IWUE from 1992 to 2010 as found by K13. We incorporated the assumed physiological driver of the trend, stomatal closure in response to rising atmospheric CO_2 concentrations, into the process-based terrestrial biosphere model JSBACH (Reick et al., 2013), thereby forcing the observed trend in the model. The implications of the increased IWUE trend to carbon and water cycling at the continental scale were subsequently investigated by comparing JSBACH simulations of ET, continental runoff, and the seasonal amplitude of atmospheric CO_2 across the extra-tropical northern hemisphere with observation-based ET products (Mueller et al., 2013), runoff measurements at major rivers, and observed atmospheric CO_2 concentrations across ground-based monitoring sites.

2.2 Materials and Methods

2.2.1 JSBACH model description

The JSBACH model (Reick et al., 2013; Knauer et al., 2015, version 3.10, revision 687) is the land component of the MPI Earth System Model (Giorgetta et al., 2013). Moisture, energy, and momentum fluxes between the land surface and the lower atmosphere are simulated using classical bulk transfer relations, in which aerodynamic land–atmosphere coupling is based on the Monin–Obukhov similarity theory (Roeckner et al., 2003). Simulated evapotranspiration (ET) comprises transpiration by vegetation, soil evaporation, and evaporation of intercepted water, all of which are affected by seasonally varying vegetation cover and leaf area. Soil hydrological processes are represented in a five-layer scheme (Hagemann and Stacke, 2014). Surface runoff and drainage enter a river routing scheme which simulates lateral water fluxes on the land surface (HD model) (Hagemann and Dümenil, 1998). Vegetation in the model is represented as plant functional types (PFTs), which differ in their biochemical and biophysical attributes. Radiative transfer in the canopy is based on the two-stream approximation (Sellers, 1985). C3 photosynthesis is simulated according to the model by Farquhar et al. (1980) and stomatal conductance (g_s) is calculated with the Ball–Berry equation (Ball et al., 1987):

$$g_s = g_0 + g_1 \frac{A_n \mathrm{rH}}{c_a} \tag{2.1}$$

where A_n is net assimilation (mol m^{-2} s^{-1}), rH is relative humidity (-), and c_a is atmospheric CO$_2$ concentration (mol mol^{-1}). g_0 (0.005 mol m^{-2} s^{-1}) and g_1 (9.3) are fitted parameters, which are kept constant across all C3 vegetation types and which represent the minimum stomatal conductance in darkness, and the sensitivity of g_s to A_n, respectively. Leaf-level values of A_n, g_s, and c_i are iteratively solved for three canopy layers, and scaled to their bulk canopy equivalents (GPP, G_c, C_i) with LAI.

2.2.2 Sensitivity of WUE to atmospheric CO$_2$ concentration

According to the Ball–Berry model (Eq. 2.1), iWUE (A_n/g_s) changes in proportion to c_a if rH and g_1 are assumed to remain unchanged with increasing c_a and $g_0 = 0$. In this case, a fractional change in c_a is expected to lead to the same fractional change in iWUE. This proportionality diminishes with increasing $\eta = g_0/g_s$, the fraction of g_s functionally not under guard cell control of the stomata and therefore not responding to an increase in c_a in the Ball–Berry model:

$$\frac{\mathrm{diWUE}}{\mathrm{iWUE}} = (1 - \eta) \frac{\mathrm{d}c_a}{c_a} \tag{2.2}$$

At the ecosystem level, the sensitivity of WUE to c_a diminishes further as a result of

two main factors: partial decoupling of the canopy from the atmosphere; and water fluxes other than transpiration (i.e. soil evaporation and interception). The strength of canopy–atmosphere decoupling depends on the ratio of aerodynamic conductance (G_a) to G_c, and was quantified as the dimensionless decoupling coefficient Ω (Jarvis and Mc-Naughton, 1986), which ranges from 0 (perfectly coupled) to 1 (completely decoupled):

$$\Omega = \frac{\epsilon + 1}{\epsilon + 1 + G_a/G_c} \tag{2.3}$$

where ϵ is the change of latent heat content relative to the change of sensible heat content of saturated air. An important implication of this concept is that with increasing Ω, the physiological control of transpiration by stomata is reduced:

$$\frac{\mathrm{d}T}{T} = (1 - \Omega)\frac{\mathrm{d}G_c}{G_c} \tag{2.4}$$

That means a given fractional change in G_c leads to a weaker fractional change in T, with the attenuation being determined by the value of Ω. In addition, soil evaporation and interception are not directly affected by changes in G_c. Consequently, the sensitivity of WUE to c_a decreases with increasing fraction of soil evaporation and interception on the total ecosystem water loss (ϕ). Accounting for these factors, and assuming that Ω does not affect plant carbon uptake, the relation between ecosystem WUE (GPP/ET) and c_a can be written as:

$$\frac{\mathrm{dWUE}}{\mathrm{WUE}} = (1 - \eta)(1 - \Omega)(1 - \phi)\frac{\mathrm{d}c_a}{c_a} \tag{2.5}$$

It can be seen from Eqs. 2.2 and 2.5 that WUE is not exactly proportional to an increase in c_a and that the responsiveness further decreases with increasing scale from leaf to ecosystem. Inserting typical values of η, Ω, and ϕ (see Table A1; Fig. A1) in Eq. 2.5 suggests that the sensitivity of WUE at ecosystem level is reduced compared with that at leaf level by c. 30% (Fig. A1).

2.2.3 Simulating increased stomatal sensitivity to atmospheric CO$_2$ concentration

To incorporate a stronger WUE response to c_a into the JSBACH model, we modified the Ball–Berry equation (Eq. 2.1) such that g_s shows an increased sensitivity to c_a:

$$g_s = g_0 + g_1 \frac{A_n \mathrm{rH}}{c_a} \frac{1}{\max(1, 1 + \xi((c_a - c_{a,\mathrm{base}})/c_{a,\mathrm{base}}))} \tag{2.6}$$

where ξ is a constant stomatal sensitivity factor to c_a, and $c_{a,\mathrm{base}}$ is the baseline atmospheric CO$_2$ concentration, set to the value observed in 1992 (355.37 ppm), the beginning of the eddy covariance observations analyzed by K13. This formulation translates into a stronger stomatal response to CO$_2$ if c_a exceeds $c_{a,\mathrm{base}}$, with the strength of the response determined by ξ. In this case, the following relation can be established at the ecosystem level:

$$\frac{\mathrm{dWUE}}{\mathrm{WUE}} = (1 - \eta)(1 - \Omega)(1 - \phi)\frac{\mathrm{d}\left(c_\mathrm{a} + \xi\dfrac{c_\mathrm{a}^2 - c_\mathrm{a,base}c_\mathrm{a}}{c_\mathrm{a,base}}\right)}{\left(c_\mathrm{a} + \xi\dfrac{c_\mathrm{a}^2 - c_\mathrm{a,base}c_\mathrm{a}}{c_\mathrm{a,base}}\right)} \tag{2.7}$$

The sensitivity factor ξ was estimated for each site by numerically solving Eq. 2.7 using simulated site values of η, Ω, and ϕ (see Table A1), such that dWUE/WUE corresponded to the median annual trend observed by K13 (2.3% yr^{-1}). Note that Eq. 2.6 has no purpose other than increasing the stomatal sensitivity in the model, thereby causing IWUE to rise at a similar rate as reported by K13.

2.2.4   Model setup and analysis

We conducted two main simulations: a standard run (ST) with the original Ball–Berry stomatal model (Eq. 2.1) and a CO_2-sensitive run (SE) with an increased stomatal sensitivity to c_a from 1992 onwards (Eq. 2.6). Both model versions were run at ecosystem level for eddy covariance sites within the FLUXNET network, and also globally at T63 spatial resolution (c. $1.875° \times 1.875°$). The focus of the analysis was on forested regions in the extratropical northern hemisphere during the period 1992–2010, consistent with the analysis conducted by K13.

Two different meteorological reanalysis datasets were used to force the JSBACH model – CRUNCEP v.6 (http://dods.extra.cea.fr/data/p529viov/cruncep/readme.htm) and WFDEI (Weedon et al., 2014) – which provide air temperature, precipitation, specific humidity, longwave and shortwave radiation, and surface wind speed at subdaily resolution. All forcing variables were brought to half-hourly resolution. Atmospheric CO_2 concentration was provided globally at annual resolution as specified in Le Quéré et al. (2015). Land cover was prescribed from the HYDE 3.1 historical land-cover inventory (Klein Goldewijk et al., 2011), combined with the SYNMAP vegetation map (Jung et al., 2006).

2.2.5   Site-level simulations

We performed site-level simulations at 21 FLUXNET sites to test the effects of the modified physiology on simulated IWUE. The sites correspond to those investigated by K13 and comprise deciduous broadleaf and evergreen needle-leaf forest ecosystems in the temperate and boreal zones. Site characteristics relevant for this study are listed in Table A1. We used reanalysis climate forcing rather than meteorological forcing from the towers to have continuous simulations for all sites over the entire 1992–2010 period, which was not available from the FLUXNET database. For overlapping years, the meteorology measured at the flux towers is in relatively good agreement with the one from the reanalyses (Fig. A2), but shows stronger trends in rH (Fig. A3). All climate variables were extracted from the pixel of the climate forcing fields (at original 0.5° resolution) where the respective site was located. For each meteorological data set, two runs were conducted, which served to attribute changes in IWUE to either c_a or other climate variables: all climate variables

19

held constant (i.e. an average site year with respect to precipitation, temperature, and air humidity was repeated throughout the entire simulation period) but ca allowed to vary; and all climate variables, including c_a, allowed to vary. Basic plant physiological (e.g. maximum carboxylation rate) and structural (LAI, vegetation height) attributes, as well as basic soil parameters (e.g. soil depth, particle size distribution) were adjusted to observed or estimated values for each site, if available. Mean annual summertime IWUE at site level was calculated as follows:

$$IWUE = Median \left(\frac{GPP \cdot VPD}{ET} \right) \tag{2.8}$$

where GPP (g C m^{-2} s^{-1}), ET (kg H$_2$O m^{-2} s^{-1}), and VPD (hPa) represent filtered half-hourly values in the summer months June, July, and August. Modeled data were filtered as described in K13 to exclude photosynthetically inactive time periods to avoid phenological effects as a result of possible shifts in the growing season. Days with precipitation and the following day were excluded to reduce the fraction of nontranspirational (i.e. not physiologically controlled) water fluxes on ET. Annual summertime IWUE trends were estimated with the Theil–Sen single median method.

To investigate whether the simulated IWUE trends are sensitive to the representation of canopy photosynthesis in the model, we tested two alternative model versions at site level, one in which photosynthesis is calculated separately for sunlit and shaded canopy fractions (Spitters, 1986, denoted as 'sunlit_shaded' run), and one in which photosynthesis and g_s were explicitly coupled to the energy balance ('leaf_EB' run), in contrast to the version used in this study, which assumed equal canopy surface and air temperatures.

2.2.6 Continental simulations and evaluation datasets

For the global runs, the model was brought into equilibrium with respect to its water and carbon cycle using preindustrial climate forcing, atmospheric CO$_2$ concentration, and land use. We then ran the model with a transient forcing from 1860 to 2010 and with annually updated land cover. The sensitivity factor ξ for the continental runs was set to the mean value of all sites ($\xi = 7.6$).

Simulated monthly ET was compared with the diagnostic datasets and reanalyses of the LandFlux-EVAL multi-dataset synthesis (Mueller et al., 2013), which were aggregated to the resolution of the model via conservative remapping. The analysis was restricted to regions north of 35°N and where forest cover (based on SYNMAP) exceeds 30%. Daily river discharge time series were downloaded from the Global Runoff Data Centre (GRDC; Koblenz, Germany: http://www.bafg.de/GRDC/EN/02_srvcs/21_tmsrs/ riverdischarge_node.html) and aggregated to mean annual discharges. Missing years were filled with the mean of the respective time series. Rivers with more than 3 years missing from 1992 to 2010 were discarded. Data from 42 river-gauging stations in America (21) and Eurasia (21), whose river catchments cover c. 19.8 Mio km^2, were used for the analysis (Table A2; Fig. A4).

The seasonal amplitude of atmospheric CO_2 from 1985 to 2010 was simulated using the atmospheric transport model TM3 (Rödenbeck et al., 2003) in Jacobian representation Kaminski et al., 1999. Input to the TM3 model comprises global net biome productivity (NBP) from the JSBACH simulations, fossil fuel emissions (CDIAC, Boden et al., 2013), and net ocean carbon fluxes from the Global Carbon Project (Le Quéré et al., 2015). Simulated CO_2 amplitudes were compared with estimates from flask and continuous measurements collected by various institutions (see Rödenbeck, 2005). We selected six remote measurement stations (Table A3) whose seasonal cycle is predominantly influenced by the terrestrial biosphere north of 35°N (Randerson et al., 1997). Both observed and simulated seasonal CO_2 amplitudes were calculated based on monthly averaged CO_2 time series as the difference between the maximum and the minimum atmospheric CO_2 concentrations in each calendar year, and normalized to the 1985–1991 reference period. Normalized amplitude trends and their uncertainties were calculated using linear mixed-effects models with station as random effect.

2.3 Results

2.3.1 Site-level simulations

The effects of the modified model formulation on simulated vegetation physiology, GPP, ET and WUE at site level are shown in Fig. 2.1 (for WFDEI forcing; see Fig. A5 for CRUNCEP forcing). Results from the CO_2-sensitive (SE) model formulation start to differ from those of the standard (ST) version after 1992, when c_a exceeds $c_{a,base}$ (Eq. 2.6). Between 1992 and 2010, the higher CO_2 sensitivity in the SE run induces strong stomatal closure, which is apparent in the $c.$ 53% reduction in g_s by the end of the simulation period (Fig. 2.1b). ET is reduced in parallel, but at an attenuated rate as a result of the contribution of nontranspirational water fluxes and canopy–atmosphere decoupling. The same holds true for IWUE when compared with the GPP/G_c response. In addition, C_i and GPP respond clearly to the partial stomatal closure and show a $c.$ 20% reduction in 2010 compared with the reference period. The stronger decrease in ET compared with GPP leads to a strong increase in IWUE between 1992 and 2010 at all sites. Mean IWUE in 2010 exceeded that of the reference period by 54% and 60% for WFDEI and CRUNCEP forcing, respectively. The simulated increases in IWUE over all sites (median of 2.0% yr^{-1} for WFDEI and 2.2% yr^{-1} for CRUNCEP forcing, respectively) closely approach the annual IWUE increase of 2.3% yr^{-1} as observed by K13 (Fig. 2.2).

To attribute the changes in modeled IWUE to c_a or other climate variables, the simulated IWUE trends were compared between model runs forced with constant climate (CO_2 effect) and variable climate (both CO_2 and climate effects) in the ST model version. c_a caused a relatively constant contribution of $c.$ 0.45% yr^{-1} to the IWUE trend across sites (Fig. 2.2), which agrees with the expected theoretical behavior and the formulation implemented in the model. All other climate variables reduced IWUE at some sites and enhanced it at others and thus introduced a large intersite variability to the IWUE trend (Fig. A6).
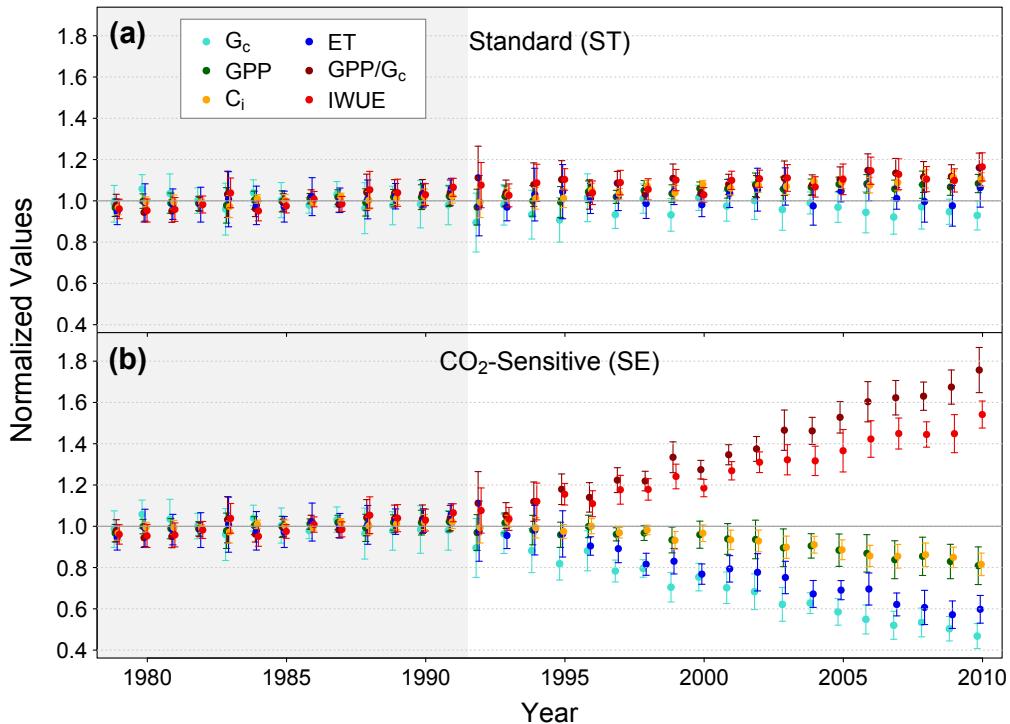
Fig. 2.1. Mean daytime summer (JJA) values ($\pm$ SD) of canopy conductance (G_c), gross primary production (GPP), intercellular CO_2 concentration (C_i), evapotranspiration (ET), GPP/G_c, and inherent water-use efficiency (IWUE = (GPP · VPD)/ET) for: (a) the standard (ST) run; and (b) the CO_2-sensitive (SE) run. All variables are normalized to the mean of the 1979–1991 period (gray shaded area). Shown are results for WFDEI climate forcing (see Fig. A5 for CRUNCEP climate forcing). Values are averaged across the 21 eddy covariance sites.

However, the median across all sites remained almost constant for both CRUNCEP and WFDEI forcing (Fig. 2.2). Compared with the ST scenario, significantly higher IWUE trends were simulated in the SE scenario for all sites. SE runs with constant climate showed a similar IWUE response to the SE runs with variable climate (Fig. 2.2). These results suggest that the simulated IWUE trend in the SE version can be primarily attributed to CO_2 effects, and not to those of other climate variables (Fig. A7).

Simulated IWUE trends at site level in both alternative model versions ('sunlit_shaded' and 'leaf_EB') were in good agreement with the ones presented here (see Figs. A8 and A9). An explicit coupling of photosynthesis and g_s to the energy balance as in the 'leaf_EB' run led to an increase in temperature and humidity at the canopy surface. However, these emerging meteorological gradients between the surface and the free air were constrained by the prescribed meteorological forcing and had little effect on the simulated IWUE trends.

2.3.2 WUE responses to atmospheric CO_2 concentration at leaf and ecosystem levels

Ecosystem WUE is less sensitive to rising c_a than its leaf-level equivalent, because factors such as nonstomatal water fluxes and aerodynamic resistance emerge at the ecosystem level that are negligible at the leaf level (Eq. 2.5). This scale dependency of the CO_2 sensitivity
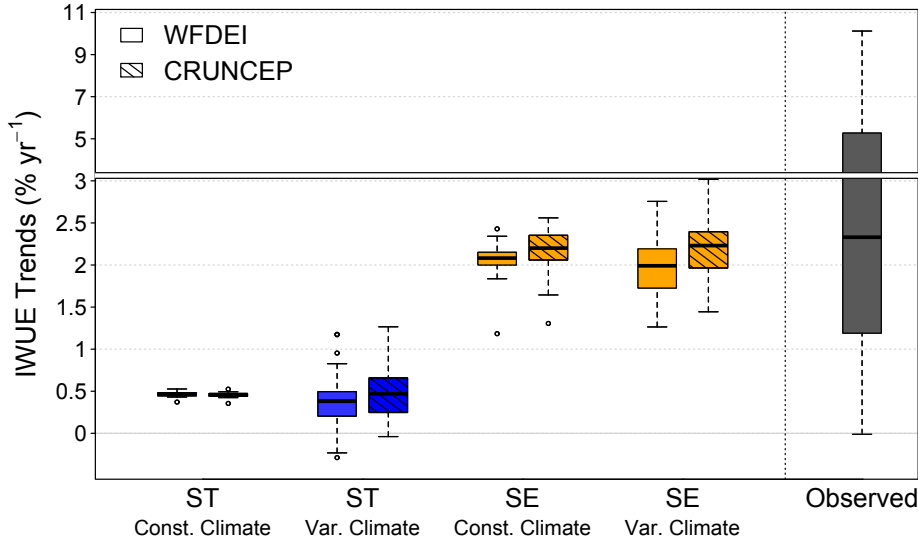
Fig. 2.2. Distribution of simulated inherent water-use efficiency (IWUE) trends (1992–2010) across all 21 flux tower sites for the standard (ST) and CO_2-sensitive (SE) runs with constant (Const.) climate, where all climate variables except atmospheric CO_2 concentrations were kept constant for an average site year, and variable (Var.) climate, where all climate variables, including atmospheric CO_2 concentrations, were allowed to vary. The boxes, bold horizontal lines, and circles indicate the interquartile ranges, medians, and data points outside 1.5 times the interquartile range, respectively. The right box depicts the corresponding observed trends reported by Keenan et al. (2013).

of WUE implies that an observed IWUE trend at ecosystem level is associated with a stronger iWUE trend at leaf level. To evaluate whether this affects the physiological interpretation of trends in ecosystem WUE, we performed idealized JSBACH simulations at the leaf and ecosystem levels using constant climate forcing to isolate the effects of increasing c_a (Fig. 2.3). The simulations at leaf and ecosystem levels were identical with respect to the calculation of photosynthesis and g_s (see section 2.2), but the ecosystem-level simulations included scale-dependent feedbacks with the physical environment that are attenuated or nonexistent in the leaf-level simulations. We evaluated two common physiological scenarios with respect to stomatal responses to a rise in c_a (Saurer et al., 2004): one in which stomatal closure leads to a constant c_i/c_a (as assumed by the Ball–Berry model), and one in which c_i remains constant over time (as proposed by K13, implying a somewhat stronger stomatal closure). Run 1 served as a reference and employed the Ball–Berry model (Eq. 2.1) with c_a as measured in 1992. According to the constant c_i/c_a scenario, the increase in c_a between 1992 and 2010 causes a slight decrease in g_s, and consequently a rise in iWUE, which is proportional to the change in c_a (run 2). Keeping c_i constant at the level of 1992 (run 3) requires an increased stomatal response to c_a which causes a larger iWUE trend between 1992 and 2010. In run 3, iWUE increases more than IWUE, which can be explained by the stronger impact of the attenuating factors (Eq. 2.5) at ecosystem level compared with leaf level. Importantly, the response associated with the constant c_i scenario is not sufficient to cause an IWUE trend in the magnitude as reported by K13 (median of 2.3 % yr^{-1}; Fig. 2.2). To obtain an IWUE response similar to the one observed

at the ecosystem level (run 4), the required physiological response at leaf level would need to involve a decrease in c_i over time.
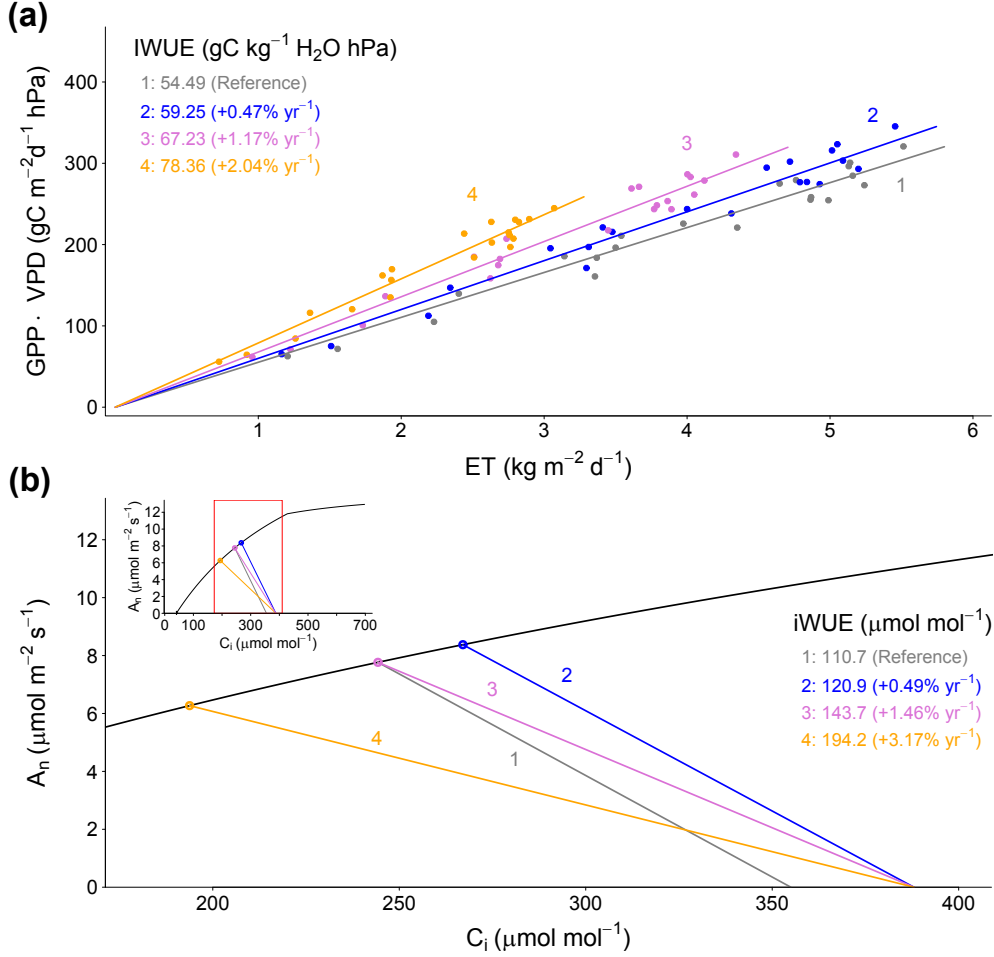
Fig. 2.3. (a) Simulated ecosystem inherent water-use efficiencies (IWUEs) and their trends for four runs differing in their stomatal response to atmospheric CO_2 concentration: (1) reference run: constant ratio of intercellular to atmospheric CO_2 concentrations (c_i/c_a) for c_a of 1992 (Ball–Berry); (2) constant c_i/c_a for ca of 2010 (Ball–Berry); (3) constant c_i; and (4) stomatal closure inducing an IWUE increase of c. 2% yr^{-1}. Numbers on the left indicate simulated IWUEs (g C kg^{-1} H_2O hPa) in 2010, and their mean annual relative trends from 1992 to 2010 (in brackets). Each point represents one site and the slopes of the lines are across-site estimates of IWUE. IWUE was simulated by the JSBACH model, forced with WFDEI reanalysis, for the 21 FLUXNET sites characterized in Table A1. Non-CO_2 climate forcing was held constant in all runs. The following model settings were used for the respective simulations: (1) standard (ST) model version with c_a of 1992; (2) ST model version with c_a of 2010; (3) CO_2-sensitive (SE) model version with a mean sensitivity factor (ξ in Eq. 2.7) of 2.85 and c_a of 2010; (4) SE model version with a mean ξ of 7.6 and c_a of 2010. (b) The corresponding behavior at leaf level, simulated as in (a) but with a stand-alone version of the coupled photosynthesis-g_s model in JSBACH (Farquhar et al., 1980; Ball et al., 1987). The slope of the line originating at the abscissa is $1/g_s$, and its intersection with the A_n/c_i curve ('operating point') gives the corresponding A_n and c_i values (Long and Bernacchi, 2003). Simulations were run with mean climate forcing from all sites (air temperature = 20.7°C, relative humidity = 52.7%, photosynthetically active photon flux density = 942 μmol m^{-2} s^{-1}) and with $V_{cmax} = 40$ μmol m^{-2} s^{-1}, $J_{max} = 76$ μmol m^{-2} s^{-1}, $g_1 = 9.3$, $g_0 = 0.005$ mol m^{-2} s^{-1} and with Rubisco kinetic parameters taken from Bernacchi et al. (2001).

2.3.3 Continental-scale implications of the observed IWUE trend

At the continental scale, the different physiological responses to c_a embedded in the ST and SE model versions are clearly reflected in ET, particularly in the summer months (Fig. 2.4a). The ST runs show a slight increase in ET across forested regions of the extratropical northern hemisphere from 1992 to 2005, which is in line with the reanalyses and the diagnostic ET products presented in Mueller et al. (2013). By contrast, the strong CO_2-induced decline in G_c in the SE scenario causes a significant decrease in ET, totaling $c.$ 1% yr^{-1}, which is not in accordance with the observation-based ET products (Fig. 2.4b). The choice of the climate forcing dataset had only minor effects on these results. The absolute mean summer values (Fig. A10a) demonstrate that simulated ET in the ST model version is underestimated compared with the data products and that their temporal dynamics are in moderate agreement (correlation coefficients (r) between 0.45 and 0.56). Although the ST and SE scenarios differ strongly, the difference between continental simulations was significantly lower than at site level as a result of the lower T/ET fraction in the absence of any data filtering, and the averaging across different vegetation types holding different aerodynamic properties.

A consequence of the modeled reduction in ET is an increase in simulated continental runoff (Fig. 2.4c,d). Across 42 river gauges (Table A2), normalized observed discharges show a slight, but not significant upward trend from 1992 to 2010. This behavior differs among rivers (Fig. A11). Simulated continental discharges in the ST versions are in agreement with the observations, but show stronger upward trends. The two SE model simulations show significantly higher discharge trends than both the ST runs and the observations (Fig. 2.4c,d). Both forcing products resulted in a good agreement of the modeled interannual variability with the observations ($r_{WFDEI} = 0.88$ and $r_{CRUNCEP} = 0.68$ for the 1992–2010 period). However, the use of WFDEI forcing yields more realistic absolute discharges (Fig. A10b) and weaker trends for the 1992–2010 time period than the CRUNCEP dataset. The strong underestimation of discharge ($c.$ 40%) in simulations forced by the CRUNCEP dataset is indicative of a negative precipitation bias in this product, probably to some extent caused by the nonapplication of a precipitation undercatch correction (e.g. Biemans et al., 2009).

The altered physiology in the SE model version had considerable implications for carbon cycling in the model. The strong stomatal closure affected vegetation carbon uptake (GPP) and NBP at large scales, which led to changes in the simulated seasonality of atmospheric CO_2 concentrations. Observations show an increase in the seasonal amplitude of atmospheric CO_2 concentrations in the northern hemisphere, corresponding to an intensified net carbon exchange across temperate and boreal terrestrial ecosystems (Graven et al., 2013; Forkel et al., 2016). The ST model runs simulated no changes to weak increases in the seasonal CO_2 amplitude at six ground-based measurement stations (Fig. 2.5). The SE runs, by contrast, showed significant decreasing trends, which are clearly unrealistic given the observations (Fig. 2.5). The progressive decrease in the CO_2 amplitude in the SE

25
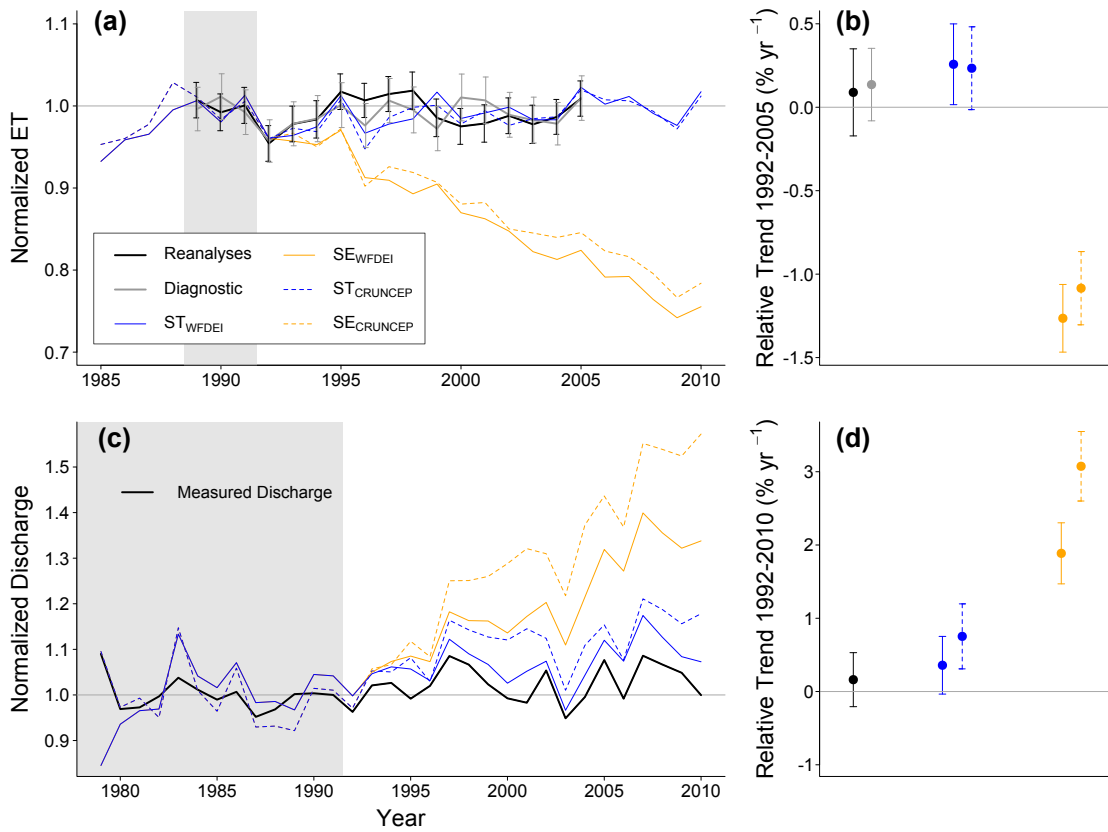
Fig. 2.4. (a) Normalized time series (gray shaded area: reference period 1989–1991) of observation-based (i.e. diagnostic and reanalysis products; see Mueller et al. (2013)) and simulated mean summer (JJA) evapotranspiration (ET). Error bars denote standard errors of the mean. (b) Confidence intervals for the trend in normalized ET from 1992 to 2005 based on ordinary least-squares (OLS) regression. (c) Normalized time series (reference period 1979–1991) of observed and simulated continental discharge, calculated as the sum of 42 individual river discharges. The location of the individual gauging stations and characteristics of the rivers are shown in Fig. A4 and Table A2, respectively. (d) Confidence intervals for the trend in normalized continental discharge from 1992 to 2010 based on OLS regression.

model version indicates a weakening of the seasonal carbon exchange in these ecosystems, which is caused by the marked decrease in GPP (Fig. A12) in response to the successively increasing stomatal limitations to photosynthesis.

To assess whether observed large-scale carbon and water fluxes are consistent with a constant C_i over time, we repeated the continental simulations using a model parameterization that yields a constant C_i at ecosystem level across FLUXNET sites (Eq. 2.6 with ξ set to 2.85). As expected, the resulting trends in ET, discharge, and atmospheric CO_2 amplitude showed an intermediate behavior between the ST and SE runs (Fig. A13). Nonetheless, this scenario is less consistent with the observations than the ST simulations, for all three observational datasets.
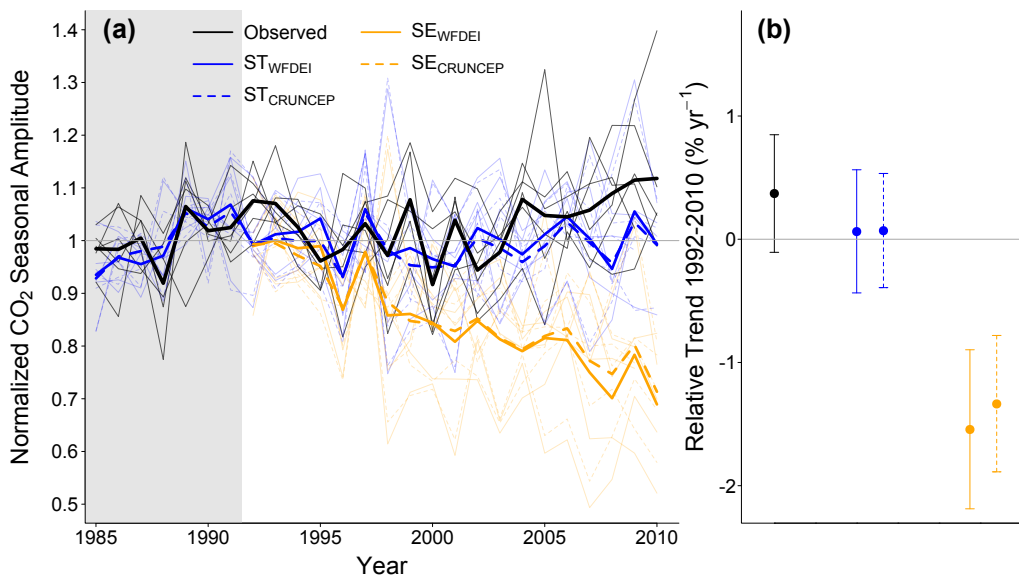
Fig. 2.5. (a) Individual (faint) and mean (bold) time series of normalized seasonal amplitudes of atmospheric CO_2 (gray shaded area: reference period), calculated as the difference between maximum and minimum CO_2 concentrations within a calendar year, based on six ground-based measurement stations (Table A3; Fig. A4). (b) Confidence intervals for the linear trends. Trends and confidence intervals were calculated using linear mixed-effects models assuming station as random effect.

2.4 Discussion

2.4.1 WUE responses to atmospheric CO_2 concentration and other factors

Rising atmospheric CO_2 concentration is expected to increase plant WUE as a result of stomatal closure, but the exact magnitude of this effect is still under debate (e.g. Saurer et al., 2004). Studies at the leaf to stand scale suggest stomatal closure commensurate with a constant c_i/c_a and iWUE at leaf level to rise in proportion to c_a ('constant c_i/c_a' scenario) (e.g. Ainsworth and Long, 2005; Frank et al., 2015). The strong iWUE trend found by K13 has been attributed to the same physiological mechanism, but their results imply a much stronger stomatal response to c_a, which, as has been argued by K13, is consistent with an invariant C_i over time. Increasing the stomatal sensitivity to c_a in the JSBACH model resulted in increases in IWUE at site level that are similar to those observed by K13 from 1992 to 2010. However, the degree of stomatal closure necessary to cause this trend led to decreasing levels of C_i, GPP, and ET, which are inconsistent with observations from the eddy covariance sites. This implies that it is unlikely that CO_2-induced stomatal closure would have been the primary driving force behind the observed IWUE trend. Our simulations support previous empirical findings of a physiological regulation towards a constant c_i/c_a as c_a increases rather than a constant c_i (Fig. A13), and suggest a constant yet moderate contribution of c_a to the increase in IWUE, accounting for approximately one-quarter of the trend found by K13.

Besides atmospheric CO_2 concentration, other abiotic and biotic factors may have contributed to the trend. Climate change, for instance, has been found to influence WUE of

27

grasslands and forests (De Boeck et al., 2006; Yu et al., 2008; Niu et al., 2011), with the sign and magnitude of the response depending on the type of ecosystem and the prevailing climatic conditions (Tian et al., 2010; Zhu et al., 2011; Zhang et al., 2014). Our model simulations at site level emphasize the strong climatic control on WUE. Climate factors other than c_a (e.g. VPD) enhanced, reduced, or, for some sites, reversed the positive effects of c_a on WUE in the ST scenario (Figs. 2.2, A7). Additionally, changing biotic factors such as LAI can involve changes in WUE (Hu et al., 2008; Zhang et al., 2014). This and other biotic (e.g. canopy height) and abiotic (e.g. surface roughness) factors show no systematic changes over the study period and thus have been excluded as drivers for the WUE trend across sites by K13. Nevertheless, variables other than ca may still have contributed to the IWUE trend nonuniformly across sites. The eddy covariance data used for the analysis by K13 might be subject to a sampling bias in space and, particularly, in time, considering that analyzed time series were as short as seven years for some sites. The magnitude of the trend found by K13 remains unexplained but might not be robust enough to draw conclusions on a 'mean' WUE response, representative across extratropical forest ecosystems, over the last two decades.

2.4.2 WUE definitions and their implications

Many different ways of calculating WUE have been proposed, depending on the scale and purpose of the investigation (see Kuglitsch et al., 2008, for an overview). For entire ecosystems, WUE is commonly defined as GPP/ET (e.g. Law et al., 2002; Ponton et al., 2006; Yu et al., 2008; Huang et al., 2015) and in some studies additional data screening is applied to ensure that ET represents mostly T (Ponton et al., 2006). However, WUE calculated in this way is strongly influenced by the effects of VPD on ET (e.g. Law et al., 2002; Ponton et al., 2006; Tang et al., 2014) with the consequence that observed dynamics in GPP/ET cannot be attributed to plant physiological function. To remove the confounding effects of VPD on WUE, an 'inherent' WUE (IWUE = (GPP · VPD)/ET) has been proposed as a proxy of iWUE at the ecosystem level (Beer et al., 2009). This formulation was adopted by subsequent studies. Recent considerations, however, have pointed out that the IWUE formulation neglects VPD effects on c_i/c_a (Zhou et al., 2014), which decreases as a result of stomatal closure in response to rising VPD (e.g. Leuning, 1995). Based on the optimality theory (Cowan and Farquhar, 1977; Lloyd and Farquhar, 1994), Zhou et al. (2014) derived a new WUE metric termed 'underlying' WUE (uWUE = GPP · $\sqrt{\text{VPD}}$/ET), which they found to better capture the GPP–ET relationship. Importantly, uWUE and IWUE predict different WUE trends depending on the concomitant change in VPD (Fig. 2.6). As most sites investigated by K13 showed an increase in VPD over time (mean over all sites $\approx$ 1.25% yr^{-1}), the magnitude of the WUE trend would probably be smaller if calculated as uWUE, the physiologically more appropriate WUE metric. Considering the large effect of the WUE metric on the calculation of WUE trends as well as the central role ascribed to VPD in future climate change (Cook et al., 2014), the choice of the WUE formulation is

key when relating changes in WUE to plant physiological behavior.
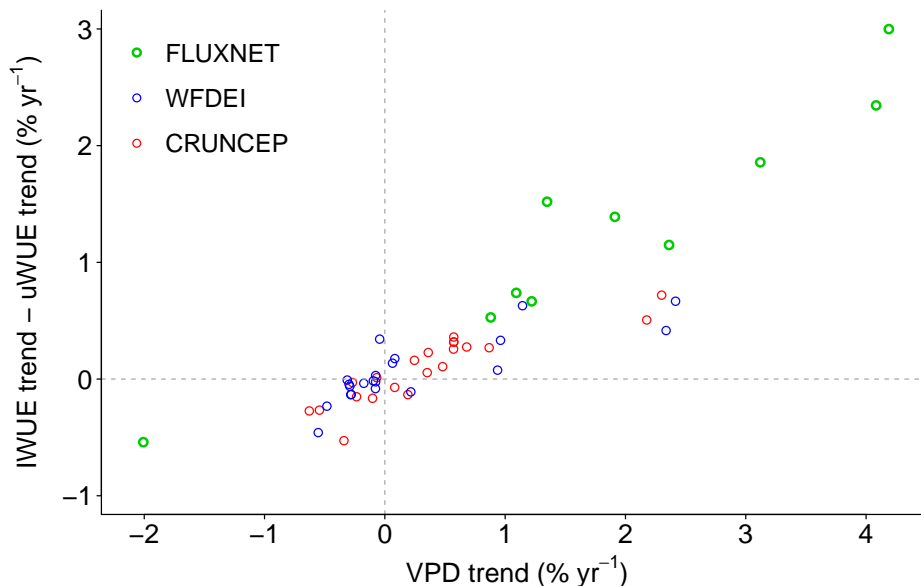
Fig. 2.6. Difference in water-use efficiency (WUE) calculated with different metrics (inherent WUE (IWUE) – underlying WUE (uWUE)) in dependence of a vapor pressure deficit (VPD) trend for observations from 10 FLUXNET sites and simulations for 21 FLUXNET sites forced with WFDEI and CRUNCEP reanalysis.

2.4.3   WUE response to atmospheric CO$_2$ concentration at leaf and ecosystem levels

Our considerations (Eqs. 2.2–2.7) suggest that the sensitivity of WUE to ca decreases with increasing scale from leaf to ecosystem, with the consequence that an observed CO$_2$ response of WUE at the ecosystem level corresponds to an even stronger physiological response within the leaves (Fig. 2.3). Thus, the required stomatal response at leaf level would have to involve a decline in c_i (Fig. 2.3), which is physiologically unlikely to happen (Saurer et al., 2004). One reason for the difference across scales is aerodynamic conductance (G_a), which, depending on vegetation type and surface roughness, can exert strong control on canopy water use. The effect of G_a was discussed extensively by Jarvis and McNaughton (1986) in their 'omega' theory, which effectively describes the sensitivity of T to changes in G_c as a consequence of canopy–atmosphere decoupling. Ω calculated from micrometeorological measurements of G_a and derived G_c in temperate forests is usually in the range of 0.2–0.3 (e.g. Magnani et al., 1998; Wullschleger et al., 2000; Wullschleger et al., 2002; Martin et al., 2001). Modeled Ω by JSBACH (Table A1) was in accordance with field studies with a daytime mean of 0.21, indicating that the strength of the canopy–atmosphere decoupling is adequately represented in the model.

Not only does T tend to get less sensitive to c_a with increasing scale, but also G_c itself has been ascribed a lower responsiveness to c_a than its leaf-level equivalent g_s. Gunderson et al. (2002) and Wullschleger et al. (2002), for instance, found that stomata at lower canopy

levels responded less to elevated ca than those in the upper canopy. In the Ball–Berry model (Eq. 2.1), as in most other state-of-the-art stomatal models (e.g. Leuning, 1995; Medlyn et al., 2011), the constant g_0 term reduces the sensitivity of g_s to c_a (Eq. 2.2) and further leads to a diminished response of G_c compared with g_s as a result of a larger g_0/g_s (η) fraction in lower canopy layers with lower photosynthetic rates. Given the firm physiological basis of g_0 and its importance for canopy transpiration (Barnard and Bauerle, 2013), its role in modeling G_c and WUE in ecosystem and land surface models deserves further investigation.

The analysis of IWUE usually relies on the assumption that ET consists almost entirely of T if an appropriate data filter is employed (see section 2.2). This a critical assumption because nontranspirational water fluxes are not directly responsive to c_a and thus reduce the sensitivity of ecosystem water loss to rising atmospheric CO_2 concentrations, regardless of the physiological state of the vegetation. Our model simulations showed a low average residual contribution of evaporation of 4% across sites, indicating that the data screening applied here is sufficient to exclude water fluxes other than transpiration. It is worth mentioning that, in the absence of any data filter, evaporation and interception comprise a much larger fraction of ET (see Schlesinger and Jasechko, 2014), which leads to a considerably lower CO_2 effect on WUE over longer timescales (e.g. annually) (e.g. Wullschleger et al., 2002; Leuzinger and Koerner, 2007), which is also apparent in our continental-scale analyses.

2.4.4   Role of stomata in the hydrological response of the land surface to rising CO_2

At the continental scale, simulated ET showed a marked reduction in response to the strong stomatal closure in the SE scenario, which is in line with previous studies that have emphasized the high sensitivity of ET to G_c even at large spatial scales (Friend and Kiang, 2005; Gedney et al., 2006). The implications of CO_2-induced stomatal closure on ET and the land surface energy budget, known as 'physiological forcing' (Betts et al., 2007) is simulated in an exaggerated manner in the SE run, but shows qualitatively the same response as previous studies (Betts et al., 2007; Boucher et al., 2009; Cao et al., 2010), including increases in continental runoff and land surface temperatures (but note Piao et al., 2007).

One consequence of the reduced ET in the SE scenario was an increase in soil water content, a major indirect ecological effect of rising c_a (e.g. Morgan et al., 2004). This effect plays only a minor role in this study as the focus was on regions where water limitation is of minor ecological importance. In water-limited regions, the simulated IWUE increase in the SE scenario is expected to be much weaker as a result of a positive feedback of increased water availability on vegetation productivity and thus ET.

In addition to its physiological effect through stomatal closure, rising c_a can affect vegetation structure through increases in biomass production and LAI (Cowling and Field, 2003).

Experimental studies have reported increases in foliage cover in response to elevated c_a except for sites where the maximum leaf area carrying capacity has already been reached (Norby and Zak, 2011). This structural CO_2 effect through increased LAI is assumed to enhance transpiration and thus counteract the physiological CO_2 effect. However, its strength is poorly constrained and so are its implications for continental runoff (Gerten et al., 2014). In simulation studies, the structural CO_2 effect was small in Betts et al. (2007), but considerable in other studies (Kergoat et al., 2002; Bounoua et al., 2010), and Piao et al. (2007) even identified an increase in runoff caused by c_a. The JSBACH model lacks a productivity–LAI feedback, which leads to an unchanged foliage cover throughout the simulation period despite clear changes in GPP. A more realistic representation of vegetation growth in the model would probably, to some extent, offset the simulated CO_2 response of both ET and GPP, leading to lower responses in continental runoff as well. In the ST runs, the simulated increase in discharge (Fig. 2.4c,d) may be partly attributed to the missing vegetation structure feedback in the model. Notwithstanding this, the trends in the SE run are strongly dominated by the pronounced simulated physiological effect (Fig. 2.2), which makes a strong compensatory effect of LAI unlikely in this model version.

Stomatal responses to atmospheric factors, including c_a and VPD, as well as the resulting ET are subject to multiple feedbacks at different scales (Field et al., 1995; Wilson et al., 1999; de Arellano et al., 2012), involving changes in the surface energy budget, temperature, convective boundary layer height, and cloud formation. The JSBACH model gives only a simplified representation of the mechanisms involved. In particular, the model was not coupled to the atmosphere, and thus any boundary layer feedbacks were precluded in the simulations. Although these additional feedbacks are assumed to stabilize the ET response at larger scales (Field et al., 1995), a coupled model run would be necessary to test this assumption and to obtain a more complete representation of land–atmosphere interactions.

2.4.5 Does the observed ecosystem IWUE trend occur throughout the northern hemisphere?

The response of the terrestrial hydrological and carbon cycles to rising atmospheric CO_2 concentrations and their feedbacks on the climate system are key issues in climate change research (Gerten et al., 2014). This work supports the majority of previous studies reporting moderate physiological responses of g_s and WUE to c_a at the plant scale compared with the recent suggestions by K13. The sensitivity of the total land–atmosphere water flux to the rise in c_a is further attenuated with increasing scale as a result of feedbacks with the physical environment. The combined implications of these two aspects are reflected in our results, which indicate that the magnitude of the ecosystem IWUE trend as reported by K13 is not in accordance with observed large-scale trends in continental discharge, ET, and the seasonal CO_2 exchange in temperate and boreal regions of the northern hemisphere over the 1992–2010 time period (Figs. 2.4, 2.5). The simulations demonstrate that changes in ecosystem IWUE in the magnitude as found by K13 would result, if they occurred at

31

the continental scale, in altered carbon and water fluxes at the land surface that would be clearly detectable in signals responding to biogeochemical changes in the terrestrial biosphere. We thus conclude that the magnitude of the IWUE trend observed at temperate and boreal forest ecosystems is not a large-scale phenomenon.

Acknowledgments

3 Sources of uncertainties in deriving iWUE metrics from EC data

Jürgen Knauer[1,2,3], Sönke Zaehle[1,4], Belinda E. Medlyn[3], Markus Reichstein[1,4], Christopher A. Williams[5], Mirco Migliavacca[1], Martin G. De Kauwe[6,7], Christiane Werner[8], Claudia Keitel[9], Pasi Kolari[10], Jean-Marc Limousin[11], and Maj-Lena Linderson[12] (2018). **Towards physiologically meaningful water-use efficiency estimates from eddy covariance data.** *Global Change Biology* 24, 694-710. doi: 10.1111/gcb.13893.

[1] Department of Biogeochemical Integration, Max Planck Institute for Biogeochemistry, Jena, Germany;

[2] International Max Planck Research School for Global Biogeochemical Cycles (IMPRSgBGC), Jena, Germany;

[3] Hawkesbury Institute for the Environment, Western Sydney University, Richmond, NSW, Australia;

[4] Michael-Stifel-Center Jena for Data-Driven and Simulation Science, Jena, Germany;

[5] Graduate School of Geography, Clark University, Worcester, MA, USA;

[6] Department of Biological Science, Macquarie University, North Ryde, NSW, Australia;

[7] ARC Centre of Excellence for Climate Extremes, University of New South Wales, Sydney, NSW, Australia;

[8] Department of Ecosystem Physiology, University of Freiburg, Freiburg, Germany;

[9] School of Life and Environmental Science, University of Sydney, Brownlow Hill, NSW, Australia;

[10] Department of Physics, University of Helsinki, Helsinki, Finland;

[11] Centre d'Ecologie Fonctionnelle et Evolutive, Université de Montpellier, Montpellier, France;

[12] Department of Physical Geography and Ecosystem Science, Lund University, Lund, Sweden

Abstract

Intrinsic water-use efficiency (iWUE) characterizes the physiological control on the simultaneous exchange of water and carbon dioxide in terrestrial ecosystems. Knowledge of iWUE is commonly gained from leaf-level gas exchange measurements, which are inevitably restricted in their spatial and temporal coverage. Flux measurements based on the eddy covariance (EC) technique can overcome these limitations, as they provide continuous and long-term records of carbon and water fluxes at the ecosystem scale. However, vegetation gas exchange parameters derived from EC data are subject to scale-dependent and method-specific uncertainties that compromise their ecophysiological interpretation as well as their comparability among ecosystems and across spatial scales. Here, we use estimates of canopy conductance and gross primary productivity (GPP) derived from EC data to calculate a measure of iWUE (G_1, "stomatal slope") at the ecosystem level at six

sites comprising tropical, Mediterranean, temperate, and boreal forests. We assess the following six mechanisms potentially causing discrepancies between leaf and ecosystem-level estimates of G_1: (i) non-transpirational water fluxes; (ii) aerodynamic conductance; (iii) meteorological deviations between measurement height and canopy surface; (iv) energy balance non-closure; (v) uncertainties in net ecosystem exchange partitioning; and (vi) physiological within-canopy gradients. Our results demonstrate that an unclosed energy balance caused the largest uncertainties, in particular if it was associated with erroneous latent heat flux estimates. The effect of aerodynamic conductance on G_1 was sufficiently captured with a simple representation. G_1 was found to be less sensitive to meteorological deviations between canopy surface and measurement height and, given that data are appropriately filtered, to non-transpirational water fluxes. Uncertainties in the derived GPP and physiological within-canopy gradients and their implications for parameter estimates at leaf and ecosystem level are discussed. Our results highlight the importance of adequately considering the sources of uncertainty outlined here when EC-derived water-use efficiency is interpreted in an ecophysiological context.

3.1 Introduction

Water-use efficiency (WUE) is an important vegetation property which characterizes the coupling of the water and carbon cycles at the leaf to global scales (Beer et al., 2009; Denmead et al., 1993; Farquhar et al., 1989; Ito and Inatomi, 2012). Understanding the physiological mechanisms that modulate WUE and being able to predict its future behavior in a changing environment is a fundamental challenge. Since the common formulation for WUE — the ratio of carbon gain to water loss — is affected by both physiological and environmental factors, alternative WUE metrics are useful that aim to extract the biological component of WUE. Such metrics have the advantage of being readily comparable across atmospheric conditions and across sites, and their dynamics can be more directly linked to the underlying physiological mechanisms. For example, many authors replace actual WUE (net photosynthesis (A_n)/transpiration) with the intrinsic WUE (iWUE = A_n/stomatal conductance (g_s)) (Osmond et al., 1980; Schulze and Hall, 1982). However, iWUE is still indirectly dependent on environmental conditions, particularly vapor pressure deficit (VPD) and atmospheric CO_2 concentration (c_a). A metric that accounts for variations in these conditions is the "stomatal slope" or "slope coefficient" ("g_1" of the optimal stomatal model derived by Medlyn et al. (2011)). This parameter is inversely related to the marginal carbon cost of water to the plant and is calculated as the slope of the relationship between g_s and A_n, normalized for VPD and CO_2 concentration (Medlyn et al., 2011). g_1 is inversely related to intrinsic water-use efficiency (iWUE), and higher values of g_1 are associated with higher intercellular CO_2 concentrations (c_i). By accounting for confounding atmospheric factors, g_1 has been shown to provide valuable insights into the ecophysiological functioning of vegetation and its water-use strategy. It could, for instance, be related to wood density, which is a proxy for various plant hydraulic traits (Lin et al., 2015). g_1 is further, and

in its original meaning, the key model parameter in stomatal conductance formulations embedded in ecosystem and Earth system models (Ball et al., 1987; Leuning, 1995; Medlyn et al., 2011). Thus, knowledge on the variation of g_1 with climate and vegetation types is essential for understanding and modeling the physiological basis of present and future terrestrial water–carbon relations.

Values of g_1 are usually inferred from gas exchange measurements on individual leaves using transparent or lighted chambers. These instruments determine A_n and g_s from gas concentration changes within the chamber and provide simultaneous measurements of CO_2 concentration and humidity at the leaf surface, information from which g_1 can be readily inferred. One advantage of this measurement setup is that it provides conditions in which feedbacks with the physical environment (e.g., leaf boundary layer conductance) are largely controlled; thus, the information gained can be considered as purely physiological — though pitfalls exist (see Long and Bernacchi, 2003). One disadvantage of the method is that it is laborious and time-consuming, with the consequence that measurements are often restricted to a few days and to a small selection of leaves, usually located at the top of the canopy. As a consequence, leaf gas exchange measurements and resulting g1 estimates are prone to spatial and temporal sampling biases.

Inferring g1 from gas exchange measurements at the ecosystem scale with the eddy covariance (EC) technique (e.g. Aubinet et al., 1999) offers the potential to circumvent these biases. This method overcomes the main limitations of leaf-level data as it provides non-invasive, continuous, and long-term measurements of carbon, water, and energy fluxes that integrate an entire ecosystem. In principle, g_1 can be estimated from EC data in the same manner as at the leaf level if A_n and g_s are replaced by their ecosystem-level analogs and meteorological conditions at the leaf level with those measured at the flux tower (Medlyn et al., 2017). Ecosystem-integrated g_s, i.e., canopy conductance (G_c), is commonly derived as surface conductance (G_s) from the inverted Penman–Monteith (PM) equation, and ecosystem net photosynthesis can be approximated by gross primary productivity (GPP) as derived from measured net ecosystem exchange (NEE) of CO_2. G_1 (capital letters denote ecosystem-level quantities in this study) at ecosystem level constitutes a WUE-related ecosystem functional property according to Reichstein et al. (2014) and has the advantage of representing a spatial and temporal integration of vegetation gas exchange, which supposedly yields more robust and representative WUE characteristics of an ecosystem than leaf gas exchange data. This aspect is especially relevant when the vegetation is of complex vertical structure or composed of multiple species with different physiological traits, in which case it is challenging to adequately represent the entire vegetation community with point measurements.

One challenge associated with EC data is that the measured fluxes are affected by physical feedback mechanisms that hinder conclusions about the underlying physiological mechanisms, an aspect that is generally of increasing importance when the scale of measurement is increased, e.g., from leaf to ecosystem (Anderson et al., 2003; Jarvis and McNaughton, 1986; Knauer et al., 2017). With the fluxes and meteorological variables measured a few

meters above the canopy, an additional aerodynamic conductance (G_a) term has to be considered. Further, the EC system is unable to distinguish purely physical (i.e., evaporation) from physiologically controlled (i.e., transpiration) water fluxes. EC data are also subject to method-specific measurement errors and uncertainties. In particular, the measured energy fluxes often do not close the energy balance (Leuning et al., 2012; Wilson et al., 2002a), and the partitioning of NEE into its component fluxes involves considerable uncertainties (Desai et al., 2008; Reichstein et al., 2005; Wehr et al., 2016). In addition, possible within-canopy gradients of g_1 cannot be directly resolved with EC measurements alone.

These aspects are especially relevant in the context of a recent study that found discrepancies between leaf- and EC-based estimates of g_1 and its patterns across vegetation types (Medlyn et al., 2017). These mismatches are unlikely to result from inadequate scaling procedures of WUE from leaf to ecosystem (Launiainen et al., 2011; Linderson et al., 2012), but might in large parts be caused by methodological uncertainties in the EC data and conceptual differences between the two data sources. Thus, identifying and quantifying the potential effects of these uncertainties will be a crucial first step to reconcile estimates across scales and enable a consistent use of the two data sources in modeling and observational studies.

Here, we analyze the sensitivity of G_1 to the factors outlined above at six forest ecosystems and compare it to leaf-level g_1 estimates at the same location. The objective of this study is to quantify the effects of confounding nonphysiological factors on ecosystem-level G_1, with the ultimate goal of deriving a physiologically meaningful WUE parameter from EC measurements that is analogous to leaf-level estimates. Such information can be used to (i) parameterize and evaluate large-scale models, (ii) obtain a characterization of ecosystem-level iWUE that is readily comparable across locations differing in their environmental conditions, and (iii) compare estimated vegetation gas exchange parameters across scales.

3.2 Materials and Methods

3.2.1 Leaf-level estimates of g_1

Gas exchange measurements at leaf level are taken from previous studies (Table 3.1) and are in parts also included in the database compiled by Lin et al. (2015). Data are publicly available under `https://bitbucket.org/gsglobal/leafgasexchange`. Measurements were made with standard instruments mostly at the top third of the canopy for the dominant species at the site. For the analysis, the unified stomatal optimization model (Medlyn et al., 2011) was used:

$$g_s = g_0 + 1.6 \left(1 + \frac{g_1}{\sqrt{D_s}}\right) \frac{A_n}{c_s} \tag{3.1}$$

where g_0 is the minimum stomatal conductance (mol m^{-2} s^{-1}), g_1 is the stomatal slope parameter (kPa$^{0.5}$), and A_n is net photosynthesis (mol m^{-2} s^{-1}). D_s is the vapor pressure

deficit (kPa), and c_s is the CO_2 concentration (ppm), both at the leaf surface. g_1 was estimated from Eq. 3.1 using nonlinear, iteratively reweighted least squares based on the R package robustbase (Maechler et al., 2016). As in Lin et al. (2015), g_0 was set to 0 for the entire analysis, as (i) the physiological meaning of a statistically fitted g_0 is unclear (e.g. Barnard and Bauerle, 2013), and (ii) g_0 correlates with g_1, thus simultaneous estimation of both parameters would hamper the comparison of g_1 across datasets and sites.

3.2.2 Ecosystem-level estimates of surface conductance and G_1

We analyzed EC data from six flux tower sites within the FLUXNET network, where colocated leaf-level measurements were available (Table 3.1). The EC data were taken from the FLUXNET2015 dataset (`http://fluxnet.fluxdata.org/data/fluxnet2015-dataset/`; accessed on 04.07.2016) and are at half-hourly or hourly resolution. The sites comprise one evergreen needle-leaf forest (FI-Hyy), two deciduous broadleaf forests (DK-Sor, US-Ha1), two evergreen broadleaf forests (AU-Tum, FR-Pue), and one evergreen tropical forest (GF-Guy). Flux data underwent standard processing, including friction velocity (u_*) filtering (Papale et al., 2006), gap filling, and flux partitioning (Reichstein et al., 2005). Only measured flux data were used.

Eddy covariance measurements were analyzed within a "big-leaf" model framework, in which vegetation is represented as a uniform, single plane, acting as the only flux source and sink in the ecosystem (e.g. Raupach and Finnigan, 1988). For the purpose of this study, a data-oriented, top-down approach based on the big-leaf framework was preferred over more detailed representations of the ecosystem, such as two-layer (vegetation–soil, (e.g. Shuttleworth and Wallace, 1985) or dual-source models (sun–shade, (e.g. De Pury and Farquhar, 1997)) as these representations would require additional parameterization that cannot be obtained from single-level flux measurements. Bulk surface conductance (G_s, m s^{-1}) was calculated from the inverted Penman–Monteith (PM) equation (Monteith, 1965):

$$G_s = \frac{\lambda E G_a \gamma}{s(R_n - G - S) + \rho c_p G_a D_a - \lambda E(s + \gamma)} \tag{3.2}$$

where λE is the latent heat flux (W m^{-2}), G_a is the bulk aerodynamic conductance for water vapor (m s^{-1}), γ is the psychrometric constant (Pa K^{-1}), s is the slope of the saturation vapor pressure curve (Pa K^{-1}), R_n is the net radiation (W m^{-2}), G is the ground heat flux (W m^{-2}), S is the sum of all energy storage fluxes (W m^{-2}), ρ is the air density (kg m^{-3}), c_p is the heat capacity of dry air (J kg^{-1} K^{-1}), and D_a is the air vapor pressure deficit (Pa). For some sites, G was measured with heat flux plates, whereas measurements of S were not available and set to 0 for all sites. The PM equation was applied at the half-hourly or hourly timescale, thereby accounting for sub-diurnal variations in meteorological drivers. The approach is further based on similar assumptions as the EC technique (see, e.g., van Dijk et al., 2015, and references therein). G_s subsumes canopy conductance (G_c), as well as conductances from the soil and water intercepted by

Table 3.1. Characteristics of eddy covariance sites and colocated leaf-level measurements used in this chapter.

Site	Climate[a]	Forest type	Max. LAI	Canopy height (m)	Reference EC site	Leaf-level g_1 (kPa$^{0.5}$)	Species sampled	Reference leaf-level data
AU-Tum	Cfb	Broadleaf evergreen	2.4	40	Leuning et al. (2005)	3.7	Eucalyptus delegatensis	Medlyn et al. (2007)
DK-Sor	Cfb	Broadleaf deciduous	4.5	25	Pilegaard et al. (2011)	4	Fagus sylvatica	Linderson et al. (2012)
FI-Hyy	Dfc	Needle-leaf evergreen	3.3	14	Vesala et al. (2005)	1.8	Pinus sylvestris	Kolari et al. (2007)
FR-Pue	Csa	Broadleaf evergreen	3.3	5.5	Rambal et al. (2003)	1.6	Quercus ilex	Martin-StPaul et al. (2012)
GF-Guy	Af	Tropical evergreen	7.0[b]	35	Bonal et al. (2008)	4.4	77 species	unpublished
US-Ha1	Dfb	Broadleaf deciduous	4.9	23	Urbanski et al. (2007)	4.9	Acer rubrum, Betula alleghaniensis, Betula papyrifera, Quercus rubra	Bassow and Bazzaz (1997)

[a] Koeppen-Geiger climate classification (Af = equatorial, rainforest; Cfb = humid, warm temperate, warm summer; Csa = summer dry, warm temperate, hot summer; Dfb = cold, humid, warm summer; Dfc = cold, humid, cold summer)

[b] Plant area index

38

the canopy. Consequently, G_s is only a physiologically meaningful quantity ($G_s \approx G_c$) in time periods when vegetation is active, and the vegetation and soil surfaces are not wet. To ensure this to be the case, precipitation events, as well as the subsequent 48 hours, were excluded, and the analysis was restricted to daylight conditions (PPFD > 200 µmol m^{-2} s^{-1}) and to time periods within the growing season. Data were considered to be in the growing season when smoothed (15-day moving average) daily GPP exceeded half of the 95th percentile of all daily GPP values in a year (e.g., Fig. B1). Further filtering criteria included the following: air temperature >5°C, relative humidity <95%, $\lambda E > 0$ W m^{-2}, and (R_n - G) > 0 W m^{-2}. A site- and year-specific u_* threshold, as provided by the FLUXNET2015 dataset, was applied. Atmospheric CO_2 data were processed as described in Medlyn et al. (2017). Analysis steps performed in this study are available in the language R under `https://bitbucket.org/juergenknauer/g1_leaf_ecosystem`.

Ecosystem-level G_1 was calculated in the same manner as at the leaf level (Eq. 3.1) but with g_s and A_n replaced by G_s and GPP (representing carboxylation minus photorespiration), respectively (Eq. 3.3, data shown in Figs. B2 and B3). Further, D_s and c_s were replaced by the respective measurements (D_a and C_a) at the flux tower:

$$G_s = G_0 + 1.6 \left(1 + \frac{G_1}{\sqrt{D_a}} \right) \frac{\text{GPP}}{C_a} \tag{3.3}$$

G_1 in Eq. 3.3 was determined on an annual basis using the same nonlinear regression method as for the determination of g_1 at leaf level.

3.2.3   Factors affecting G_1 estimates

Non-transpirational water fluxes

G_s as calculated from Eq. 3.2 is affected by both transpiration and solely physically driven water fluxes (i.e., bare soil and interception evaporation); thus, G_c and G_1 are expected to be increasingly overestimated with increasing contribution of non-transpirational water fluxes to ET (Paw U and Meyers, 1989). To analyze the sensitivity of G_1 to these contributions, we calculated G_1 for successively increasing time periods following a rainfall event. Time after rainfall is considered as an inverse proxy for the contribution of physical water fluxes to ET, which have been observed to decrease exponentially with time after rainfall (e.g. Kelliher et al., 1998), but not in all ecosystems (e.g. Dubbert et al., 2014). Since dew evaporation is, unlike soil and interception evaporation, not necessarily excluded by the rainfall filter, we additionally tested the effect of a simple dew evaporation filter on estimated annual values of G_1. The dew filter was applied if the likelihood of dew evaporation was high, which was considered the case if relative humidity exceeded 95% and the radiation balance turned negative ($R_n < 0$ W m^{-2}) at night. If these conditions were met, the PPFD threshold was raised to 600 µmol m^{-2} s^{-1} in the following morning.

Aerodynamic conductance

The bulk aerodynamic conductance for water vapor (G_a) between the evaporating surface and the measurement height of the flux is an integral part of the PM equation (Eq. 3.2). G_a can be conceptualized as the inverse of two resistances in series: $G_a = 1/R_a = (R_{am} + R_b)^{-1}$, where R_{am} is the turbulent aerodynamic resistance for momentum, and R_b is the (bulk) canopy boundary layer resistance or "excess resistance" (Verma, 1989).

We tested the effect of calculating G_a in Eq. 3.2 using three different approaches of increasing complexity:

1. G_a set to infinity, corresponding to the assumption that the ecosystem is aerodynamically fully coupled to the atmosphere:

$$G_{a,\text{fcoupled}} = \infty \tag{3.4}$$

2. G_a calculated from wind speed u (m s^{-1}) and friction velocity u_* (m s^{-1}) under the assumption of a logarithmic wind profile above the canopy. R_b follows an empirical dependence on u_* according to Thom (1972):

$$1/G_{a,\text{empGb}} = \frac{u}{u_*^2} + 6.2u_*^{0.67} \tag{3.5}$$

Note that the first term of Eq. 3.5 implicitly accounts for the effects of atmospheric stability on G_a.

3. As Eq. 3.5 but with the empirical R_b model replaced by a physically based formulation according to Su et al. (2001), a simplification of the model developed by Massman (1999):

$$1/G_{a,\text{physGb}} = \frac{u}{u_*^2} + \frac{\dfrac{kC_d}{4C_t\dfrac{u_*}{u(z_h)}}f_c^2 + kB_s^{-1}(1 - f_c)^2}{ku_*} \tag{3.6}$$

where $k = 0.41$ is the von Kármán constant, C_d is a foliage drag coefficient, assumed constant with a value of 0.2 (Massman, 1999), C_t is the heat transfer coefficient of the leaf, f_c is fractional canopy cover, $u(z_h)$ is wind speed at canopy height (m s^{-1}), and B_s^{-1} is the inverse Stanton number for bare soil surface. C_t depends primarily on the leaf characteristic dimension D_l (m; values are taken from the literature, Table B1), and f_c was estimated from LAI (for further details, see chapter B).

To test the sensitivity of G_1 to different formulations of G_a, G_s (Eq. 3.2) and G_1 (Eq. 3.3) were calculated with G_a given by Eqs. 3.4–3.6. Throughout the following analysis, $G_{a,\text{empGb}}$ (Eq. 3.5) was used.

Meteorological deviations between measurement height and canopy surface

A finite G_a causes the meteorological conditions at the canopy surface to differ from those measured a certain distance above the canopy (e.g. Grantz and Meinzer, 1990). These deviations are important to consider since the conditions at the canopy surface are physiologically more relevant than those in the air above the canopy. Obtaining representative measurements of canopy surface micrometeorology is challenging, but surface temperature and humidity can be readily inferred from the inverted bulk transfer equations of sensible and latent heat if an estimate of G_a is available. Aerodynamic canopy surface temperature (T_0) is then given by:

$$T_0 = T_a + \frac{H}{\rho G_a c_p} \tag{3.7}$$

where T_a is air temperature (°C) measured at sensor height, and H is sensible heat flux (W m^{-2}). Vapor pressure at the canopy surface e_0 (Pa) is given by:

$$e_0 = e_a + \frac{\lambda E \gamma}{\rho G_a c_p} \tag{3.8}$$

where e_a is air vapor pressure (Pa). VPD at the canopy surface (D_0) is given by Eqs. 3.7 and 3.8:

$$D_0 = E_{sat}(T_0) - e_0 \tag{3.9}$$

where $E_{sat}(T_0)$ is the saturation vapor pressure at temperature T_0. Likewise, CO_2 concentration at the canopy surface (C_0) can be approximated by:

$$C_0 = C_a + \frac{\text{NEE}}{G_a} \tag{3.10}$$

where G_a is for CO_2 and in mol m^{-2} s^{-1}.
G_1 (Eq. 3.3) was recalculated with D_a and C_a at measurement height replaced by their equivalents at the canopy surface (D_0 and C_0, respectively), as given by Eqs. 3.9 and 3.10. Note that the calculated G_s (Eq. 3.2) remains unchanged as the PM equation already accounts for meteorological deviations between the surface and measurement height.

Energy balance closure

The PM equation that is inverted to estimate G_s (Eq. 3.2) in this study assumes that the energy balance at the land surface is closed, i.e.:

$$A = R_n - G - S = \lambda E + H \tag{3.11}$$

where A is the available energy, R_n is the net radiation, G is the ground heat flux, S is the sum of all ecosystem storage terms (see e.g. Leuning et al., 2012), λE is the latent heat flux, and H is the sensible heat flux (all in W m^{-2}). A common issue observed for EC data

is that the energy balance is not closed, as the turbulent fluxes (right part of Eq. 3.11) typically do not sum up to the available energy. We tested the sensitivity of an unclosed energy balance to estimates of G_s derived from the PM equation and the corresponding G_1 considering three hypothetical extreme cases which differ with respect to the attribution of the residual of the energy balance closure (residual $= A - (H + \lambda E)$):

1. All error in H (denoted as $G_{s,H}$; $G_{1,H}$): Both A and λE are assumed to be correctly measured, and the residual is entirely ascribed to H. This case is implied by the PM equation (Eq. 3.2).

2. All error in λE ($G_{s,\lambda E}$; $G_{1,\lambda E}$): Both A and H are assumed to be correctly measured, and the residual is entirely ascribed to λE, i.e., λE is recalculated as $\lambda E = A - H$.

3. All error in A ($G_{s,A}$; $G_{1,A}$): The turbulent fluxes H and λE are assumed to be correctly measured, and the energy imbalance is caused by an overestimation of A as a result of missing or inappropriate measurements of G and/or the components of S (i.e. $A = \lambda E + H$).

For comparison, G_s was additionally calculated using λE adjusted according to the Bowen ratio method (Twine et al., 2000), which assumes that the residual of the energy balance is attributed to H and λE according to the Bowen ratio ($H/\lambda E$; see `http://fluxnet.fluxdata.org/data/fluxnet2015-dataset/data-processing/` for details on the calculation). Note that this approach, in contrast to the three cases considered above, does not force the energy balance to be closed at the sub-diurnal timescale.

The degree of the energy balance non-closure was quantified as the energy balance ratio (EBR):

$$\text{EBR} = \frac{\sum(\lambda E + H)}{\sum(R_n - G - S)} \tag{3.12}$$

where the individual energy balance components are either half-hourly/hourly values or summed up over a specified time period.

NEE partitioning

The eddy covariance technique measures the NEE of CO_2 between the ecosystem and the atmosphere, but not its component fluxes GPP and ecosystem respiration (R_{eco}), which have to be estimated using flux partitioning algorithms. These algorithms, described below, can be classified into two main approaches: one that extrapolates nighttime NEE data to daytime, and one that fits light response curves to daytime NEE measurements. We calculate G_1 (Eq. 3.3) using GPP derived from both approaches to assess the uncertainty in G_1 arising from uncertainties in the GPP estimates. The nighttime data-based approach (Reichstein et al., 2005) (denoted as GPP_{nt}; $G_{1,nt}$) relies on the use of a temperature response function fitted to nighttime NEE ($= R_{eco}$), which is then extrapolated to daytime conditions. The temperature response function (based on air temperature Lloyd and

Farquhar, 1994) considers a time-varying base respiration, which implicitly accounts for additional environmental factors affecting R_{eco}. The daytime data-based approach (Lasslop et al., 2010) (GPP_{dt}; $G_{1,\text{dt}}$) fits a hyperbolic light response curve to daytime NEE. The function additionally accounts for temperature effects on R_{eco} and for VPD effects on GPP. We compared values of $G_{1,\text{nt}}$ and $G_{1,\text{dt}}$.

Within-canopy gradients

Gradients of g_1 within the canopy cannot be directly inferred from eddy covariance data. Instead, the g_1 gradients were assessed with an integrative approach using both the EC data and a simple canopy model. The model simulates radiative transfer separately for sunlit and shaded fractions of the canopy (Spitters, 1986), which is separated into three vertical layers. Stomatal conductance and photosynthesis are modeled according to Eq. 3.1 (Medlyn et al., 2011) and Farquhar et al. (1980) for each layer and are upscaled to the canopy level with the leaf area index (LAI). The model simulations were used to calculate the relative contribution of G_{c} from each layer to the total G_{c}. This fraction was considered as a proxy of the fraction of the G_1 signal coming from a certain layer (e.g., if G_{c} of the lowest layer contributed 20% to the total G_{c}, its contribution to the derived G_1 value was also assumed 20%). The EC data were then binned according to the relative contribution of G_{c}, and G_1 was estimated for each bin using Eq. 3.3. Thus, the sun–shade radiation model served only to estimate the relative contribution of each canopy layer to G_{c}, whereas G_1 was directly estimated from the EC data and not from the modeled fluxes. Conditions where λE exceeded A were excluded. A random forest model (see chapter B) was used to explain the response of G_1 to the contribution of the respective canopy layer as well as other variables. Subsequently, the marginal effect of the contribution of the respective layer on G_1 was calculated, and a linear regression model was fitted to the resulting partial dependence function. An extrapolation of this linear regression fit to 1 gave an estimate of the corresponding G_1 value of the layer. The estimated within-canopy gradients were then compared to the estimated g_1 from leaf-level measurements made at different levels in the canopy for the sites DK-Sor and US-Ha1.

3.3 Results

Fig. 3.1 shows time series of G_1 for the EC sites considered in this study as well as available leaf-level estimates of g_1 collected at the same location. The two estimates show a relatively good agreement for AU-Tum, but different magnitudes at the other sites, where both lower (GF-Guy, US-Ha1) and higher (FI-Hyy, FR-Pue) estimates were estimated from EC data. Ecosystem-level G_1 values were robust against alternative data filters with respect to the applied growing season and radiation thresholds (Fig. B4), but showed high interannual variability which could not be attributed to a single cause. In the following sections, we present the potential effects of different factors possibly contributing to the mismatch between the estimates from the two different data sources.
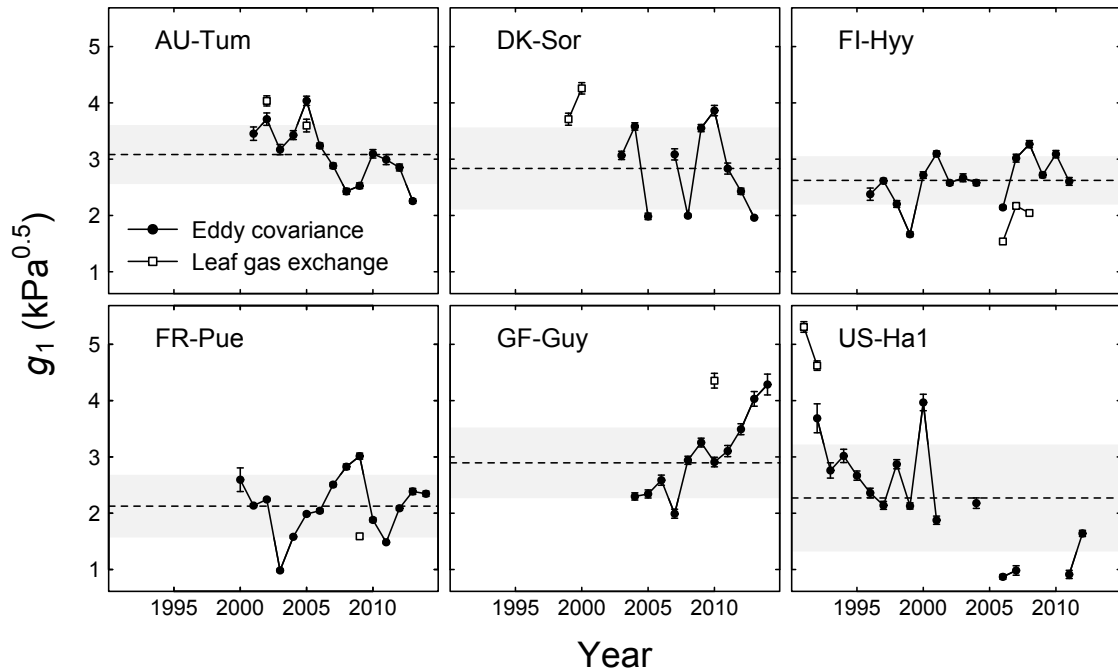
Fig. 3.1. Time series of annual estimates of G_1 from eddy covariance (EC) data (filled circles) and g_1 from leaf gas exchange data taken at the top third of the canopy (open squares). For the EC data, G_1 was calculated using the following settings: 48 hours after rainfall removed, G_a calculated from Eq. 3.5 ($G_{a,empGb}$), surface conditions, and $G_{1,H}$. Error bars indicate standard errors, dashed lines the mean across all years, and gray shaded areas the standard deviation of all annual G_1 values

3.3.1 Non-transpirational water fluxes

G_1 calculated with successively longer time periods after the last rainfall event removed (Fig. 3.2) showed the steepest decrease in the first hours after rain followed by a more moderate decline for all sites except US-Ha1. This pattern is likely to reflect the decreasing fraction of soil and interception evaporation on ET with time after rainfall, which is associated with a decrease of nonphysiological contributions to the inferred G_s (Eq. 3.2). Similar effects are expected from dew evaporation. However, the removal of time periods that are likely to be affected by dew evaporation did not result in noticeable changes in the G_1 estimates (Fig. B5). The calculated G_1 still shows a significant decrease after 3 days for some sites (e.g. 9% for FR-Pue, 19% for DK-Sor), which suggests a significant contribution of sustained soil evaporation. However, there is no clear relationship between the sensitivity of G_1 to the excluded time period after rainfall events and the LAI of the ecosystem, which indicates that the ongoing decline in G_1 is not driven solely by soil evaporation. Data several days after the last rainfall might, in addition, be affected by the onset of drought stress, albeit the most severe drought conditions are filtered out by the GPP-based growing season filter (Fig. B1).

44
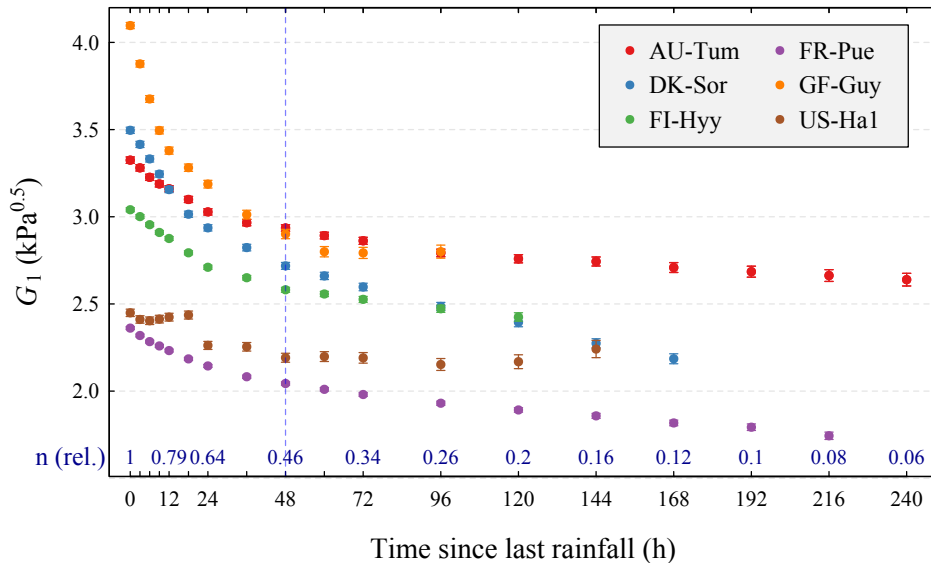
Fig. 3.2. G_1 calculated excluding successively longer time periods after the last rainfall event removed (time since rainfall is considered as a proxy for the contribution of physical evaporation on ET). G_1 is only shown if the number of data exceeds 10% of all filtered data. n (rel.) denotes the relative amount of remaining data compared to no filter applied. The dashed blue line indicates the rainfall filter as applied in this study (48 hours). Error bars indicate standard errors.

3.3.2 Aerodynamic conductance

The different G_a formulations (Eqs. 3.4–3.6; Fig. B6) inserted into the inverted PM equation (Eq. 3.2) resulted in similar G_1 estimates, except for the formulation where G_a was assumed infinite ($G_{a,fcoupled}$; Eq. 3.4) (Fig. 3.3). The fully coupled assumption significantly overestimates G_s (Fig. B7a) and consequently G_1 (Fig. 3.3a) for all site years. Compared to the reference formulation ($G_{a,empGb}$; Eq. 3.5), the overestimation of G_1 resulting from neglecting G_a varied between 17% and 80% (site averages; mean of 50% over all site years) and depended not only on the magnitude of G_a but also on the evaporative fraction ($\lambda E/R_n$; Fig. B8) (Raupach and Finnigan, 1988). The $G_{a,physGb}$ model gave similar results for G_1 than the simpler $G_{a,empGb}$ formulation. The two estimates did not differ by more than 10% for 90% of all site years. Differences between $G_{a,empGb}$ and $G_{a,physGb}$ resulted solely from the boundary layer part (R_b, second term in Eqs. 3.5 and 3.6), which depends only on u_* in the empirical formulation ($G_{a,empGb}$), whereas it is affected by various additional aerodynamic properties in the physically based model $G_{a,physGb}$. In both formulations, R_b accounts for one-third to more than one half of the total aerodynamic resistance (Table B1). The $G_{a,physGb}$ model tends to predict lower G_a for broad-leaved vegetation (e.g. DK-Sor, GF-Guy) which reflects the formation of a thicker boundary layer around larger leaves (Fig. B6). The strong dependence of G_a on the leaf characteristic dimension (D_l) in this formulation (see Eqs. B.7 and B.8) is associated with large uncertainties in G_a that propagate to G_s (Fig. B7b) and G_1. Assuming a standard deviation of 25% of the average D_l resulted in uncertainties in G_1 that mostly encompassed the G_1 values calculated using the empirical $G_{a,empGb}$ formulation (Fig. 3.3b).

45
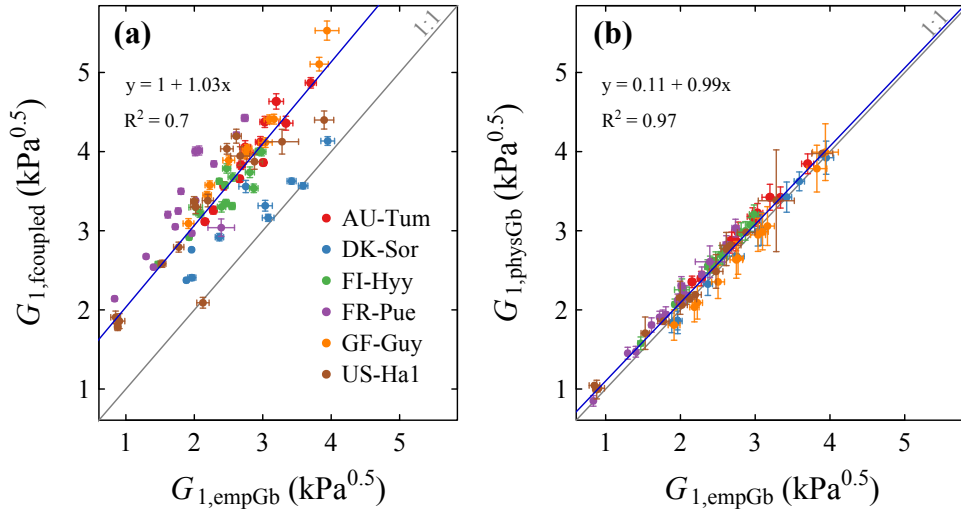
Fig. 3.3. Mean annual G_1 estimated (Eq. 3.3) with different calculation methods of aerodynamic conductance (G_a) used for the calculation of surface conductance (G_s; Eq. 3.2). Estimated G_1 using G_a estimated from wind speed and friction velocity and an empirical canopy boundary layer conductance (G_b) model ($G_{a,empGb}$; Eq. 3.5) is compared to (a) the fully coupled case ($G_{a,fcoupled}$; Eq. 3.4) and (b) a physically based G_b formulation ($G_{a,physGb}$; Eq. 3.6). Blue lines indicate reduced major axis (RMA) regression fits. Error bars indicate standard errors.

3.3.3 Surface conditions

The inferred canopy surface conditions from the inverted bulk transfer equations for λE and H (Eqs. 3.7–3.9 using $G_{a,empGb}$ (Eq. 3.5) indicate that the canopy surface is in most conditions warmer (median $c.2°C$) and more humid (median $c.$ 0.1 kPa) than the air at measurement height (Fig. B9a,b). The temperature effect on VPD through an increase in E_{sat} was stronger than the effect of an increase in humidity, resulting in a mostly higher VPD (median $c.$ 0.1–0.2 kPa) at the vegetation surface compared to the air above ($D_0 > D_a$; Figs. 3.4a and B9c). Based on the theory elaborated by Jarvis and McNaughton (1986), Magnani et al. (1998) have shown that the difference between D_0 and D_a can be expressed as a rather complex function of the relative importance of imposed and equilibrium ET, the degree of canopy-atmosphere decoupling, and G_c. In general, the deviations are expected to be large when the degree of decoupling is high, G_c is low, and the difference of equilibrium and imposed ET is large (Magnani et al., 1998). The predominantly high deviations found for FR-Pue, for instance, can be linked to the low G_c relative to the other sites. The inferred molar concentration of CO_2 at the canopy surface (C_0) was lower than that in the air (C_a) as a consequence of vegetation uptake. The effect varied among sites depending on GPP and G_a (Eq. 3.10), and typically ranged between 0 and 15 ppm.

The estimated G_1 using C_0 (Eq. 3.3) was only marginally lower than the original estimate using C_a (2%–4%; Fig. 3.4c). Replacing D_a in Eq. 3.3 with D_0 had the opposite effect and led to slightly higher G_1 estimates, but the effect was again small (5% − 15%). Owing to their minor and opposite effects on G_1, the substitution of both D_a and C_a with their

analogs at the canopy surface D_0 and C_0 in Eq. 3.3 resulted in marginal increases in G_1 (2%–13%; Fig. 3.4c).
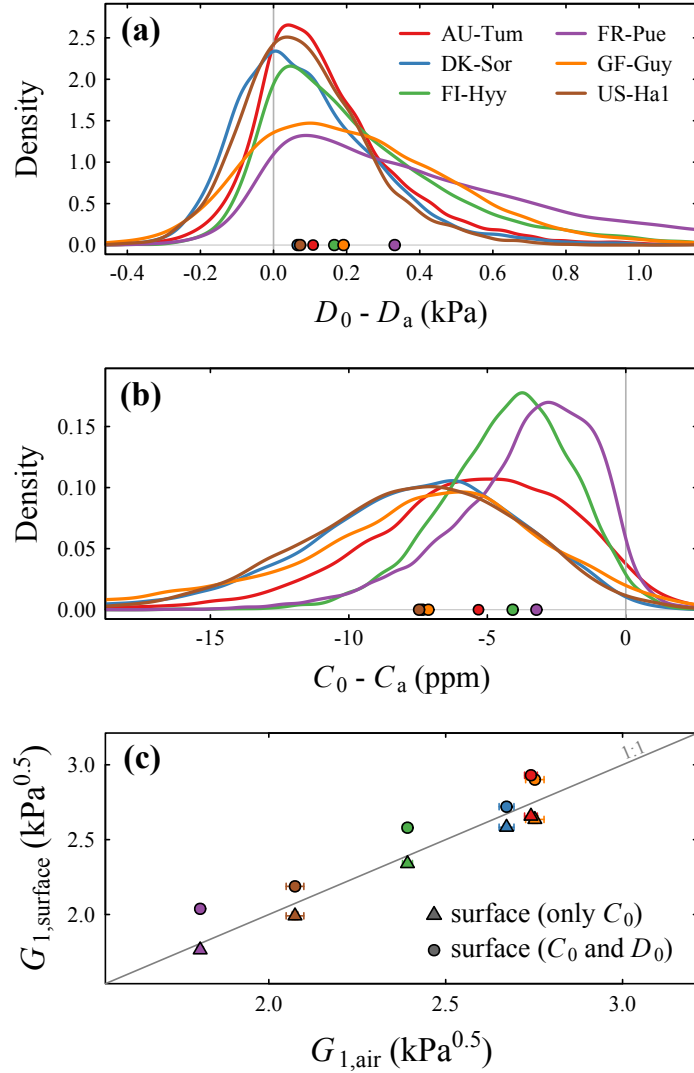
Fig. 3.4. Difference between inferred canopy surface conditions and measurements above the canopy for (a) vapor pressure deficit (D) and (b) CO_2 concentration (C), as well as (c) the resulting effects on G_1. Canopy surface D (D_0) was calculated from the inverted bulk transfer relations of latent and sensible heat flux (Eqs. 3.7–3.9), and the CO_2 concentration at the canopy surface (C_0) was calculated from measured net ecosystem exchange (Eq. 3.10). For all calculations, G_a from Eq. 3.5 was used. The filled circles in (a) and (b) indicate the medians of the distribution functions. G_1 in (c) represents the site mean over all available years (error bars indicate standard errors)

3.3.4 Energy balance

Fig. 3.5a–c depicts mean diurnal courses of the measured energy balance components for the three sites FI-Hyy, AU-Tum, and FR-Pue. The available energy A, represented by $A = R_n - G$ (black line), almost always exceeds the sum of the turbulent energy fluxes ($H + \lambda E$; green line), indicating a non-closed energy balance. The degree of closure of the energy balance was represented by the energy balance ratio (EBR, Eq. 3.12; orange line).

The deviation from a closed energy balance (i.e., the difference between A and $H + \lambda E$ or the residual of the energy balance closure, respectively) varied among sites. The mean EBR amounts to 0.83, 0.85, and 0.68 for FI-Hyy, AU-Tum, and FR-Pue, respectively, and is thus in the range of previously reported average values for the FLUXNET network (Stoy et al., 2013; Wilson et al., 2002a). The diurnal course of the EBR changed markedly throughout the day for all sites but in a different manner. FI-Hyy and AU-Tum showed a consistent increase in the EBR from the morning to the evening with the energy balance being closed in the late afternoon and evening hours (EBR $\sim$ 1). This pattern is characteristic for FLUXNET sites (Wilson et al., 2002a). FRPue, in contrast, showed the opposite pattern and a mostly decreasing EBR throughout the day.

The fact that the EBR is smaller than 1 for most conditions has consequences for G_s inferred from the inverted PM equation (Eq. 3.2), as this equation was derived under the assumption of a closed energy balance. The error associated with the inferred G_s depends on which components of the surface energy balance (Eq. 3.11) are inadequately measured or (not) accounted for. Assigning the residual entirely to either H, λE, or A served to assess the maximum uncertainty in G_s arising from a non-closed energy balance. The assumption that the energy balance non-closure is completely a result of an underestimate of H ("all error in H" case), as implicitly assumed by the PM equation, consistently led to the lowest G_s values in case of an EBR < 1. Assigning the residual energy entirely to A by recalculating it as $A = H + \lambda E$ gives slightly higher estimates compared to the first case. By contrast, assuming that all the error is in λE (i.e. λE recalculated as $\lambda E = A - H$) yields significantly higher G_s estimates, reaching more than 100% overestimation compared to the reference case (all error in H) for all three sites. The difference between the G_s estimates from the three cases scales with the EBR. These three G_s estimates are identical if EBR $= 1$ and deviate for both lower and higher EBR values. The "Bowen ratio adjusted" case shows intermediate G_s values for most conditions but it may give higher G_s and G_1 values as the "all error in λE" case, as it does not force the energy balance to be closed on the sub-diurnal timescale. Importantly, diurnal variations in the EBR as found for all three sites affect the temporal behavior of G_s throughout the day (Fig. 3.5d–f).

The uncertainty in G_s due to the non-closure of the energy balance propagates to the uncertainty in G_1, which shows a similar behavior as G_s and the highest values if the residual is attributed to λE (Fig. 3.5g–i). G_1 shows an even higher sensitivity to the EBR. This can be explained by the fact that the estimated G_1, in addition to G_s, responds to VPD and C_a, whose diurnal courses amplify the response of G_1 to the EBR (Eq. 3.3). Importantly, not only the magnitude of G_1 but also its diurnal course is affected. For instance, G_1 at FI-Hyy and AU-Tum show a steady decrease if the residual is assigned to λE, but constant or slightly increasing values through most parts of the day if it is assigned to H or A (Fig. 3.5g,h).
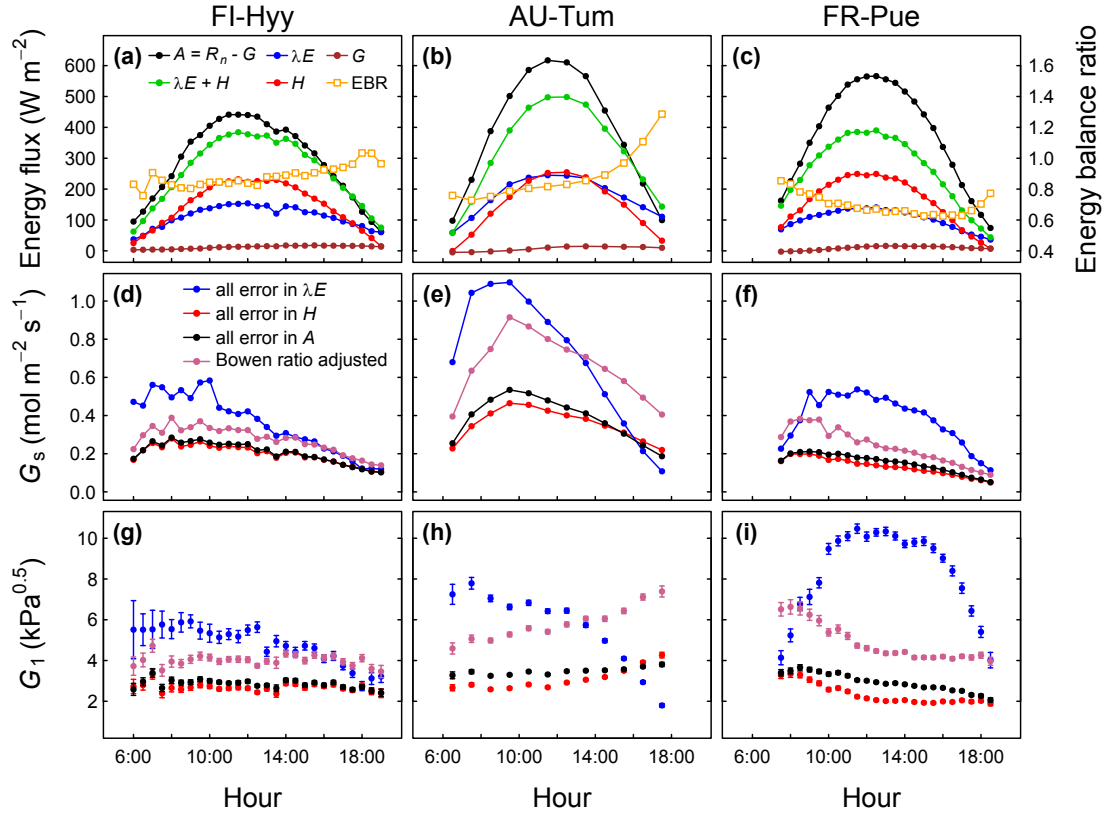
Fig. 3.5. Mean diurnal courses (over all available site years) of (a–c) energy balance components and the energy balance ratio (EBR), (d–f) surface conductance (G_s), and (g–i) the corresponding G_1 for the sites FI-Hyy, AU-Tum, and FR-Pue. G_s was calculated from Eq. 3.2 for three hypothetical extreme cases with respect to the attribution of the residual of the energy balance closure to either H, λE, or A, as well as for the Bowen ratio adjusted case. G_1 was estimated for all data in the respective half-hourly/hourly bin (Eq. 3.3). Error bars indicate standard errors

The sensitivity of G_s to an unclosed energy balance as quantified by the EBR (Eq. 3.12) is illustrated in Fig. 3.6. There is a high variability of the half-hourly EBR at each site, though most of the data are characterized by an EBR between 0.5 and 1.2, depending on the time of day (Fig. 3.5a–c) and most likely other conditions (e.g., turbulence intensity, Wilson et al., 2002a; Leuning et al., 2012). The y-axis shows the ratio of the two most extreme estimates of G_s, which are given by $G_{s,\lambda E}$ (i.e., G_s calculated from Eq. 3.2 assuming that the residual is entirely attributed to λE, i.e., $\lambda E = R_n(-G) - H$) and $G_{s,H}$ (i.e., assuming that the residual is entirely attributed to H). $G_{s,\lambda E}$ and $G_{s,H}$ are identical in case of a closed energy balance and yield the highest and lowest G_s estimates if the EBR < 1 and vice versa if the EBR > 1. Any deviation in the EBR from 1 (positive or negative) causes the ratio of the two extreme estimates of G_s to change exponentially with the EBR. The sensitivity of $G_{s,\lambda E}/G_{s,H}$ to the EBR is similar for all sites (fitted lines in Fig. 3.6b) and varies only slightly with VPD and other variables (results not shown). A typical value of $G_{s,\lambda E}/G_{s,H}$ is *c.* 2 for sites with an average EBR of *c.* 0.8 (as, for example, in FI-Hyy) and exceeds 3 for sites with a poor energy balance closure (as, e.g., FR-Pue). It has to be noted that the ratio $G_{s,\lambda E}/G_{s,H}$ represents the maximum uncertainty in G_s. This uncertainty is

considerably lower if the residual is to large parts the result of an overestimation of A. The "true" G_s and G_1 will most likely not reach the two extreme cases $G_{s,\lambda E}$ and $G_{s,H}$, but lie somewhere in between. Their exact values can only be determined if the values of A, λE, and H are correctly known.
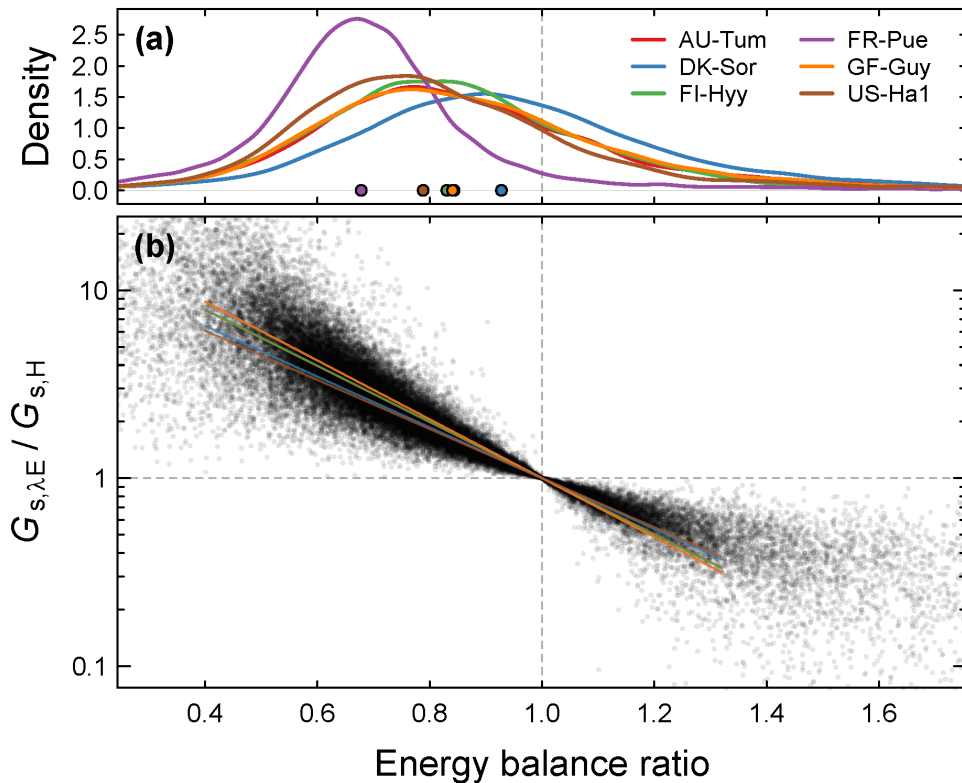
Fig. 3.6. (a) Distribution of the halfhourly/hourly energy balance ratio (Eq. 3.12) and (b) the maximum uncertainty in G_s (derived from the Penman–Monteith equation) resulting from an unclosed energy balance. The points in (a) indicate the median of the energy balance ratio. $G_{s,\lambda E}$ and $G_{s,H}$ in (b) are calculated from Eq. 3.2 with $\lambda E = R_n - G - H$ (or $\lambda E = R_n - H$ if G is unavailable) and λE as measured from the eddy covariance data, respectively. Lines in (b) are fitted with weighted least squares regression.

3.3.5 NEE partitioning algorithm

The two algorithms ("daytime" (dt) and "nighttime" (nt)) that were used to partition NEE into its component fluxes GPP and R_{eco} yielded similar average GPP values for the filtered daytime data within the growing season ($R^2 = 0.97$; Fig. 3.7a). Depending on the year, the nighttime method gave either higher or lower GPP estimates than the daytime method. Over all years, there was no consistent difference between the two methods across sites, but the nighttime approach tended to estimate higher GPP averages than the daytime method (Fig. 3.7a). The patterns in GPP are clearly reflected in the G_1 values calculated using the two different GPP versions (Fig. 3.7b). Higher estimates in GPP generally result in lower estimates of G_1 and vice versa. G_1 was further found to be relatively sensitive to GPP. On average, a change in GPP of 1 µmol m^{-2} s^{-1} led to a change of 0.2 kPa$^{0.5}$ in G_1 across sites (Fig. B10).

50
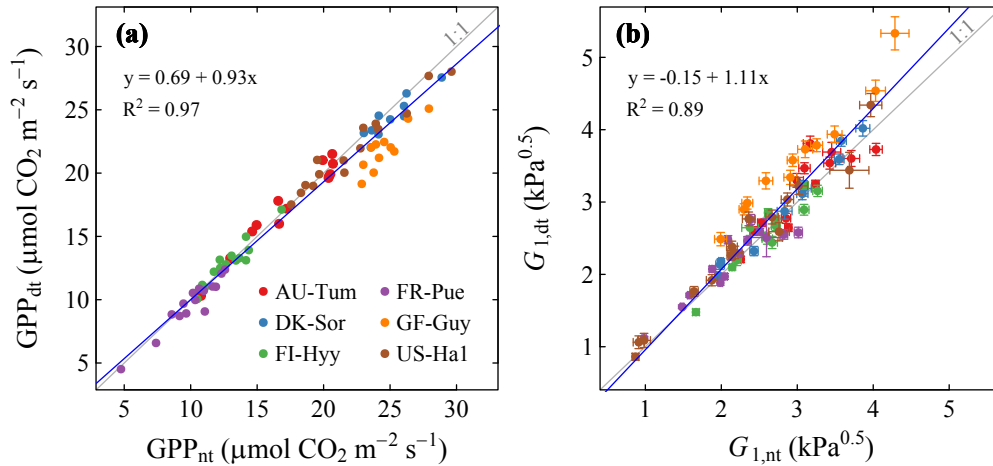
Fig. 3.7. Estimates of (a) mean growing season gross primary productivity (GPP) and (b) G_1 (Eq. 3.3) with GPP derived from a daytime (dt; Lasslop et al., 2010) and nighttime (nt; Reichstein et al., 2005) partitioning approach of net ecosystem exchange (NEE). Data are filtered as described in Materials and methods. Blue lines indicate reduced major axis (RMA) regression fits.

3.3.6 Within-canopy gradients

The partial dependence plots in Fig. 3.8 display the marginal effects of the relative contributions of the top and bottom layer ($G_{c,layer}/G_{c,total}$; x-axis) on the ecosystem-level G_1 as estimated from the EC data (y-axis). All subplots (except Fig. 3.8d (FR-Pue)) indicate that the contribution of the bottom layer G_c to the total G_c (black lines) increases along with the estimated G_1. In other words, under conditions when a comparatively large proportion of the G_1 signal comes from the lowest 1/3 of the canopy, G_1 as estimated from the EC data (Eq. 3.3) tends to be higher than when the lowest layer's contribution is small. As expected, the pattern is reverted for the contribution of the top layer (blue lines), in which case an increase in the relative contribution of the top layer is associated with a decrease in G_1. The two marginal effects are consistent across sites in that they imply higher G_1 values at the canopy bottom compared to the top, a behavior that is present at all sites except FR-Pue. An estimate of the within-canopy gradient was further made by fitting a linear model to the partial dependence plots, and extrapolating the fitted line to 1, the hypothetical value at which the entire G_1 signal comes from the respective layer (dots in Fig. 3.8). The ratio of the two values (representing the G_1 value of the bottom and top layer, respectively) is then an indication of the gradient within the canopy (denoted as "Ratio" in Fig. 3.8). The gradients differed from site to site. We found a moderately high correlation ($r = 0.76$) between the implied gradients and the degree of aerodynamic vegetation-atmosphere decoupling (results not shown). This may be an indication that relatively poorly coupled forests with tall and dense canopies (e.g., GF-Guy) are associated with higher within-canopy gradients. However, the low number of sites included in this study did not allow to investigate this aspect in more detail. The approach is further strongly affected by the effects of the energy balance non-closure on G_1, which are exceptionally critical for half-hourly/hourly data as used here (see Fig. 3.5).

51

At leaf level, g_1 estimates from different levels in the canopy did not indicate gradients at DK-Sor and US-Ha1 (insets in Fig. 3.8b,f). It is important to note that G_1 gradients within the canopy can result from vertical gradients within plants of the same species or physiological differences between overstory and understory vegetation, information that can only be resolved with a more detailed knowledge on the vegetation at the site.
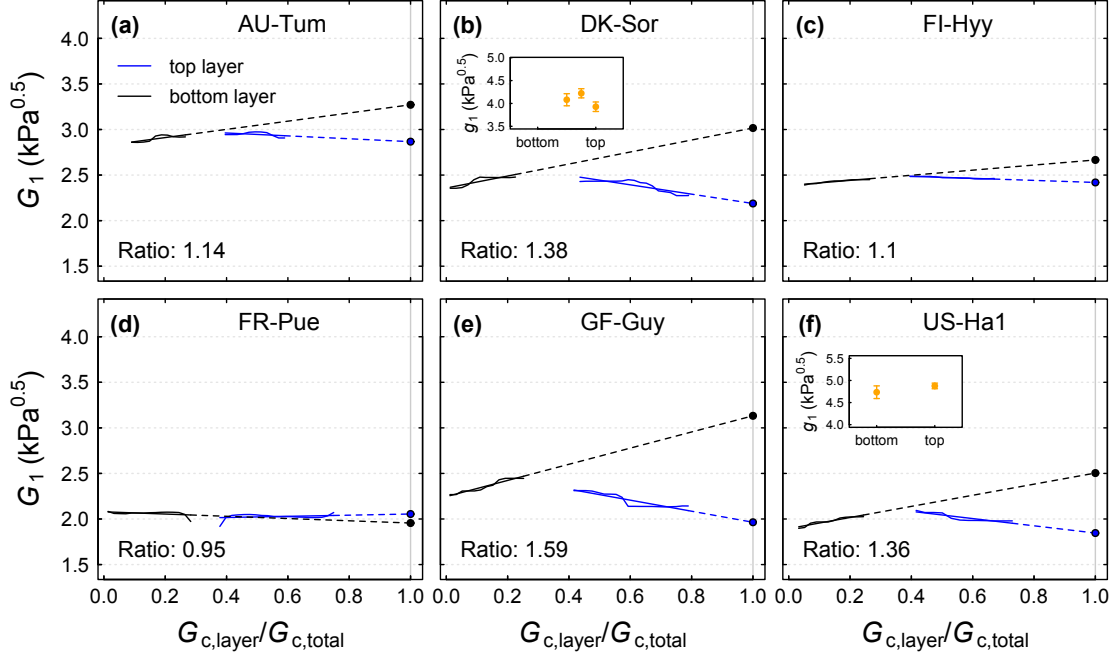
Fig. 3.8. Partial dependence plots (solid lines) of the contribution of the top (blue line) and bottom layer (black line) (approximated as $G_{c,layer}/G_{c,total}$) on the estimated G_1 (Eq. 3.3). The straight lines represent the ordinary least squares fit to the partial dependences (solid) and their extrapolation to 1 (dashed). The ratio of the extrapolated values at 1 (i.e., $G_{1,bottom}/G_{1,top}$) is indicated at the bottom left of each panel. Conditions where $\lambda E > A$ were excluded. Insets show g_1 estimates from available leaf gas exchange data at different positions in the canopy

3.4 Discussion

In this study, we show that values of G_c and the intrinsic WUE metric G_1 inferred from EC data are affected by confounding physical factors and methodological uncertainties (Table 3.2). We demonstrated that factors that are often overlooked in an ecophysiological context (e.g., energy balance non-closure, aerodynamic conductance) can be more critical for the accurate estimation of WUE than factors which are more commonly acknowledged (e.g., NEE partitioning algorithm, soil evaporation). The fact that observed discrepancies between the two data sources (Fig. 3.1) could not be fully resolved may be attributed to the low level of scientific understanding (and corresponding high uncertainty) of the factors considered here (Table 3.2), or to issues of representativeness in the sense that species contributing to the ecosystem fluxes are not sampled in the same proportion at the leaf level (Table 3.1).

Table 3.2. Effects of the factors investigated in this study on the derived ecosystem-level intrinsic water-use efficiency measure G_1 and their uncertainties

Factor	Impact on G_1		Uncertainty of the effect
1) Interception and soil evaporation	Medium	$-$ 10 - 50%	Medium - High
2) Aerodynamic conductance	Medium - High	$-$ 10 - 70%	Low
3) Meteorological gradients canopy-air	Low	$+$ 0 - 15%	Medium
4) Energy balance non-closure	High	$+$ 0 - 400%	High
5) NEE partitioning	Low	$+/-$ 0 - 20%	Medium
6) Within-canopy gradients in g_1 [a]	Low	$-$ 0 - 20%	High

[a] Numbers refer to the canopy-integrated estimate of G_1 relative to g_1 from the top third of the canopy only (as measured by leaf gas exchange).

3.4.1 Non-transpirational water fluxes

The physiological interpretation of G_s is compromised if measured λE comprises substantial non-transpirational contributions from the soil or canopy interception, in which case $G_s \gg G_c$ (Kelliher et al., 1995; Paw U and Meyers, 1989). The effects of non-transpirational λE on G_s can be assessed by either extrapolating G_s from dry periods to rainfall periods (e.g. Knohl and Buchmann, 2005), or by excluding time periods following rainfall events, as was done here. Our results (Fig. 3.2) underline the need to exclude time periods following precipitation in order to avoid an overestimation of G_c and thus G_1. An additional exclusion of time periods affected by dew evaporation was found not to be necessary for the sites studied here, possibly because the overall contribution of dew to the total evapotranspiration is minor (see e.g. Jacobs et al., 2006), or because the radiation threshold used here (200 µmol m^{-2} s^{-1}) was sufficient to exclude major dew evaporation fluxes. Our Results confirm previous approaches in which the excluded time period is restricted to 2 days after rainfall (e.g. Beer et al., 2009; Ponton et al., 2006), a practical approach with regard to the tradeoff between physiologically meaningful G_s estimates and a sufficient amount of data.

3.4.2 Aerodynamic conductance and surface conditions

The effect of G_a on G_1 was found to be important for all ecosystems investigated here and is likely to be especially important for short-statured (poorly coupled) vegetation. Fig. 3.3a demonstrates that the occasionally made assumption of a full aerodynamic coupling between the vegetation and the atmosphere (e.g. Beer et al., 2009; Groenendijk et al., 2011; Keenan et al., 2013) is, even for comparatively well coupled forests, not justified.
A simple estimate of G_a (Eq. 3.5 or similar) is often embedded in the PM equation (e.g. Blanken and Black, 2004; Launiainen et al., 2016). This formulation only requires measurements of wind speed and u_* and gives values similar to more complex approaches (Fig. 3.3b).
A major difficulty in the derivation of G_a at ecosystem level is the canopy boundary layer

conductance (G_b) (e.g. Verhoef et al., 1997). Replacing the empirical G_b model (Eq. 3.5) with a physically based formulation (Eq. 3.6) (Massman, 1999; Su et al., 2001) considers a more comprehensive set of aerodynamically relevant properties of the ecosystem, but also introduces additional uncertainties. This is problematic due to the high sensitivity of this formulation (and that of others, e.g. McNaughton and Van den Hurk, 1995) to the characteristic leaf dimension (Eqs. B.2, B.7, and B.8); Fig. 3.3b), information that is not always available and presumably highly variable at EC sites.

Using G_a to infer the micrometeorology at the big-leaf surface as the physiologically relevant conditions (Grantz and Meinzer, 1990) resulted in better model fits (Table B2), but had minor effects on the mean growing season G_1 values for the ecosystems investigated here. It appears unlikely that G_1 will be significantly affected by meteorological gradients within the canopy, as they have often been found to be even less pronounced than those between canopy and tower height (Linderson et al., 2012; Schurgers et al., 2015). However, meteorological gradients are likely to be more relevant for more decoupled ecosystems (e.g., grasslands, croplands) but this also strongly depends on site-specific micrometeorological conditions (Magnani et al., 1998).

3.4.3   Energy balance closure

Energy balance non-closure, i.e., the phenomenon that the sum of the measured turbulent fluxes H and λE is smaller than the available energy, is observed at most EC sites (Stoy et al., 2013; Wilson et al., 2002a). Potential reasons for this issue are manifold (Foken, 2008; Leuning et al., 2012), but involve either an underestimation of the turbulent fluxes by EC measurement systems (due to, e.g., low-frequency losses resulting from mesoscale circulations (Foken, 2008; Stoy et al., 2013)) or an overestimation of A, which arises predominantly when energy storage terms (S) are neglected. Yet, not all components of S can be readily determined. For example, the energy storage flux into and out of the aboveground biomass, which can sum up to approximately half of S in forest ecosystems (Lindroth et al., 2010), has to be estimated from biomass temperature, mass of the aboveground biomass as well as its heat capacity (see e.g. Haverd et al., 2007), information that is not available for most sites.

An unclosed energy balance affects the derivation of G_s from the inverted PM equation, since the latter assumes the energy balance to be closed. Our results demonstrate that the inferred G_s is sensitive to a violation of this assumption, in agreement with the analysis for a grassland and a shrub ecosystem by Wohlfahrt et al. (2009). The error in G_s that is made due to the energy balance nonclosure depends on which component of the energy balance is misrepresented in the measurements. An important implication is that the PM equation (Eq. 3.2) implicitly assigns the residual entirely to H and, therefore, underestimates (overestimates) G_s when the EBR < 1 (EBR > 1). G_s is less sensitive to errors in S, but highly sensitive to errors in λE, with potential errors rising exponentially with a decline in the EBR (Fig. 3.6b). In addition, an often observed diurnal cycle in the

EBR also affects the diurnal courses of G_s (Fig. 3.5d–f). Thus, both the magnitude and the temporal dynamics of G_s are strongly confounded by (and dependent on) the degree of closure in the energy balance, which is problematic as the EBR is not expected to be a physiologically relevant driver of iWUE. The uncertainty in G_s propagates to G_1 (Fig. 3.5), which further depends on to what extent carbon fluxes are affected by the energy balance closure problem (see Barr et al., 2006).

Our results call for accurate measurements of the surface energy storage terms (S in Eq. 3.11) and their diurnal courses at EC sites. This information would help to constrain uncertainties in G_s and ultimately allow application of flux correction procedures (Twine et al., 2000, "Bowen ratio adjusted" case in Fig. 3.5), which "overcorrect" half-hourly/hourly turbulent fluxes if S and/or G are neglected, particularly in ecosystems with tall vegetation and high biomass. Careful consideration of all energy balance terms (as e.g. in Blanken et al., 1997; Barr et al., 2006; Jacobs et al., 2008) and, where appropriate, adjustment of the turbulent fluxes are crucial for the derivation and physiological interpretation of EC-derived gas exchange characteristics on a sub-daily time scale.

3.4.4 NEE partitioning and uncertainties across scales

Fig. 3.7 suggests that ecosystem-level G_1 is relatively robust to choices made on the partitioning approach, which is in line with the general good agreement between the two GPP products (Lasslop et al., 2010). Nonetheless, the high sensitivity of G_1 to GPP emphasizes the importance of correctly estimating GPP from EC data, which also relies on the use of a representative driving temperature for R_{eco} (Lasslop et al., 2012). Also relevant for the direct comparison of g_1 at leaf and ecosystem levels are differences in the carbon uptake term used in Eqs. 3.1 and 3.3 net photosynthesis (A_n) at the leaf level and GPP at the canopy level. The two have to be interpreted differently for two main reasons: (i) GPP estimated from flux partitioning algorithms integrates carboxylation (V_c) minus photorespiration (R_p) and is thus not equivalent to (and to some extent larger than) net photosynthesis ($A_n = V_c - R_p - R_l$) measured from leaf-level gas exchange. (ii) Leaf respiration in the dark (R_d) has been found to exceed that in daylight (R_l) (Atkin et al., 1997; Brooks and Farquhar, 1985), though a recent study suggests that this "Kok effect" could also be explained by changes in the chloroplastic CO_2 concentration (C_c) caused by a reduced mesophyll conductance at low light (Farquhar and Busch, 2017), in which case R_d would not necessarily be down-regulated in the light. The consequence of a larger R_d compared to R_l would be that an extrapolation of nighttime respiration to daytime overestimates GPP (Wohlfahrt and Gu, 2015). This effect is not considered in common flux partitioning approaches because it would require additional modeling efforts (e.g., light distribution within the canopy), knowledge of the fraction of leaf respiration to ecosystem respiration (Wohlfahrt et al., 2005), and because the inhibition effect (i.e., the ratio R_l/R_d) is not well constrained (Niinemets and Keenan, 2014). Both these issues lead to a lower estimate of G_1 at the ecosystem level compared to the leaf level. Estimates

55

of canopy-scale R_l from our simulations amount to 3.4% of GPP on average across sites, whereas overestimation of GPP due to a possible light inhibition of R_d would be in the order of 15% (Janssens et al., 2001; Wehr et al., 2016; Wohlfahrt et al., 2005), indicating that the latter is the more relevant source of disagreement between across-scale estimates of G_1, but clearly a better process understanding is needed (Farquhar and Busch, 2017).

3.4.5 Within-canopy gradients

Pronounced canopy gradients of G_1 as estimated in this study for some sites (Fig. 3.8) were not supported by leaf-level measurements at DK-Sor and US-Ha1. However, canopy gradients were in agreement with several observational studies reporting a lower iWUE (corresponding to a higher g_1) in the understory both across (Domingues et al., 2007) and within species (Sellin et al., 2010), a pattern that results from the maintenance of a relatively high g_s at the canopy bottom compared to the top (Chazdon, 1988). As EC measurements integrate G_1 over the existing canopy gradients whereas leaf measurements do not, the former are expected to give higher values than the latter (if taken at the top of the canopy). This effect depends both on the gradient itself as well as the relative flux contribution from the different layers. Our results indicate that within-canopy gradients of g_1 are site- and possibly species-specific, highlighting the need for additional leaf-level measurements at different levels in the canopy, as well as a more comprehensive characterization of the understory vegetation and its contribution to total ecosystem fluxes.

3.4.6 Recommendations for future studies

In this study, we aimed to derive a physiologically meaningful WUE metric (G_1) from EC data that can be used in modeling and for the characterization of the physiological control of ecosystem water–carbon coupling. We were limited to forest sites in this study by the availability of leaf gas exchange data, but it would be useful to extend this analysis to non-forest sites or to include carbon isotope data as an independent dataset (as e.g. in Medlyn et al., 2017). We demonstrate that EC-derived G_s and G_1 are strongly affected by (i) confounding physical factors and (ii) methodological uncertainties, and are subject to (iii) conceptual differences to leaf-level estimates. Ignoring these factors compromises the ecophysiological interpretation of EC-derived vegetation gas exchange characteristics as well as their direct comparison to leaf-level estimates. Based on our analysis, we have the following recommendations for the calculation of G_1:

- Exclusion of time periods for at least 24 hr after rainfall.

- The assumption $G_a = \infty$ is inappropriate; the use of physically based G_a models is only recommended if site-specific aerodynamic properties are known.

- The derivation of canopy surface meteorology (e.g., VPD) is meaningful, but of secondary importance for average growing season values.

- Critical evaluation and (if appropriate) correction of all energy balance terms is pivotal.

- Both daytime and nighttime NEE partitioning algorithms can be used for WUE studies.

- EC data should be complemented by physiological (leaf level) and meteorological measurements made at different levels in the canopy.

Acknowledgements

4 The bigleaf R package

This chapter is a copy-edited version of the following published article:

Jürgen Knauer[1], Tarek S. El-Madany[1], Sönke Zaehle[1,2], Mirco Migliavacca[1] (2018). **Bigleaf - An R package for the calculation of physical and physiological ecosystem properties from eddy covariance data.** *PLoS ONE* 13(8), e0201114. doi:10.1371/journal.pone.0201114.

[1] Department of Biogeochemical Integration, Max Planck Institute for Biogeochemistry, Jena, Germany;

[2] Michael-Stifel-Center Jena for Data-Driven and Simulation Science, Jena, Germany

Abstract

We present the R package `bigleaf` (version 0.6.5), an open source toolset for the derivation of meteorological, aerodynamic, and physiological ecosystem properties from eddy covariance (EC) flux observations and concurrent meteorological measurements. A 'big-leaf' framework, in which vegetation is represented as a single, uniform layer, is employed to infer bulk ecosystem characteristics top-down from the measured fluxes. Central to the package is the calculation of a bulk surface/canopy conductance ($G_\mathrm{s}/G_\mathrm{c}$) and a bulk aerodynamic conductance (G_a), with the latter including formulations for the turbulent and canopy boundary layer components. The derivation of physical land surface characteristics such as surface roughness parameters, wind profile, aerodynamic and radiometric surface temperature, surface vapor pressure deficit (VPD), potential evapotranspiration (ET), imposed and equilibrium ET, as well as vegetation-atmosphere decoupling coefficients, is described. The package further provides calculation routines for physiological ecosystem properties (stomatal slope parameters, stomatal sensitivity to VPD, bulk intercellular CO_2 concentration, canopy photosynthetic capacity), energy balance characteristics (closure, biochemical energy), ancillary meteorological variables (psychrometric constant, saturation vapor pressure, air density, etc.), customary unit interconversions and data filtering. The target variables can be calculated with a different degree of complexity, depending on the amount of available site-specific information. The utilities of the package are demonstrated for three single-level (above-canopy) eddy covariance sites representing a temperate grassland, a temperate needle-leaf forest, and a Mediterranean evergreen broadleaf forest. The routines are further tested for a two-level EC site (tree and grass layer) located in a Mediterranean oak savanna. The limitations and the ecophysiological interpretation of the derived ecosystem properties are discussed and practical guidelines are given. The package provides the basis for a consistent, physically sound, and reproducible characterization of biometeorological conditions and ecosystem physiology, and is applicable to EC sites across vegetation types and climatic conditions with minimal ancillary data requirements.

4.1 Introduction

The eddy covariance (EC) technique provides direct and continuous measurements of the exchange of heat, water vapor, carbon dioxide, and other trace gases between the surface and the lower atmosphere (Aubinet et al., 1999; Baldocchi et al., 2001). The method has significantly contributed to our understanding of how this mass and energy exchange is controlled by environmental drivers such as radiation (Knohl and Baldocchi, 2008; Mercado et al., 2009), temperature, vapor pressure deficit (VPD) (Law et al., 2002; Novick et al., 2016), or soil water stress (Keenan et al., 2010a), and how it is modulated by meteorological extreme events such as heatwaves (Ciais et al., 2005a; Teuling et al., 2010). EC data have proven useful to characterize climate and vegetation controls on the partitioning of available energy at the land surface (Wilson et al., 2002b) and the resulting surface hydrology (Williams et al., 2012). EC data have further allowed a more detailed insight into the coupling of biogeochemical cycles, in particular carbon and water, and its modification by climate and surface conditions (Beer et al., 2009; Zhou et al., 2014).

These findings have been achieved by a large scientific community (Baldocchi, 2008; Pastorello et al., 2017), which maintains several hundred EC measurement sites around the globe. The increasing length of available EC data in combination with freely available data processing tools (Beringer et al., 2017; Kljun et al., 2015), which are partly available in R (Metzger et al., 2017; Wutzler et al., 2018), underline the important role of EC data in present and future ecological and climate change research.

The analysis of EC data does not have to be restricted to direct or partitioned energy and mass flux measurements, but additional ecosystem properties can be derived from a joint analysis of fluxes and meteorological variables. Such additional information can help in obtaining a more comprehensive understanding of the biological and physical processes underlying the measured fluxes (Fig. 4.1). For instance, the aerodynamic conductance (G_a) between the land surface and the instrument height is a key variable describing how effective the ecosystem can transfer mass and energy to the atmosphere. Knowledge of both G_a and the measured energy or mass fluxes allows to infer average conditions at the surface (e.g. temperature, atmospheric humidity, CO_2 concentration). This is of interest as conditions at the canopy surface are in general more relevant for ecophysiological processes than those measured at instrument height some distance above the canopy (Grantz and Meinzer, 1990).

An important ecophysiological ecosystem property is the surface conductance (G_s). Its vegetation component (canopy conductance (G_c)) is an integrated measure of stomatal conductance and constitutes the main biological control on the exchange of water and carbon dioxide at the land surface. These two central bulk conductances (G_a and G_s) can be combined to assess the aerodynamic coupling between the vegetation and the atmosphere (Jarvis, 1986), which again indicates the relative importance of key meterological drivers and the degree of physiological control on evapotranspiration (ET) (Jarvis, 1986; McNaughton and Jarvis, 1991). Ecosystems well coupled to the atmosphere, such as aero-

dynamically rough forests, are more likely to exhibit stronger stomatal control on transpiration than low-statured ecosystems such as grasslands (Jarvis, 1986). At the same time, ET is under stronger control of VPD in well-coupled ecosystems, whereas available energy has been identified as the decisive factor in poorly coupled ecosystems (McNaughton and Jarvis, 1991).

The derived G_s can be used to infer additional ecophysiological variables at ecosystem level such as intrinsic water-use efficiency metrics (Knauer et al., 2018), intercellular CO_2 concentration (C_i) (Kosugi et al., 2013), stomatal sensitivity to VPD (Migliavacca et al., 2009; Novick et al., 2016), or photosynthetic capacity (Kosugi et al., 2013; Ueyama et al., 2016). Many of these quantities can be seen as ecosystem scale analogues of parameters derived from leaf level measurements, and in theory constitute time-invariant quantities that characterize ecosystem functioning in a more comparable manner than flux measurements alone (Reichstein et al., 2014).

Since the EC method in its traditional application (i.e. single-level and time-averaged measurements) cannot resolve the vertical and horizontal distribution of ecosystem flux sources and sinks, the above described quantities inevitably lack information on the vertical and horizontal structure of the ecosystem as well as on its components (e.g. soil and vegetation) when they are inferred directly from the measured fluxes. Approaches directed to circumvent this limitation are two-level sensor systems (Baldocchi et al., 1997; Blanken and Black, 2004), techniques resolving the spatio-temporal variability of the fluxes (Xu et al., 2018), or the inversion of more detailed models which separate e.g. sunlit from shaded canopy fractions (De Pury and Farquhar, 1997; Wang and Leuning, 1998), soil from canopy components (Shuttleworth and Wallace, 1985), or which represent the canopy as a multi-layered system (Baldocchi and Harley, 1995). These alternative modeling approaches are able to give more detailed and more realistic insights into the underlying physical and physiological mechanisms. However, the additional complexity comes at the cost of higher computational demands as well as higher requirements on ancillary data for model parameterization. A much simpler and more direct way to infer ecosystem properties from EC data is to invert a 'big-leaf' model, in which measured fluxes are assumed to origin from a single, homogenous plane. This approach requires little site-specific ancillary information, is widely applicable across sites, and has been shown to give meaningful results within its limits of applicability and validity (Raupach and Finnigan, 1988; Kelliher et al., 1995). Bulk ecosystem properties derived with a top-down 'big-leaf' approach are thus commonly presented in EC studies and have proven useful in characterizing vegetation behavior in various ecosystems and under contrasting conditions (Wilson et al., 2002b; Kumagai et al., 2004; Blanken and Black, 2004; Launiainen, 2010; Khatun et al., 2011; Baldocchi and Ma, 2013; Medlyn et al., 2017).

Despite their relevance for global change research and their widespread appearance, little effort has been put into the development of harmonized calculation protocols for these quantities, and as a consequence, calculated metrics are often not easily comparable, especially with respect to the wide variety of existing methodologies and formulations (e.g.

Goldberg and Bernhofer, 2008). In this paper, we describe the R package `bigleaf`, which provides functions to infer G_a, G_s and further physical as well as physiological bulk ecosystem properties from EC data and concurrent meteorological measurements in a consistent and standardized manner. In the following, the main equations are presented and their use is demonstrated for four contrasting EC sites. The limitations of the calculations, arising from methodological constraints and inherent limitations of the 'big-leaf' approach, as well as the consequences for the interpretation of the resulting variables, are discussed. The paper ends with practical guidelines on how to use the `bigleaf` package.

4.2 The `bigleaf` R package

4.2.1 Package design and availability

The `bigleaf` package is entirely written in the open source software R (R Core Team, 2017). The package is available as a stable version from CRAN (`https://cran.r-project.org/web/packages/bigleaf`) or as a development version (continously updated with git version control) from `http://www.bitbucket.org/juergenknauer/bigleaf`. This paper describes package version 0.6.5 (git commit: fcada22). An overview of the main functions is illustrated in Fig. 4.1. In the following, the theory underlying the package's key functions is shortly presented. For technical details on the functions, the reader is directed to the functions' help pages and examples therein.

4.2.2 The 'big-leaf' framework

All functions provided in this package are based on the 'big-leaf' framework (Fig. 4.1) (Monteith, 1965), which assumes that a single plane located at height $d + z_{0h}$ (d=displacement height, z_{0h}=roughness length for heat) is the single source and sink of all mass and energy fluxes, and that wind speed is zero at height $d + z_{0m}$ (z_{0m}=roughness length for momentum) and increases exponentially with height. This approach does not distinguish fluxes from different compartments of the ecosystem (e.g. soil and vegetation), nor does it account for vertical variations within the canopy or horizontal heterogeneity due to e.g. different species. The derived quantities at the 'big-leaf' surface must thus be regarded as average (but representative) conditions of the tower footprint. The main principle of the `bigleaf` package is to derive ecosystem surface properties from the observations using a top-down (inversion) approach.
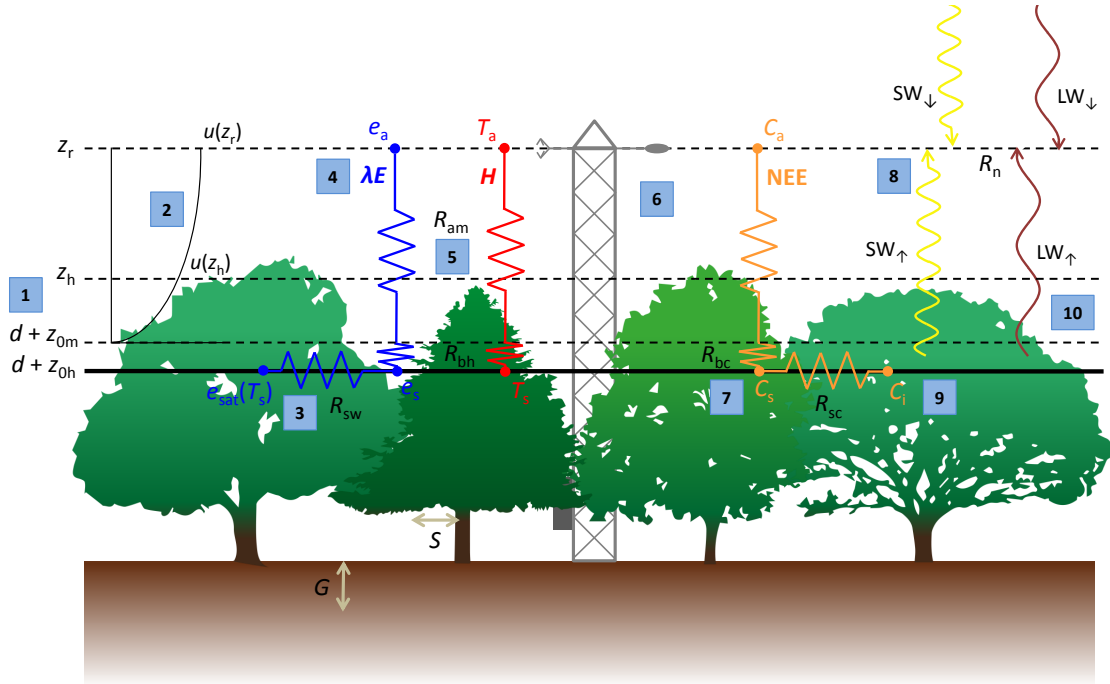
Fig. 4.1. Illustration of the 'big-leaf' concept and main functions included in the `bigleaf` R package. d is the displacement height, z_{0h} is the roughness length for heat, z_{0m} is the roughness length for momentum, z_h is the average vegetation height, z_r is the reference (=measurement) height, u is the horizontal wind speed, R_{sw} is the surface resistance to water vapor, R_{sc} is the surface resistance to CO_2, R_{bh} is the canopy boundary layer resistance to heat transfer, R_{bc} is the canopy boundary layer resistance to CO_2 transfer, R_{am} is the aerodynamic resistance to momentum transfer, e_{sat} is the saturation vapor pressure at the 'big-leaf' surface, e_s is the vapor pressure at the 'big-leaf' surface, e_a is the vapor pressure at reference height, λE is the latent heat flux, T_s is the aerodynamic surface temperature, T_a is the air temperature, H is the sensible heat flux, C_i is the bulk intercellular CO_2 concentration, C_s is the CO_2 concentration at the 'big-leaf' surface, NEE is the net ecosystem exchange of CO_2, SW↓ and SW↑ are the incoming and outgoing shortwave radiation, respectively, LW↓ and LW↑ are the incoming and outgoing longwave radiation, respectively, and R_n is the net radiation. Numbers denote the following functions: 1) `roughness.parameters()`; 2) `stability.parameter()`, `stability.correction()`, `wind.profile()`; 3) `surface.conductance()`, `stomatal.sensitivity()`, `stomatal.slope()`; 4) `potential.ET()`, `equilibrium.imposed.ET()`, `WUE.metrics()`; 5) `aerodynamic.conductance()`, `decoupling()`; 6) `energy.closure()`; 7) `surface.conditions()`; 8) `light.response()`, `light.use.efficiency()`; 9) `intercellular.CO2()`, `photosynthetic.capacity()`, `biochemical.energy()`, `energy.use.efficiency()`; 10) `radiometric.surface.temp()`. For details on the functions, see section 'Package content' or the respective R package help pages.

4.2.3 Package content

Data filtering

The `bigleaf` package does not provide functionalities to pre-process raw EC data or to assess the quality of individual datapoints. Instead, the package relies on correctly pre-processed, aggregated, quality-flagged, and friction velocity (u_*) filtered fluxes and meteorological measurements (e.g. Papale et al., 2006; Wutzler et al., 2018). Further, some analyses presented in this paper are only meaningful if certain meteorological conditions are met (e.g. daytime or rainfree periods, see below).

The package offers a basic data filtering routine (function `filter.data()`), which filters EC

data based on the aforementioned criteria. The function consists of two parts: 1) Quality control: data points of bad quality (e.g. gap-filled with poor confidence) are discarded, and 2) Meteorological filtering: variables falling out of the (purpose-specific) accepted range (e.g. nighttime values, precipitation events) are filtered out. The `filter.data()` function returns the input data frame in wich time periods that do not fulfill the filter criteria are set to `NA`.

Constants, unit interconversions, and sign convention

The package combines all required constants into one list that can be evoked by calling `bigleaf.constants()`. This list is passed as a default argument to all functions that use one or more constants. Thus, individual constants do not have to be provided for any function call, but can be changed by calling the argument explicitly. As a basis for many calculation steps, common unit interconversions are provided:

- Conductances between mass and molar units (m s^{-1} and mol m^{-2} s^{-1})

- Water fluxes between mass and energy units (kg m^{-2} s^{-1} and W m^{-2})

- Carbon fluxes between mass and molar units (g C m^{-2} d^{-1} and µmol CO$_2$ m^{-2} s^{-1})

- Atmospheric humidity between vapor pressure deficit (kPa), vapor pressure (kPa), specific humidity (kg kg^{-1}), and relative humidity

- Radiation between energy and molar units (W m^{-2} and µmol m^{-2} s^{-1})

The sign convention is that fluxes directed away from the surface are positive and those directed toward the surface are negative. Thus, negative net CO$_2$ ecosystem exchange (NEE) values indicate a net uptake of CO$_2$ by the ecosystem.

Meteorological variables

Most of the central functions in the `bigleaf` package require meteorological variables that are not commonly provided by the processed EC products, but which can be readily calculated from standard meteorological variables like air temperature, humidity, and atmospheric pressure. For reasons of space, the individual formulations are not presented here, instead the user is directed to the help page of the respective function and the references therein. All functions apply textbook calculations and include:

- latent heat of vaporization: `latent.heat.vaporization`(T_a)

- psychrometric constant: `psychrometric.constant`(T_a,p)

- saturation vapor pressure and slope of the saturation vapor pressure curve: `Esat.slope`(T_a)

- air density: `air.density`(T_a,p)

- virtual temperature: `virtual.temp`(T_a,q)

63

- wet-bulb temperature: `wetbulb.temp($T_a$,$p$,$D_a$)`

- dew point: `dew.point($T_a$,$D_a$)`

where T_a is the air temperature (°C), p is the atmospheric pressure (kPa), q is the specific humidity (kg kg^{-1}), and D_a is the vapor pressure deficit (kPa). If p is not available, it can be approximated by the hypsometric equation as a function of site elevation (`pressure.from.elevation()`).

Aerodynamic conductance

Aerodynamic conductance to heat transfer (G_{ah}) is central to the 'big-leaf' concept and multiple formulations have been proposed. G_{ah} can be written as

$$G_{ah} = 1/R_{ah} = (R_{am} + R_{bh})^{-1} \tag{4.1}$$

where R_{am} is the aerodynamic resistance to momentum transfer with turbulence as the principal transport mechanism, and R_{bh} is the canopy (quasi-laminar) boundary layer resistance ("excess resistance") to heat transfer, which is characterized by molecular diffusion as the dominant transport mechanism (Verma, 1989; Massman, 1999)).

At EC sites, G_{am} can be calculated directly as (e.g. Monteith and Unsworth, 2008; Verma, 1989)(`aerodynamic.conductance()`):

$$G_{am} = \frac{u_*^2}{u(z_r)} \tag{4.2}$$

where u_* is friction velocity (m s^{-1}) and $u(z_r)$ is wind speed (m s^{-1}) at reference (=measurement height)(m) .

Eq. 4.2 implicitly accounts for the effects of atmospheric stability on G_{am}. Nevertheless, an alternative and frequently used formulation is provided, which explicitly accounts for the effects of atmospheric stability (Verma, 1989):

$$G_{am} = \frac{k u_*}{\ln\left[\dfrac{z_r - d}{z_{0m}}\right] - \psi_h} \tag{4.3}$$

where k is the von Kármán constant (0.41), d is the zero plane displacement height (m), z_{0m} is the roughness length for momentum (m), and ψ_h is the integrated form of the stability correction function for heat and water vapor. ψ_h is a function of the atmospheric stability parameter $\zeta = (z_r - d)/L$, where L is the Monin-Obukhov length. The function `stability.correction()` can be used to calculate ψ_h based on formulations suggested by Businger et al. (1971) or Dyer and Hicks (1970). The two roughness parameters d and z_{0m} have to be determined a priori. The function `roughness.parameters()` provides three options: 1) an empirical approach assuming d and z_{0m} as constant fractions of canopy height z_h (by default $d = 0.7z_h$ and $z_{0m}=0.1z_h$), 2) a semi-empirical approach estimating both z_{0m} and d based on z_h and leaf area index (LAI) according to Choudhury and Monteith

(1988) for data presented in Shaw and Pereira (1982), and 3) an approach that calculates $z_{0\mathrm{m}}$ from the logarithmic wind profile equation with a prescribed d. Note that d and z_{0m}, as well as all other ancillary variables (e.g. LAI), can be provided as time-varying vectors with the same length as the input data frame.

Multiple formulations have been suggested for the calculation of the canopy (quasi-laminar) boundary layer conductance to heat transfer (G_{bh}), which range from empirical to physically-based (see Hong et al., 2012; Verhoef et al., 1997, for an overview). Thom (1972) suggested a simple empirical relationship between G_{bh} and u_* (`Gb.Thom()`):

$$G_{\mathrm{bh,Thom}} = \left(6.2 u_*^{-0.67}\right)^{-1} \tag{4.4}$$

Several further (semi-) empirical formulations have been suggested, but we restricted the functions to those best applicable to EC sites. In that respect, relationships based on the Reynolds number, which have been found to show a biphasic behavior (Garratt and Hicks, 1973), are currently not implemented. More mechanistic, but also parameter-rich approaches commonly require LAI and aerodynamically-relevant foliage characteristics (leaf width or leaf characteristic dimension). The formulation suggested by Choudhury and Monteith (1988) is given by (`Gb.Choudhury()`):

$$G_{\mathrm{bh,Choudhury}} = \mathrm{LAI}(0.02/\alpha)\sqrt{u(z_{\mathrm{h}})/w}(1 - \exp(-\alpha/2)) \tag{4.5}$$

where α is an attenuation coefficient modeled in dependence on LAI according to data presented in McNaughton and Van den Hurk (1995), $u(z_{\mathrm{h}})$ is wind speed (m s^{-1}) at canopy height z_{h}, and w is leaf width (m). Wind speed at height z_{h} (or any other height $z > d+z_{0\mathrm{m}}$ can be estimated from the logarithmic wind profile equation (`wind.profile()`):

$$u(z) = (u_*/k)\ln((z - d)/z_{0\mathrm{m}}) - \psi_{\mathrm{m}} \tag{4.6}$$

where ψ_{m} is the integrated form of the stability correction function for momentum (as calculated in `stability.correction()`). A third model currently implemented in the `bigleaf` package was developed by Massman (1999) and simplified by Su et al. (2001)(`Gb.Su()`):

$$G_{\mathrm{bh,Su}} = \frac{ku_*}{\dfrac{kC_{\mathrm{d}}f_{\mathrm{c}}^2}{4C_{\mathrm{t}}\dfrac{u_*}{u(z_{\mathrm{h}})}} + kB_s^{-1}(1 - f_{\mathrm{c}})^2} \tag{4.7}$$

where C_{d} is a foliage drag coefficient (assumed constant with a value of 0.2 (Massman, 1999)), f_{c} is fractional vegetation cover, C_{t} is a heat transfer coefficient, and B_s^{-1} is the inverse Stanton number for bare soil surface (Su et al., 2001). C_{t} mainly depends on the leaf characteristic dimension and the number of leaf sides participating in heat transfer, see Massman (1999) and Su et al. (2001) for details. The denominator of Eq. 4.7 is often referred to as the kB_{h}^{-1} parameter (e.g. Verhoef et al., 1997), which is defined as:

$$kB_{\mathrm{h}}^{-1} = \ln\left(\frac{z_{0\mathrm{m}}}{z_{0\mathrm{h}}}\right) = \frac{ku_*}{G_{\mathrm{bh}}} \tag{4.8}$$

From Eq. 4.8 the roughness length for heat ($z_{0\mathrm{h}}$) can be determined.

Note that G_{am} is identical for different scalars in the atmosphere (heat, water vapor, CO_2, and other trace gases), whereas G_{b} differs with respect to the quantity of interest. G_{b} of quantity x can be calculated based on G_{bh} (Hicks et al., 1987):

$$1/G_{\mathrm{bx}} = 1/G_{\mathrm{bh}} \left(\frac{\mathrm{Sc}_x}{\mathrm{Pr}}\right)^{0.67} \tag{4.9}$$

where Pr is the Prandtl number (0.71), and Sc_{x} is the Schmidt number for quantity x. For simplicity, the assumption is made that G_{b} is identical for heat and water vapor transfer (i.e. $G_{\mathrm{bh}} = G_{\mathrm{bw}}$). The more realistic difference of a few percent (Hicks et al., 1987) is considered small compared to other uncertainties (see also Jarvis and McNaughton, 1986). Since the calculations of G_{am} and G_{bh} are independent, the bulk aerodynamic conductance to heat transfer (G_{ah}) can be calculated as the sum of the inverse versions of Eqs. 4.2-4.3 and 4.4-4.7. The main function `aerodynamic.conductance()` returns G_{am}, G_{ah}, G_{bh}, G_{ac} (aerodynamic conductance to CO_2 transfer), G_{bc}, the corresponding resistances, and kB_{h}^{-1}, ζ, as well as ψ_{h}. If one or more additional Schmidt numbers are provided, G_{a} and G_{b} are calculated for the respective quantities as well. Due to the modular structure of the functions, each of these components can also be calculated individually.

Surface conditions

EC measurements are accompanied by meteorological measurements taken at approximately the same height as the flux measurements, usually several meters above the canopy. If G_{a} is determined, the bulk transfer relations can be inverted and solved for the surface variable (Blanken and Black, 2004; Knauer et al., 2018)((`surface.conditions()`)):

$$T_{\mathrm{s}} = T_{\mathrm{a}} + \frac{H}{\rho G_{\mathrm{ah}} c_p} \tag{4.10}$$

$$e_{\mathrm{s}} = e_{\mathrm{a}} + \frac{\lambda E \gamma}{\rho G_{\mathrm{ah}} c_p} \tag{4.11}$$

$$D_{\mathrm{s}} = e_{\mathrm{sat}}(T_{\mathrm{s}}) - e_{\mathrm{s}} \tag{4.12}$$

$$C_{\mathrm{s}} = C_{\mathrm{a}} + \frac{\mathrm{NEE}}{G_{\mathrm{ac}}} \tag{4.13}$$

where H is the sensible heat flux (W m^{-2}), ρ is the air density (kg m^{-3}), c_p is the heat capacity of dry air (J K^{-1} kg^{-1}), e is vapor pressure (kPa), λE is the latent heat flux (W m^{-2}), γ is the psychrometric constant (kPa K^{-1}), e_{sat} is the saturation vapor pressure, D is the vapor pressure deficit (kPa), and C is the CO_2 concentration. Subscripts a and s

denote air and surface, respectively. Note that in Eqs. 4.10-4.13 "surface conditions" refer to the notional canopy surface. It is also possible to infer conditions in the intercanopy airspace by replacing G_{ah} in Eqs. 4.10 and 4.11 or G_{ac} in Eq. 4.13 with G_{am}. The function `surface.conditions()` returns T_s, $e_{sat}(T_s)$, e_s, D_s, q_s, rH_s, and C_s. This method can be applied to other atmospheric constituents measured at EC sites (e.g. methane, nitrogen oxides, ozone), provided that the corresponding G_a is known (see above).

An alternative estimate of surface temperature is based on the physical principle that any object emits longwave radiation in dependence of its temperature as described by the Stephan-Boltzmann relation. This radiometric surface temperature (T_r, in Kelvin) is given by ((e.g. Wang et al., 2008), `radiometric.surface.temp()`):

$$T_r = \left(\frac{LW_\uparrow - (1 - \epsilon)LW_\downarrow}{\sigma \epsilon} \right)^{1/4} \tag{4.14}$$

where $LW_\uparrow$ and $LW_\downarrow$ are longwave upward and longwave downward radiation (W m^{-2}), respectively, σ is the Stefan-Boltzmann constant (W m^{-2} K^{-4}), and ϵ is the emissivity of the surface.

Surface conductance

Surface conductance to water vapor (G_{sw} in m s^{-1}), describes the conductance of the entire surface, i.e. including soil and plant canopy components. It is commonly calculated by inverting the Penman-Monteith (PM) equation (`surface.conductance()`):

$$G_{sw} = \frac{\lambda E G_{ah} \gamma}{s(R_n - G - S) + \rho c_p G_{ah} D_a - \lambda E(s + \gamma)} \tag{4.15}$$

where s is the slope of the saturation vapor pressure curve (kPa K^{-1}), R_n is the net radiation (W m^{-2}), G is the ground heat flux (W m^{-2}), and S is the sum of all energy storage fluxes (W m^{-2}).

Eq. 4.15 implicitly assumes that G_a for water vapor equals G_a for heat, i.e. $G_{ah} = G_{aw}$ which corresponds to an amphistomatous vegetation where the transfer of both heat and water vapor occurs at both leaf sides. The hypostomatous case (water vapor transfer from one side only) is conceptually not straightforward at the canopy level (McNaughton and Jarvis, 1991; Goldberg and Bernhofer, 2008), and is thus currently not implemented in this package. Eq. 4.15 further assumes that the energy balance is closed (i.e. $R_n - G - S = \lambda E + H$). The derived G_{sw} and all subsequent derivations are sensitive to violations of this assumption (Wohlfahrt et al., 2009; Knauer et al., 2018).

The function `surface.conductance()` offers the calculation of G_{sw} according to Eq. 4.15, and a simplified (but also less realistic) formulation based on a simple flux-gradient approach, which assumes infinite G_{ah}: $G_{sw} = \lambda E / \lambda / (D_a/p)$. This formulation is equivalent to the one proposed by McNaughton and Black (1973).

Vegetation-atmosphere decoupling

With both G_{ah} and G_{sw} available, the degree of aerodynamic decoupling between the land surface and the atmosphere can be assessed with the decoupling coefficient Ω, which takes values between 0 and 1. Low values indicate well-coupled conditions and a high degree of physiological control on ET. Values close to 1 indicate the opposite, i.e. poorly coupled conditions and a low sensitivity of ET to G_{sw} (Jarvis, 1986; McNaughton and Jarvis, 1991). In its simplest and most commonly used form, Ω is given by Jarvis (1986) (`decoupling()`):

$$\Omega_{\text{Jarvis}} = \frac{s/\gamma + 1}{s/\gamma + 1 + G_{ah}/G_{sw}} \tag{4.16}$$

Eq. 4.16 was modified by Martin (1989), who included the effects of radiative coupling between the vegetation and the atmosphere:

$$\Omega_{\text{Martin}} = \frac{s/\gamma + 1 + G_r/G_{ah}}{s/\gamma + 1 + G_{ah}/G_{sw} + G_r/G_{sw} + G_r/G_{ah}} \tag{4.17}$$

where G_r is the longwave radiative transfer conductance of the canopy (m s^{-1}), calculated as $G_r = 4\sigma T_a^3 \text{LAI}/c_p$ (`longwave.conductance()`). Note that, as in the PM equation (Equation 4.15), Eqs. 4.16 and 4.17 assume that the vegetation is amphistomatous (Jarvis, 1986).

Imposed and equilibrium evapotranspiration

The concept of decoupling is often used to characterize physiological and energy controls on transpiration. In addition it can help to quantify radiation and VPD controls on λE (e.g. Martin et al., 2001). λE can be written in an alternative way (Jarvis, 1986)(`equilibrium.imposed.ET()`):

$$\lambda E = \Omega \lambda E_{eq} + (1 - \Omega)\lambda E_{imp} \tag{4.18}$$

where

$$\lambda E_{eq} = \frac{s(R_n - G - S)}{s + \gamma} \tag{4.19}$$

and

$$\lambda E_{imp} = \frac{\rho c_p G_{sw} D_a}{\gamma} \tag{4.20}$$

Eqs. 4.19 and 4.20 are derived directly from the PM equation by letting G_{ah} approach 0 or ∞, respectively. Thus, λE_{eq} is the λE rate that would occur if the surface was completely decoupled from the atmosphere. In this case, λE is strongly controlled by R_n. Likewise, λE_{imp} can be interpreted as the λE rate that would occur under fully coupled conditions, in which case λE is mainly dependent on G_{sw} and D_a.

Potential evapotranspiration

Potential evapotranspiration (λE_{pot}) is frequently used to characterize atmospheric demand and the degree of climatic aridity (e.g. Williams et al., 2012). Here, λE_{pot} is by default calculated from the Priestley-Taylor equation (Priestley and Taylor, 1972) (`potential.ET()`):

$$\lambda E_{\text{pot,PT}} = \frac{\alpha s(R_{\text{n}} - G - S)}{s + \gamma} \tag{4.21}$$

where α is the Priestley-Taylor coefficient, which accounts for large-scale advection effects. Its value is usually set to 1.26, but it likely varies with surface conditions (De Bruin, 1983). λE_{pot} can further be calculated from the PM equation with a prescribed G_{sw} (Novick et al., 2016), which may correspond to typical maximum values (e.g. 95% quantile) found in the ecosystem :

$$\lambda E_{\text{pot,PM}} = \frac{s(R_{\text{n}} - G - S) + \rho c_p D_{\text{a}} G_{\text{ah}}}{s + \gamma(1 + G_{\text{ah}}/G_{\text{sw}})} \tag{4.22}$$

Energy balance

The package contains basic functionalities to characterize energy balance closure at EC sites. The function `energy.closure()` quantifies the energy balance closure ($R_{\text{n}} - G - S = \lambda E + H$) with both the slope method and the energy balance ratio (EBR) as described in Wilson et al. (2002a). The package further enables the calculation of biochemical energy (S_{p}), a small and therefore often neglected component of the energy balance: $S_{\text{p}} = \alpha\text{NEE}$, where $\alpha = 0.422$ J mol^{-1} denotes the biochemical energy taken up/released by photosynthesis/respiration per mole of CO_2 fixed/respired (Meyers and Hollinger, 2004). The function `energy.use.efficiency()` provides a simple estimate of the energy use efficiency (EUE) of the ecosystem: $\text{EUE} = S_{\text{p}}/R_{\text{n}}$.

Physiological ecosystem quantities

For ecosystems that have a largely closed vegetation cover, and under conditions when canopy and soil surfaces are not wet, the derived G_{s} can be interpreted as a proxy for the canopy-integrated stomatal conductance (i.e. canopy conductance G_{c}) (Kelliher et al., 1995). G_{s} may then be used to calculate additional physiological quantities. The function `stomatal.slope()` returns an estimate of the stomatal slope parameter G_1 at ecosystem level, analogous to g_1 at leaf level (Medlyn et al., 2017) (Note that in this paper, uppercase and lowercase letters denote physiological quantities at ecosystem and leaf-level, respectively). G_1 is estimated using non-linear regression from the unified stomatal model (USO) (Medlyn et al., 2011):

$$G_{\text{sw}} = G_0 + 1.6\left(1 + \frac{G_{1,\text{USO}}}{\sqrt{D_{\text{s}}}}\right)\frac{\text{GPP}}{C_{\text{s}}} \tag{4.23}$$

where G_0 is the minimum canopy conductance (mol m^{-2} s^{-1}), and GPP is gross primary productivity (µmol CO$_2$ m^{-2} s^{-1}). D_s and C_s represent conditions at the notional 'big-leaf' surface in this case (Eq. replaced by the measured values at instrument height (i.e. D_a and C_a 4.12) and Eq. 4.13, respectively), but they are often (Medlyn et al., 2017). G_0 can either be estimated along with G_1, or fixed to a user-defined value (e.g. set to 0). In addition to Eq. 4.23, G_1 can be calculated from the stomatal model proposed by Ball et al. (1987), or from its modified version suggested by Leuning (1995). Note that absolute values and units of G_1 differ across models. GPP is not directly measured at EC sites but inferred from NEE-partitioning algorithms (e.g. Reichstein et al., 2005; Lasslop et al., 2010). GPP is further not directly analogous to leaf-level net photosynthesis (A_n), and ecosystem leaf day respiration, if available, may be subtracted from GPP to better represent canopy-level A_n (Kosugi et al., 2013; Wohlfahrt and Gu, 2015).

The package further includes several alternative water-use efficiency (WUE) metrics (`WUE.metrics()`) which can be calculated more readily from the measured fluxes, but which contain less physiological information (Knauer et al., 2018). Examples are WUE (=GPP/ET), inherent WUE (IWUE=(GPP D_a)/ET) (Beer et al., 2009), or underlying WUE (uWUE=(GPP $\sqrt{D_a}$)/ET) (Zhou et al., 2014).
Stomatal sensitivity to VPD, a relevant indicator of vegetation water-use strategy, can be characterized with the following function (Oren et al., 1999) (`stomatal.sensitivity()`):

$$G_{sw} = -m \ln(D_s) + b \tag{4.24}$$

where the two parameters m (mol m^{-2} s^{-1} ln(kPa)$^{-1}$) and b (mol m^{-2} s^{-1}) represent the sensitivity of G_{sw} to D_s (D_a can be used alternatively) and the reference G_{sw} at D_s of 1 kPa, respectively (Oren et al., 1999; Novick et al., 2016).
Bulk canopy intercellular CO$_2$ concentration (C_i in µmol mol^{-1}) can be inferred from Fick's first law analogously to the calculation of c_i at leaf level (see e.g. Keenan et al., 2010b; Kosugi et al., 2013, `intercellular.CO2()`):

$$C_i = C_s - \text{GPP}/G_{sc} \tag{4.25}$$

where C_s is the CO$_2$ concentration at the 'big-leaf' surface (µmol mol^{-1}; Eq. 4.13), which can also be approximated by C_a. G_{sc} denotes the surface conductance to CO$_2$ (mol CO$_2$ m^{-2} s^{-1}) and is calculated as $G_{sc} = G_{sw}/1.6$.
With C_i available, the 'big-leaf' concept may be further expanded to calculate an estimate of basic photosynthetic parameters such as the maximum carboxylation rate (V_{cmax}) and maximum electron transport rate (J_{max}) at canopy level (e.g. Rayment et al., 2002; Kosugi et al., 2013; Ueyama et al., 2016), `photosynthetic.capacity()`). The calculation is once more analogous to that at leaf level, where commonly the model developed by Farquhar et al. (1980) is employed. Note however, that especially for V_{cmax} and J_{max} the interpretation differs from that at leaf level (see discussion). From the Rubisco-limited photosynthesis

rate (when carboxylation is the rate limiting process i.e. GPP = GPP_c, usually under high radiation), V_{cmax} (µmol m^{-2} s^{-1}) can be calculated as:

$$V_{cmax} = \frac{GPP_c(C_i + K_c(1 + O_i/K_o))}{C_i - \Gamma^*}$$ (4.26)

where K_c (µmol mol^{-1}) and K_o (mmol mol^{-1}) are the Michaelis-Menten constants for CO_2 and O_2, respectively, O_i (mol mol^{-1}) is the O_2 concentration, and Γ^* (µmol mol^{-1}) is the photorespiratory CO_2 compensation point (µmol mol^{-1}). All photosynthetic parameters and their temperature responses (activation energies) are taken from Bernacchi et al. (2001) and assume infinite mesophyll conductance to CO_2 transfer. Under conditions when Ribulose 1,5-bisphosphate (RuBP)-regeneration is limiting photosynthesis (i.e. GPP = GPP_j), the electron transport rate J (µmol m^{-2} s^{-1}) is given by:

$$J = \frac{GPP_j(4C_i + 8\Gamma^*)}{C_i - \Gamma^*}$$ (4.27)

J_{max} is then calculated from the following relation:

$$J = \frac{APPFD_{PSII} + J_{max} - \sqrt{(APPFD_{PSII} + J_{max})^2 - 4\Theta APPFD_{PSII} J_{max}}}{2\Theta}$$ (4.28)

where $APPFD_{PSII}$ is absorbed photosynthetic photon flux density (PPFD) by photosystem II (µmol m^{-2} s^{-1}), and Θ is a curvature parameter. $APPFD_{PSII}$ is currently assumed to be a constant fraction of PPFD (by default $APPFD_{PSII} = 0.8PPFD$), but a more realistic estimate of APPFD, depending on solar elevation angle and LAI, will be implemented in the future. Bulk canopy photosynthesis is assumed to be limited by either Rubisco activity (GPP=GPP_c) or RuBP-regeneration (GPP=GPP_j) at high and low radiation, respectively, and simple radiation thresholds are applied to separate the two limitation states. V_{cmax} and J_{max} are temperature-dependent and are normalized to the reference temperature of 25°C (i.e. $V_{cmax,25}$ and $J_{max,25}$) using a modified Arrhenius equation as described in e.g. Medlyn et al. (2002) with default parameter values from Bernacchi et al. (2001) and Bernacchi et al. (2003).

Ecosystem light response curves (LRCs) are useful to characterize both the CO_2 uptake rate at light saturation as well as the light utilization efficiency (i.e. the initial slope). The most frequently used model is the rectangular hyperbolic LRC, which can be written in a general form as (Falge et al., 2001, (`light.response()`)):

$$\text{-NEE} = \frac{\alpha PPFD}{(1 - (PPFD/PPFD_{ref}) + (\alpha PPFD/GPP_{ref}))} - R_{eco}$$ (4.29)

where α is the initial slope of the light-response curve (µmol CO_2 m^{-2} s^{-1} (µmol quanta m^{-2} s^{-1})$^{-1}$), R_{eco} is ecosystem respiration (µmol CO_2 m^{-2} s^{-1}), and $PPFD_{ref}$ is the PPFD value at which GPP_{ref} (µmol CO_2 m^{-2} s^{-1}) is calculated (usually at saturating light, e.g. at 2000 µmol m^{-2} s^{-1}). Additionally, a simple light-use efficiency (LUE) metric, defined as the ratio of cumulative GPP to cumulative PPFD, is available in the package

```
(light.use.efficiency()).
```

4.3 Case studies

4.3.1 Single-level EC sites

Three sites with EC measurements at a single level above the canopy were chosen for the demonstration of the formulations described above: AT-Neu (Neustift), a managed grassland in Austria (Wohlfahrt et al., 2008), DE-Tha (Tharandt), a high-statured (mean canopy height = 26.5m) spruce forest in Eastern Germany (Grünwald and Bernhofer, 2007), and FR-Pue (Puechabon), a Mediterranean evergreen oak forest in southern France, which is subject to seasonal water stress (Rambal et al., 2003). The location as well as basic ecosystem properties for these sites are listed in Table 4.1. Data are freely available from the FLUXNET2015 dataset (http://fluxnet.fluxdata.org/data/fluxnet2015-dataset/; accessed on 2016-11-09). Subsetted dataframes are included in the package and are automatically loaded when the package is attached. Data underwent standard postprocessing (e.g u_* filtering, gap-filling, NEE-partitioning) as detailed on the FLUXNET2015 webpage (http://fluxnet.fluxdata.org/data/fluxnet2015-dataset/data-processing/; accessed on 2018-04-19).

Table 4.1. Characteristics of the three single-level case study sites.

site	lon (°)	lat (°)	elevation (m)	MAP (mm)	MAT (°C)	vegetation type	z_h (m)	max. LAI
AT-Neu	11.32	47.12	970	852	6.30	grassland	0.5[a]	6[a]
DE-Tha	13.57	50.96	385	843	8.20	spruce forest	26.5	7.6
FR-Pue	3.60	43.74	48	883	13.50	holm oak forest	5.5	3.3

[a] highly variable throughout the growing season (Wohlfahrt et al., 2008). LAI=5 in subsequent calculations

Seasonal courses of G_s, G_a and vegetation-atmosphere decoupling

We calculated seasonal dynamics of aerodynamic and surface conductance to water vapor, as well as the decoupling coefficient Ω (Fig. 4.2). The results reveal that G_{ah} is relatively constant over the course of the year, but differs in magnitude across sites. As expected, highest values can be found in the aerodynamically rough spruce forest DE-Tha, and lowest values in the meadow AT-Neu. FR-Pue shows intermediate values. Differences between the different G_{ah} versions result from different models of the bulk boundary layer conductance (G_{bh}; Eqs. 4.4-4.7). The different G_{bh} formulations agree well for AT-Neu and FR-Pue, but lead to clear differences in estimated G_{ah} for DE-Tha. This is likely because the Choudhury (Eq. 4.5) and Su (Eq. 4.7) models consider additional aerodynamic properties (e.g. leaf size, LAI) that are neglected in the Thom model (Eq. 4.4). Thus, accounting for the low leaf characteristic dimension / leaf width and high LAI in DE-Tha leads to a higher G_{ah} in the Su and especially in the Choudhury formulation compared to the Thom

model. The differences in G_{ah} among the formulations do not have strong effects on the derived G_{sw} and Ω. G_{sw} shows pronounced seasonal dynamics at all three sites. Lowest values correspond to inactive vegetation, as e.g. caused by soil water stress (DOY 190-240 in FR-Pue). The dynamics in G_{sw} are clearly reflected in Ω, the magnitude of which differs considerably across sites. AT-Neu (grassland) is relatively poorly coupled, whereas DE-Tha (forest) shows a high degree of coupling. All three sites show typical values for the respective vegetation type (De Kauwe et al., 2017).
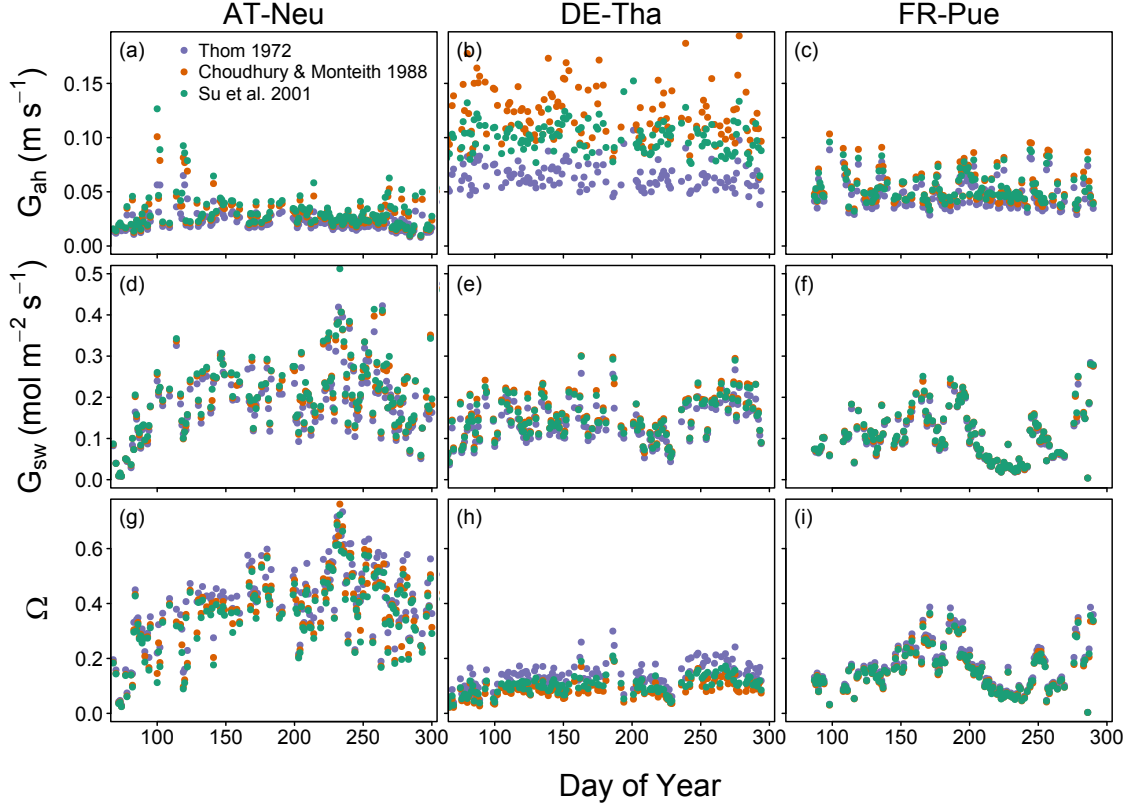
Fig. 4.2. Seasonal courses of mean daily values of aerodynamic conductance to heat transfer (G_{ah}), surface conductance to water vapor (G_{sw}), and decoupling coefficient (Ω) for the year 2012. Data were filtered for rainfree periods (24h after rainfall excluded), daylight (PPFD > 200 µmol m^{-2} s^{-1}), and positive λE. G_{sw} was calculated according to Eq. 4.15, and Ω according to Eq. 4.16. Three different G_{ah} formulations (Eqs. 4.2 and 4.4-4.7), denoted by different colors, were used as input variables for the respective functions.

Surface conditions

Fig. 4.3 depicts mean diurnal courses of air temperature, vapor pressure, VPD, and CO_2 concentration and the respective surface variables as calculated from Eqs. 4.10 - 4.13 for the summer months June, July, and August (JJA) of all available site years. At all three sites, aerodynamic surface temperature T_s (Eq. 4.10) exceeds air temperature at daytime and is lower at nighttime. T_s - T_a is largely parallel to the course of H throughout the day. The inferred temperature difference depends not only on the magnitude of H, but also on G_{ah}. It follows that the grassland AT-Neu has a more pronounced temperature difference

for the same H than the forest DE-Tha owing to its lower efficiency to transfer heat to the atmosphere (i.e. lower G_{ah}). Temperature gradients are most pronounced at FR-Pue (approx. 4°C at midday) where a large fraction of the available energy goes into H. Radiometric surface temperature (T_r; Eq. 4.14) generally agrees well with T_s, but shows biases at some timeperiods (e.g. AT-Neu at night). Differences between T_s and T_r can be caused by inappropriate emissivity values, biases in the estimated G_{ah}, or differences in the spatial representativeness of radiation ($LW_{\uparrow}$) and flux (H) measurements.

The derived vapor pressure at the 'big-leaf' surface (e_s) exceeds the measured values at instrument height (e_a) at all three sites during daytime. The water vapor gradient at AT-Neu is significantly higher than at the other two sites, which is caused by the relatively high λE and low G_{ah}. The high e_s at AT-Neu leads to a decrease of surface VPD (D_s) compared to air VPD (D_a). In contrast, the temperature effect on VPD is stronger than the moisture effect in DE-Tha and FR-Pue, with the consequence that D_s exceeds D_a at daytime at these two sites. Future analyses should be directed to the question whether these patterns hold across sites and vegetation types.

The difference of CO_2 concentration at the 'big-leaf' surface (C_s) to the concentration in the atmosphere (C_a) follows the diurnal pattern of NEE (Fig. 4.3j-l). Daytime photosynthetic CO_2 uptake and nocturnal ecosystem respiration lead to lower or higher CO_2 concentrations, respectively, at the surface compared to the air. The absolute differences are generally low (< 10 µmol mol^{-1}), but may exceed 20 µmol mol^{-1} under conditions of high biological activity and low turbulent mixing.
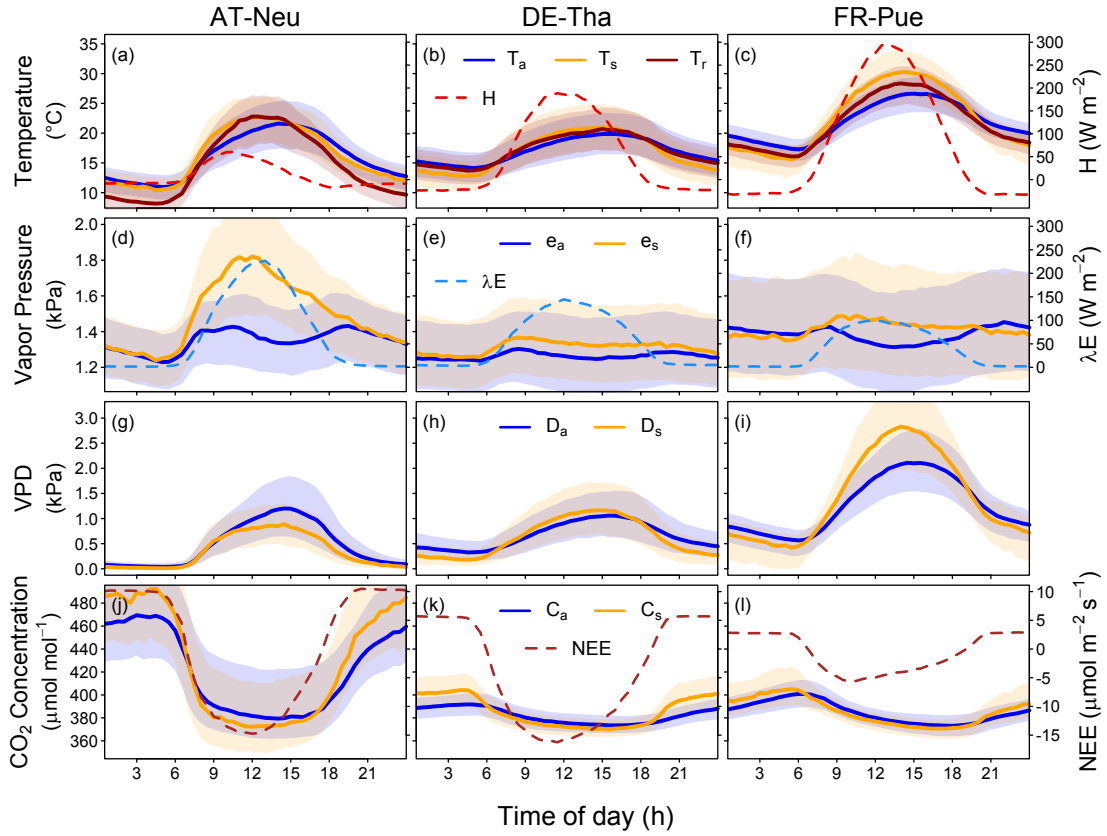
Fig. 4.3. Median diurnal courses of measured air and respective derived 'big-leaf' surface variables for the summer months of all available site years (JJA). Lines depict median diurnal courses of all available site years and shaded areas the interquartile range. Surface conditions were calculated with G_a calculated from Eqs. 4.2 and 4.7 (with D_l taken as 0.02, 0.008, and 0.035 m for AT-Neu, DE-Tha, and FR-Pue, respectively). Radiometric surface temperature in panels a-c was calculated according to Eq. 4.14 assuming a constant longwave emissivity of 0.98.

Relationship between G_s and GPP

Fig. 4.4 illustrates the relationship between G_{sw} and the "stomatal index", i.e. GPP adjusted for VPD and CO_2 concentration (Medlyn et al., 2017) for the year 2012. The relationship between these two quantities characterizes intrinsic WUE (iWUE) at ecosystem level and provides essential information on the physiological basis of ecosystem WUE. The slope of the depicted relationship approximates the $G_{1,USO}$ parameter ("stomatal slope") with higher slopes corresponding to a lower iWUE. Points in Fig. 4.4 are colored according to the C_i/C_s ratio, which is again closely related to iWUE. High C_i/C_s correspond to high stomatal slopes and lower WUE, and the opposite is the case for low C_i/C_s. The relationship between G_{sw} and the "stomatal index" shows large scatter, especially at AT-Neu, which indicates variations of iWUE throughout the growing season. Such variations within one year may be caused by changes in phenology, LAI (as e.g. caused by mowing) or the onset of water stress.
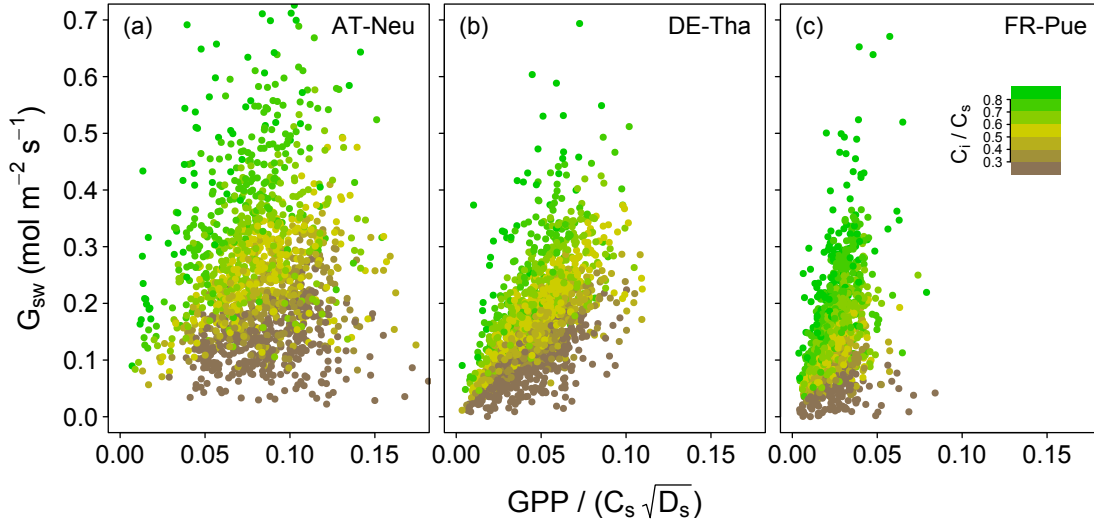
Fig. 4.4. Surface conductance (G_{sw}) plotted against $GPP/(C_s\sqrt{D_s})$. The slope of the relationship corresponds approximately to the $G_{1,USO}$ parameter (Eq. 4.23). Different colors denote the ratio of bulk intercellular CO_2 concentration (C_i; Eq. 4.25) to 'big-leaf' surface CO_2 concentration (C_s; Eq. 4.13). Shown are data for rainfree periods in the growing season of 2012 (see text for details on data filtering).

4.3.2   Two-level EC site

The package was further applied to data from the site ES-LMa (Majadas de Tietar), where fluxes and meteorology were measured at two different heights. The site (39°56'N; 5°46'W, 260 m a.s.l.) is an open woodland with a tree canopy cover (mainly *Quercus ilex*) of about 20% (Casals et al., 2009). Ecosystem fluxes were measured at 15.5 m above ground (7 m above tree canopy height) and grass layer fluxes were measured with a second tower at 1.65 m height. Tree fluxes were derived as the differences of the ecosystem fluxes and the grass layer fluxes similar to Blanken and Black (2004) and Baldocchi et al. (1997).

$G_{1,USO}$ and uWUE were calculated for a moving window of +/- 3 weeks which was shifted by one week for each calculation. This procedure was done for the ecosystem, grass layer and trees. Minimum, maximum and mean of mean daily air temperature and soil water content were calculated for the same period.

Differences in $G_{1,USO}$ follow clear seasonal patterns (Fig. 4.5) depending on water availability, VPD (which follows air temperature), and the associated growth and senescence of the grass layer. Ecosystem $G_{1,USO}$ is relatively constant during the growing periods of 2016 and 2017 (winter and spring). $G_{1,USO}$ of the grass layer is more variable as compared to the ecosystem. This mirrors the seasonal dynamics and fast responses of the grass layer to environmental conditions. For $G_{1,USO}$ of the grass layer a pronounced increase is visible before $G_{1,USO}$ drops during the summer drought. The increase is due to the rapid drop in GPP as the grasses start wilting due to drying of the top soil, while λE reduces much slower due to soil evaporation from deeper layers. The subsequent drop in $G_{1,USO}$ is then caused by the continuous reduction in λE during the dry period as the deeper soil layers are also drying out. *Q. ilex* trees are rather isohydric and react to increasing VPD by

closing their stomata to reduce water losses, which results in a decreasing $G_{1,\mathrm{USO}}$. In 2017, $G_{1,\mathrm{USO}}$ of the trees decreases more slowly compared to 2016, which is most likely caused by several rain pulses that increased the water availability and reduced VPD as compared to the long lasting dry period in 2016. $G_{1,\mathrm{USO}}$ (Fig. 4.5a) and the uWUE (Fig. 4.5b) show strongly anti-correlated patterns. As $G_{1,\mathrm{USO}}$ increases the uWUE reduces and vice versa. The trees are able to strongly increase their uWUE as atmospheric humidity and soil water availability are reduced.
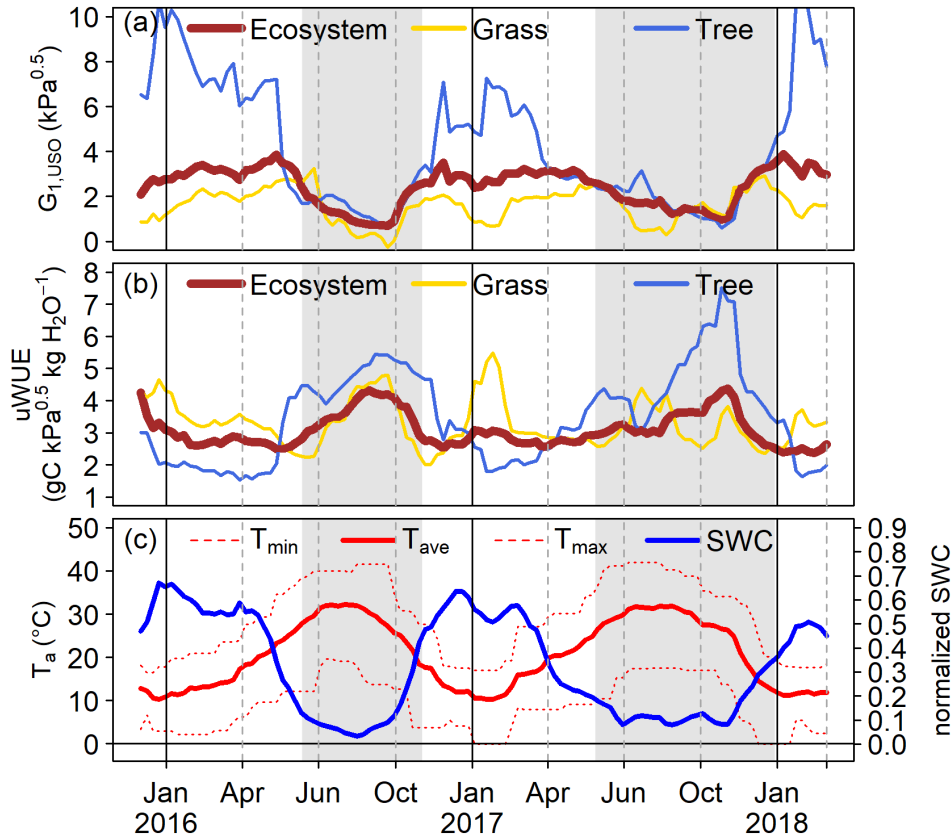
Fig. 4.5. (a) Time series of the stomatal slope parameter $G_{1,\mathrm{USO}}$ and (b) underlying water-use efficiency (uWUE) calculated for the whole ecosystem (brown), the grass layer (yellow) and the trees (blue) between December 2015 and March 2018. (c) Time series of minimum, maximum and mean daily air temperature and normalized soil water content for the same period. Grey shaded areas denote dry periods associated with a wilted grass layer.

4.3.3 Calculated ecosystem characteristics

Tables 4.2 and 4.3 present physical and physiological ecosystem properties, respectively, of the four study sites. All quantities represent median growing season values of multiple site years, i.e. have to be interpreted as multi-year averages. Site years used for the calculations were 2002-2012 for AT-Neu, 1996-2014 for DE-Tha, 2000-2014 for FR-Pue, and November 2015 - November 2017 for ES-LMa. Growing season was delineated using `filter.data()` with `tGPP=0.5`, `ws=15`, `min.int=5` (relative GPP threshold, window size (days), minimum interval (days)). Data were filtered using site-specific, multi-year aver-

aged u_* thresholds, daytime conditions (PPFD > 200 µmol m^{-2} s^{-1}), and rainfree periods (24h after rainfall excluded). Data were further filtered for $D_a > 0.01$ kPa, $\lambda E > 0$ W m^{-2} and $T_a > 5$°C. G_{ah} was calculated according to Eqs. 4.2 and 4.7, unless stated otherwise. More information on the ancillary data used for the calculations can be found under http://www.bitbucket.org/juergenknauer/bigleaf/src/master/ancillary. Note that for this study, ancillary variables (e.g. LAI, z_h, z_r) were assumed to be constant throughout all site years. In many cases, however, they vary across the growing season or among years. Thus, for a more realistic representation of the calculated ecosystem properties, required ancillary variables, if available, should be provided at an adequate temporal resolution. In general, computations in the `bigleaf` package are fast, e.g. with a state-of-the-art PC it takes < 0.1 seconds to calculate G_s for 10 site years and 2-3 seconds to calculate all properties as shown in Tables 4.2 and 4.3.

Table 4.2. Median daytime physical ecosystem properties in the growing season calculated with the `bigleaf` package.

	AT-Neu	DE-Tha	FR-Pue	ES-LMa	ES-LMa$_\mathrm{grass}$	ES-LMa$_\mathrm{trees}$
R_am (s m^{-1})	31.6	7.1	10.9	13.0	28.7	11.6
$R_\mathrm{ah,Thom}$ (s m^{-1})	47.3	15.6	20.4	23.9	46.2	21.8
$R_\mathrm{ah,Choudhury}$ (s m^{-1})	38.0	8.1	18.1	21.3	74.4	21.2
$R_\mathrm{ah,Su}$ (s m^{-1})	36.3	9.6	16.3	21.1	36.5	21.1
$R_\mathrm{ac,Su}$ (s m^{-1})	37.8	10.3	18.0	23.6	39.2	24.0
$R_\mathrm{bh,Thom}$ (s m^{-1})	15.6	8.5	9.4	10.9	17.7	10.0
$R_\mathrm{bh,Choudhury}$ (s m^{-1})	6.3	1.0	7.0	8.0	41.9	9.3
$R_\mathrm{bh,Su}$ (s m^{-1})	4.8	2.5	5.3	8.0	8.3	9.4
$kB^{-1}_{h,\mathrm{Thom}}$	1.6	2.2	2.1	1.9	1.5	2.0
$kB^{-1}_{h,\mathrm{Choudhury}}$	0.7	0.3	1.6	1.5	3.8	1.9
$kB^{-1}_{h,\mathrm{Su}}$	0.5	0.7	1.2	1.5	0.7	1.9
Ω_Jarvis	0.49	0.13	0.14	0.22	0.41	0.08
Ω_Martin	0.38	0.10	0.12	0.19	0.35	0.07
$z_{0m_{zh}}$ (m)	0.05	2.65	0.55	0.80	0.02	0.80
$z_{0m_{zh\ \&\ \mathrm{LAI}}}$ (m)	0.04	1.42	0.48	0.78	0.02	0.86
$z_{0m_{\mathrm{wind\ profile}}}$ (m)	0.05	1.74	0.43	0.38	0.05	0.48
ζ	-0.021	-0.085	-0.034	-0.052	-0.030	-0.017
L (m)	-11.8	-137.1	-87.7	-62.7	-12.1	-153.2
$u(z_h)/u(z_r)$	0.29	0.62	0.48	0.60	0.02	0.56
$T_s - T_a$ (°C)	1.0	1.3	2.1	1.9	1.6	0.9
$T_r - T_a$ (°C)	0.2	0.5	0.9	2.5	2.7	2.6
$e_s - e_a$ (kPa)	0.35	0.06	0.09	0.15	0.27	0.04
$D_s - D_a$ (kPa)	-0.16	0.12	0.23	0.11	-0.03	0.09
$C_s - C_a$ (µmol mol^{-1})	-13.8	-3.3	-2.8	-3.1	-4.7	-1.8
$\lambda E_\mathrm{pot,PT}$ (W m^{-2})	247.5	310.7	353.0	333.9	187.3	152.9
$\lambda E_\mathrm{pot,PM}$ (W m^{-2}) [a]	265.5	226.7	227.1	268.5	214.5	132.2
λE_eq (W m^{-2})	196.4	246.6	280.1	265.0	148.6	121.3
λE_imp (W m^{-2})	163.4	91.7	71.4	98.0	129.3	28.3
EBR	0.80	0.81	0.69	0.70	0.99	0.59
EB slope	0.72	0.76	0.64	0.67	0.98	0.43
EB intercept (W m^{-2})	21	18	19	10	3	27
Sp (W m^{-2})	6.2	5.5	2.8	2.3	2.0	1.3
EUE	0.038	0.022	0.012	0.012	0.021	0.008

[a] with $G_\mathrm{sw,ref}$ taken as the 95% quantile of G_sw

Table 4.3. Median daytime physiological ecosystem properties in the growing season calculated with the `bigleaf` package.

	AT-Neu	DE-Tha	FR-Pue	ES-LMa	ES-LMa$_{grass}$	ES-LMa$_{trees}$
WUE (g C (kg H_2O)$^{-1}$)	4.8	5.2	3.1	2.3	2.7	2.2
IWUE (g C kPa (kg H_2O)$^{-1}$)	5.3	5.4	4.2	3.1	3.4	3.1
uWUE (g C kPa$^{0.5}$ (kg H_2O)$^{-1}$)	5.1	5.3	3.6	2.7	3.0	2.6
G_{sw} (mol m^{-2} s^{-1})	0.301	0.195	0.119	0.157	0.223	0.047
m (mol m^{-2} s^{-1} ln(kPa)$^{-1}$)	0.080	0.091	0.089	0.099	0.067	0.060
b (mol m^{-2} s^{-1})	0.349	0.231	0.184	0.229	0.282	0.094
$G_{0,\mathrm{USO}}$ (mol m^{-2} s^{-1})	0.090	-0.007	-0.015	0.014	0.040	0.034
$G_{1,\mathrm{USO}}$ (kPa$^{0.5}$) [a]	1.4	1.5	2.3	3.5	4.1	2.9
$G_{1,\mathrm{BB}}$ [a]	6.6	7.7	10.4	13.7	14.8	11.9
$G_{1,\mathrm{LEU}}$ [a,b]	5.5	6.0	10.7	9.7	9.0	26.0
D_0 (kPa)	1.7	1.5	0.9	2.1	4.7	0.3
C_i (µmol mol^{-1})	231	213	233	297	316	310
C_i/C_s	0.61	0.57	0.62	0.74	0.79	0.77
$V_{\mathrm{cmax},25}$ (µmol m^{-2} s^{-1})	177.4	135.1	68.9	53.8	55.4	12.0
$J_{\mathrm{max},25}$ (µmol m^{-2} s^{-1})	457.5	188.4	65.1	50.1	83.2	15.4
α (µmol CO_2 m^{-2} s^{-1} (µmol quanta m^{-2} s^{-1})$^{-1}$)	0.106	0.079	0.037	0.037	0.044	0.098
GPP$_{ref}$ (µmol m^{-2} s^{-1}) [c]	34.8	24.0	12.9	12.5	13.8	8.6
LUE (mol mol^{-1})	0.027	0.020	0.010	0.008	0.009	0.002

[a] assuming $g_0 = 0$;   [b] assuming $D_0 = 1.5$ kPa;   [c] at 2000 µmol m^{-2} s^{-1}

4.4 Discussion

4.4.1 Potential and limitations of the 'big-leaf' approach

All calculations implemented in the `bigleaf` package are based on the 'big-leaf' framework (Monteith, 1965; Raupach and Finnigan, 1988), which reduces the ecosystem to a single, uniform plane (Fig. 4.1). This approach thus assumes that vegetation as well as meteorological conditions are vertically and horizontally homogenous. One advantage of the 'big-leaf' approach is that calculations require no additional information on the EC site or commonly available variables only (e.g. LAI, vegetation height). Ecosystem properties are inferred directly from EC measurements, with no assumptions on the underlying ecosystem structure. The 'big-leaf' approach is further applicable to both single-level and two-level EC systems. In the latter case ecosystem properties can be derived for two 'big leafs', e.g. whole ecosystem and understory (Blanken and Black, 2004; Baldocchi et al., 1997) or whole ecosystem and grass layer (this study, Fig. 4.5).

It is important to clarify that the `bigleaf` package exclusively applies a top-down approach, in which the 'big-leaf' framework is used to estimate ecosystem properties inversely from the measured fluxes. The package does not provide bottom-up model formulations, which apply a 'big-leaf' framework to up-scale simulated fluxes from leaf- to canopy-level. This up-scaling approach has been shown to be prone to integration errors (De Pury and Farquhar, 1997; Luo et al., 2018). However, this type of error does not apply to the calculations in the `bigleaf` package because the 'big-leaf' framework is solely used for the derivation of bulk ecosystem properties and no up- or down-scaling is performed.

The fact that the top-down 'big-leaf' approach as applied in this package can only de-

rive bulk ecosystem properties is also its most critical limitation. It is not possible to resolve the vertical distribution of the derived properties. For example, soil and vegetation components cannot be distinguished and the resulting properties will inevitably contain signals from both the soil and the vegetation. These drawbacks can only be circumvented by modeling approaches such as two-layer (soil/canopy) (Shuttleworth and Wallace, 1985; Choudhury and Monteith, 1988) or dual-source (sun/shade) models (De Pury and Far-quhar, 1997), which attempt to resolve the flux contribution of different canopy fractions or ecosystem compartments. These alternative modeling frameworks are more complex and consequently require additional site-specific information (e.g. canopy clumping, canopy ni-trogen profiles, etc.). They are thus mostly applied to a few sites where these additional model parameters are sufficiently well known (e.g. Reichstein et al., 2003; Wolf et al., 2006). The 'big-leaf' framework is thus most suitable for multi-site comparisons or for sites where little ancillary information is available, and where no detailed knowledge on the derived variable (e.g. canopy gradients) is required.

4.4.2 Interpretation of the derived physiological properties

The `bigleaf` package provides functions to calculate ecosystem-scale physiological vari-ables such as G_s, G_1, C_i, V_{cmax}, J_{max}, and GPP_{ref} in the same manner as it is commonly done at leaf-level. Important in this context is that the interpretation of these bulk canopy variables is not as straightforward as that of their leaf-level analogues (see also Knauer et al., 2018). This is due to 1) conceptual uncertainties (as discussed above), and 2) the pres-ence of confounding physical factors. For instance, the intensity of the before-mentioned mixing of soil and vegetation signals increases with a decrease of vegetation density (i.e. LAI) of the ecosystem. Kelliher et al. (1995) for instance showed that G_c is substantially overestimated in ecosystems with an LAI less than approx. 2. This does not mean that the calculation of G_s is meaningless in low-LAI ecosystems, but its physiological interpretation as G_c is increasingly compromised as vegetation cover decreases. For ecosystems with an LAI lower than 2-3, the inversion of a soil/canopy model (Shuttleworth and Wallace, 1985) is likely more appropriate than the inversion of the 'big-leaf' model for the derivation of physiological variables.

In all ecosystems, confounding physical factors, which are non-existent or negligible at leaf-level, must be taken into account in order to extract a meaningful physiological sig-nal. For example, evaporation (i.e. water fluxes not under plant control) occurring after rainfall will lead to an overestimation of the stomatal slope parameter G_1, and thus to an underestimation of WUE, if such time-periods are not filtered out (see Knauer et al., 2018, for an overview of confounding factors and their associated uncertainties).

In general, uncertainties of physiological variables propagate with each calculation step. For example, C_i as calculated by Eq. 4.25 is affected by uncertainties in both input variables G_s and GPP. Photosynthetic parameters are affected by the same uncertainties and in addition by assumptions made for their calculation. It follows that with increasing

number of calculation steps following the derivation of G_s, uncertainties increase and the meaningfulness of the derived variables depends critically on the applied data filtering and the quality of the (original or partitioned) data.

As discussed above, all physiological variables are integrated over the entire canopy and represent bulk canopy properties (expressed in units per ground area instead of leaf area). They are thus not directly comparable to leaf-level measurements taken at a particular location in the canopy. The discrepancies between leaf and ecosystem values will be most pronounced for variables with a distinct profile within the canopy (e.g. V_{cmax} and J_{max} (De Pury and Farquhar, 1997)), and probably less relevant for G_1.

4.4.3   General package usage guidelines

Data filtering

For most applications, it is recommended to apply a basic data filter that removes unreliable measurements or certain meteorological conditions. The optimal type of filter depends on the purpose of the study and the variable of interest. For example, it is advisable to exclude negative λE values from the calculation of G_s in order to minimize the occurrence of negative G_s estimates which are not readily interpretable. Furthermore, periods outside the growing season or following rainfall should be removed if G_s is interpreted in an ecophysiological context. G_a and surface conditions on the other hand can in principle be calculated for all conditions. In general, data that do not fulfill the assumptions of the EC method, or that were gap-filled with low confidence, should be discarded. Depending on the filter settings and the conditions at the site, this can lead to a considerable fraction of missing values in the dataset. This is generally not a problem for the subsequent analyses in this package (missing input data simply return `NA` again), but some (regression-based) functions may require a minimum number of available data in order to return robust results.

Treatment of uncertainties

The derived variables in the `bigleaf` package are affected by several sources of uncertainty, which may be classified as 1) random errors in the measured fluxes (Hollinger and Richardson, 2005; Richardson et al., 2012), 2) systematic errors in the fluxes due to e.g. energy-balance non-closure, advection problems (Leuning et al., 2012; Finnigan, 2008) and 3) conceptual uncertainties. The complex nature of uncertainties in EC measurements and the associated computational challenges to adequately account for and propagate all sources of uncertainty in the derived variables are the main reasons why the `bigleaf` package does not offer uncertainty estimates for each output interval. To account for one or more of the outlined sources of uncertainties, the use of wrapper functions is the most meaningful approach. These functions (often in specialized R packages) apply e.g. Monte Carlo (parameter sensitivity on the derived variables) or bootstrapping (random data sampling with replacement) techniques without the need to modify the functions in `bigleaf`.

Some simple examples on the use of such wrapper functions are given in the vignette of the `bigleaf` package (accessible in `R` with `browseVignettes("bigleaf")`).

Use of the derived properties

The majority of the derived properties in the `bigleaf` package are intended to be primarily diagnostic, i.e. results serve to provide a more mechanistic understanding of the observed fluxes, which enables a more comprehensive analysis and interpretation of ecosystem surface-atmosphere gas exchange. These diagnostics provide additional insights on the underlying physical or physiological processes and are often directly comparable across sites and climatic conditions. Some variables may further be helpful for the parameterization, calibration, or evaluation of bottom-up models. For that purpose, two major prerequisites must be fulfilled: (1) the variable of interest derived with a top-down (inversion) approach must be at the same organizational scale as the one calculated in the bottom-up model, and (2) the framework and the assumptions made in the two approaches must be consistent. For example, both the dynamics and magnitude of the simulated degree of atmosphere-canopy decoupling (Ω) by land surface models can be directly compared with the Ω values derived from this package (De Kauwe et al., 2017). This also applies to other characteristics such as G_a, G_s, or WUE and LUE metrics that are simulated as (emergent) bulk surface properties in models. In contrast, physiological bulk canopy parameters such as C_i should not be compared to leaf-level c_i values as simulated by multi-layer models. Likewise, bulk canopy or $V_{cmax,25}$ cannot be used to parameterize leaf-level $v_{cmax,25}$ in multi-layer models. In any case, it is imperative that uncertainties specific to the EC-method (as summarized in the previous section) are taken into account when derived properties are used for bottom-up modeling purposes.

4.5 Conclusions

The presented R package `bigleaf` provides a framework for the derivation of physical and physiological ecosystem properties at EC sites in a consistent and reproducible manner and with minimal requirements regarding ancillary site data. The package thus has the potential to increase the comparability of the provided calculations as well as their applicability across sites. The functions will be useful in complementing the analysis of land-atmosphere mass and energy fluxes by providing a basic level of process understanding. The availability of additional ecosystem surface characteristics as provided by the `bigleaf` package will be key in interpreting ever-increasing records of EC data and the responses of land-atmosphere exchange to global environmental change. The open source and version control environment further enable the continuous development of the package and encourage community input.

Acknowledgements

5 Effects of mesophyll conductance on vegetation responses to elevated CO$_2$ concentrations

This chapter is a copy-edited version of the following submitted article:

Jürgen Knauer[1,2], Sönke Zaehle[1,3], Martin G. De Kauwe[4], Nur H.A. Bahar[5], John R. Evans[6], Belinda E. Medlyn[7], Markus Reichstein[1,3], Christiane Werner[8]. **Effects of mesophyll conductance on vegetation responses to elevated CO$_2$ concentrations in a land surface model.** Under review in *Global Change Biology*, submitted on 07. September 2018.

[1] Department of Biogeochemical Integration, Max Planck Institute for Biogeochemistry, 07745 Jena, Germany;

[2] International Max Planck Research School for Global Biogeochemical Cycles (IMPRS gBGC), 07745 Jena, Germany;

[3] Michael-Stifel Center Jena for Data-Driven and Simulation Science, 07745 Jena, Germany;

[4] ARC Centre of Excellence for Climate Extremes and the Climate Change Research Centre, University of New South Wales, Sydney, 2052, NSW, Australia;

[5] ARC Centre of Excellence in Plant Energy Biology, Division of Plant Sciences, Research School of Biology, Australian National University, Canberra, 2601, ACT, Australia;

[6] ARC Centre of Excellence for Translational Photosynthesis, Division of Plant Sciences, Research School of Biology, Australian National University, Canberra, 2601, ACT, Australia;

[7] Hawkesbury Institute for the Environment, Western Sydney University, Richmond, 2751, NSW, Australia;

[8] Department of Ecosystem Physiology, University of Freiburg, 79110 Freiburg, Germany

Abstract

Mesophyll conductance (g_m) is known to affect plant photosynthesis. However, g_m is rarely explicitly considered in land surface models (LSMs), with the consequence that its role in ecosystem and large-scale carbon and water fluxes is poorly understood. In particular, the different magnitudes of g_m across plant functional types (PFTs) are expected to cause spatially divergent vegetation responses to elevated CO$_2$ concentrations. Here, an extensive literature compilation of g_m across major vegetation types is used to parameterize an empirical model of g_m in the LSM JSBACH and to adjust photosynthetic parameters based on simulated $A_n - c_i$ curves. We demonstrate that an explicit representation of g_m changes the response of photosynthesis to environmental factors, which cannot be entirely compensated by adjusting photosynthetic parameters. These altered responses lead to changes in the photosynthetic sensitivity to atmospheric CO$_2$ concentrations which depend both on the magnitude of g_m and the climatic conditions, particularly tempera-

ture. We then conducted simulations under ambient and elevated (ambient + 200 µmol mol^{-1}) CO_2 concentrations for contrasting ecosystems and for historical and anticipated future climate conditions (representative concentration pathways; RCPs) globally. The g_m-explicit simulations using the RCP8.5 scenario resulted in significantly higher increases in gross primary productivity (GPP) in high latitudes (+10-25%), intermediate increases in temperate regions (+5-15%), and slightly lower to moderately higher responses in tropical regions (-2-5%), which summed up to moderate GPP increases globally. Similar patterns were found for transpiration, but with a lower magnitude. Our results suggest that the effect of an explicit representation of g_m is most important for simulated carbon and water fluxes in the boreal zone, where a cold climate coincides with evergreen vegetation.

5.1 Introduction

The representation of photosynthesis in land surface models (LSMs) is critical for simulating the response of the terrestrial biosphere to global environmental change (Booth et al., 2012; Rogers et al., 2017), accurately simulating the land uptake of CO_2 as well as the coupling of the water and carbon cycles. The photosynthesis schemes embedded within state-of-the-art LSMs commonly assume that the CO_2 concentration available for carboxylation equals the CO_2 concentration in the sub-stomatal cavity, i.e. the intercellular CO_2 concentration (c_i). This corresponds to the assumption that the conductance to CO_2 transfer within the leaf (mesophyll conductance, g_m) is infinite, and that the CO_2 concentration at the actual place of carboxylation in the chloroplast stroma (chloroplastic CO_2 concentration, c_c) equals c_i. However, recent evidence has clearly shown that g_m is finite (Flexas et al., 2008; Warren, 2008) and that it causes a clear drawdown of the CO_2 concentration between the sub-stomatal cavity and the chloroplast stroma. The magnitude of this drawdown depends both on g_m and the photosynthetic capacity of the leaf, as can be seen from the definition of g_m: $g_m = A_n/(c_i\text{-}c_c)$, where A_n is net photosynthesis. Replacing c_i with c_c as the available CO_2 concentration for photosynthesis has been shown to change the response of simulated photosynthesis to environmental drivers (Niinemets et al., 2009b), which has important implications for large-scale simulations of land carbon uptake (Sun et al., 2014b). g_m is a complex physiological property which integrates several leaf-internal sub-conductances in both the gaseous and liquid phase, including the intercellular airspace, cell walls, plasma membranes, cytoplasm, and the chloroplast envelopes and stroma (Evans et al., 2009). g_m is known to change dynamically in response to several environmental stimuli at the time scale of minutes (Warren, 2008). At the same time, its absolute magnitude is constrained by leaf anatomical and structural traits (e.g. cell wall thickness, chloroplast surface area attached to the intercellular airspaces), with the consequence that the values of g_m differ considerably among vegetation types (Flexas et al., 2008). Despite its important role in photosynthesis and the distinct differences across plant functional types, g_m is at present not explicitly considered in the vast majority of LSMs for two main reasons: (1) the current process understanding of g_m is severely lim-

ited (Rogers et al., 2017) as its response to environmental drivers, foremost light and CO_2 concentration but also temperature, is largely unknown and currently an area of intensive research (Tazoe et al., 2009; Gu and Sun, 2014; von Caemmerer and Evans, 2015; Xiong et al., 2015; Théroux-Rancourt and Gilbert, 2017), and (2) the effects of g_m are implicitly included in current models since the overestimation of CO_2 available for photosynthesis is compensated for by an underestimated (apparent) photosynthetic capacity. This means that parameters representing photosynthetic capacity, which are currently estimated on a c_i-basis, would need to be re-estimated on a c_c-basis if g_m were to be explicitly considered in models (Sun et al., 2014a). It is likely for these two complications that so far only one study (Sun et al., 2014b) focused on the effects of an explicit representation of g_m in a LSM (the Community Land Model 4.5). Sun et al. (2014b) showed that the overestimation of the available CO_2 concentration for photosynthesis due to the assumption of an infinite g_m leads to an underestimation of the photosynthetic sensitivity to rising atmospheric CO_2 concentrations (c_a). As a consequence, replacing the implicit simulation of g_m with an explicit one significantly increased the responsiveness of gross primary productivity ($+16\%$ from 1901-2010) to rising c_a as long as c_a was not saturating. The stronger response of photosynthesis to rising atmospheric CO_2 concentrations with an explicitly modeled g_m as shown in the study by Sun et al. (2014b) implies that the physiological responses to rising atmospheric CO_2 concentrations will vary among plant groups that have intrinsically different values of g_m. Consequentially, it might be hypothesized that photosynthesis of plants with a low g_m (e.g. evergreen species) are more responsive to rising atmospheric CO_2 concentrations than plants with a higher g_m (e.g. herbaceous plants), which potentially gives the former plant group a relative advantage over the latter in a high CO_2 world (Niinemets et al., 2011). A stronger response of photosynthesis to c_a is likely to also affect stomatal conductance (g_s) given that g_s and A_n are tightly coupled (Wong et al., 1979). As a consequence, the consideration of g_m is expected to have important implications for both terrestrial carbon and water fluxes, as well as their coupling (e.g. water-use efficiency Flexas et al., 2016). Such plant type-specific physiological responses would thus not only have important implications for the future global distribution of vegetation types, but also for large-scale patterns of biogeochemical cycles and associated physical climate feedbacks (e.g. evaporative cooling). In this paper, we explore whether g_m has implications for simulations of future global carbon and water fluxes, and to what extent the effects are expected to differ among vegetation types and climatic conditions. In the following, we (1) compile a global database of g_m measurements, (2) describe the g_m model and its incorporation into the land surface model JSBACH (Reick et al., 2013; Knauer et al., 2015), (3) outline the model parameterization and the necessary adjustment of photosynthetic parameters, (4) analyze the effects of an explicit g_m on the photosynthetic sensitivity to C_a at the leaf- and ecosystem level, and (5) investigate its relevance for future carbon and water fluxes globally.

5.2 Methods

To investigate the effects of g_m on simulations of water and carbon fluxes, we tested two different approaches in the LSM JSBACH:

Implicit g_m: Effects of g_m are considered implicitly by employing apparent (c_i-based) photosynthetic parameters. This represents the current scenario in most LSMs. Rubisco kinetic parameters were taken from Bernacchi et al. (2001). This model version is denoted as *Imp*.

Explicit g_m: g_m is modeled explicitly as described in section 5.2.1. Rubisco kinetic constants were taken from Bernacchi et al. (2002), and were determined on a c_c-basis. Four sub-versions (denoted as *Exp*, *ExpC*, *ExpL*, *ExpCL*) were implemented, which differ with respect to whether g_m is affected by c_i and/or light (Table 5.1). The effect of these two factors is contentious in the literature (Gu and Sun, 2014; Théroux-Rancourt and Gilbert, 2017), hence it is relevant to investigate their potential sensitivities to simulations of photosynthesis at the leaf to the global scale.

Table 5.1. Environmental responses considered in the g_m model versions implemented in this study.

Model version	Temperature	Soil moisture	Canopy profile	Intercellular CO_2 concentration	Light
Exp	x	x	x		
ExpC	x	x	x	x	
ExpL	x	x	x		x
ExpCL	x	x	x	x	x

Note that the two approaches differ only in the assumed values of g_m and the Rubisco kinetic parameters (Michaelis-Menten constants for CO_2 (K_c) and O_2 (K_o), photorespiratory CO_2 compensation point (Γ_*)) as well as their temperature responses (see Table C1 for parameter values).

5.2.1 Mesophyll conductance model

The g_m model implemented here is a multiplicative formulation, in which a PFT-specific maximum (i.e. unstressed) value of g_m at the reference temperature of 25°C ($g_{m,max25}$) is modified by environmental factors:

$$g_m = g_{m,max25} f_1(N) f_2(T_l) f_3(\Theta) f_4(c_i) f_5(\text{aPPFD}) \tag{5.1}$$

Where N is leaf nitrogen content, T_l is leaf temperature, Θ is soil moisture content, c_i is intercellular CO_2 concentration, aPPFD is absorbed photosynthetic photon flux density, and f denotes 'function of'. In Eq. 5.1, $g_{m,max25}$ and f_1 represent leaf structural determinants of g_m, whereas $f_2 - f_5$ describe instantaneous physiological responses. Note that the last two terms in Eq. 5.1 (f_4 and f_5) are not considered in all model versions (Table 5.1).

Canopy profile

g_m generally declines with depth through the canopy, and is usually higher in sun than in shade leaves (Hanba et al., 2002; Piel et al., 2002). It has been found that g_m varies in a similar manner to photosynthetic capacity (or N) across the canopy profile (Montpied et al., 2009). This decline with canopy depth might be related to the relatively low mesophyll thickness and the lower chloroplast surface area exposed to the intercellular airspaces in shade-adapted leaves (Evans et al., 1994; Hanba et al., 2002). Here, we implemented the following canopy profile of g_m:

$$f_1(N) = e^{-k_n \text{LAI}} \tag{5.2}$$

Where k_n is the canopy nitrogen extinction coefficient and LAI is the leaf area index. k_n was assumed to be 0.11 following Zaehle and Friend (2010). Thus, the canopy gradient of g_m equals the one of V_{cmax} and J_{max} in the model. Such a behavior was confirmed by several studies (Warren et al., 2007; Montpied et al., 2009; Han et al., 2010), but also higher (Zhang and Yin, 2012) and lower (Cano et al., 2011) gradients for g_m compared to V_{cmax} have been found, suggesting that k_n is site- and probably PFT-specific (Warren et al., 2007).

Temperature response

The temperature response of g_m is the result of different physical and physiological processes in mesophyll cells (e.g. solubility and diffusivity of CO_2 in water), and the response is likely to differ across cell compartments, e.g. membranes and cell walls (Evans and Von Caemmerer, 2013). The overall response of g_m to leaf temperature can be described by a modified Arrhenius function (Johnson et al., 1942):

$$f_2(T_l) = \exp\left(\frac{H_a(T_l - T_{ref})}{T_{ref}RT_l}\right) \frac{1 + \exp\left(\dfrac{T_{ref}\Delta S - H_d}{T_{ref}R}\right)}{1 + \exp\left(\dfrac{T_l\Delta S - H_d}{T_l R}\right)} \tag{5.3}$$

where H_a is the activation energy (J mol^{-1}), H_d is the deactivation energy (J mol^{-1}), ΔS is the entropy term (J mol^{-1} K^{-1}), T_l is the leaf temperature (K), T_{ref} is the reference temperature (298.15 K), and R is the universal gas constant (8.314 J mol^{-1} K^{-1}). Eq. 5.3 was parameterized according to Bernacchi et al. (2002) and shows a temperature optimum close to 35.5°C. The use of the parameter values reported in Bernacchi et al. (2002) is consistent with the c_c-based Rubisco kinetic constants used in this study (K_o, K_c, Γ_*), which were derived assuming the same temperature response of g_m (Eq. 5.3). Published temperature responses of g_m differ with respect to the behavior at high temperatures, and both hump-shaped (Egea et al., 2011b), as well as monotonously increasing responses (Scafaro et al., 2011) have been documented. Similarly, H_a is likely to be species-specific (Walker et al., 2013), though no clear patterns across species and growth conditions have

been identified (von Caemmerer and Evans, 2015). Thus, parameters in Eq. 5.3 were assumed to be identical for all vegetation types.

Soil moisture response

The decline of g_m with increasing soil water stress has been widely reported (e.g. Galmés et al., 2007; Misson et al., 2010; Varone et al., 2012), and has been attributed to the role of aquaporins in leaf-internal CO_2 transport (Perez-Martin et al., 2014). Here, we implemented the following soil moisture dependence of g_m:

$$f_3(\Theta) = \begin{cases} 1 & \Theta \geq \Theta_{crit} \\ \left[\frac{\Theta - \Theta_{wilt}}{\Theta_{crit} - \Theta_{wilt}}\right]^{q_m} & \Theta < \Theta_{crit} \\ f_{min} & \Theta \leq \Theta_{wilt} \end{cases} \tag{5.4}$$

Where Θ is soil moisture (m), Θ_{wilt} is the permanent wilting point (m), below which water stress is at its maximum, and Θ_{crit} is the critical soil moisture content (m), which marks the onset of soil water stress. f_{min} denotes the minimum possible g_m as a fraction of $g_{m,max25}$ ($f_{min} = 0.15$ for all PFTs). Eq. 5.4 is applied to g_s, g_m, and leaf biochemistry (V_{cmax} and J_{max}) but with different sensitivities (i.e. different values of the exponent q). Using the same formulation, Egea et al. (2011a) found that imposing the highest sensitivity to g_m, then to g_s, and finally to V_{cmax} and J_{max} best captured the behavior of photosynthesis under water stressed conditions. The q parameters were defined accordingly as $q_m = 0.75$, $q_s = 0.50$, and $q_b = 0.25$ for all PFTs.

Response to intercellular CO_2 concentration

Most studies investigating the response of g_m to c_i have found a continuous decrease of g_m with increasing c_i under field conditions (i.e. c_i above c. 200 µmol mol^{-1}) (Flexas et al., 2007; Hassiotou et al., 2009; Xiong et al., 2015), but see Tazoe et al. (2009)). However, there is currently no physiological explanation to link the response of g_m to c_i, and some concerns on the reliability of these measurements have been raised (Gu and Sun, 2014). We have implemented a c_i response function which was derived empirically based on leaf-level measurements as shown in Fig. C6:

$$f_4(c_i) = f_{min} + 1.5(1 - e^{(-c_i/38)})e^{(-c_i/460)} \tag{5.5}$$

Eq. 5.5 describes an abrupt increase of g_m at low c_i (until approx. 100 µmol mol^{-1}), and an exponential decline thereafter (Fig. C6).

Light response

The effect of absorbed radiation on g_m and the underlying mechanisms driving this potential response are currently unresolved. Studies in which g_m was measured at different

light levels have reported either no clear responses of g_m to variations in light (Tazoe et al., 2009; Yamori et al., 2010; Loucos et al., 2017), or clear increases with light (Yin et al., 2009; Douthe et al., 2012; Cai et al., 2017) (see Fig. C7). The following function was used to simulate the potential effects of light on g_m:

$$f_5(\text{aPPFD}) = 1 - (1 - f_{\min})e^{-0.003\text{aPPFD}} \tag{5.6}$$

where aPPFD is absorbed photosynthetic photon flux density (μmol m^{-2} s^{-1}). Eq. 5.6 corresponds to a light response curve that takes the values of approx. $f_{\min}$ and approx. 1 at PPFD values of 0 and 1500 μmol m^{-2} s^{-1}, respectively (see Fig. C7). The function corresponds to a steep increase of g_m at low aPPFD, a relative g_m of 0.8 at approx. 500 μmol m^{-2} s^{-1} and a shallow response at high aPPFD.

5.2.2 C4 plants

In C4 plants, g_m describes the conductance to CO_2 transfer from the intercellular airspace to the cytosol of the mesophyll cells only, where the first binding of CO_2 occurs. Thus, the main difference to C3 plants is that the chloroplast components are not part of the diffusion pathway (von Caemmerer and Furbank, 1999). This means that g_m in C4 plants causes a CO_2 concentration drawdown from c_i to c_m, the CO_2 concentration in the mesophyll cytosol (i.e. $g_m = A_n/(c_i - c_m)$). Recent methodological advances have enabled measurements of g_m in C4 plants (Barbour et al., 2016; Ubierna et al., 2016). These measurements indicate that g_m is considerably higher in C4 plants than in C3 plants (see Fig. 5.1). The response of g_m to environmental factors was assumed to be identical to that in C3 plants (Eqs. 5.2-5.6). This assumption could not be confirmed due to the scarcity of g_m measurements in C4 plants, but recent studies indicate that the temperature as well as the c_i response are qualitatively similar to that in C3 plants (Ubierna et al., 2016; Kolbe and Cousins, 2017). C4 photosynthetic parameter ratios were kept constant as in von Caemmerer and Furbank (1999) (see Table C1).

5.2.3 Implementation into the land surface model JSBACH

The developed g_m model was incorporated into the LSM JSBACH (Reick et al., 2013; Knauer et al., 2015), which is the land component of the MPI Earth system model (Giorgetta et al., 2013). Vegetation in JSBACH is classified into plant functional types (PFTs), which differ with respect to key physiological and biophysical properties. Land-atmosphere water fluxes are calculated with a bulk transfer approach (Schulz et al., 2001), and A_n, as well as g_s and g_m are scaled to canopy-level with the LAI. Canopy radiative transfer is modeled as described in Wang (2003) based on the model of Goudriaan (1977) and considers sun-lit and shaded canopy fractions in nine vertical layers. g_s is modeled according to Medlyn et al. (2011) with PFT-specific stomatal slope parameters (g_1) taken from Lin et al. (2015). A_n is simulated according to Farquhar et al. (1980) and von Caemmerer and Furbank (1999) for C3 and C4 vegetation, respectively. In the photosynthesis routine of the

model, g_m is calculated first according to Eq. 5.1, and A_n, g_s, c_i, and c_c are subsequently solved iteratively.

5.2.4 Maximum mesophyll conductance values ($g_{m,max25}$)

To parameterize the key parameter in the model, $g_{m,max25}$ (Eq. 5.1), we compiled an extensive literature review of leaf-level g_m-measurements. This dataset (available online at `https://bitbucket.org/juergenknauer/gm_data`) comprises 609 individual g_m measurements of 319 species from 295 studies. Measurements were performed using all common methods used to estimate g_m (see e.g. Pons et al., 2009) and represent unstressed, fully expanded, and sun-exposed leaves. If necessary, measurements were converted to units of mol m^{-2} s^{-1} and standardized to 25°C using Eq. 5.3. If g_m was assumed to be light-dependent (model versions *ExpL* and *ExpCL*), measurements were standardized to high light (1500 µmol m^{-2} s^{-1}) according to Eq. 5.6. If g_m was assumed to be c_i dependent (model versions *ExpC* and *ExpCL*), $g_{m,max25}$ was adjusted according to the c_i measured along with g_m. This adjustment accounts for the fact that different vegetation types operate at different c_i/c_a. The g_m values were assigned to PFTs and the mean, median and standard error of the median were calculated (see Fig. 5.1, Table 5.3). More details on the conducted literature survey and the subsequent analysis can be found in chapter C.

5.2.5 Adjustment of c_i-based to c_c-based photosynthetic parameters

The explicit representation of g_m in photosynthesis models requires that photosynthetic parameters represent c_c-based rather than c_i-based values, as the latter implicitly include the effects of g_m (Ethier and Livingston, 2004). This typically requires that existing (i.e. c_i-based) parameters are adjusted to c_c-based parameters. Previous approaches for this parameter adjustment focused on the simultaneous derivation of g_m, V_{cmax} and J_{max} from $A_n - c_i$ curves using curve fitting techniques (Gu et al., 2010; Sun et al., 2014a). An alternative approach as applied in this study makes use of independent g_m estimates which allow the conversion of $A_n - c_i$ curves to $A_n - c_c$ curves and the subsequent re-estimation of photosynthetic parameters on a c_c basis. This alternative approach consists of three main steps (illustrated in Fig. C1; R code available at `https://bitbucket.org/juergenknauer/gm_data`):

1. Simulation of a PFT-specific $A_n - c_i$ curve under unstressed conditions, saturating light, and 25°C using the current (implicit g_m) photosynthesis routine of the model with c_i-based Rubisco parameters from Bernacchi et al. (2001). Under these conditions, g_m is assumed to equal $g_{m,max25}$.

2. Calculation of c_c from Fick's first law: $c_c = c_i - A_n/g_m$ and construction of the corresponding $A_n - c_c$ curve. Depending on whether g_m is assumed to be independent of c_i or not, g_m is either assumed to be constant or a function of c_i (Eq. 5.5).

3. Simultaneous fitting of V_{cmax25} and J_{max25} to the $A_n - c_c$ curve calculated in Step 2 using the same model as in step 1, but with c_c-based Rubisco parameters taken from Bernacchi et al. (2002). The fitting is done with a non-linear regression routine.

Compared to parameter adjustments based on measured $A_n - c_i$ curves, this approach has the advantage of being universally applicable across model types and model structures, and to both C3 and C4 photosynthesis models. This is achieved by an internally consistent parameter adjustment which is ensured by the employment of the exact same photosynthesis model and parameter values (e.g. leaf day respiration, Γ_*) for both the parameter adjustment and the actual simulations. In addition, this approach circumvents uncertainties associated with the determination of g_m from $A_n - c_i$ curves (e.g. assignment of limitation states) by taking independent g_m measurements. It follows that no raw data (i.e. $A_n - c_i$ curves) are required, but instead a sufficient number of g_m measurements, from which representative estimates of g_m can be inferred.

5.2.6 Site-level simulations

The JSBACH model was run for eight eddy covariance sites within the FLUXNET network. The sites were selected to cover different PFTs and contrasting hydro-climates (Table 5.2). Flux and forcing data for all sites are freely available from the FLUXNET2015 webpage (`http://fluxnet.fluxdata.org/data/fluxnet2015-dataset/`; accessed 2017-11-09). All sites were run with meteorological forcing from the flux towers. Vegetation height, roughness length, and LAI were adjusted according values reported in the literature, and c_i-based photosynthetic capacity ($V_{cmax25,ci}$ and $J_{max25,ci}$) was adjusted to match the flux measurements. $g_{m,max25}$ was calculated as the cover fraction-weighted $g_{m,max25}$ values of the PFTs present at the site. For all sites, all model versions (*Imp, Exp, ExpC, ExpL, ExpCL*) were forced with (1) observed meteorological conditions and (2) elevated CO_2 concentrations (ambient + 200 µmol mol^{-1}), and the same meteorological forcing as in the ambient CO_2-runs.

5.2.7 Global simulations

To investigate the large-scale implications of an explicit representation of g_m in JSBACH, we conducted global runs for the *Imp, Exp*, and *ExpCL* model versions under historic (1970-2004) and projected future conditions (2070-2100). Bias-corrected daily meteorological forcing (0.5° spatial resolution) for both the historic and future runs was obtained from the Inter-Sectoral Impact Model Intercomparison Project (ISIMIP) (Hempel et al., 2013; Frieler et al., 2017), using output from the HadGEM2-ES model (Martin et al., 2011). Future runs were conducted with RCP4.5 and RCP8.5 scenarios. Land cover was obtained from Pongratz et al. (2007) and assumed to be unchanged in the historic and future runs. $g_{m,max25}$ as well as V_{cmax25} and J_{max25} parameter values are listed in Table 5.3.

Table 5.2. Characteristics of eddy covariance sites used in this study.

Site	Vegetation type	Simulation period	MAP[a] (mm)	MAT[b] (°C)	Max. LAI	Vegetation height (m)	$V_{cmax25,ci}$ (µmol m^{-2} s^{-1})	$g_{m,max25}$ (mol m^{-2} s^{-1})	Site reference
AT-Neu	C3 grasses/herbs	2008-2012	852	6.3	6	0.5	70	0.197	Wohlfahrt et al. (2008)
DE-Geb	C3 crops	2005-2014	470	8.5	5	0.5	39	0.295	Kutsch et al. (2010)
FI-Hyy	Evergreen needle-leaf forest	1996-2014	709	3.8	3.3	14	41	0.09	Vesala et al. (2005)
FR-LBr	Evergreen needle-leaf forest	2003-2008	900	13.6	3.1	18	42	0.09	Berbigier et al. (2001)
FR-Pue	Evergreen broadleaf forest	2005-2014	883	13.5	3.3	5.5	24	0.106	Rambal et al. (2003)
GF-Guy	Tropical rain-forest	2006-2014	3041	25.7	7	35	36	0.152	Bonal et al. (2008)
US-Ha1	Deciduous broadleaf forest	1992-2012	1071	6.6	4.9	23	45	0.176	Urbanski et al. (2007)
US-Ne1	C4 crops (irrigated maize)	2002 - 2012	790	10.1	6	3	32	0.739	Verma et al. (2005)

[a] mean annual precipitation

[b] mean annual temperature

5.3 Results

5.3.1 Unstressed g_m values across PFTs

Fig. 5.1 shows the results of the literature review, revealing distinct patterns in unstressed g_m across PFTs. Lowest values were found in needle-leaf and evergreen broadleaf trees, followed by tropical evergreen trees and deciduous broadleaf trees. Generally, herbaceous species had higher g_m values than woody species. Within herbaceous PFTs, crops had higher g_m values than grasses and wild herbs, and C4 plants had significantly higher values than C3 plants. The number of measurements is unequally distributed among the PFTs and 87% of all measurements were performed in only four PFTs (C3C, EBF, C3G, DBF). It follows that most PFTs are poorly sampled and the corresponding g_m measurements are less robust than in the well-sampled PFTs. However, the four highly sampled PFTs also show a large spread, reflecting the large range of g_m values among different species within each PFT. Results in Fig. 5.1 show g_m values that were not standardized to a given c_i or to high light. Accounting for a potential response of g_m to light or c_i led to only minor changes in the magnitude of g_m and its pattern across PFTs (Tables 5.3, C4).

5.3.2 Parameter adjustment

The required parameter adjustment procedure as described in section 5.2.5 led to significant changes to the two key photosynthetic parameters in the model, V_{cmax25} and J_{max25} (Table 5.3). The c_c-based parameters ($V_{cmax25,cc}$ and $J_{max25,cc}$) account for the lower available CO_2 concentration due to the effects of g_m, and are thus usually higher than their c_i-based counterparts. For all PFTs, V_{cmax25} is more strongly affected than J_{max25}, which results in a decrease of the J_{max25}/V_{cmax25} ratio. The difference between the c_i-based
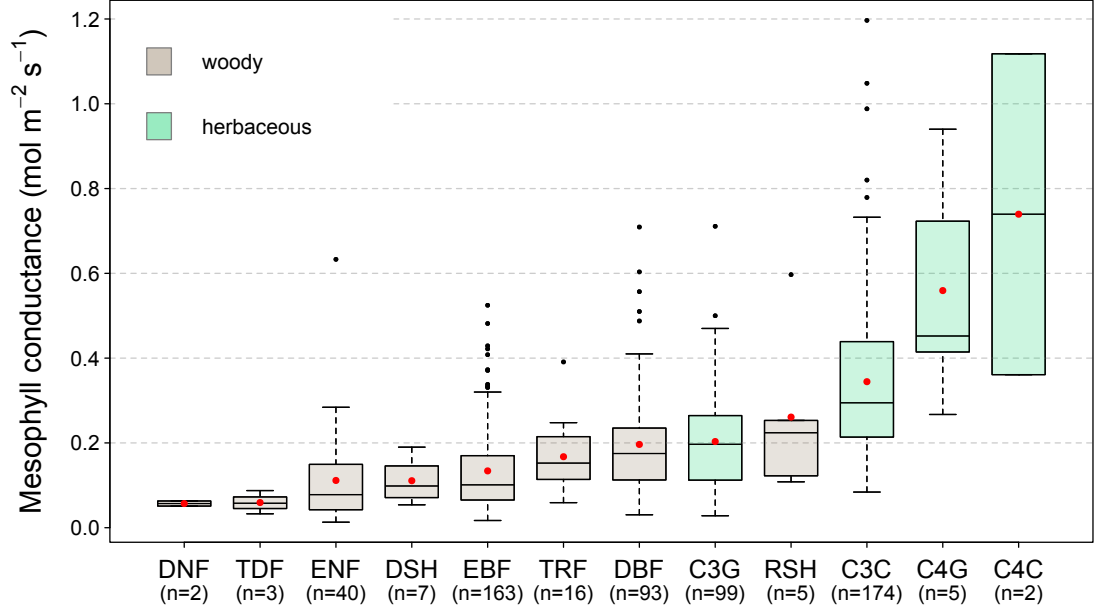
Fig. 5.1. Maximum (unstressed) mesophyll conductance values for different Plant Functional Types (PFTs) at 25°C. Horizontal lines within boxes represent medians, red dots represent means, the lower and upper boundaries of the boxes represent the first and third quantile, respectively, and whiskers represent 1.5 times the interquartile range. PFT abbreviations are: DNF = deciduous needle-leaf trees, TDF = tropical deciduous trees, ENF = evergreen needle-leaf trees, DSH= deciduous shrubs, EBF = evergreen broadleaf trees/shrubs, TRF = tropical evergreen trees, DBF = deciduous broadleaf trees, C3G = C3 herbs and grasses, RSH = raingreen shrubs, C3C = C3 crops, C4G = C4 grasses and herbs, C4C = C4 crops.

and c_c-based parameters depends both on the magnitude of g_m and the magnitude of $V_{cmax25,ci}$ and $J_{max25,ci}$, and are highest when g_m is low and photosynthetic capacity is high (as e.g. in ENF). The decrease of the $J_{max25,cc}/V_{cmax25,cc}$ ratio leads to a shift of the inflection point (the c_i where photosynthetic limitation changes from Rubisco-limited to RuBP (ribulose-1,5-bisphosphate)-limited) to lower c_i, which is associated with a higher fraction of photosynthesis occurring in the electron transport-limited domain (see e.g. Fig. C1).

In the model versions where g_m is affected by c_i (*ExpC* and *ExpCL*), g_m is assumed to change throughout the $A_n - c_i$ curve according to Eq. 5.5, i.e. increases sharply at low c_i and decreases continuously thereafter. By accounting for this potential response, the re-adjusted photosynthetic parameters, in particular $J_{max25,cc}$, are considerably higher compared to the default version (*Exp*). To compensate for the low g_m simulated at higher c_i where RuBP-regeneration is limiting, $J_{max25,cc}$ needs to be greater in order to maintain the same A_n as in the implicit case. This results in significantly higher $J_{max25,cc}/V_{cmax25,cc}$ ratios compared to the explicit model versions (Table 5.3). The model versions accounting for a light response of g_m (*ExpL* and *ExpCL*) do not show systematic deviations from the corresponding versions without a light response (*Exp* and *ExpC*, respectively; see Table C4).

Table 5.3. $g_{m,max25}$, c_i-based and c_c-based V_{cmax25} and J_{max25}, and J_{max25}/V_{cmax25} ratios for different plant functional types (PFTs) in the JSBACH model and for the *Exp* and *ExpC* model versions. Adjustments of c_i- to c_c-based parameters were performed as described in section 5.2.5. $V_{cmax25,ci}$ were taken from Kattge et al. (2009), and if applicable re-calculated based on N_a (leaf nitrogen per area) data in Kattge et al. (2011). PFT abbreviations are as in Fig. 5.1

PFT	$g_{m,max25} \pm$ SEM[a] (mol m^{-2} s^{-1})	$V_{cmax25,ci}$ (µmol m^{-2} s^{-1})	$J_{max25,ci}$ (µmol m^{-2} s^{-1})	$J_{max25,ci}/V_{cmax25,ci}$	$V_{cmax25,cc}$ (µmol m^{-2} s^{-1})	$J_{max25,cc}$ (µmol m^{-2} s^{-1})	$J_{max25,cc}/V_{cmax25,cc}$	$g_{m,max25}$[b] (mol m^{-2} s^{-1})	$V_{cmax25,cc}$ (µmol m^{-2} s^{-1})	J_{max25} (µmol m^{-2} s^{-1})	$J_{max25,cc}/V_{cmax25,cc}$
	Exp	*Imp*	*Imp*	*Imp*	*Exp*	*Exp*	*Exp*	*ExpC*	*ExpC*	*ExpC*	*ExpC*
DNF	0.057 ± 0.008	33.1	62.9	1.9	59.3	65	1.1	0.054	68.1	89.9	1.32
TDF	0.058 ± 0.020	31	58.9	1.9	49.8	60.4	1.21	0.056	50.4	76.9	1.41
ENF	0.078 ± 0.021	52.7	100.1	1.9	118.8	105.5	0.89	0.074	113.3	145.3	1.28
DSH	0.098 ± 0.025	49.8	94.7	1.9	75.7	96.9	1.28	0.1	78.1	112.1	1.44
EBF	0.101 ± 0.010	61.4	116.7	1.9	117.8	121.1	1.03	0.1	126.7	167.4	1.32
TRF	0.152 ± 0.026	39	74.1	1.9	42.1	74.1	1.76	0.151	43.7	76.9	1.76
DBF	0.175 ± 0.016	52.1	98.9	1.9	58.6	99.2	1.69	0.172	61.3	104.2	1.7
C3G	0.197 ± 0.015	50.1	95.2	1.9	54	95.1	1.76	0.198	55.8	98.7	1.77
RSH	0.224 ± 0.111	49.8	94.7	1.9	52.1	94.4	1.81	0.23	53.6	97.3	1.82
C3C	0.295 ± 0.017	80.2	152.4	1.9	87.9	152.5	1.73	0.305	90.3	158.5	1.76
		$V_{pmax25,ci}$ (µmol m^{-2} s^{-1})			$V_{pmax25,cc}$ (µmol m^{-2} s^{-1})				$V_{pmax25,cc}$ (µmol m^{-2} s^{-1})		
C4G	0.452 ± 0.151	40			118.9			0.382	189		
C4C	0.739 ± 0.474	60			145.4			0.62	193.6		

[a] standard error of the median

[b] standardized to a c_i of 260 µmol mol^{-1} (Eq. 5.5)

95

In the C4 photosynthesis model described by von Caemmerer and Furbank (1999), the only parameter affected by the parameter adjustment is the maximum PEP-carboxylation rate (V_{pmax25}) (see Fig. C2). In case of a $g_{\mathrm{m,max25}}$ of 0.739 mol m^{-2} s^{-1}, the median value observed in C4 crops, V_{pmax25} increases strongly from 60 (c_i-based) to approx. 145 µmol m^{-2} s^{-1} (c_m-based; Table 5.3).

5.3.3 Effects on simulated leaf-level photosynthesis
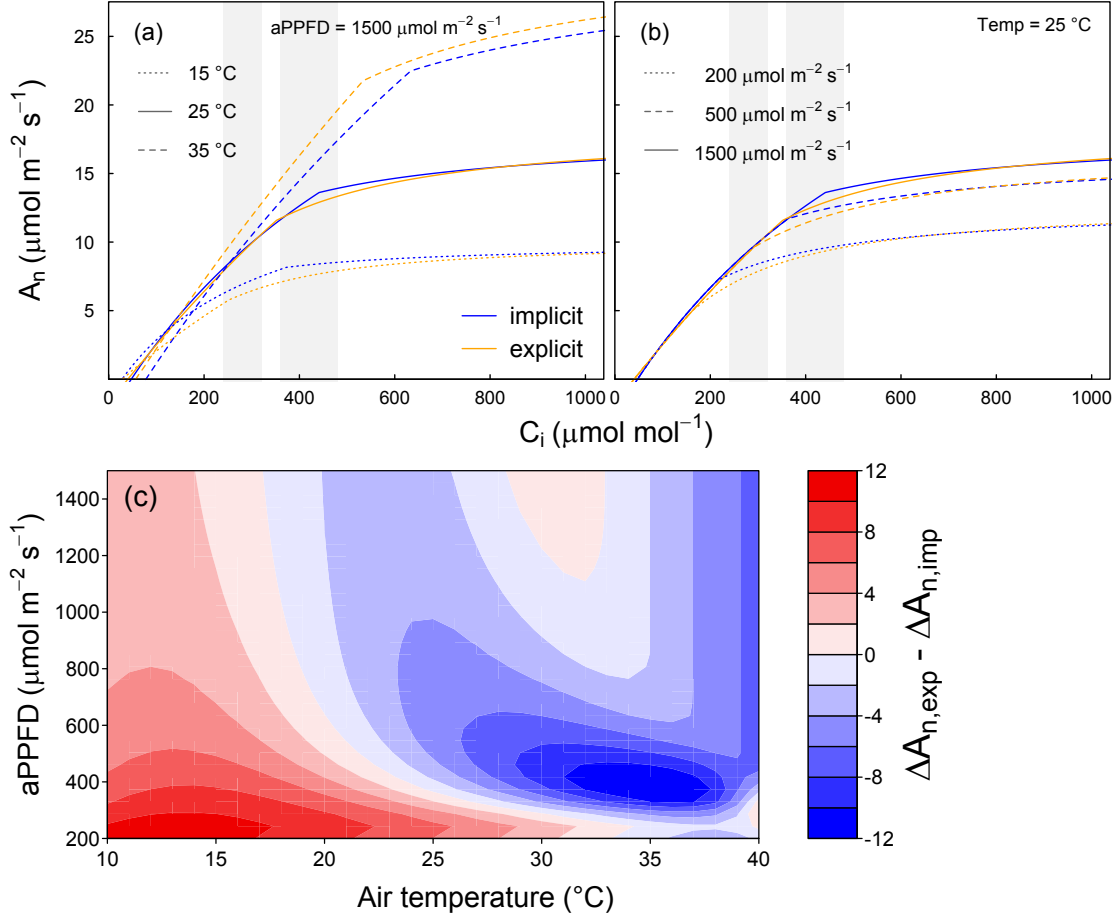
Fig. 5.2. (a) $A_n - c_i$ curves for the implicit (blue) and explicit (orange) model versions for three different temperatures (b) and light conditions and (c) the resulting differences in photosynthetic sensitivity to CO_2 between the implicit and the explicit model version for the shaded c_i regions in (a) and (b). ΔA_n in (c) is defined as $\Delta A_n = (A_{\mathrm{n,eCO2}} - A_{\mathrm{n,aCO2}})/A_{\mathrm{n,aCO2}}$, where aCO2 denotes the intercellular CO_2 concentration (c_i) range 240 – 320 µmol mol^{-1}($= 0.6 \cdot 400 - 0.8 \cdot 400$ µmol mol^{-1}) and eCO2 denotes the c_i range between 360-480 µmol mol^{-1}($= 0.6 \cdot 600 - 0.8 \cdot 600$ µmol mol^{-1}). Positive values of ΔA_n indicate that A_n in the implicit model is more sensitive to CO_2 than A_n in the explicit model, negative values of ΔA_n indicate the opposite. Shown are leaf-level simulations using the C3 photosynthesis model described in Farquhar et al. (1980) with the following parameters: $V_{\mathrm{cmax25,ci}} = 40$ µmol m^{-2} s^{-1}; $J_{\mathrm{max25,ci}} = 76$ µmol m^{-2} s^{-1}; $g_{\mathrm{m,max25}} = 0.1$ mol m^{-2} s^{-1}; $V_{\mathrm{cmax25,cc}} = 50.8$ µmol m^{-2} s^{-1}; $J_{\mathrm{max25,cc}} = 76.86$ µmol m^{-2} s^{-1}; $R_l = 0.44$ µmol m^{-2} s^{-1}; and Rubisco kinetic parameters as listed in Table C1

Simulated photosynthesis in the implicit and the explicit model versions are compared in Fig. 5.2. Shown are $A_n - c_i$ curves calculated from leaf-level simulations under contrasting temperature and light conditions. The adjustment of V_{cmax25} and J_{max25} is always

performed under reference conditions (i.e. temperature of 25°C and saturating light) and aims to minimize the difference between the implicit and explicit simulations under these reference conditions (Fig. 5.2a, solid lines). The achieved goodness of fit depends on the magnitude of g_m, with lower g_m resulting in a poorer fit to the implicit $A_n - c_i$ curve under otherwise equal conditions (Table C3). Importantly, when temperature and light deviate from the reference conditions, the agreement between the implicit and explicit model deteriorates. This is especially relevant when temperature changes, because g_m exhibits a strong temperature response (Eq. 5.3), leading to higher and lower A_n at temperatures higher and lower than 25°C, respectively (Fig. 5.2a). The model comparison at lower light conditions (Fig. 5.2b) does not necessarily lead to a poorer agreement between the model versions, but the comparison exemplifies that the mismatch between the model versions and thus the sensitivities to CO_2 strongly depend on the prevailing conditions. The *ExpC* model leads to similar curves as shown in Fig. 5.2 (Fig. C4). Assuming that g_m responds to light (*ExpL*) leads to much lower simulations of A_n under low light, as well as to higher sensitivities to rising CO_2 throughout the whole c_i range (Fig. C5). The deviations between the implicit and explicit model versions causes changes in the sensitivity of A_n to changes in c_a compared to the reference conditions (Fig. 5.2c). In general, g_m shows a stronger response to c_i in the explicit compared to the implicit model at lower temperatures, but the opposite behavior at high temperatures. These contrasts are more pronounced at lower light conditions. It has to be noted that the sensitivities and their relation between the implicit and explicit model version change with the c_i-range of interest (shaded areas in Fig. 5.2a,b).

5.3.4 Site-level simulations

The implications of the above changes for the integrated response of canopy-level A_n and canopy conductance (G_c) to changes in atmospheric CO_2 concentrations at the ecosystem level are analyzed in Fig. 5.3 for an exemplary set of ecosystems from the FLUXNET database. In the implicit model version (*Imp*), A_n increases under eCO_2 at all sites with C3 vegetation. The relative increases depend on temperature as described previously (Kirschbaum, 1994), and are more pronounced in warm (e.g. GF-Guy) than in cold climates (e.g. FI-Hyy). In the explicit model versions, the changes in the responses of A_n at the ecosystem-level represent the effects of the observed changes to the sensitivity at leaf-level (Fig. 5.2c), integrated over the whole canopy. The explicit model version that does not consider a light and c_i response (*Exp*) shows higher sensitivities of A_n to eCO_2 for most sites, but a significantly lower sensitivity for GF-Guy, which can be explained by the lower photosynthetic sensitivity to CO_2 at higher temperatures (Fig. 5.2). Model configurations that simulate a response of g_m to light (*ExpL* and *ExpCL*) show the highest responsiveness of A_n to CO_2, which is a consequence of the continuously higher sensitivity under low light in the *ExpL* and *ExpCL* versions due to the marked decrease of g_m at low light (Eq. 5.6). This effect is amplified at the canopy level, as a considerable fraction of a

closed canopy continuously operates at low light conditions. The situation is different for the model configuration responding to c_i only (*ExpC*). These runs show similar or slightly lower responses compared to the *Exp* model version, which is likely due to the fact that the lower simulated g_m is largely compensated by the higher c_c-based photosynthetic capacity (Table 5.3).
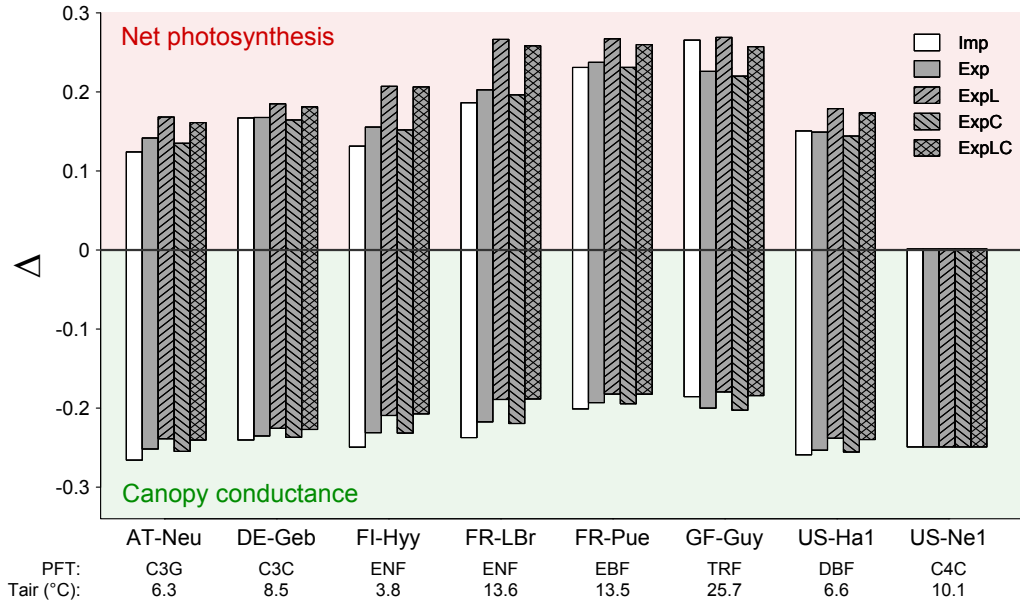
Fig. 5.3. Relative responses of ecosystem-level net photosynthesis and canopy conductance to elevated atmospheric CO_2 concentrations for the five main model versions tested in this study (*Imp* = implicit g_m; *Exp* = explicit g_m; L = light response of g_m; C = c_i response of g_m). Δ is defined as $(X,eCO_2 - X,aCO_2)/X,aCO_2$ where X denotes either net photosynthesis or canopy conductance, and aCO_2 and eCO_2 denote ambient and elevated (ambient + 200 µmol mol^{-1}) atmospheric CO_2 concentrations, respectively. PFT abbreviations are as in Fig. 5.1. Tair represents the mean annual temperature (see also Table 5.2).

The positive responses in A_n are accompanied by negative responses in G_c, i.e. stomatal closure. A consistent pattern in Fig. 5.3 is the opposite response of G_c compared to A_n in the sense that a stronger response of A_n is associated with a weaker response of G_c, with the result that the response of ecosystem level intrinsic water-use efficiency (iWUE=A_n/G_c) to eCO_2 does not vary among the model runs (i.e. it always increases by the same amount). This can be explained as an intrinsic property of the stomatal model employed here (Medlyn et al., 2011), in which c_i/c_a is assumed to stay constant with rising CO_2 concentrations. This model behavior is unchanged in the explicit model version with the consequence that stronger positive responses of A_n to eCO_2 are accompanied by weaker decreases in g_s, the combination of which keep c_i/c_a constant. Hence, the changes in g_s are not direct effects of g_m, but indirect ones via A_n that are caused by the coupling between A_n and g_s in the model. This relationship holds regardless of whether g_m is assumed to stay constant or to decrease over time, as it is the case in the *ExpC* model runs.

For C4 plants, none of the explicit model versions led to any changes in simulations of A_n and G_c compared to the implicit model. All model runs do not show a response of A_n to eCO_2, and a constant decrease of 25% for G_c. The reason for this is that c_i does not

fall in the range where photosynthesis is limited by V_{pmax} (e.g. low c_i). This behavior depends on the parameterization of the model, and g_m effects might be more important under conditions of water stress.
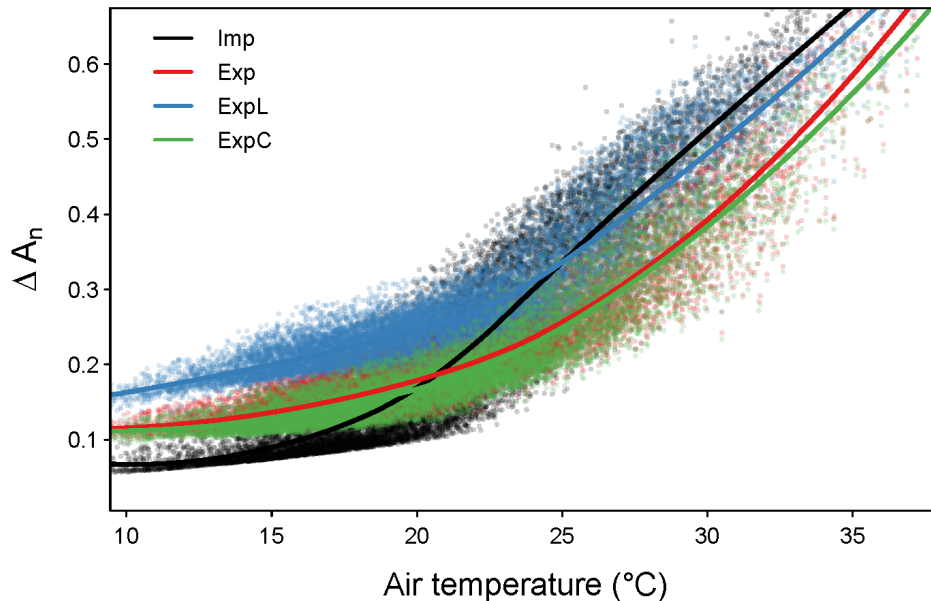
Fig. 5.4. Sensitivity of canopy-level net assimilation to elevated CO_2 concentrations in the implicit (*Imp*) and explicit model versions (*Exp*, *ExpL*, *ExpC*) for the Mediterranean pine forest site FR-LBr. Points are half-hourly simulation results, and lines indicate local polynomial regression fits (loess) to the points. Δ is defined as in Fig. 5.3.

As shown in Fig. 5.2, the fact that g_m responds to temperature causes significant changes to the temperature response of A_n. It follows that the photosynthetic sensitivity to CO_2 shows a different response to temperature in the explicit compared to the implicit model versions (Fig. 5.4). The sensitivity of A_n to CO_2 increases with temperature in all model versions, but with a different functional response (i.e. slope). In particular at low temperatures ($< 20°C$), the explicit model versions simulate a higher photosynthetic sensitivity to CO_2 compared to the implicit version. This behavior is reversed at approx. 20°C, above which *Exp* and *ExpC* simulate a lower photosynthetic sensitivity to CO_2 compared to *Imp*. The *ExpL* version shows the highest sensitivity at low temperatures due to the above mentioned amplification of the light response at canopy level. At high temperatures (above c. 25°C), *ExpL* and *Imp* show similar temperature sensitivities.
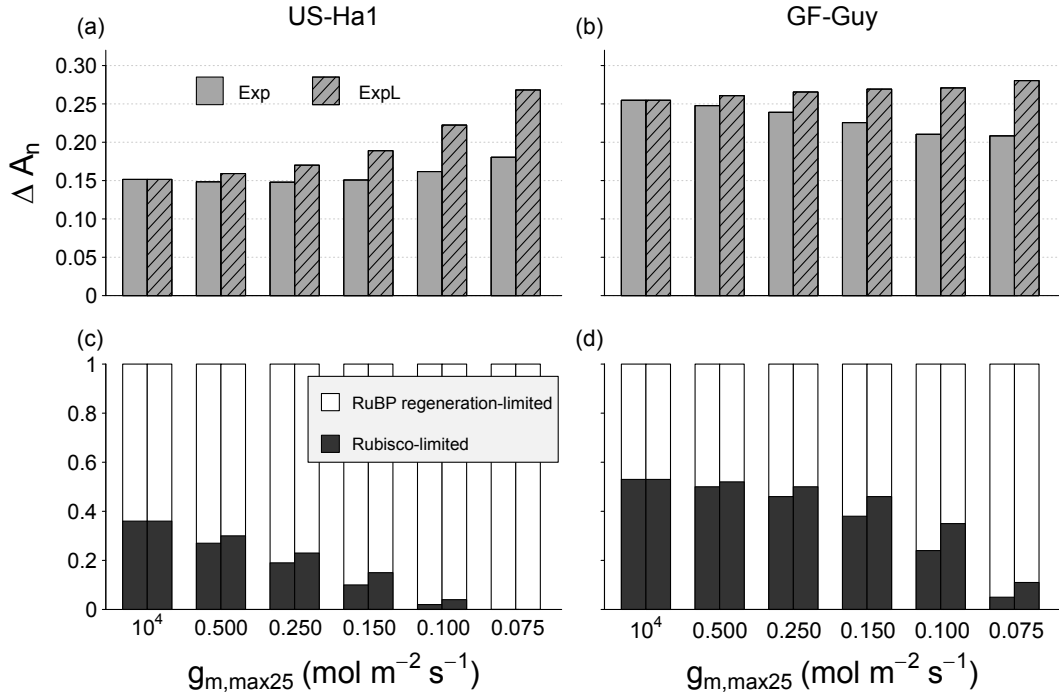
Fig. 5.5. Site-level simulations for the sites US-Ha1 and GF-Guy with differing values of $g_{m,max25}$. V_{cmax25} and J_{max25} were re-adjusted for each $g_{m,max25}$ value as described in section 5.2.5. Δ is defined as in Fig. 5.3. (c,d): Proportions of canopy level net photosynthesis limited by the two limitation states of the photosynthesis model in the ambient CO_2 simulations.

As demonstrated in Figs. 5.2-5.4, the effects of g_m on the photosynthetic responses to eCO_2 depend not only on the magnitude of g_m (and thus PFT) but also on the environmental conditions, foremost temperature and radiation. To investigate the isolated effects of g_m without any confounding meteorological factors, we conducted additional ecosystem-level simulations for the sites US-Ha1 and GF-Guy, in which $g_{m,max25}$ was varied while keeping the climate forcing unchanged. For these simulations, $g_{m,max25}$ was reduced stepwise from 10000 (i.e. non-limiting) to 0.075 mol m^{-2} s^{-1}, and V_{cmax} and J_{max} were re-adjusted for each change in $g_{m,max25}$ as described above. The results demonstrate that the effects of g_m on simulations of photosynthesis strengthen when its magnitude decreases (Fig. 5.5). This is a consequence of the increasing mismatch between the implicit and explicit model versions when g_m decreases (Table C2), an effect that amplifies when conditions deviate from those that were used for the parameter adjustment (Fig. 5.2). In the *Exp* model version, the high temperatures in the tropical site GF-Guy thus cause the photosynthetic sensitivity to CO_2 to decrease when g_m decreases, whereas the opposite is the case in the temperate site US-Ha1. The *ExpL* version causes a stronger sensitivity with decreasing g_m for all sites. At US-Ha1, this leads to a significant increase of the photosynthetic sensitivity to CO_2 at low g_m. At GF-Guy, in contrast, a potential light response of g_m offsets the increase caused by a reduced g_m, with the consequence that the *ExpL* model version shows a similar sensitivity for all g_m values.

At both sites, the proportion of Rubisco-limited A_n at canopy level decreases when $g_{m,max25}$

decreases. Again, this is a consequence of the parameter adjustment (see section 5.2.5), in which the stronger changes in V_{cmax25} compared to J_{max25} lead to a shift of the inflection point to a lower c_i, which is associated with a higher fraction of photosynthesis occurring in the RuBP regeneration-limited domain. This effect (i.e. the change in J_{max25}/V_{cmax25}) increases with a decrease in g_m under otherwise equal conditions. In general, this shift towards lower proportions of Rubisco-limited photosynthesis on total canopy level photosynthesis counteracts the higher photosynthetic sensitivity to CO_2 caused by an explicit g_m, as photosynthesis in the RuBP regeneration limited region generally shows a lower sensitivity to rising CO_2 concentrations.

5.3.5 Global simulations
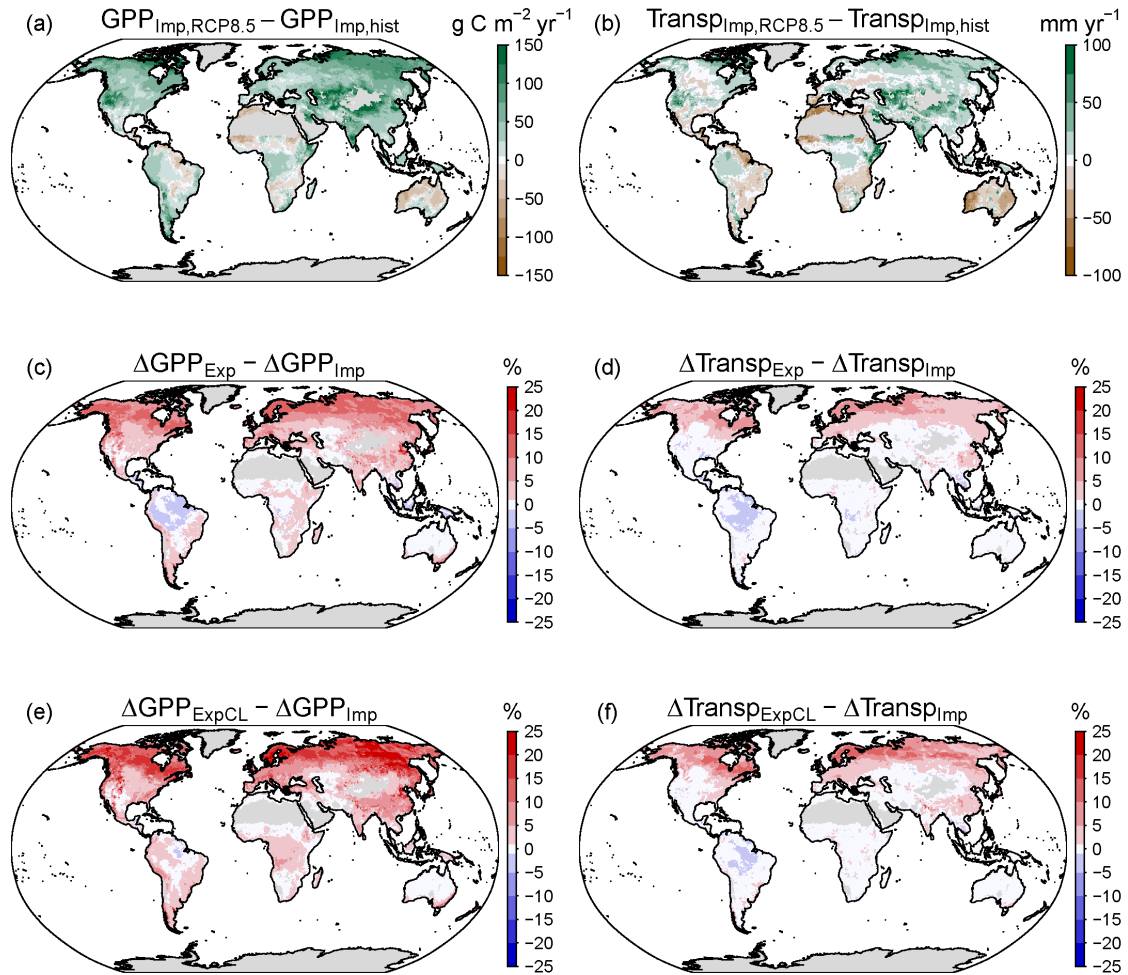
Fig. 5.6. (a-b) Simulated differences between the RCP8.5 future scenario (2070-2099) and the historical (hist) runs (1975-2004) in mean annual gross primary productivity (GPP) and Transpiration (Transp). (c-f) Relative differences from the *Exp* (c,d) and *Exp CL* (e,f) model versions. Δ is defined as $\Delta = (X_{RCP8.5} - X_{hist})/X_{hist}$, where X is either GPP or Transpiration. Regions with an average annual GPP < 200 g C m^{-2} yr^{-1} were masked out. Red colors in panels c-f denote stronger increases in GPP or Transpiration in the g_m-explicit simulations compared to the g_m-implicit simulations

At the global scale, the widespread substantial increases in mean annual GPP from the historical (1975-2004) to the future RCP8.5 (2070-2099) simulation illustrate the commonly observed CO_2-fertilization effect (Fig. 5.6a). Exceptions from this upward trend are found in some semi-arid regions, as well as in parts of the Amazon basin, which experience a drying trend in the climate projections by HadGEM2-ES. Transpiration (Fig. 5.6b), shows a weaker absolute responses and a more diverse pattern throughout the globe. In contrast to GPP, transpiration tends to be reduced due to stomatal closure, but this reduction may be offset by increasing VPD in some regions of the earth (Kala et al., 2016). The more moderate RCP4.5 future scenario shows similar patterns, but smaller absolute differences (Fig S8). Fig. 5.6 further reveals that g_m has spatially contrasting effects on the photosynthetic sensitivity to CO_2. The differences in the Δ values between the *Exp* and the *Imp* version largely reflect both the magnitude of g_m (and thus vegetation type), and the environmental conditions as described earlier. It follows that the largest changes can be found in high latitudes, in particular in boreal forests, which show a combination of vegetation with a low g_m (ENF and DNF) and a cool climate, both of which increase the photosynthetic sensitivity to CO_2 when g_m is modeled explicitly. Changes are moderately positive throughout large parts of the temperate (5-15%) and semi-arid regions of the earth (0-5%) and slightly negative in large parts of the tropical forests (-2-0%). This decrease in the CO_2 sensitivity of photosynthesis is in accordance with the site-level results, and is mostly attributable to the high temperatures in these regions. The *ExpCL* model version (Fig. 5.6e,f) shows similar spatial patterns as the *Exp* model, but consistently stronger positive responses. The reason for the stronger response is the light response function that amplifies at canopy level, as described earlier. The changes in transpiration in both the *Exp* and *ExpCL* model versions mirror those found for GPP, but are generally weaker. The weaker responses of transpiration compared to GPP are likely caused by aerodynamic decoupling, that cause a lower sensitivity of modeled transpiration to atmospheric CO_2 compared to G_c (Knauer et al., 2017).

The differences among plant types are more clearly demonstrated in Fig. 5.7. As stated earlier, the differences among the PFTs are not only caused by differences in g_m, but also by differences in the prevailing climatic conditions. For example, the lower response of TDF compared to DNF, despite similar $g_{m,max25}$ values, can be attributed to the higher temperatures the TDF are exposed to (Fig. 5.4). Nonetheless, the comparison of co-occurring PFTs in the same model grid cells (i.e. PFTs experiencing identical climate forcing), show significant differences in the simulated photosynthetic sensitivity, indicating that changes therein can primarily be attributed to differences in g_m, and not to climate (Fig. C10).

The widespread increases in plant carbon uptake in the explicit model versions relative to the implicit version of 5-25% (Figs. 5.6,5.7) lead to clear increases in simulations of global GPP (Fig. C11). Differences between simulated global GPP values in the RCP8.5 scenario amount to 3.6 and 6.6 Pg C yr^{-1} in the *Exp* and *ExpCL* model version, respectively. In both cases, about two-third of the increase is caused by regions north of 30°N (Fig. C11),
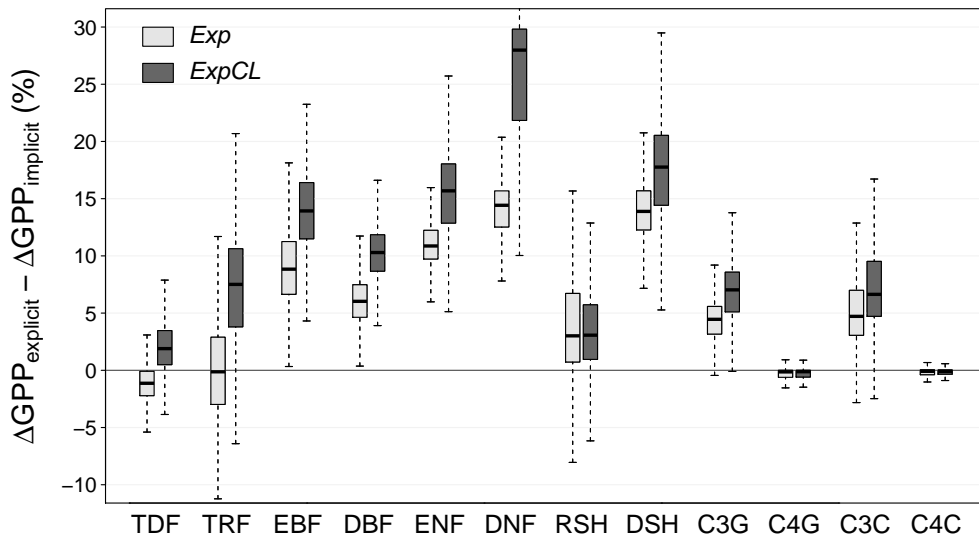
Fig. 5.7. Photosynthetic sensitivity to future climate conditions for different plant functional types (PFTs), expressed as the differences between the ΔGPP of the explicit and implicit g_m model versions. ΔGPP was calculated as $(\mathrm{GPP_{RCP8.5}} - \mathrm{GPP_{hist}})/\mathrm{GPP_{hist}}$, where $\mathrm{GPP_{RCP8.5}}$ and $\mathrm{GPP_{hist}}$ denote GPP simulated in the RCP8.5 future scenario (2070-2099) and the historical runs (1975-2004), respectively. Shown are values of grid cells where the cover fraction of the respective PFT was at least 10%. PFT abbreviations are as in Fig. 5.1

in particular in boreal forests (Fig. 5.7).

5.4   Discussion

5.4.1   Required adjustments to the Farquhar et al. 1980 photosynthesis model

The explicit consideration of g_m in models of photosynthesis requires that photosynthetic parameters are adjusted from their apparent (c_i-based) to true (c_c-based) values, as the former implicitly account for the effects of g_m. The Rubisco kinetic parameters (K_o, K_c and Γ_*) as well as their activation energies have been determined by Bernacchi et al. (e.g. 2002) on a c_c basis. These parameters are commonly assumed to be conserved across C3 plants (but see e.g. Walker et al., 2013), which leaves the species-specific parameters V_{cmax25} and J_{max25} left to adjust. Here, we suggest a simple and flexible parameter adjustment scheme that is applicable across model structures and that is capable of accounting for a potential c_i-response of g_m. The method converts V_{cmax25} and J_{max25} in accordance with the individual structure of the model and does not require measured $A_n - c_i$ curves, but instead independent g_m estimates. The adjustment from apparent to true values resulted in changes to the key parameters V_{cmax25} and J_{max25} that are qualitatively comparable to the results of previous adjustments (Sun et al., 2014a), and that compare well with independently adjusted parameters by Bahar et al. (2018) (results not shown). The adjustment again underlines the asymmetrical effects that g_m has on V_{cmax25} and J_{max25}. The stronger change in V_{cmax25} compared to J_{max25} as a result of the re-adjustment decreases the J_{max25}/V_{cmax25} ratio and shifts the inflection point towards lower c_i values. In general,

103

these changes to the photosynthesis model result in an altered response of photosynthesis to key environmental factors like temperature and light. Further, it also changes the sensitivity of photosynthesis to eCO_2 in dependence on the environmental conditions. This can mostly be attributed to the fact that the parameter adjustment is performed under reference conditions of 25°C and saturating light. Under these conditions, the agreement between the explicit and implicit model versions is the best, but it deteriorates when conditions deviate from the reference conditions, an effect that was previously asserted by Sun et al. (2014b). Most relevant in this context is the strong temperature response of g_m (Eq. 5.5), which leads to a significant deviation of simulated photosynthesis under higher and lower temperatures in the explicit model version. It may be noted that these introduced deviations could be avoided by additionally re-adjusting the activation energy of $V_{cmax,cc}$. This would, however, not be in accordance with the adjustment of the Rubisco kinetic constants as performed in Bernacchi et al. (2002), where changes in the temperature response of A_n were entirely attributed to K_c, and K_o, thereby assuming an unchanged activation energy of V_{cmax}. This approach is also justified theoretically since $V_{cmax,cc}$, the substrate-saturated photosynthesis rate, is by definition unaffected by g_m. We thus argue that - under the assumption that Rubisco kinetic parameters as determined in tobacco (i.e. following Bernacchi et al., 2002) adequately represent all PFTs - the observed changes in the photosynthesis response to temperature are not an artifact.

5.4.2 Implications for water and carbon fluxes at ecosystem level

The adjustments to the photosynthesis model cause modest changes to the CO_2 sensitivity of A_n and G_c at ecosystem level. However, the responses depend on the type of g_m model that is implemented. In the *Exp* version (no light and c_i response), the sensitivity of A_n and G_c to eCO_2 depends both on the magnitude of g_m and the climatic conditions, foremost temperature. Strongest effects were found in cold ecosystems with a low g_m (FI-Hyy), but this response does not hold across all climate types, and the tropical site GF-Guy showed the reverse response and a decreasing responsiveness to eCO_2.

The *ExpC* version (c_i response) does not differ markedly from the *Exp* version described above for any of the ecosystems investigated here. This indicates that the parameter adjustment is capable of completely offsetting the g_m response to c_i by a concomitant increase in $J_{max25,cc}$. This is an important implication for models as our results indicate that a potential response of g_m to c_i is not expected to have an impact on the simulated response of carbon and water fluxes to eCO_2 in LSMs.

Contrarily, the *ExpL* version (light response) leads to a stronger responsiveness of eCO_2 in all ecosystem types. This effect can best be demonstrated with leaf level simulations under low light conditions, where the CO_2 responsiveness of A_n is higher in the *ExpL* compared to the *Imp* model, so long as c_i is not saturating (Fig. C5). This effect is amplified at the ecosystem level, where a certain fraction of the canopy operates in sub-saturating light conditions regardless of the incident radiation. This potential light response of g_m thus sig-

nificantly increases the CO_2 sensitivity of all C3 ecosystems investigated here and amplifies the strong positive changes in photosynthetic responsiveness to CO_2 in cold climates, or compensates for the negative response in warmer climates.

The explicit representation of g_m did not change simulations of iWUE (A_n/G_c), which increased at the same rate as in the implicit model version regardless of the g_m model employed. This behavior is a consequence of the implemented stomatal conductance model (Medlyn et al., 2011), which is based on the strong coupling between A_n and g_s, that causes the c_i/c_a ratio to stay constant regardless of the atmospheric CO_2 concentration. Since most LSMs employ similar g_s models as the one used here (see e.g. Sato et al., 2015, for an overview), our results are in that respect likely representative for most LSMs.

Our results do not indicate changes to simulations of C4 photosynthesis when g_m is considered explicitly. This is because the explicit consideration of g_m was compensated by an increase in the PEP-carboxylation rate (V_{pmax}) in the course of the parameter adjustment. While we acknowledge that we lack sufficient data to confidently parameterize the C4 photosynthesis model employed here (von Caemmerer and Furbank, 1999) at the global scale, we argue that, from a modeling point of view, results would be similar if the simpler and more widely used model by Collatz et al. (1992) (as described in e.g. Bonan et al. (2011)) was used, in which case the consideration of g_m would affect the slope of the initial CO_2 response curve in a similar manner as it affected V_{pmax} in the model of von Caemmerer and Furbank (1999) (see Fig. C3).

5.4.3 Global implications

Global simulations of GPP and transpiration under anticipated future climate suggest clear and regionally contrasting increases in GPP. The differences between the g_m-implicit and g_m-explicit simulations depend on the projected climate, and on the PFT distribution through vegetation-type differences in the magnitude of g_m. The fact that plant groups with a low g_m showed stronger responses to eCO_2 than those with a high g_m under the same climate, generally supports an earlier hypothesis that evergreen species are more likely to have a competitive advantage over other plant types in a high CO_2 world (Niinemets et al., 2011). However, our analysis suggests that this hypothesis does not hold in the tropics, where a low g_m led to a decrease in the photosynthetic CO_2 responsiveness (Figs. 5.5b,5.6). However, the actual relevance of g_m in present and future vegetation dynamics must still be investigated using experimental and modeling approaches.

The replacement of the g_m-implicit with a g_m-explicit model causes significant changes to simulations of GPP, ranging from 2.3 Pg C yr^{-1} in the *Exp* model and the RCP4.5 scenario to 6.6 Pg C yr^{-1} in the *ExpCL* model and the RCP8.5 scenario (Fig. C11). About two thirds of this increase are caused by regions north of $>30°N$, where it mostly occurs in regions covered by boreal forests. Changes of this magnitude are likely large enough to significantly affect the amplitude of atmospheric CO_2 in the high latitudes, hence g_m, which is so far neglected in this context (Zeng et al., 2014; Forkel et al., 2016), should be

considered as an additional explanatory factor.

Although our results are broadly consistent with those of Sun et al. (2014b), our estimates of the GPP response to CO_2 are more moderate. Compared to the 16% increase in the cumulative GPP found by Sun et al. (2014b), our results (calculated from Fig. C13 using Eq. 2 in Sun et al. (2014b)) suggest smaller changes in the order of 6% in the *Exp* model version and the RCP8.5 scenario (but similar values of 15% in the *ExpCL* scenario). However, these numbers may not be directly comparable due to different simulation periods. With respect to the latitudinal patterns of the g_m effects, our results agree with those by Sun et al. (2014b), as in both cases, the weakest and strongest effects were found in the tropics and the northern latitudes, respectively. Our simulations (Fig. C12) further suggest clear differences in ET between the two model versions, which may have impacts on other physical land surface properties, such as land surface temperature, soil moisture, or sensible heat fluxes.

5.4.4 Future model developments and research needs

Our results emphasize that the absolute value of g_m is important for the adjustment of photosynthetic parameters and the associated effects on simulations of photosynthesis. The magnitude of g_m is relatively robust for well-sampled PFTs, and similar to the results of earlier data compilations (Flexas et al., 2008), but more measurements are needed for tropical species, deciduous needle-leaf species, and C4 plants. The parameterization of these plant types is important for large-scale simulations, but their maximum g_m values can at the moment not be confidently parameterized due to the lack of data.

It is clearly desirable to bring empirical formulations of g_m as used here and in previous studies (Suits et al., 2005; Sun et al., 2014b) to a more process-based representation. While existing leaf-level models of g_m (Tholen and Zhu, 2011; Tomás et al., 2013) are likely too complex to be parameterized at large scales, global models of g_m could be readily improved by relating key model parameters (e.g. $g_{m,max25}$) to other plant traits, which would allow the prediction of $g_{m,max25}$ from commonly measured traits. Although relationships between $g_{m,max25}$ and other plant traits such as specific leaf area (SLA) (Piel et al., 2002; Niinemets et al., 2009a), or leaf nitrogen content and V_{cmax25} (von Caemmerer and Evans, 1991; Yamori et al., 2011; Xue et al., 2017) have been identified, more research is needed to confirm the validity of these relationships across plant types.

Currently, one factor hampering future model development is the poor process understanding of g_m, which is associated with the fact that measurements of g_m are challenging (Pons et al., 2009). It is particularly critical that the role of environmental factors such as c_i and light is unresolved. Here, we tested the potential effects of these two drivers on large-scale simulations of carbon and water fluxes. We found that a potential c_i response does not change model predictions, as its effects would be offset by the adjustment of V_{cmax25} and J_{max25} from their apparent to true values. A potential light response of g_m, however, would be amplified at canopy level and lead to a significantly higher responsiveness of A_n to ris-

ing CO_2. Extrapolated to the global scale, such a leaf-level response would significantly increase global carbon uptake and water loss. It is thus highly relevant that potential measurement artifacts are ruled out (Gu and Sun, 2014), and that the recently put forward hypothesis of an apparent light response (Théroux-Rancourt and Gilbert, 2017) is investigated further, as its existence would mean that the light response of g_m as observed at the leaf level should not be implemented in models.

5.4.5 Acknowledgments

6 Summary and Outlook

This thesis provides insights into several aspects of water-carbon coupling at different spatial scales. From chapter 2, two main conclusions can be drawn: First, the strong IWUE trend in the EC data as observed by Keenan et al. (2013) is not a large-scale phenomenon because it is not in accordance with large-scale observational data sets of both carbon and water fluxes (Figs. 2.4,2.5). Second, the physiological interpretation of WUE trends observed at ecosystem-level needs to account for scale-dependent attenuation factors, which was not done by Keenan et al. (2013). Considering these factors, it could be shown that a IWUE trend in the magnitude as observed by Keenan et al. (2013) would require a strong stomatal closure to an extent that is physiologically implausible (i.e. a decrease in c_i with rising c_a), and that any increase in IWUE of more than approx. $1\%\ \mathrm{yr}^{-1}$ would require a decrease in c_i (Fig. 2.6). Chapter 3 extends on chapter 2 by focusing on methodological and scale-dependent uncertainties present in EC data and their impact on the interpretation of the stomatal slope parameter G_1, a key parameter closely related to iWUE. The analysis demonstrates that confounding factors which are often overlooked in an ecophysiological context (e.g. aerodynamic conductance, energy-balance non-closure) are often more critical for the derivation of iWUE than other, more commonly accepted sources of uncertainty (e.g. non-transpirational water fluxes, NEE partitioning algorithm)(Table 3.2). These results call for an adequate consideration of these confounding factors when EC data are interpreted in an ecophysiological context, an aspect that is of growing scientific importance considering the increasing length of available EC time series. Chapter 4 provides a description of a software package in the language R that allows for an efficient and reproducible calculation of G_1 as well as other physiological and biometeorological ecosystem properties from EC data. The study critically evaluates the 'big-leaf' framework, and provides guidelines for the use of variables obtained from such calculations. In chapter 5, the effects of g_m on GPP and transpiration at the leaf to the global scale is investigated. It is shown that the incorporation of g_m into the widely used Farquhar et al. (1980) photosynthesis model changes the simulated response of photosynthesis to environmental factors, and that the effects of g_m cannot be captured by adjusting other photosynthetic parameters in the model. It is further demonstrated that the consideration of g_m in large-scale model simulations increases the projected CO_2 fertilization in the boreal zone significantly (Figs. 5.6,5.7). An extensive literature compilation presented in this study is useful to constrain the magnitude of g_m across major plant types (Fig. 5.1). The presented simple model conversion scheme further allows for the incorporation of g_m into all model types, including those simulating C4 vegetation. A better understanding of g_m is an important prerequisite for the application of a more comprehensive photosynthetic discrimination model and for using atmospheric $\delta^{13}C$ isotope data as an additional large-scale constraint on water-carbon coupling, as detailed in section 6.3. In the following, the results obtained in this thesis are discussed with respect to potential future research activities.

6.1 Use of EC data for current and future ecophysiological research

EC data are an invaluable source of ecological information because of the continuous and long-term measurements as well as the wide spatial (ecosystem level) coverage they provide. The data are further well-maintained by an active research community that operates hundreds of sites worldwide (Pastorello et al., 2017) and that provides sophisticated pre- and postprocessing tools (e.g. Fratini and Mauder, 2014; Beringer et al., 2017; Metzger et al., 2017; Wutzler et al., 2018). These tools also deal with uncertainties in the EC measurements (e.g. systematic and random measurement errors, caveats in data pre-processing), which are important to consider in order to derive robust estimates of land-atmosphere exchange. However, chapters 2, 3, and 4 have shown that these basic quality checks are not sufficient when the analysis involves the derivation of physiological ecosystem properties (e.g. G_c, G_1) from EC data, in which case it has proven to be essential to additionally account for methodological and environmental confounding factors.

However, studies using EC data for ecophysiological research often neglected the latter aspect. One example is the study by Keenan et al. (2013), in which a strong trend in IWUE was interpreted without taking confounding scale-dependent factors (e.g. canopy-atmosphere decoupling) into account. The physiological interpretation of the IWUE trend was consequently that plants regulate gas exchange in a way that keeps the c_i constant, a scenario which is, according to leaf-level data, commonly considered to be unlikely (Ainsworth and Rogers, 2007), but not impossible to happen (Saurer et al., 2004; Battipaglia et al., 2013). In chapter 2 it was shown that the physiological interpretation is significantly different if these scale-dependent factors are considered. Particularly, a trend of this magnitude would require a decrease of c_i over time (Fig. 2.6), which is physiologically implausible. More generally, the analysis performed in chapter 2 highlights two important aspects for future EC research: 1) EC time series must be long enough and cover a sufficient number of sites in order to derive robust trends. The fact that the IWUE trend is significantly lower when longer time series of the same sites are analyzed (Mastrotheodoros et al., 2017) supports the assumption laid out in chapter 2 that the trend in IWUE found by Keenan et al. (2013) was indeed a sampling bias. 2) confounding, mostly non-physiological factors and scale-dependent feedbacks must be taken into account in order to correctly represent the sensitivity of physiological processes to environmental changes (Wilson et al., 1999; Anderson et al., 2003).

The aforementioned confounding factors often comprise physical feedbacks that are absent or negligible at leaf level, and that consequently lead to the fact that the same metric must be interpreted differently at leaf and ecosystem level (chapters 3 and 4, Fig. 1.3). Two main factors in this respect are G_a and non-transpirational water fluxes (i.e. interception and soil evaporation). G_a (or its inverse value, R_a) is well characterized based on a long-standing physical theory (Monteith and Unsworth, 2008). Future work should focus on the boundary layer resistance at ecosystem level, which accounts for approx. 1/3 to 1/2 of the total aerodynamic resistance (Table B1). Existing physically-based approaches (Massman, 1999;

Su et al., 2001) will benefit from a more rigorous validation using independent datasets such as surface temperature (Rigden et al., 2018a). Ideally, this validation will involve the effects of structural (broadleaf vs. evergreen, canopy clumping) and physiological (hypostomatous and amphistomatous) vegetation characteristics.

A persisting challenge lies in the separation of ET into its components evaporation and transpiration. The knowledge on the magnitude as well as the temporal dynamics of the E/ET fraction has proven to be important for the interpretation of derived physiological ecosystem properties (chapter 3) as well as for the hydrological sensitivity to rising atmospheric CO_2 concentrations (chapter 2). Currently, many different ET partitioning approaches are being developed (Scanlon and Kustas, 2010; Zhou et al., 2016; Scott and Biederman, 2017; Rigden et al., 2018b). Valuable future contributions will comprise method intercomparisons (Berkelhammer et al., 2016; Wei et al., 2017), as well as their evaluation with independent measurements (Perez-Priego et al., 2017; Zhou et al., 2018)). Robust ET partitioning algorithms would further allow the replacement of the widely used simple rainfall filtering approach (Ponton et al., 2006; Keenan et al., 2013; Dekker et al., 2016, Fig. 3.2) with more meaningful estimates.

In contrast to the effects of the E/ET ratio, the energy balance non-closure, though a well acknowledged issue in EC research (Wilson et al., 2002a; Foken, 2008; Leuning et al., 2012), is often ignored when EC data are interpreted in an ecophysiological context. Chapter 3 illustrates that a typical degree of energy balance non-closure present at EC sites (approx. 20%, Stoy et al. (2013)) can critically bias absolute values of G_1, and confound its temporal dynamics (Figs. 3.5,3.6). The bias in the derived G_1 parameter strongly depends on the component(s) of the energy balance the residual energy must be attributed to (Fig. 3.5). These results highlight the need to better characterize the causes for the energy balance non-closure not only over longer time periods but also at the sub-diurnal time scale. Such an analysis would first need to quantify the diurnal course of the energy storage fluxes (S), and subsequently assign the remaining energy residual to the turbulent fluxes λE and H. The characterization of S could either be based on detailed models on the individual energy storage terms involved (e.g. Haverd et al., 2007; Jacobs et al., 2008), or alternatively, simpler, empirical estimates of S based on readily available parameters such as biomass or trunk diameter could be developed. The second step should focus on the validation of existing approaches (e.g. the Bowen ratio approach (Twine et al., 2000)). An improvement in these aspects would largely increase the interpretability of the physiological response of ecosystems to global environmental change, but would also greatly increase the value of EC-based analyses which are sensitive to absolute flux values such as water balance calculations.

In chapters 3 and 4, a parsimonious, data driven "big-leaf" approach was used to derive physiological key parameters "top-down" from the measured fluxes. At this point, the question remains whether the inversion of more complex models (e.g. sun-shade models, multi-layer canopy models) is better suited for the derivation of physiological ecosystem properties from EC data. To address this question, two aspects must be considered (see

chapter 4): the availability of site-specific information (i.e. values of the parameters required for the employed models), and the variable of interest. A more complex modeling approach is only useful if sufficient ancillary information is available, and if the variable of interest shows a pronounced gradient within the canopy, which means that its leaf-to-canopy scaling effects are expected to be significant. In case of G_1, the variation within the canopy is not yet measured across multiple sites (leaf-level measurements are commonly performed on top of the canopy only) and its behavior could not be conclusively answered in chapter 3. Thus, future scientific efforts should involve leaf-level measurements at multiple levels within the canopy and in different forest types. Investigating whether g_1 shows pronounced variations within the canopy would clarify the suitability of the "big-leaf" approach for its derivation, but would also have important implications for the parameterization of LSMs, which commonly assume a fixed value of the g_1 parameter within the canopy.

From chapter 3 it can be concluded that EC data are unlikely to provide reasonable constraints on ecophysiological parameters as required by most LSMs. The parameterization of physiological key parameters such as V_{cmax25}, J_{max25}, photosynthetic light response, g_1, or g_0 should be primarily based on compilations of leaf-level measurements across plant types and climatic conditions. Advantages of leaf-level measurements in that respect are that they are performed at the same organizational scale as required by most LSMs (i.e. leaf level), and that the estimated parameters are usually not as critically confounded as those derived from EC data (chapter 3). Promising recent developments in that respect are compilations of Lin et al. (2015) or Miner et al. (2017) for the g_1 parameter and Walker et al. (2014) or the TRY database (Kattge et al., 2011) for photosynthetic capacity. The parameters compiled in these databases can in addition be related to other key plant traits (Walker et al., 2014; Lin et al., 2015), which potentially simplifies their representation in models. Chapter 4 suggests that EC data are most efficiently used in model evaluation, where the focus should shift from the evaluation of absolute fluxes to a more pattern-oriented evaluation. The latter approach helps to evaluate aspects of models which are not directly parameterized, but which emerge at the canopy/ecosystem level as the result of various interacting processes in the model. Examples for such metrics are the aerodynamic decoupling between the canopy and the atmosphere (De Kauwe et al., 2017), the water- and light-use efficiency of ecosystems (Li et al., 2018), as well as the sensitivity of bulk canopy physiological behavior (e.g. canopy conductance) to meteorological drivers (e.g. VPD Migliavacca et al., 2009; Knauer et al., 2015).

6.2 Potential of process-based modeling in water-carbon research

Ecosystem and land surface models consider the interplay of key biological and physical processes as well as their response to environmental drivers. This process-based setup allows the application of these models to new conditions. This extrapolation may be temporally, e.g. predicting the future response of the climate system to anthropogenic

perturbations (e.g. Friedlingstein et al., 2014), or comprise the testing of hypotheses to investigate the effects of e.g. structural or physiological changes of the vegetation at large scales as has been performed in chapter 2 as well as in other studies (Kleidon et al., 2000; Zhao et al., 2001; Brovkin et al., 2009). Such an approach is especially powerful when model simulations are applied in a factorial setup, and when large-scale, multiple observations are used to evaluate (and eventually constrain) model simulations. Factorial sensitivity experiments are powerful because they allow to disentangle the effects of individual drivers (e.g. CO_2 concentration, climate, land use change) on the variability or trends of the model output (e.g. WUE) (Saurer et al., 2014; Zhou et al., 2017, chapter 2). In addition, there is currently a large, probably under-exploited, potential in using multiple data streams as large-scale constraints on terrestrial water and carbon fluxes. Future modeling studies should take full advantage of high-quality records of continental discharge (as in chapter 2), as well as terrestrial water storage (e.g. GRACE, Tapley et al., 2004). For carbon fluxes, atmospheric constraints have proven invaluable (Keeling et al., 1996; Forkel et al., 2016; Zeng et al., 2014), but also remotely sensed products may have the potential to provide constraints on physiological (Guanter et al., 2014; Frankenberg et al., 2014) and structural (Donohue et al., 2013; Houborg et al., 2015; Jiang et al., 2017) vegetation properties represented in models.

The synergistic use of model experiments and large-scale data sets can help to answer two central research questions that emerged from chapter 2. One key question underpinning the CO_2 response of vegetation is to what extent the "structural CO_2 effect" (i.e. increases in LAI) offsets the "physiological CO_2 effect" (i.e. decreases in g_s) (Gerten et al., 2014). So far, this question could not be answered because the CO_2 effect on LAI is poorly constrained by observations (Norby et al., 2010), with the consequence that a wide range of effects, including complete offsets of stomatal closure by increases in LAI (Kergoat et al., 2002; Piao et al., 2007; Bounoua et al., 2010), as well as minor effects of LAI (Betts et al., 2007), were simulated. Future research needs to focus on how far the structural CO_2 effect can be quantified using remotely sensed data products. Important is to quantify the carrying capacity of LAI (i.e. the LAI when no further increases are expected (Norby et al., 2010)) for different biomes of the earth, and whether and to what extent this carrying capacity has already been reached. To investigate these effects in models, also other confounding factors, which are not directly responsive to atmospheric CO_2 (e.g. land use change (Piao et al., 2007)), must be taken into account. The second research question addresses the response of water-stressed regions to rising atmospheric CO_2 concentrations. Considerations made in chapter 2 as well as in other studies (Hungate et al., 2002; Morgan et al., 2004; Holtum and Winter, 2010) suggest that CO_2-induced stomatal closure increases plant available soil moisture, which is likely to trigger a positive feedback that diminishes the physiological CO_2 effect in water-stressed regions (i.e. higher water availability is expected to lead to an increase in g_s which counteracts the initial decreases in g_s caused by increasing CO_2). Given that this question is closely entangled with the first one - higher soil moisture is also expected to increase LAI, especially in low-LAI ecosystems -

it would be meaningful to address the two questions simultaneously. Relevant large-scale observations in semi-arid regions are streamflow measurements (Ukkola et al., 2016), but also the potential of satellite products should be exploited (de Jong et al., 2011; Donohue et al., 2013).

All model simulations must be evaluated against observations. However, as Prentice et al. (2015) pointed out, the evaluation of model output "is necessary, but not sufficient". It has been shown, for instance, that models may give the "right" results (e.g. accurate flux simulations) for the "wrong" reasons (e.g. compensating errors in model formulations) (e.g. Zaehle et al., 2014). Such a model behavior severely compromises the capability of LSMs to predict future vegetation-climate feedbacks, and emphasizes that a substantial part of future modeling work needs to focus on the improvement of existing model structures and formulations. Relevant future fields of model improvement relevant for the physiological controls on water-carbon coupling comprise, but are not limited to, the following aspects:

- The representation of soil water stress on A_n, g_s and g_m, as well as a more mechanistic representation of the β soil moisture stress factor (e.g. Eq. 5.1), by e.g. considering soil water potential instead of volumetric soil moisture.

- The role of nutrients, in particular nitrogen and phosphorous in plant physiology and their effects on future CO_2 fertilization.

- the acclimation of key photosynthetic parameters (V_{cmax} and J_{max}, g_1) to elevated CO_2.

- Improved modeling of the g_0 parameter. g_0 functionally represents the part of g_s that is not under guard cell control (i.e. the residual conductance through the leaf cuticula and due to incomplete stomatal closure). Owing to its small values, g_0 is in many cases not deemed relevant, however previous studies have pointed out that g_0 is important for global carbon and water fluxes (Barnard and Bauerle, 2013; Lombardozzi et al., 2017), and that it is likely more important under high CO_2 concentrations when g_s is expected to decrease (Voelker et al., 2016). In particular, it needs to be tested whether g_0 as currently included in models (e.g. Eq. 2.1) is suitable to represent the lower boundary of g_s under both day- and nighttime conditions.

- The role of mesophyll conductance in photosynthesis and stomatal conductance, as discussed in chapters 5 and 6.3.

6.3 Role of mesophyll conductance in future water-carbon coupling research

6.3.1 Future improvements in modeling g_m at large scales

The incorporation of g_m into the LSM JSBACH is an example of a structural model improvement. In other state-of-the-art LSMs the overestimation of the available CO_2 concentration for photosynthesis resulting from the assumption of an infinite g_m constitutes a structural model deficiency, which is to large parts, but not completely, compensated by the underestimation of other photosynthetic parameters. The results in chapter 5 confirm that the c_i-based model does not fully account for the effects of g_m, and that the explicit representation of g_m changes the sensitivity of photosynthesis to environmental factors, which affects future projections of terrestrial carbon uptake and transpiration. This study is also in accordance with Sun et al. (2014b), who found that g_m increases CO_2 fertilization particularly in the boreal zone. One remaining question is to clarify to what extent g_m can explain the overprediction of atmospheric CO_2 by global models (Sun et al., 2014b), as well as the observed increase in the seasonal cycle of atmospheric CO_2. Given that the uncertainties at larger scales arise in large parts from the fact that the instantaneous light response of g_m is unresolved (compare Fig. 5.6c,d and 5.6e,f), future research should focus on understanding the frequently observed g_m light response at leaf level (Théroux-Rancourt and Gilbert, 2017).

Chapter 5 describes two main steps that are required to include g_m routinely in LSMs: First, it provides the hitherto best constrained estimates of the magnitude of unstressed g_m of different vegetation types (the $g_{m,max25}$ parameter). Second, it presents a simple and universally applicable scheme to re-adjust photosynthetic parameters from apparent (c_i-based) to true (c_c-based) values. This approach ensures that no artifacts are introduced when LSMs are restructured from a g_m-implicit to a g_m-explicit model version, and may thus prove useful for other modeling groups.

One aspect that warrants further research is the question of how g_m should be modeled in LSMs. The current model formulation (Eq. 5.1) suffers from the fact that it contains in total eleven empirical parameters, the majority of which does not have a clear physiological meaning. This overparameterization problem is mainly the result of the high degree of empiricism required to model g_m, which is again a consequence of the poor process understanding of g_m (Warren, 2008; Rogers et al., 2017). A meaningful starting point for future model development is the prediction of $g_{m,max25}$ (i.e. the maximum/unstressed g_m at 25°C) from other, commonly measured plant traits. When establishing such a relationship, both physiological and structural traits need to be taken into account. The reason for considering physiological traits is that g_m must be, to a certain extent, correlated with photosynthetic capacity following first order principles. From Fick's first law ($A_n = g_s(c_a - c_i) = g_m(c_i - c_c)$) it can be seen that a high leaf photosynthetic capacity (allowing a high A_n) is only advantageous when diffusional limitations are low enough (i.e. g_s and g_m are sufficiently high) to allow this high A_n. The reason why structural traits need

to be taken into account is that leaf physiology is overlaid by anatomical constraints (e.g. evergreen leaves need a certain cell thickness for stability). Thus, a promising approach would be to relate $g_{m,max25}$ to a small number of readily available traits describing both photosynthetic capacity (e.g. leaf nitrogen content) and leaf anatomical features (e.g. cell wall thickness, mesophyll surface per unit leaf area), an analysis that should make use of the full database described in section 5.

6.3.2 Relevance of g_m in using carbon isotope discrimination as a constraint on WUE

As addressed at the beginning of this chapter, knowledge on g_m and its variation in time and space is valuable for the interpretation of carbon isotope measurements, which can provide an additional observational constraint on the behavior of vegetation gas exchange in past, present, and future climate. In the following, the theoretical background on carbon isotope discrimination and its relation to physiological variables is provided, and two potential future research applications - a bottom-up and a top-down approach - are presented.

As described in chapter 1, basic physiological quantities such as c_i/c_a or iWUE can be inferred from the observed Δ using photosynthetic discrimination models. The most commonly used discrimination model is a simplified formulation, which considers only the fractionation by diffusion through the stomata and the carboxylation by Rubisco (the "simple" model):

$$\Delta_{\text{simple}} = a + (b' - a)\frac{c_i}{c_a} \qquad (6.1)$$

where a is the fractionation due to diffusion in air (4.4 ‰), and b' is the fractionation by Rubisco ($\approx$ 27 ‰). As summarized in e.g. Ubierna and Farquhar (2014), photosynthetic fractionation occurs also as an effect of other processes, including diffusion through the leaf boundary layer, the mesophyll, as well as during respiration and photorespiration. In the simple model (Eq. 6.1), b' implicitly accounts for all other isotopic effects during photosynthetic fractionation (Ubierna and Farquhar, 2014). An alternative (the "classical") discrimination model considers two additional fractionation factors, g_m and photorespiration, explicitly but neglects further factors such as discrimination through the leaf boundary layer or ternary effects. The classical model can be written as (Farquhar et al., 1982):

$$\Delta_{\text{classical}} = a\frac{c_a - c_i}{c_a} + a_m\frac{c_i - c_c}{c_a} + b\frac{c_c}{c_a} - f\frac{\Gamma_*}{c_a} \qquad (6.2)$$

where a_m is the fractionation associated with the transfer of CO_2 from the intercellular airspace to the chloroplast (1.8 ‰), f is the fractionation during photorespiration (8-16 ‰), and b is the fractionation by carboxylation (30 ‰; note the difference between b' in Eq. 6.1 and b in Eq. 6.2). Corresponding equations can be written for C4 plants (see e.g.

Cernusak et al., 2013), but are not presented here. By combining Eq. 6.2 with Fick's first law ($A_n = g_m(c_i - c_c)$), replacing A_n by the ratio g_s/g_m and solving for c_i/c_a, the following equation can be derived (Seibt et al., 2008):

$$\frac{c_i}{c_a} = \frac{\Delta_{\text{classical}} - a + (b - a_m)\dfrac{g_s}{1.6 g_m} + f\dfrac{\Gamma_*}{C_a}}{b - a + (b - a_m)\dfrac{g_s}{1.6 g_m}} \quad (6.3)$$

Eq. 6.3 demonstrates that for the same Δ measured, the derived values of c_i/c_a (and thus iWUE) depend, among other factors, on the values of g_m and Γ_* (see Seibt et al., 2008, for further details). More generally, it points to the fact that the derived gas exchange characteristics depend on the discrimination model and thus on the choice of the fractionation processes that are considered explicitly. Γ_* is well constrained by leaf-level measurements and known to be conserved across C3 plants (von Caemmerer, 2000), thus the main source of uncertainty in Eq. 6.3 lies in the magnitude and dynamics of g_m. It should be noted that also one of g_s or A_n are needed to infer c_i/c_a, however they are generally considered to be better known than g_m. Fig. 6.1 illustrates the effects of the different photosynthetic discrimination models (Eqs. 6.1 and 6.2) assuming a constant c_i/c_a over time. The simple leaf-level calculations demonstrate important differences between calculations using the "simple" and the "classical" model, but also between different plant types differing in g_m and other photosynthetic characteristics.
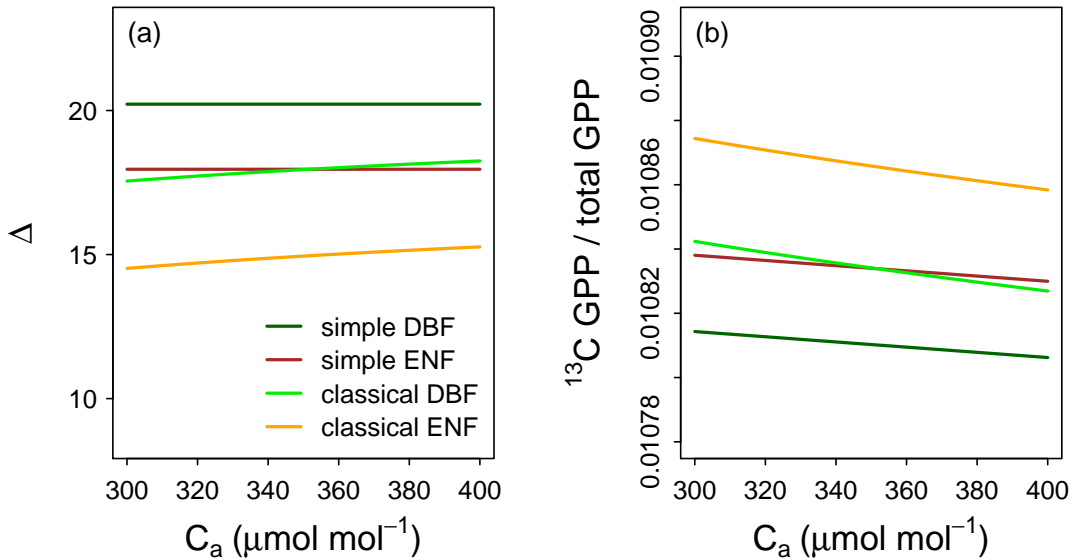
Fig. 6.1. (a) calculated Δ and (b) the ratio of ^{13}C GPP to total (^{12}C + ^{13}C) GPP using the "simple" and the "classical" isotope fractionation model (Eqs. 6.1 and 6.2, respectively) over an atmospheric CO_2 concentration of 300 - 400 µmol mol^{-1}. Shown are differences between deciduous broadleaf (DBF) and needle-leaf evergreen (ENF) vegetation, for which the following parameters were assumed: DBF: $A_n = 7$ µmol m^{-2} s^{-1}, $g_m = 0.2$ mol $^{-2}$ s^{-1}, c_i/c_a=0.7; ENF: $A_n = 4$ µmol m^{-2} s^{-1}, $g_m = 0.1$ mol $^{-2}$ s^{-1}, c_i/c_a=0.6. A_n was assumed to increase by 20% over a C_a between 300 and 400 µmol mol^{-1}.

Despite these clear effects, photosynthetic fractionation associated with g_m and other frac-

tionation processes are commonly ignored in isotope studies (Feng, 1999; McCarroll and Loader, 2004; Belmecheri et al., 2014; Frank et al., 2015; Walker et al., 2015; Voelker et al., 2016), which is most likely due to the fact that the magnitude of g_m is poorly quantified and that its variation with environmental factors is not well understood (Warren, 2008; Flexas et al., 2012).

The compilation of unstressed g_m values (Fig. 5.1), as well as the observed responses of g_m to environmental factors (Eqs. 5.2-5.6) can be effectively used in two different research perspectives that aim to provide additional observational constraints on WUE. The first approach is a bottom-up approach which primarily aims to re-evaluate tree ring $\delta^{13}C$ data as presented in e.g Belmecheri et al. (2014) or Frank et al. (2015) using Eq. 6.2 instead of Eq. 6.1. g_m in Eq. 6.2 can be obtained from the compiled database as presented in chapter 5. This database comprises enough measurements to robustly estimate the magnitude of g_m at PFT level (including evergreen needle-leaf trees and deciduous broadleaf trees) and in some cases also at species level (see `https://bitbucket.org/juergenknauer/gm_data` for all species available in the database). Important in this context is the possibility to not only account for the effects of g_m, but also for the differences among plant types, an aspect that has not yet been considered with respect to isotopes, but which may have important implications of the spatial patterns of inferred iWUE trends (see Fig. 6.1). A back-of-the-envelope estimate of the effects of Γ_* and g_m was recently made by Keeling et al. (2017), who found that the inferred iWUE trends using Eq. 6.2 are 14% higher than those inferred from Eq. 6.1. iWUE trends over the 20th century were corrected from 14% to 28%, and from 22% to 36% for broadleaf and needle-leaf evergreen trees, respectively, and 60% of this correction were attributed to the effects of g_m, and the rest to photorespiration. However, it should be noted that Keeling et al. (2017) assumed a value of g_m (0.2 mol m^{-2} s^{-1}) which is at the higher end of what is usually measured in temperate trees (Fig. 5.1), and importantly, which ignores physiological differences between deciduous broadleaf and needle-leaf evergreen trees (Figs. 5.1, 6.1). Lastly, it is important to note that this analysis should not be restricted a priori to the classical model (Eq. 6.2), i.e. more comprehensive model versions should be considered first. The effects of other discrimination factors (Farquhar et al., 1982; Ubierna and Farquhar, 2014) needs to be tested using sensitivity analysis. The effects of fractionation during respiration should be analyzed, and in particular for broadleaf trees it needs to be clarified whether the fractionation during diffusion through the leaf boundary layer is negligible under field conditions.

The second potential future research application is a top-down approach, in which modeled atmospheric $\delta^{13}C$ values are confronted with measurements. This analysis will consist of two main steps: first, the net biosphere-atmosphere ^{13}C flux needs to be calculated from a process-based biosphere model which takes various isotopic fractionation factors of ^{13}C into account. The net ^{13}C fluxes will then be transported in the atmosphere to remote measurement stations (see chapter 2 for description of the CO_2 measurement stations) with an atmospheric transport model using prescribed ocean net fluxes and fossil fuel

emissions of ^{13}C. This analysis will build on existing carbon isotope models embedded in global models (e.g. Kaplan et al., 2002; Suits et al., 2005; Scholze et al., 2008), but in addition include a more detailed discrimination model of carbon assimilation, as described in the previous paragraphs. As stated in earlier studies, several additional factors need to be accounted for when carbon isotope fractionation is investigated at ecosystem to global scales. Land use, especially the C3-C4 cover fractions and their change over time, needs to be reasonably well constrained due to the fact that C4 plants fractionate ^{13}C much less than C3 plants (Farquhar et al., 1982). Important is also to account for isotopic disequilibrium, i.e. the fact that respired δ^{13}C was fixed at a time when atmospheric δ^{13}C differed from the current value (Ciais et al., 2005b). This effect requires that all ^{13}C pools, as well as their residence times, must be adequately presented in the model in order to obtain robust ^{13}C flux fields (Scholze et al., 2008). The final analysis could involve both the comparison of the simulated atmospheric δ^{13}C to the observed trend as well as to the trend in the seasonal amplitude of δ^{13}C. This comparison could ultimately be used to constrain the dynamics of c_i/c_a over time (Eq. 6.3) and thus provide an additional large-scale constraint on the behavior of vegetation gas exchange.

Appendices

A   Supplementary Information for Chapter 2

Table A1. Characteristics of flux tower sites used in chapter 2.

Site	Lon (°)	Lat (°)	Climate[a]	Vegetation[b]	LAI	ζ^c	η^c	Ω^c	ϕ^c	Reference
BE-Bra	4.52	51.3	Cfb	DBF/ENF	3.6	7.1	0.07	0.21	0.04	Carrara et al. (2004)
BE-Vie	6	50.3	Cfb	DBF/ENF	5.1	6.8	0.08	0.15	0.04	Aubinet et al. (2002)
CA-Man	-98.48	55.87	Dfc	ENF	4.2	9.5	0.18	0.22	0.03	Dunn et al. (2007)
DE-Tha	13.57	50.96	Cfb	ENF	7.0	8.2	0.11	0.27	0.01	Grünwald and Bernhofer (2007)
DK-Sor	11.65	55.49	Cfb	DBF	5.0	7.0	0.08	0.20	0.03	Pilegaard et al. (2003)
FI-Hyy	24.29	61.84	Dfc	ENF	3.3	7.4	0.09	0.23	0.02	Launiainen (2010)
FI-Sod	26.64	67.36	Dfc	ENF	1.7	7.0	0.09	0.14	0.06	Thum et al. (2007)
FR-Hes	7.06	48.67	Cfb	DBF	5.6	7.9	0.09	0.27	0.02	Granier et al. (2000)
FR-LBr	-0.77	44.72	Cfb	ENF	3.5	7.8	0.07	0.25	0.05	Berbigier et al. (2001)
NL-Loo	5.74	52.17	Cfb	ENF	2.0	6.6	0.04	0.18	0.06	Dolman et al. (2002)
RU-Fyo	32.92	56.46	Dfb	ENF	3.5	7.4	0.08	0.14	0.09	Milyukova et al. (2002)
SE-Fla	19.46	64.11	Dfc	ENF	3.4	7.2	0.12	0.14	0.04	Lindroth et al. (2008)
US-Bar	-71.29	44.06	Dfb	DBF	4.3	7.8	0.08	0.20	0.07	Jenkins et al. (2007)
US-Blo	-120.63	38.90	Csa	ENF	2.0	9.4	0.14	0.18	0.06	Tang et al. (2005)
US-Ha1	-72.17	42.54	Dfb	DBF	5.4	8.0	0.09	0.28	0.02	Urbanski et al. (2007)
US-Ha2	-72.18	42.54	Dfb	ENF	4.4	7.7	0.09	0.23	0.03	Hadley and Schedlbauer (2002)
US-Ho1	-68.74	45.20	Dfb	ENF	6.0	8.2	0.11	0.27	0.02	Hollinger et al. (2004)
US-LPH	-72.19	42.54	Dfb	DBF	4.5	7.7	0.08	0.25	0.03	Hadley et al. (2008)
US-MMS	-86.41	39.32	Cfa	DBF	4.8	8.1	0.10	0.23	0.03	Schmid et al. (2000)
US-UMB	-84.71	45.56	Dfb	DBF	3.5	7.5	0.07	0.25	0.04	Nave et al. (2011)
US-WCr	-90.08	45.81	Dfb	DBF	5.4	7.4	0.10	0.18	0.04	Cook et al. (2004)

[a] Köppen-Geiger climate classification (Cfa = warm temperate, fully humid, hot summer; Cfb = warm temperate, fully humid, warm summer; Csa = warm temperate, dry and hot summer; Dfb = snow, fully humid, warm summer; Dfc = snow, fully humid, cool summer).
[b] DBF = deciduous broadleaf forest, ENF = evergreen needle-leaf forest.

[c] filtered mean summer (JJA) values, simulated in JSBACH with WFDEI climate forcing.

120

Table A2. Characteristics of rivers and associated discharge gauging stations used in chapter 2.

River	Mean annual discharge 1992-2010		Catchment area	Gauging station			Missing years
	m^3 s^{-1}	%	(km^2)	GRDC number	Lon (°)	Lat (°)	1992-2010
Yenisey	19444	14.3	2,440,000	2909150	86.5	67.48	0
Lena	17632	13	2,430,000	2903420	127.65	70.7	0
Ob	13102	9.6	2,950,000	2912600	66.53	66.57	1
Mackenzie	9067	6.7	1,660,000	4208025	-133.74	67.46	2
Ohio	8478	6.2	525770	4123050	-88.74	37.15	0
Volga	8202	6	1,360,000	6977100	44.59	48.8	0
St. Lawrence	7456	5.5	773,892	4143550	-74.79	45.01	0
Danube	6527	4.8	807,000	6742900	28.72	45.22	2
Columbia	5014	3.7	613,830	4115200	-121.17	45.61	0
Pechora	4834	3.6	312,000	6970700	52.2	67.6	1
Yukon	3404	2.5	508,417	4103550	-149.72	65.88	0
Nelson	3393	2.5	1,060,000	4213711	-94.37	56.4	0
Missouri	2690	2	1,357,678	4122900	-91.44	38.71	0
Fraser	2663	2	217,000	4207900	-121.45	49.38	0
Neva	2485	1.8	281,000	6972430	30.53	59.84	0
Rhine	2308	1.7	160,800	6435060	6.11	51.84	0
Stikine	1583	1.2	51,593	4204900	-132.13	56.71	0
Arkansas	1395	1	409,298	4125804	-92.36	34.79	0
Olenek	1237	0.9	198,000	2999910	123.22	72.12	0
Kuskokwim	1178	0.9	80,549	4102100	-158.1	61.87	2
Yana	1114	0.8	224,000	2998110	136.08	70.75	3
Susquehanna	1152	0.8	70,189	4147703	-76.17	39.66	0
Alsek	961	0.7	28,024	4102050	-138.08	59.39	0
Alabama	914	0.7	55,615	4149401	-87.55	31.61	0
Skeena	904	0.7	42,200	4206250	-128.43	54.63	0
Churchill	857	0.6	244,000	4214262	-100.05	56.49	0
Apalachicola	674	0.5	49,728	4149632	-85.02	29.95	0
Elbe	717	0.5	131,950	6340110	10.89	53.23	0
Glomma	700	0.5	40,540	6731400	11.12	59.61	3
Vuoksi	615	0.5	61,061	6855400	28.78	61.21	0
Mezen	637	0.5	56,400	6970500	45.62	65.03	2
Sacramento	563	0.4	55,040	4146281	-121.6	38.77	0
Angermanaelven	521	0.4	30,638	6233650	17.27	63.17	0
Oder	517	0.4	109,564	6357010	14.14	52.87	0
Kemijoki	567	0.4	50,683	6854700	24.55	65.79	0
Daugava	481	0.4	64,500	6973300	26.53	55.88	2
Neman	512	0.4	81,200	6974150	22.58	55.08	2
Klamath	473	0.3	31,339	4146110	-124	41.51	3
Altamaha	353	0.3	35,224	4148720	-81.83	31.65	0
Weser	335	0.2	37,720	6337200	9.12	52.96	0
Kymijoki	300	0.2	36,275	6855200	26.82	60.7	0
San Joaquin	137	0.1	35,058	4146360	-121.27	37.68	0
All	136,096	100	19,767,775				

Table A3. List of CO$_2$ monitoring stations used in chapter 2.

Code	Name, Geographic Location	Longitude (°)	Latitude (°)
ALT	Alert, Canada	-62.52	82.45
BRW	Barrow, Alaska	-156.60	71.32
CBA	Cold Bay, Alaska	-162.72	55.20
MID	Sand Island, Midway, Pacific	-177.37	28.22
MLO	Mauna Loa, Hawaii	-155.58	19.53
STM	Station 'M', Atlantic	2.00	66.00
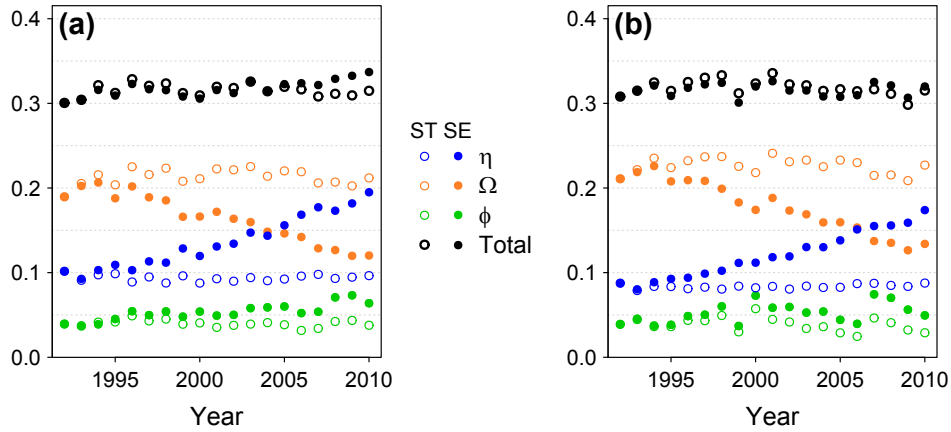
Fig. A1. Mean summer (JJA) values for the fraction of minimum stomatal conductance (g_0) to stomatal conductance (η), vegetation-atmosphere decoupling (Ω) (Eq. 2.3), and fraction of non-transpirational water fluxes on evapotranspiration (ϕ), averaged across all sites for (a) WFDEI and (b) CRUNCEP forcing. Total refers to the combined effect of the three factors, given by $(1 - \eta)(1 - \Omega)(1 - \phi)$ (see Eq. 2.5).
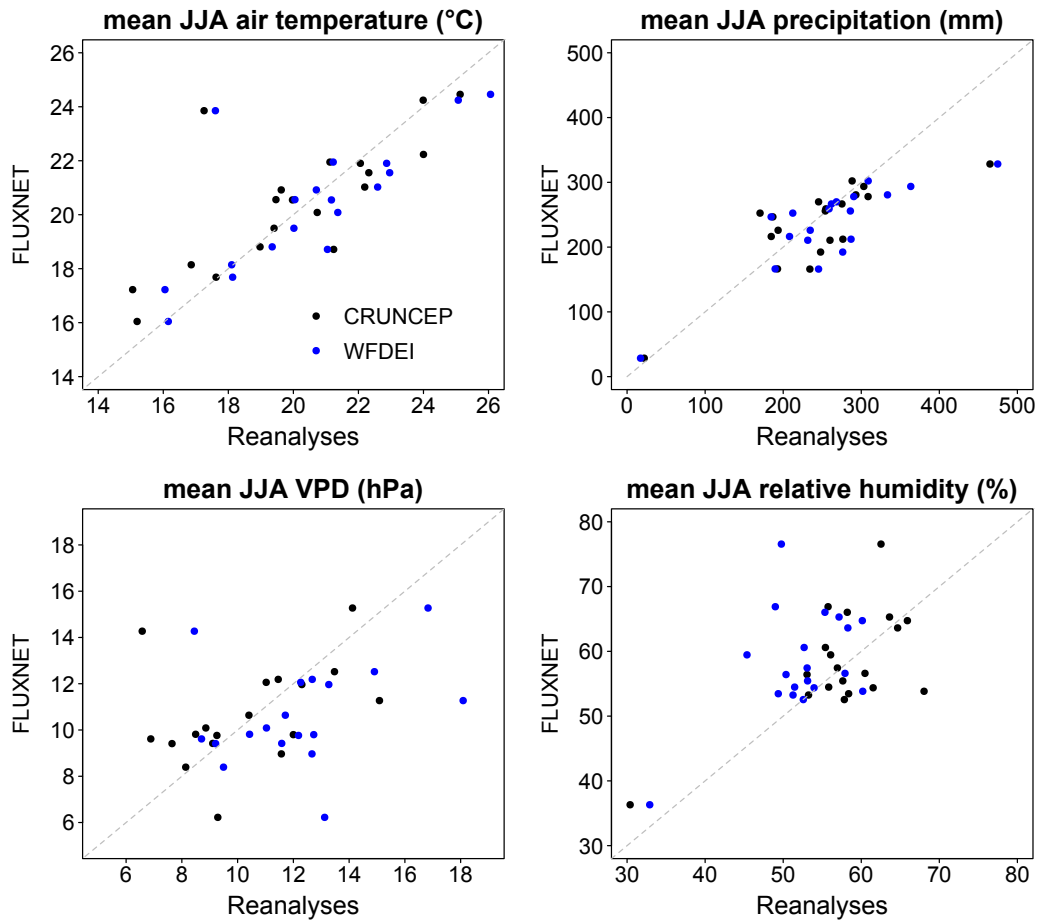
Fig. A2. Mean summer (JJA) air temperature, precipitation, VPD, and relative humidity as measured at the eddy flux towers and the reanalysis products.
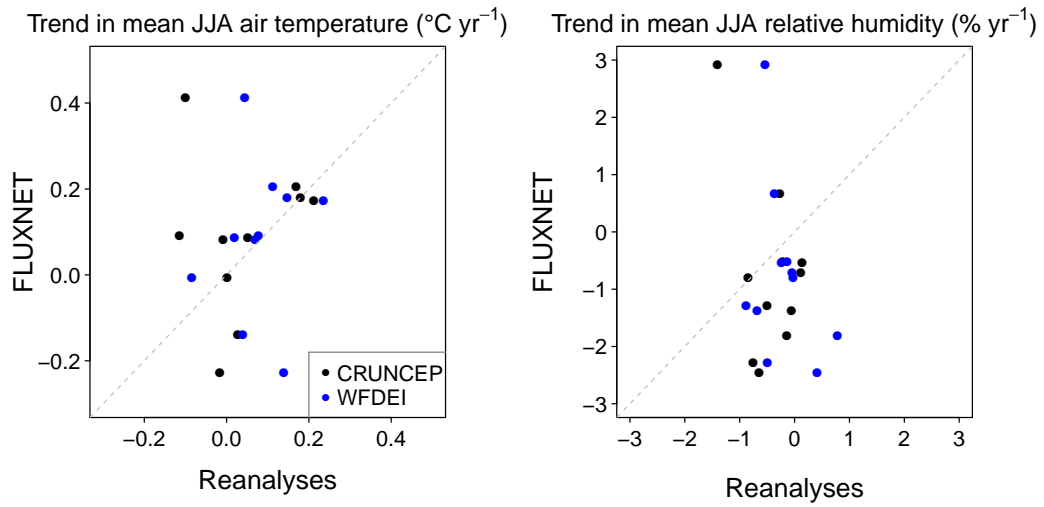
Fig. A3. Mean summer (JJA) trends in air temperature, precipitation, VPD, and relative humidity as measured at the eddy flux towers and the reanalysis products.
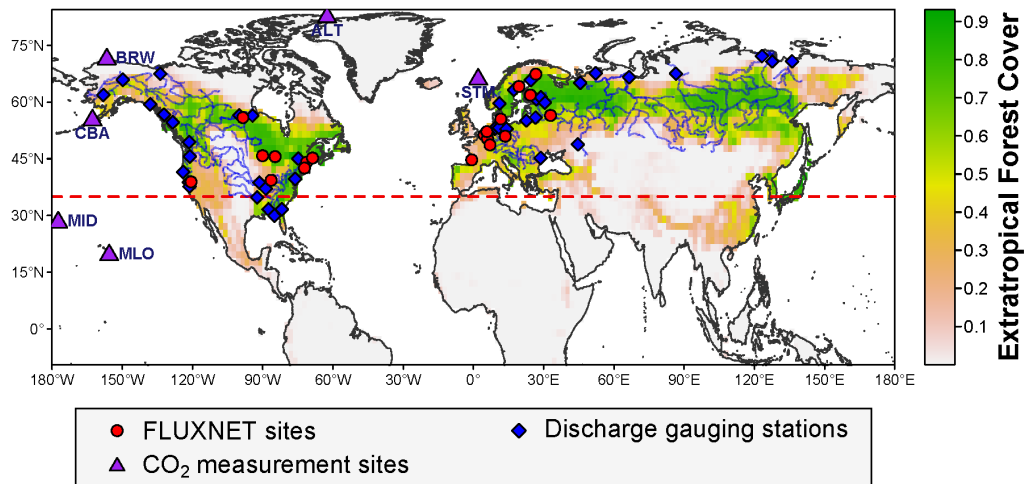
Fig. A4. Location of FLUXNET sites, ground-based CO_2 measurement stations, and discharge gauging stations analyzed in this study. Simulated and observed ET was analyzed for regions north of $35°N$ (dashed red line) and where forest cover exceeds 30%.
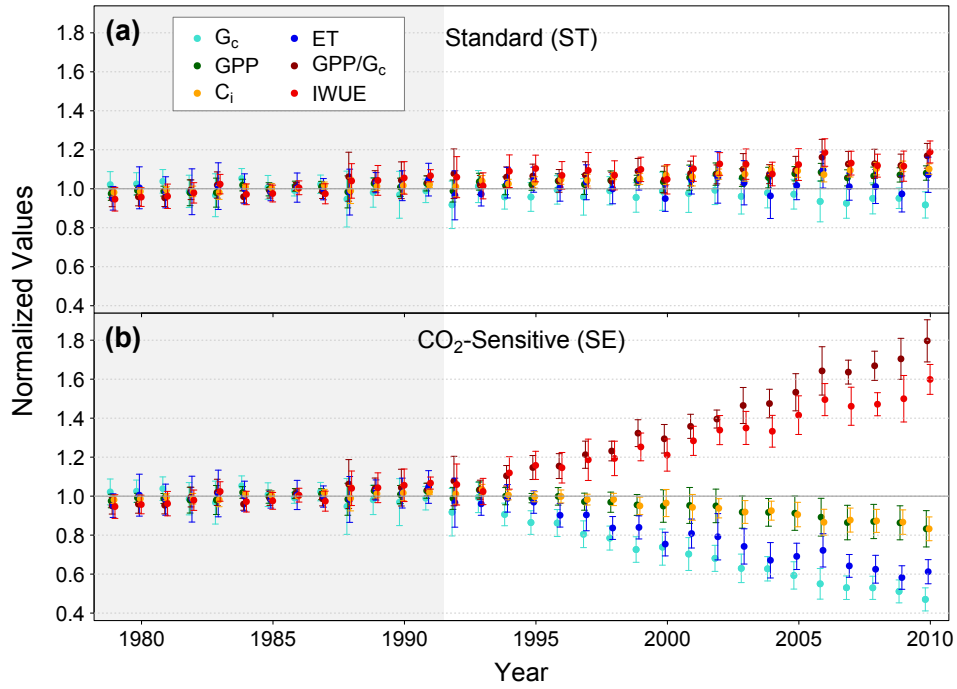
Fig. A5. As Fig. 2.1, but with CRUNCEP climate forcing
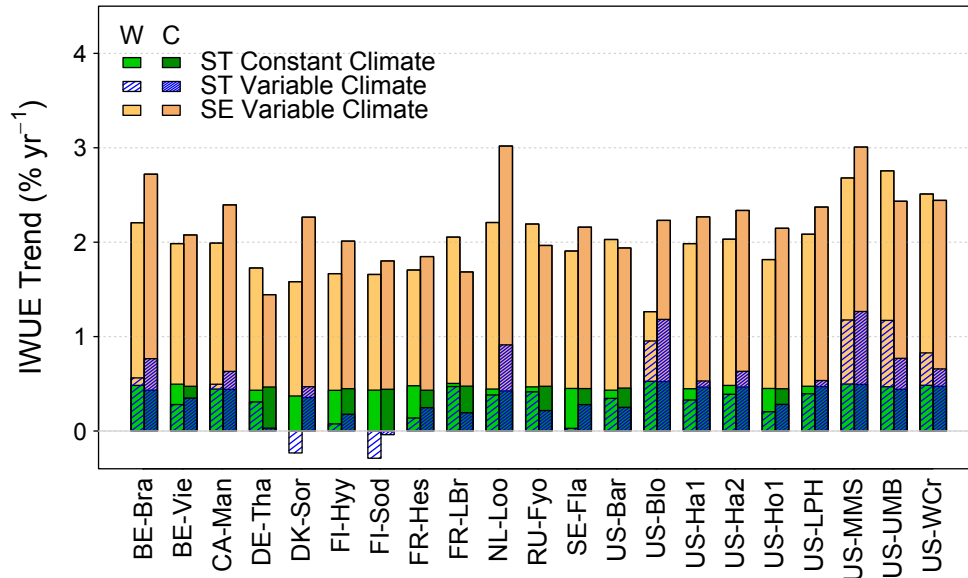
Fig. A6. IWUE trends (1992-2010) for all sites simulated with constant and variable climate in the standard (ST) model formulation, and for variable climate in the CO_2-sensitive (SE) model formulation, for both WFDEI (W) and CRUNCEP (C) climate forcing.
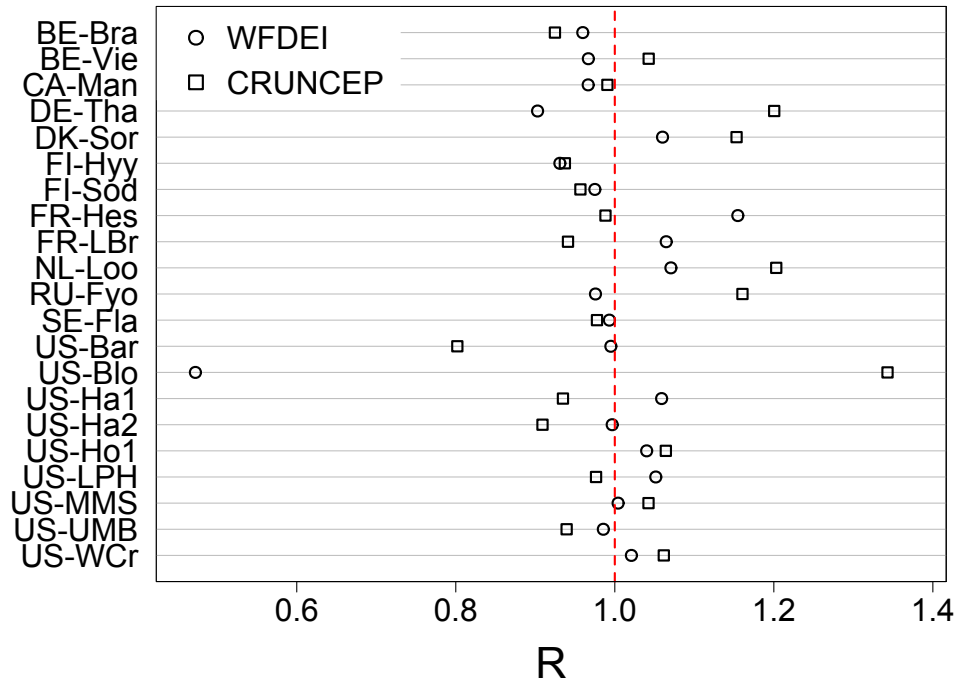
Fig. A7. Contribution of climate variables other than atmospheric CO_2 concentration (c_a) to the IWUE trend in the SE scenario, calculated as $R = \dfrac{\text{Trend,SE}_{varclim} - \text{Trend,ST}_{varclim}}{\text{Trend,SE}_{constclim} - \text{Trend,ST}_{constclim}}$. A value of R close to 1 indicates that the trend in IWUE is predominantly driven by c_a. $R > 1$ indicates that climate variables other than c_a increase the trend compared to the isolated effects of c_a; $R < 1$ indicates the opposite.
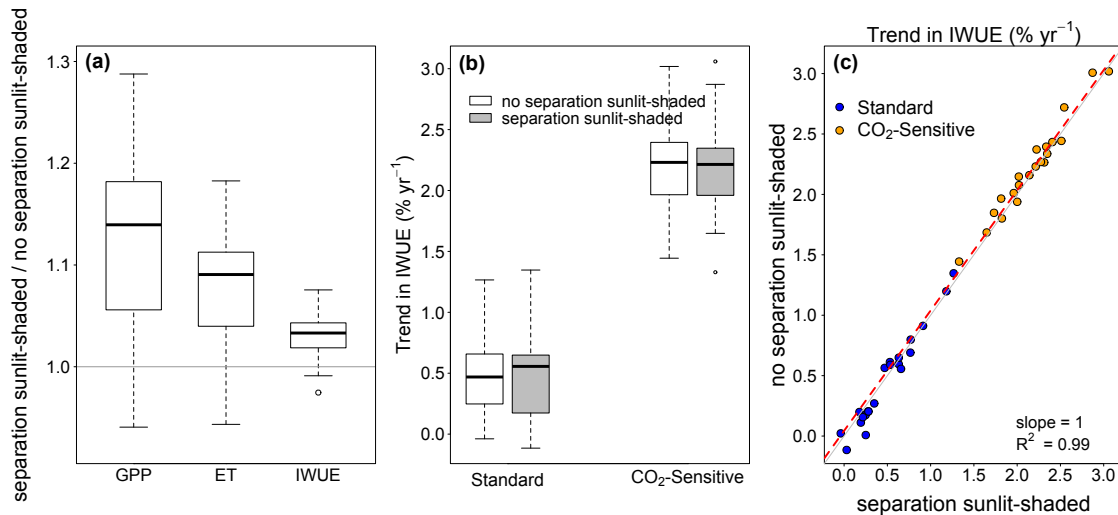
Fig. A8. Results from an alternative model version ("sunlit_shaded"), in which photosynthesis was calculated separately for sunlit and shaded fractions of the canopy. (a) Resulting changes in GPP, ET, and IWUE expressed as the ratio between the model results from the "sunlit_shaded" run and the standard model run. (b) Boxplots and (c) scatterplots showing relative trends in IWUE in the two model versions for both Standard and CO_2-Sensitive runs. The dashed blue line is the regression line. Model runs were forced with the CRUNCEP reanalysis product.

125
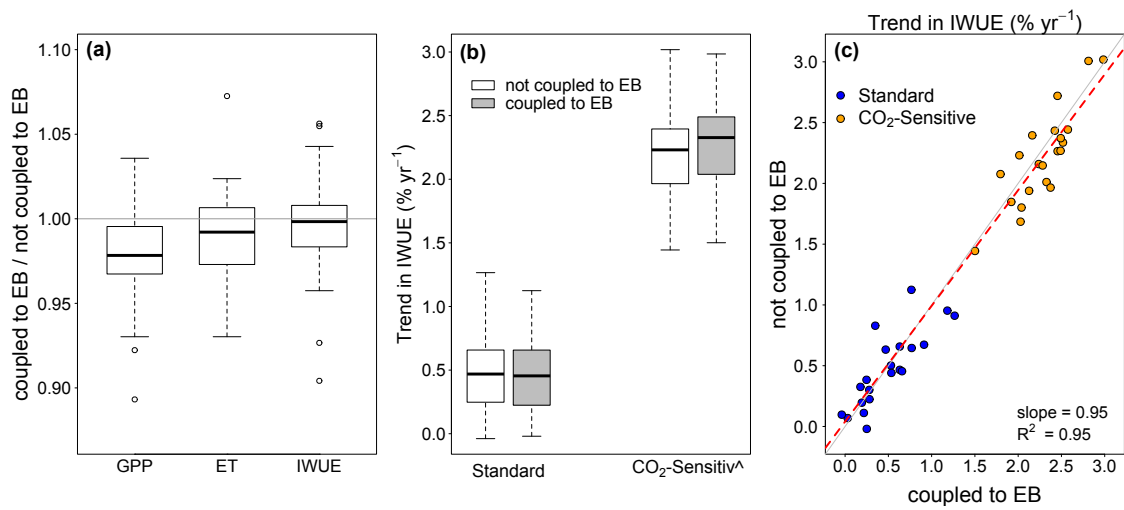
Fig. A9. Results from an alternative model version ("leaf_EB"), in which photosynthesis and stomatal conductance were explicitly coupled to the energy balance (EB). (a) Resulting changes in GPP, ET, and IWUE expressed as the ratio between the model results from the "leaf_EB" run and the standard model run. (b) Boxplots and (c) scatterplots showing relative trends in IWUE in the two model versions for both Standard and CO₂-Sensitive runs. The dashed blue line is the regression line. Model runs were forced with the CRUNCEP reanalysis product.
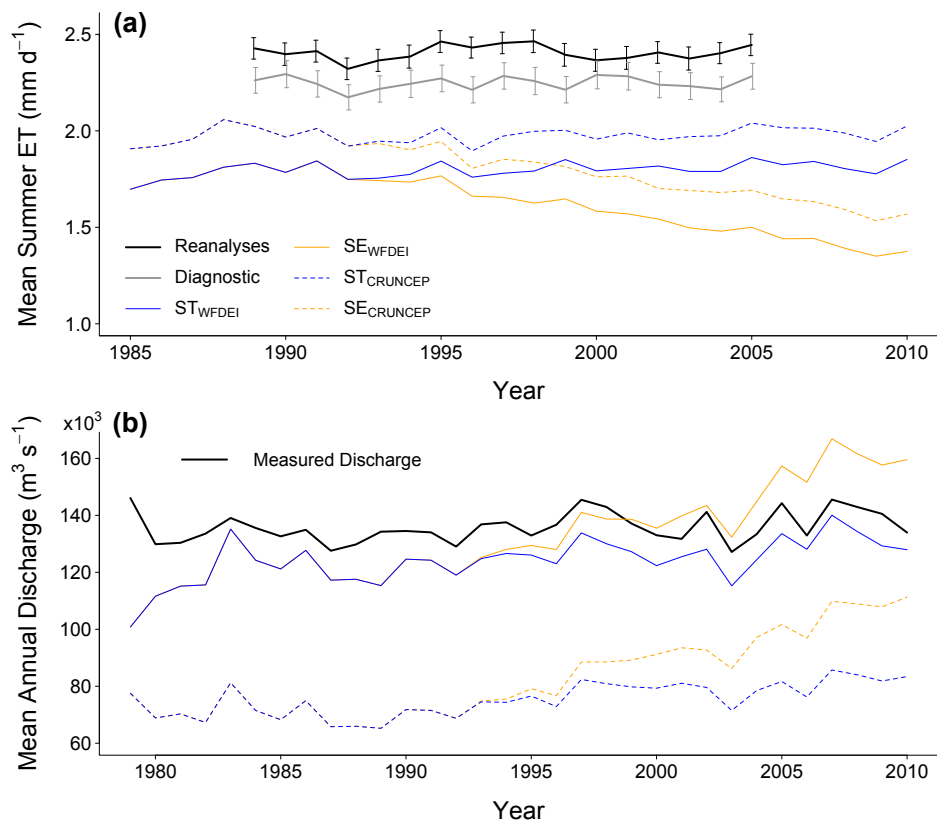
Fig. A10. (a) Mean summer (JJA) ET of diagnostic and reanalysis products described in Mueller et al. (2013), and (b) mean annual discharges
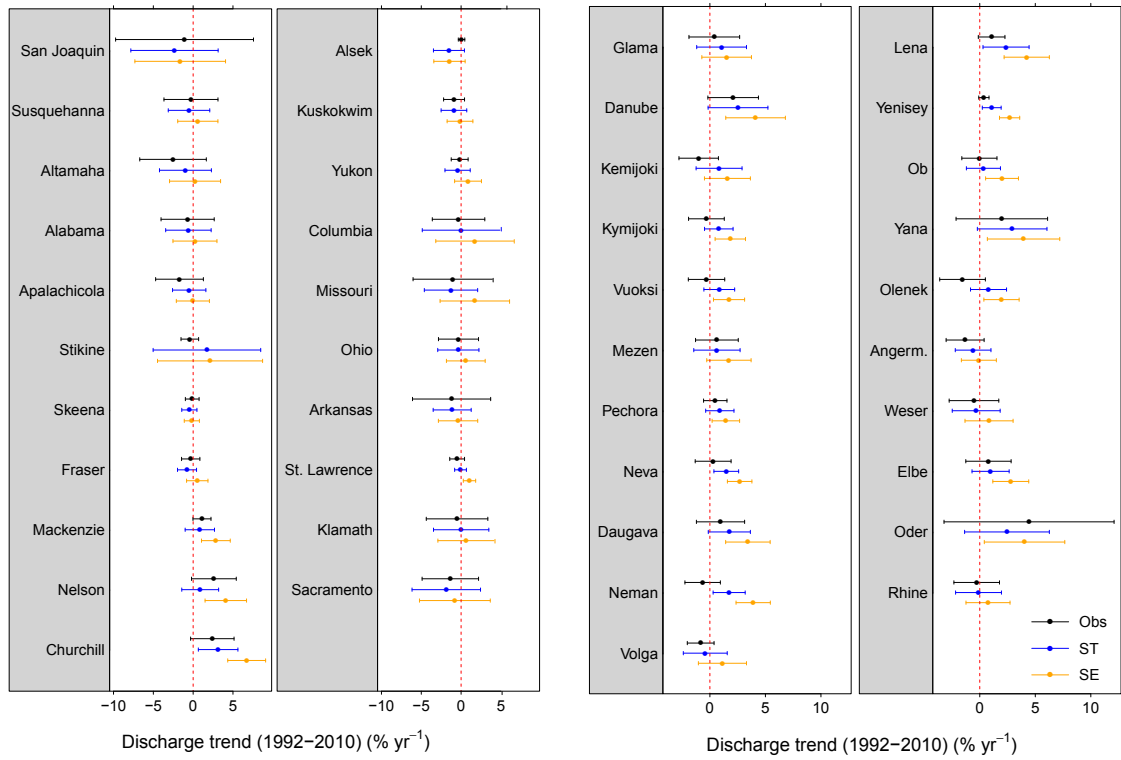
Fig. A11. Relative trends in measured and simulated discharge (with WFDEI climate forcing) for rivers accounted for in this study. Trends and confidence intervals were calculated using generalized least squares, a regression method that accounts for serial correlation in the time series.
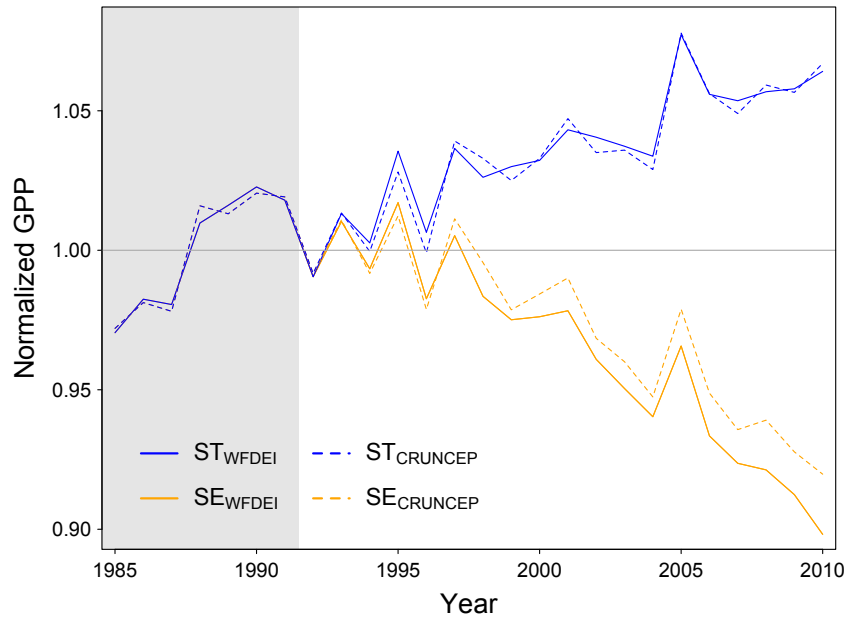
Fig. A12. Time series of simulated gross primary production (GPP) for the Standard (ST) and CO_2-Sensitive (SE) runs and WFDEI and CRUNCEP climate forcing, normalized to the 1985-1991 reference period. Considered are regions north of 35°N and where forest cover (according to SYNMAP) exceeds 30%.
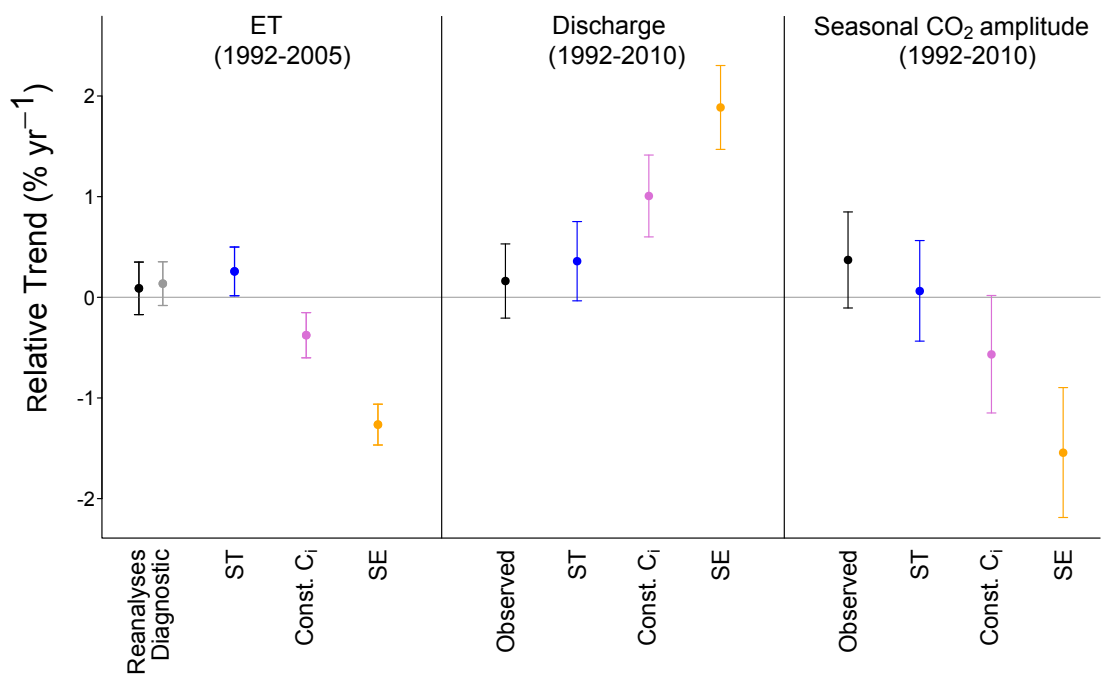
Fig. A13. Confidence intervals for the trend in ET (as in Fig. 2.4b), continental discharge (as in Fig. 2.4d), and the seasonal CO_2 amplitude (as in Fig. 2.5b), including the "constant C_i" scenario, model simulations in which stomatal sensitivity to atmospheric CO_2 concentrations at site level was adjusted to yield constant intercellular CO_2 concentrations (C_i) over time.

B   Supplementary Information for Chapter 3

Physically-based canopy boundary layer conductance model

The non-turbulent component of G_a is often expressed as the kB^{-1} parameter (Verhoef et al., 1997; Massman, 1999), which is related to the boundary layer resistance (R_b) as follows (e.g. Verma, 1989):

$$R_b = \frac{kB^{-1}}{ku_*} \tag{B.1}$$

where k is the von-Kármán constant (0.41), u_* is the friction velocity (m s^{-1}), and B^{-1} is the inverse Stanton number (Owen and Thomson, 1963). The kB^{-1} model used in this study (second term in Eq. 3.6) was originally developed by Massman (1999), and simplified by Su et al. (2001):

$$kB^{-1} = \frac{kC_d}{4C_t\dfrac{u_*}{u(z_h)}}f_c^2 + kB_s^{-1}(1-f_c)^2 \tag{B.2}$$

where C_d is a foliage drag coefficient, assumed constant with a value of 0.2 (Massman, 1999), C_t is the heat transfer coefficient of the leaf, $u(z_h)$ is the wind speed at canopy height (m s^{-1}), f_c is fractional canopy cover, and B_s^{-1} is the inverse Stanton number for bare soil surface (Su et al., 2001). f_c was calculated from LAI for all sites:

$$f_c = (1 - \exp(-0.5LAI)) \tag{B.3}$$

The kB^{-1} value for bare soil surface kB_s^{-1} is given by:

$$kB_s^{-1} = 2.46\text{Re}^{0.25} - \log(7.4) \tag{B.4}$$

where Re is the Reynolds number for bare soil Re=$h_s u_*/v$ (Su et al., 2001), where h_s is the roughness length of the soil, set to 0.01 m, and v is the kinematic viscosity of air (m^2 s^{-1}). Wind speed at canopy height $u(z_h)$ was calculated from the logarithmic wind profile equation:

$$u(z_h) = \frac{u_*}{k}\left(\ln\left[\frac{(z_h - d)}{z_{0m}}\right] - \psi_m\right) \tag{B.5}$$

where z_r is measurement height (m) and ψ_m the integrated stability correction function for momentum (Paulson, 1970), which is a function of the stability parameter ζ ($\zeta = (z_r-d)/L$), where L is the Monin-Obukhov length. The zero-plane displacement height d (m) was fixed as a constant fraction of the canopy height ($d = 0.7z_h$), and the roughness length for momentum z_{0m} (m) was estimated from the following relation:

$$z_{0m} = (z_r - d)\exp(-ku/u_* - \psi_m) \tag{B.6}$$

Note that z_{0m} as estimated from Eq. B.6 implicitly accounts for changes in z_r and/or d

(along with e.g. an increase in canopy height), for which information was not available on an annual basis. As a consequence, z_{0m} in this study has to be interpreted as an effective parameter, integrating any changes in the aerodynamic properties of the ecosystem.

The heat transfer coefficient C_t is given by:

$$C_t = \text{Pr}^{-2/3}\text{Re}_h^{-1/2}N \tag{B.7}$$

where N is the number of leaf sides participating in heat transfer (Massman, 1999), Pr is the Prandtl number (0.71), and Re_h is the Reynolds number, defined as:

$$\text{Re}_h = D_l u/v \tag{B.8}$$

where D_l is the characteristic leaf dimension (m), which was approximated by the geometric mean of the average leaf width and leaf length of the dominant species at the site (Table B1). N in Eq. B.7 was set to 2 for both water vapor and heat, thus assuming that both kB^{-1} and R_b are equal for the two scalars. This is one assumption made in the PM equation (Eq. 3.2), which was supported experimentally (Verma, 1989).

Random forest model

The random forest algorithm is implemented in R using the `randomForest` package (Liaw and Wiener, 2002). The following regression model was constructed:

$$G_1 \ EBR_{\text{halfhourly}} + \lambda E + \text{PPFD} + T_0 + G_{a,\text{empGb}} + \text{DOY} + \text{hour} + G_{c,\text{layer}}/G_{c,\text{tot}}$$

where DOY is day of year. The focus was on the relationship between G_1 and the fraction of G_c coming from a certain layer (i.e. $G_{c,\text{layer}}/G_{c,\text{tot}}$ as a proxy for the contribution of $G_{1,\text{layer}}$ to total G_1). The marginal effect of $G_{c,\text{layer}}/G_{c,\text{tot}}$ on G_1 was calculated with the function `partialPlot()`.

Table B1. Basic observed and calculated aerodynamic properties of the sites investigated in this study. (z_h = mean canopy height; ζ = stability parameter; D_l = characteristic leaf dimension; R_{am} = aerodynamic resistance for momentum; $R_{b,empGb}$ = canopy boundary layer resistance for heat, calculated according to Thom (1972); $R_{b,physGb}$ = canopy boundary layer resistance for heat, calculated according to Su et al. (2001); kB^{-1}_{physGb} = kB^{-1} parameter, calculated according to Su et al. (2001); $R_{a,empGb}$ = total aerodynamic resistance for heat, calculated according to Eq. 3.5; $R_{a,physGb}$ = total aerodynamic resistance for heat, calculated according to Eq. 3.6). Shown are median values over all site years. Data were filtered as described in the Materials and methods section.

Site	z_h (m)	ζ	D_l (m)	R_{am} (s m^{-1})	$R_{b,empGb}$ (s m^{-1})	$R_{b,physGb}$ (s m^{-1})	$kB^{-1}_{,physGb}$	$R_{a,empGb}$ (s m^{-1})	$R_{a,physGb}$ (s m^{-1})
AU-Tum	40	-0.20	0.06	5.95	7.63	5.02	1.64	13.70	11.11
DK-Sor	25	-0.08	0.06	9.43	8.06	10.64	3.13	17.54	20.41
FI-Hyy	14	-0.08	0.01	10.10	8.55	4.74	1.26	18.52	14.92
FR-Pue	5.5	-0.07	0.03	10.53	9.17	5.31	1.34	20.00	16.13
GF-Guy	35	-0.17	0.06	9.43	8.47	11.24	3.09	17.86	20.83
US-Ha1	23	-0.07	0.10	6.80	9.01	7.35	1.95	15.87	13.89

Table B2. Standard error of the regression (SER) for all sites and multiple model versions.

G_1 version[a]	AU-Tum	DK-Sor	FI-Hyy	FR-Pue	GF-Guy	US-Ha1
fcoupled, air, nt	0.160	0.156	0.065	0.052	0.185	0.159
empGb, air, nt	0.171	0.228	0.070	0.046	0.255	0.166
physGb, air, nt	0.169	0.238	0.067	0.045	0.268	0.169
empGb, surface, nt	0.167	0.211	0.065	0.044	0.248	0.161
physGb, surface, nt	0.166	0.226	0.064	0.044	0.263	0.164
empGb, surface, dt	0.175	0.231	0.076	0.049	0.255	0.169
physGb, surface, dt	0.173	0.245	0.076	0.050	0.272	0.173

[a] denoted as: G_a formulation, air or surface conditions, nighttime (nt) or daytime (dt) NEE-partitioning.
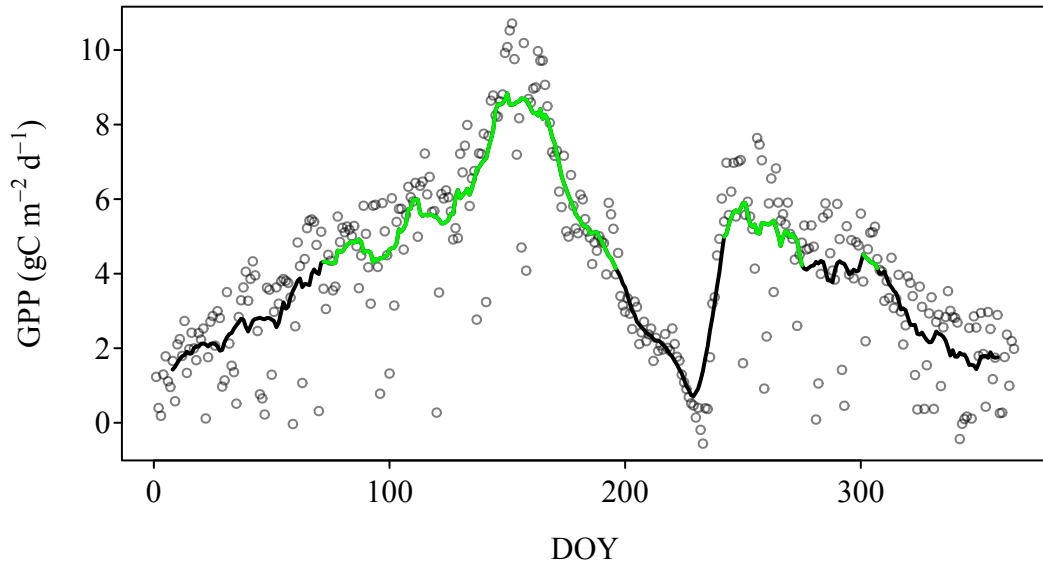
Fig. B1. GPP-based growing season filter used in this study shown for the site FR-Pue for the year 2002. Grey dots are daily GPP sums, the black line is the smoothed GPP time series (window width = 15 days), and the green line is the time period that was considered to be in the growing season.
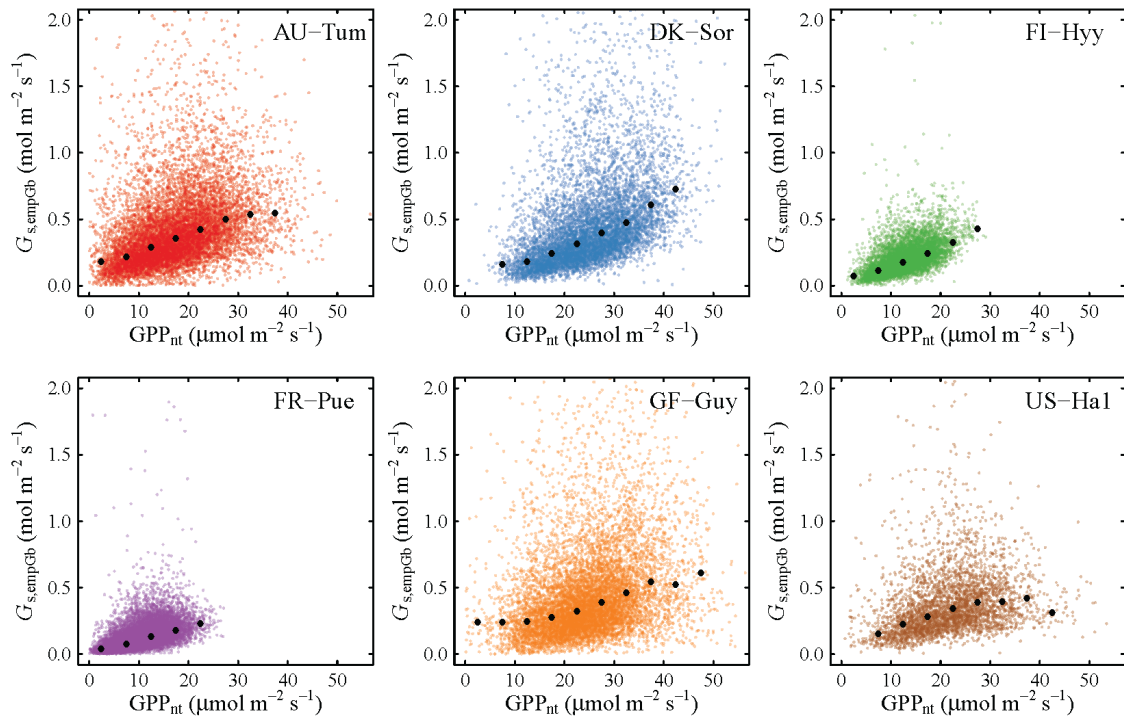
Fig. B2. Surface conductance (G_s, calculated using the G_a version $G_{a,empGb}$ (Eq. 3.5) plotted against GPP (derived from NEE using the nighttime approach according to Reichstein et al. (2005)). Black dots indicate the median of the respective bins.

132
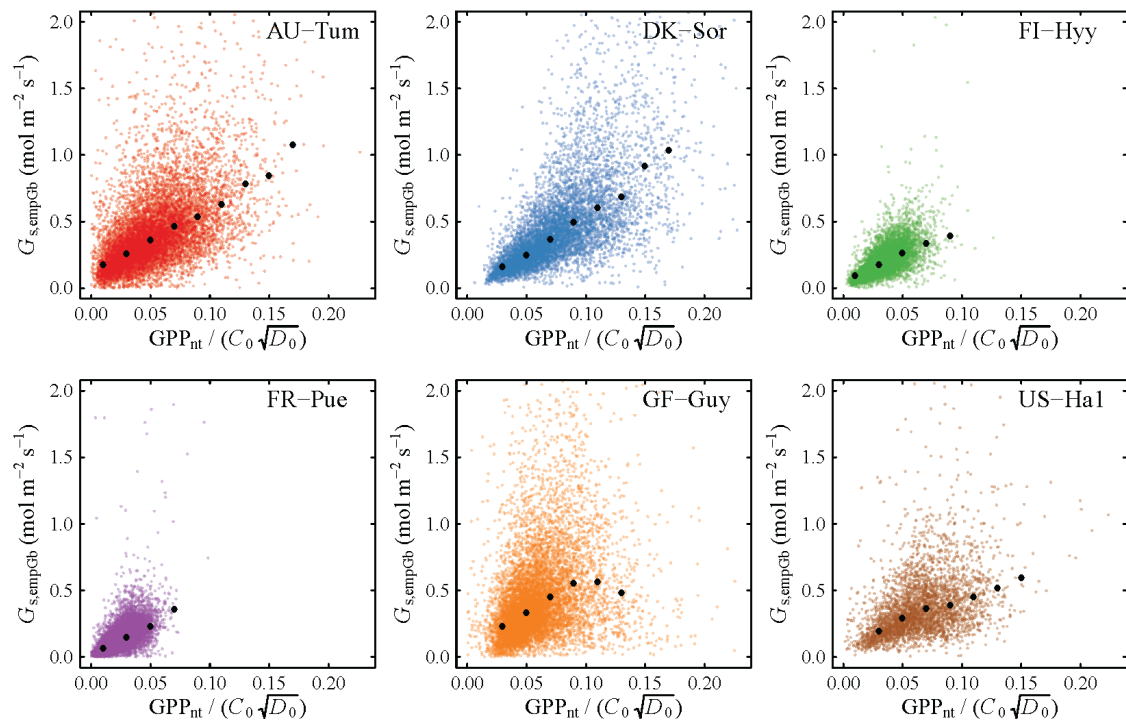
Fig. B3. Surface conductance (G_s, calculated using the G_a version $G_{a,empGb}$ (Eq. 3.5) plotted against GPP / ($C_0 \sqrt{D_0}$) (with GPP derived from NEE using the nighttime approach according to Reichstein et al. (2005)). Black dots indicate the median of the respective bins.
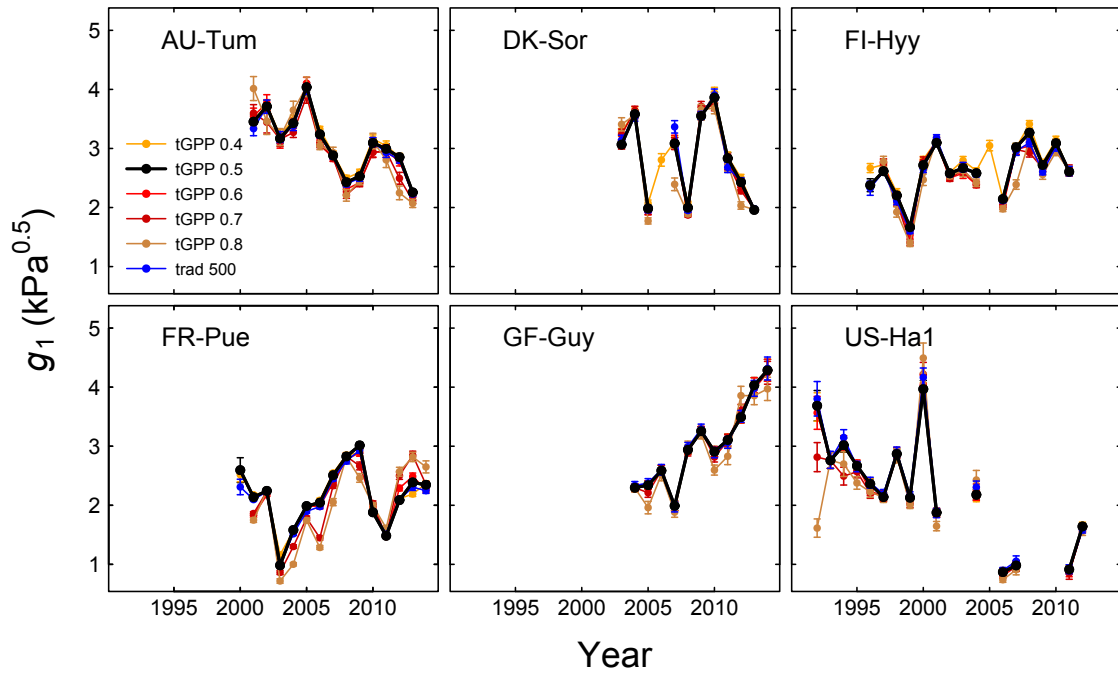
Fig. B4. Sensitivity of annual G_1 estimates to alternative data filters with respect to growing season and radiation thresholds. tGPP 0.4, tGPP 0.5, tGPP 0.6, tGPP 0.7, and tGPP 0.8 denote GPP thresholds corresponding to 40, 50, 60, 70, and 80%, respectively, of the 95th percentile of smoothed daily GPP time series, above which the data were considered to be in the growing season (see Fig. B1). trad 500 denotes an increased radiation threshold of 500 µmol m^{-2} s^{-1}. The thick black line denotes the filter as applied in this study (GPP threshold of 0.5 (50%) and radiation threshold of 200 µmol m^{-2} s^{-1}). Error bars indicate standard errors.
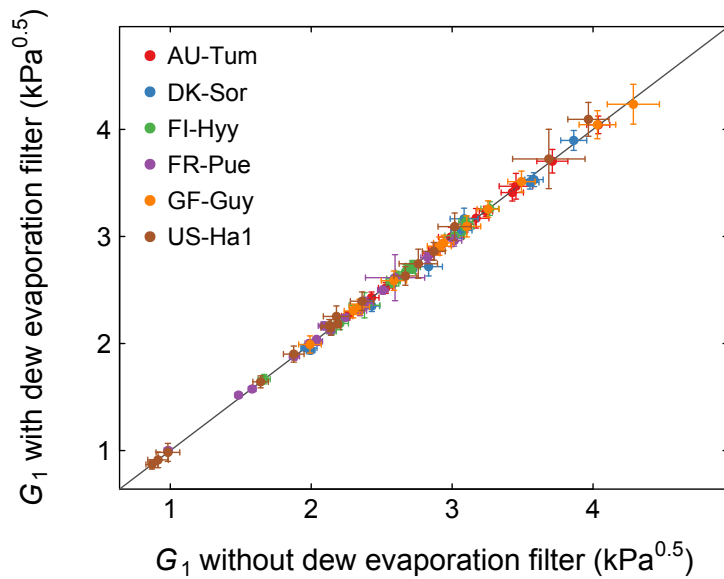
Fig. B5. Effect of the implemented dew evaporation filter on the estimated G_1. The filter excludes time periods that have a high probability of being affected by dew evaporation.

134
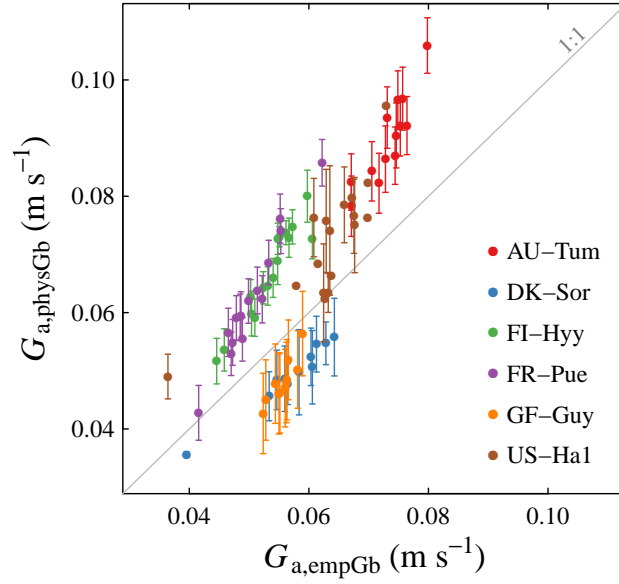
Fig. B6. Comparison of median annual values of aerodynamic conductance (G_a) calculated from different formulations (Eqs. 3.5,3.6).
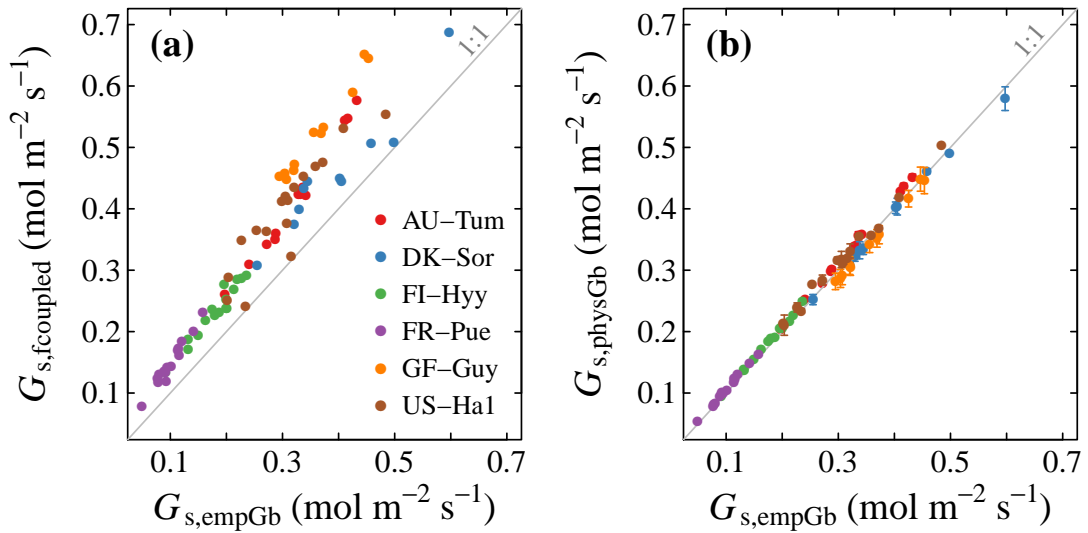
Fig. B7. Same as Fig. B6 for surface conductance (G_s)
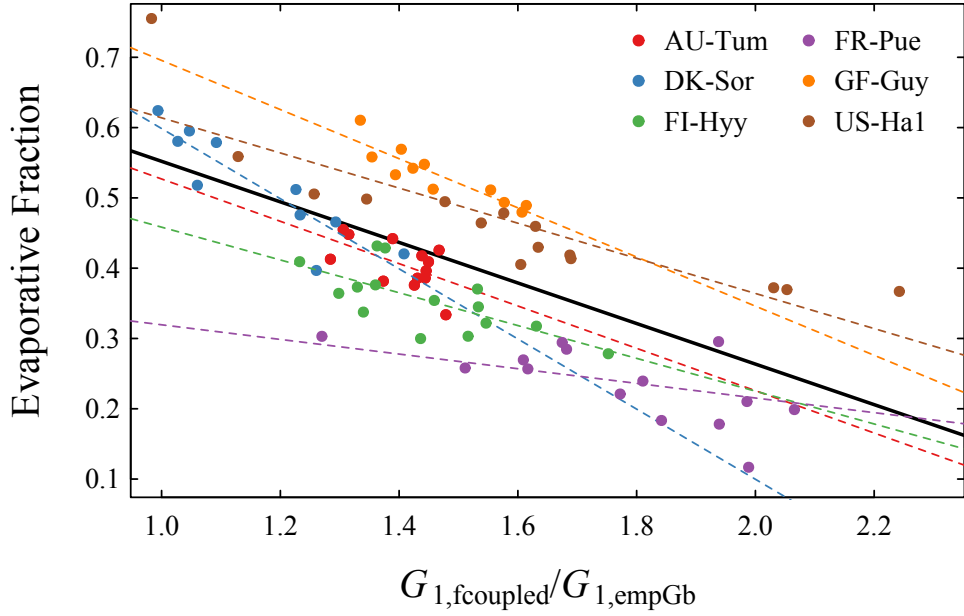
Fig. B8. The relation between evaporative fraction ($\lambda E/R_n$) and the effects of G_a on the estimated G_1. Dashed colored lines and the bold black line are ordinary least squares fits for individual sites and all sites, respectively.
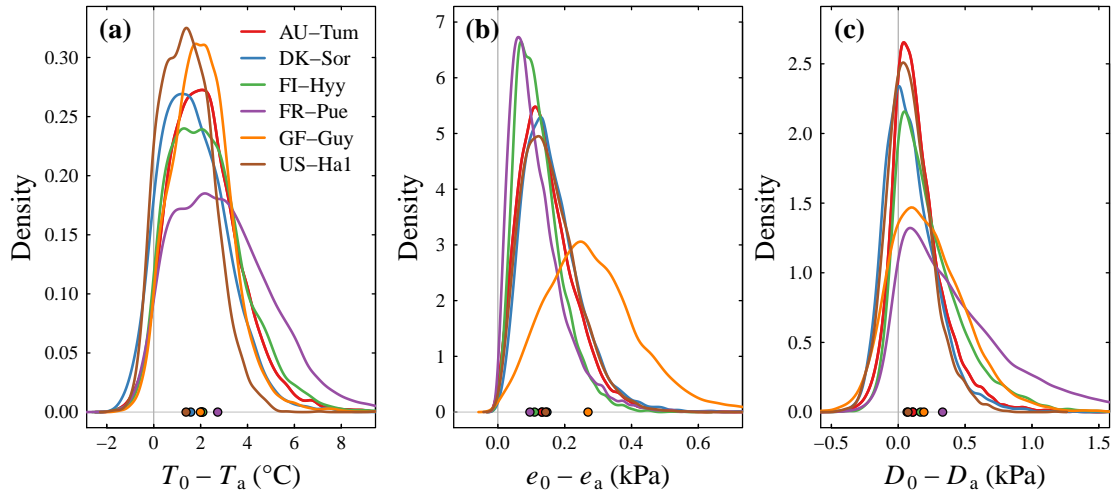
Fig. B9. Deviations of (a) Canopy surface temperature, (b) vapor pressure, and (c) the resulting vapor pressure deficit (as in Fig. 3.4) from those measured in the air. Surface conditions are derived from inverted bulk transfer equations (Eqs. 3.7 - 3.9) with G_a estimated from Eq. 3.5.
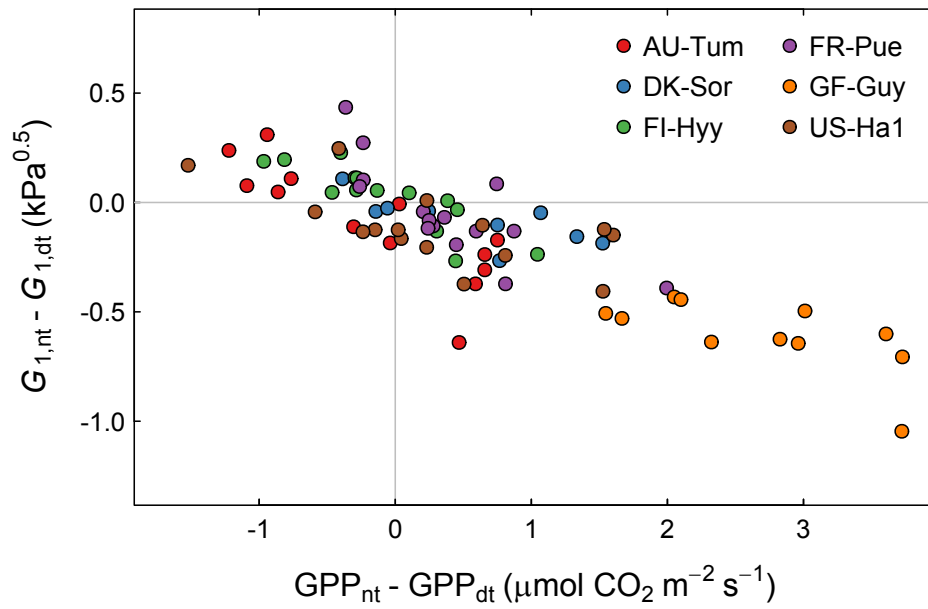
Fig. B10. Differences in GPP as a result of the two different NEE partitioning algorithms (nighttime approach (Reichstein et al., 2005) and daytime approach (Lasslop et al., 2010)) and their effects on G_1.

C Supplementary Information for Chapter 5

Literature survey on mesophyll conductance (g_{m}) and data processing

The literature survey was conducted using Google Scholar. Search terms were "mesophyll conductance" and "internal conductance". The search included peer-reviewed literature published until 31.12.2017 (with the exception of Bahar et al. (2018)).

Only studies were used in which g_{m} is defined as $g_{\mathrm{m}} = A_{\mathrm{n}}/(c_{\mathrm{i}} - c_{\mathrm{c}})$. Alternative definitions such as $g_{\mathrm{m}} = A_{\mathrm{n}}/(c_{\mathrm{i}}$ or g_{m} as the initial slope of the $A_{\mathrm{n}}/(c_{\mathrm{i}}$ curve were excluded. Reported values represent unstressed, fully expanded, non-senescent, young leaves exposed to full sun (note that not always all of these criteria (except the first one) were stated explicitly and had to be assumed for some studies). If data were presented in figures, individual data points were retrieved from the graphs using Plot Digitizer (version 2.6.8, Joseph A. Huwaldt). In a few cases, g_{m} was calculated from A_{n}, c_{i} and c_{c} using $g_{\mathrm{m}} = A_{\mathrm{n}}/(c_{\mathrm{i}} - c_{\mathrm{c}})$.

If units were reported in pressure units (mol m^{-2} s^{-1} bar^{-1} or µmol m^{-2} s^{-1} Pa^{-1}), they were converted to mol m^{-2} s^{-1} using atmospheric pressure (p) at the measurement location. If P was not reported, it was estimated from the hypsometric equation using the altitude of the measurement location. If altitude was not reported or below 200 m, p was assumed to equal approx. 100 kPa (=1 bar) and units were not converted.

g_{m} was standardized to 25°C using Eq. 5.2 with parameter values from Bernacchi et al. (2002). In cases where leaf temperature was not reported, cuvette temperature was taken as a proxy. Measurements for which temperature was not reported were discarded. In case of model versions *ExpL* and *ExpCL*, which assume a light dependency of g_{m}, g_{m} was standardized to high light (1500 µmol m^{-2} s^{-1}) using Eq. 5.6 .

Records obtained with all measurement methods were included in the analysis. If g_{m} was measured with both the curve fitting technique and an additional method (e.g. gas exchange and chlorophyll fluorescence or gas exchange and carbon isotope discrimination), only the additional method was taken, as they are considered more reliable than the curve fitting method (Pons et al., 2009). A basic outlier removal procedure was implemented at PFT-level. Records were flagged as outliers and removed if the distance of g_{m} values exceeded 1.5 times the interquartile range of the log-transformed g_{m} data within each PFT. The log-transformation was necessary to obtain normally distributed data, which enabled the detection of both high and low outliers. This procedure led to the exclusion of 23 records (3.6%).

In total 325 studies were analyzed which contained 821 measurements from 407 species. Among them, 319 species from 295 studies and 609 individual measurements fulfilled all criteria described above and could be assigned to a PFT considered by JSBACH. These measurements (see Fig. 5.1; available under `https://bitbucket.org/juergenknauer/gm_data`) were then used to parameterize the model.

Table C1. c_i- and c_c-based photosynthetic parameters used in this study.

Vegetation type	Parameter	c_i-based				c_c-based			
		Value at 25°C	H_a (kJ mol⁻¹)	H_d (kJ mol⁻¹)	ΔS (J mol⁻¹ K⁻¹)	Value at 25°C	H_a (kJ mol⁻¹)	H_d (kJ mol⁻¹)	ΔS (J mol⁻¹ K⁻¹)
C3 vegetation	g_m (mol m⁻² s⁻¹)	∞	-	-	-	PFT-specific	49.6	437.4	1400
	V_{cmax} (µmol m⁻² s⁻¹)	PFT-specific	65.33	200	635	PFT-specific	65.33	200	635
	J_{max} (µmol m⁻² s⁻¹)	PFT-specific	43.9	200	640	PFT-specific	43.9	200	640
	R_l (µmol m⁻² s⁻¹)	0.011V_{cmax25}	46.39	200	640	0.011 V_{cmax25}	46.39	200	640
	K_c (µmol mol⁻¹)	404.9	79.43	-	-	272.38	80.99	-	-
	K_o (mmol mol⁻¹)	278.4	36.38	-	-	165.82	23.72	-	-
	Γ_* (µmol mol⁻¹)	42.75	37.83	-	-	37.43	24.46	-	-
C4 vegetation	V_{cmax} (µmol m⁻² s⁻¹)	PFT-specific	67.29	144.6	472	PFT-specific	67.29	144.6	472
	J_{max} (µmol m⁻² s⁻¹)	PFT-specific	77.9	191.9	627	PFT-specific	77.9	191.9	627
	R_l (µmol m⁻² s⁻¹)	0.01 V_{cmax25}	46.39	200	640	0.01 $V_{cmax,25}$	46.39	200	640
	V_{pmax} (µmol m⁻² s⁻¹)	PFT-specific	70.37	117.9	376	PFT-specific	70.37	117.9	376
	K_p (µmol mol⁻¹)[a]	80	68.1	-	-	80	68.1	-	-
	g_{bs} (mol m⁻² s⁻¹)[b]	0.003	-	-	-	0.003	-	-	-

[a] K_p = Michaelis-Menten constant of PEP-carboxylase for CO_2

[b] bundle-sheath conductance to CO_2

Table C2. Sensitivity analysis of the parameter adjustment approach described in this paper with respect to the c_i-range and leaf day respiration (R_l) values used.

c_i-based parameters	c_c-based parameters (c_i range 0-1500 µmol mol^{-1}; R_l = 0.55 µmol m^{-2} s^{-1})	c_i range 0-1200 µmol mol^{-1}	c_i range 0-1800 µmol mol^{-1}	R_l = 0.44 µmol m^{-2} s^{-1}	R_l = 0.66 µmol m^{-2} s^{-1}
$g_{m,max25}$	∞	0.15	0.15	0.15	0.15
$V_{cmax25,ci}$	50	**58.42**	58.39	58.45	58.66	58.18
$J_{max25,ci}$	95	**95.52**	95.85	95.32	95.54	95.51
$J_{max25,ci}/V_{cmax25,ci}$	1.9	1.635	1.642	1.631	1.629	1.642

140

Table C3. Goodness of fit metrics for simulated A_n of the explicit (*Exp*) model version compared to the implicit (*Imp*) model over a c_i range of 0-1500 µmol mol^{-1}. Other parameters were: $V_{cmax25,ci} = 40$ µmol m^{-2} s^{-1}, $J_{max25,ci} = 76$ µmol m^{-2} s^{-1}.

$g_{m,max25}$ (mol m^{-2} s^{-1})	RMSE[a] (µmol m^{-2} s^{-1})	MAE[b] (µmol m^{-2} s^{-1})
0.3	0.056	0.025
0.2	0.073	0.051
0.15	0.123	0.097
0.1	0.249	0.202
0.075	0.416	0.334

[a] root mean square error
[b] mean absolute error

Table C4. As Table 5.3, but for the *ExpL* and *ExpCL* model versions.

PFT	$g_{m,max25}$ [a] $\pm$ SEM[b] (mol m^{-2} s^{-1})	$V_{cmax25,cc}$ (µmol m^{-2} s^{-1})	$J_{max25,cc}$ (µmol m^{-2} s^{-1})	$J_{max25,cc}/V_{cmax25,cc}$	$g_{m,max25}$ [c] (mol m^{-2} s^{-1})	$V_{cmax25,cc}$ (µmol m^{-2} s^{-1})	$J_{max25,cc}$ (µmol m^{-2} s^{-1})	$J_{max25,cc}/V_{cmax25,cc}$
r	ExpL	ExpL	ExpL	ExpL	ExpCL	ExpCL	ExpCL	ExpCL
DNF	0.060 ± 0.010	55.3	64.7	1.17	0.056	64.1	85.1	1.33
TDF	0.062 ± 0.022	52.7	64.3	1.22	0.061	49.6	70.4	1.42
ENF	0.088 ± 0.022	98.8	103.8	1.05	0.083	116.6	152.1	1.3
DSH	0.113 ± 0.026	67.1	96.1	1.43	0.114	70.2	106.6	1.52
EBF	0.109 ± 0.010	105.4	120.2	1.14	0.107	113.6	152.6	1.34
TRF	0.156 ± 0.027	41.9	74	1.77	0.151	43.7	76.9	1.76
DBF	0.187 ± 0.017	58.6	99.3	1.69	0.184	60	103.6	1.73
C3G	0.201 ± 0.015	53.7	95.1	1.77	0.202	55.5	98.5	1.78
RSH	0.228 ± 0.112	52	94.3	1.82	0.235	53.2	97	1.82
C3C	0.312 ± 0.018	86.6	152.3	1.76	0.323	88.9	157.8	1.77
		$V_{pmax25,cc}$ (µmol m^{-2} s^{-1})				$V_{pmax25,cc}$ (µmol m^{-2} s^{-1})		
C4G	0.453 ± 0.154	118.3			0.382	189		
C4C	0.743 ± 0.477	142.7			0.623	185.6		

[a] standardized to a c_i of 260 µmol mol^{-1} (Eq. 5.5)
[b] standard error of the median

[c] standardized to a aPPFD of 1500 µmol m^{-2} s^{-1} (Eq. 5.6)
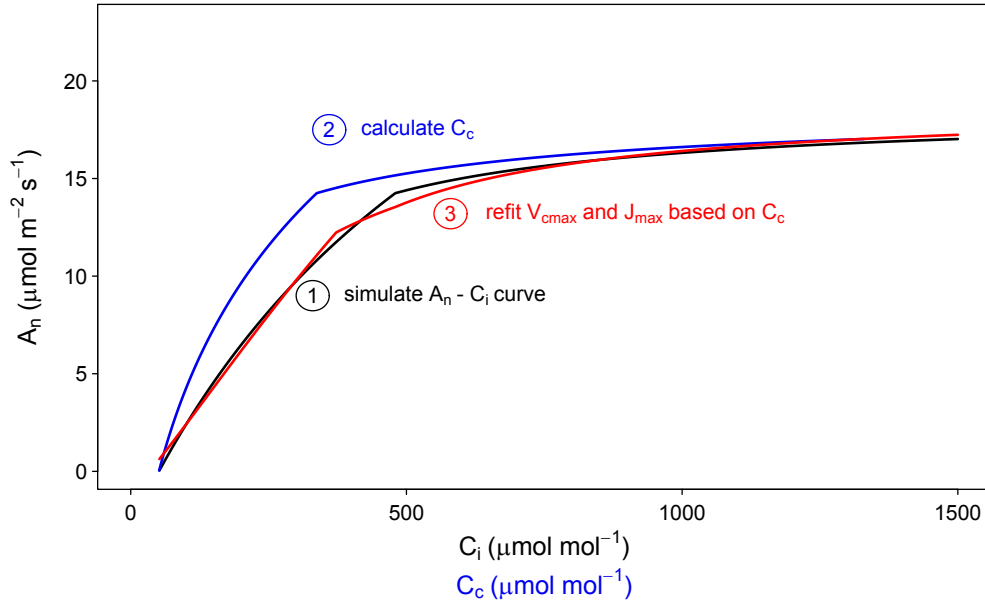
Fig. C1. Illustration of the parameter adjustment procedure implemented in this chapter. Parameters of the c_i-based model (step 1) are: $V_{cmax25,ci} = 45$ µmol m^{-2} s^{-1}; $J_{max25,ci} = 85.5$ µmol m^{-2} s^{-1}; $R_l = 0.495$ µmol m^{-2} s^{-1}; Rubisco kinetic parameters are listed in Table C1. $g_{m,max25} = 0.1$ mol m^{-2} s^{-1} and is assumed to be independent of c_i (step 2). The resulting c_c-based parameters are (step 3): $V_{cmax25,cc} = 61.6$ µmol m^{-2} s^{-1}; $J_{max25,cc} = 86.9$ µmol m^{-2} s^{-1}.
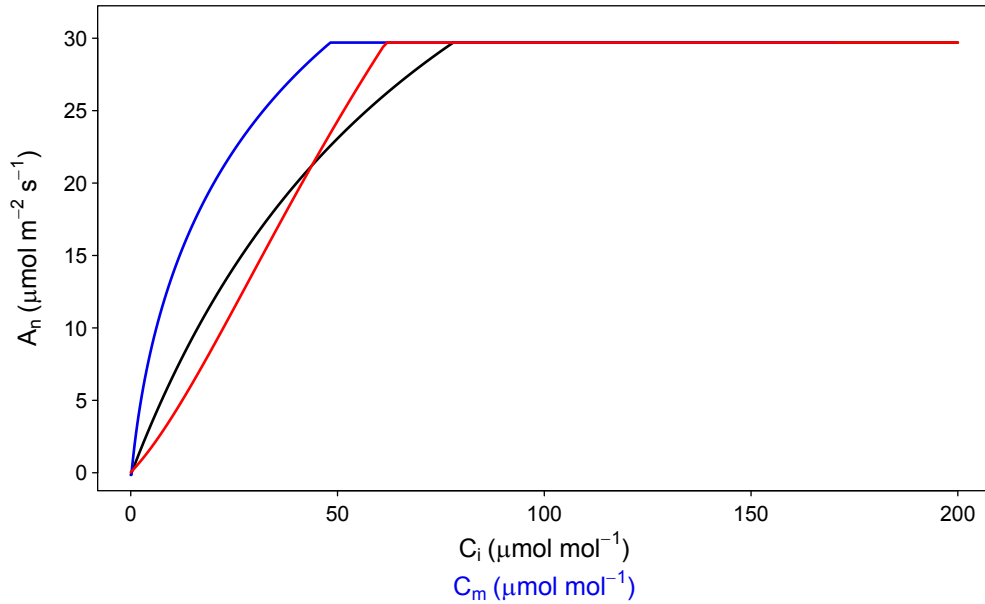
Fig. C2. Same as Fig. C1 but for the C4 photosynthesis model of von Caemmerer and Furbank (1999). Parameters of the c_i-based model (black line) are: $V_{cmax25,ci} = 30$ µmol m^{-2} s^{-1}; $J_{max25,ci} = 200$ µmol m^{-2} s^{-1}; $V_{pmax25,ci} = 60$ µmol m^{-2} s^{-1}; $R_l = 0.3$ µmol m^{-2} s^{-1}. $g_{m,max25} = 1$ mol m^{-2} s^{-1} and is assumed to be independent of c_i. The resulting c_c-based parameters (red line) are: $V_{pmax25,cc} = 96.7$ µmol m^{-2} s^{-1} and all other parameters are unchanged.

142
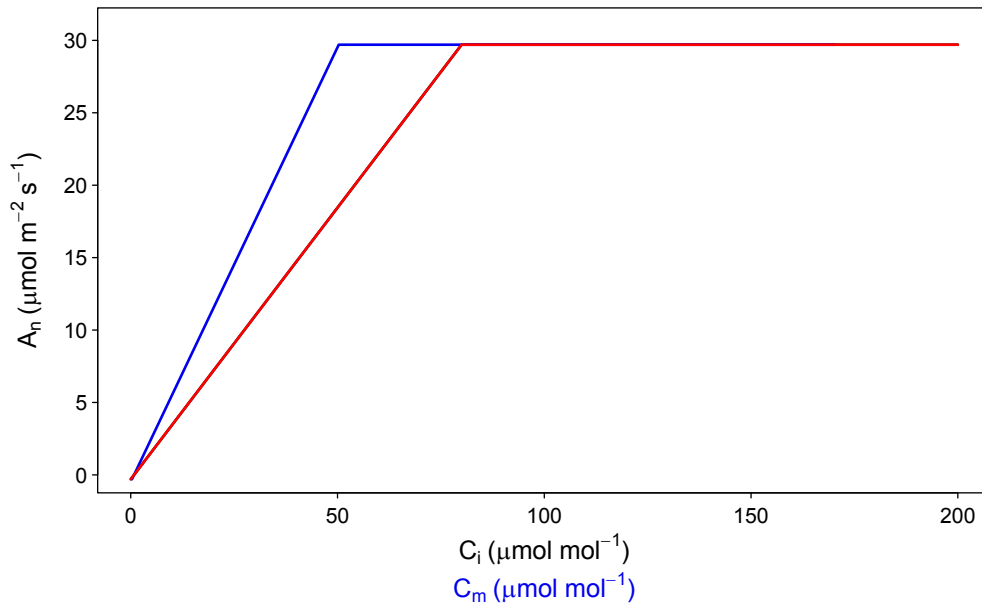
Fig. C3. Same as Fig. C1 but for the C4 photosynthesis model of Collatz et al. (1992) as implemented in Bonan et al. (2011). Parameter values were $V_{cmax25,ci} = 30$ µmol m^{-2} s^{-1}; k_{ci} (initial slope of the CO_2 response curve) $= 0.375$; $g_m = 1.0$ mol m^{-2} s^{-1};. The resulting $k_{cc} = 0.258$. For this model, the c_i-based and c_c-based model versions are identical.
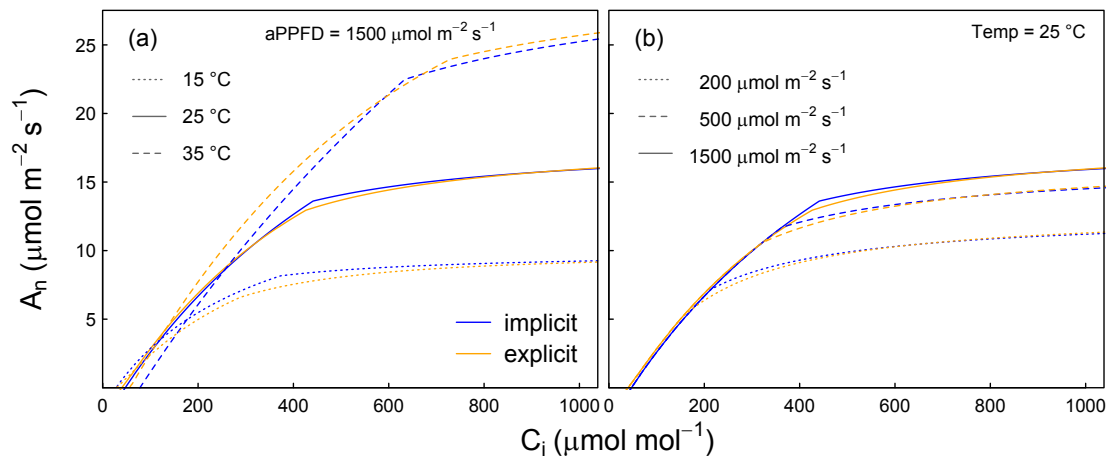
Fig. C4. Same as Fig. 5.2a,b, but for the *ExpC* model version (g_m assumed to respond to intercellular CO_2 concentration (c_i) according to Eq. 5.5)
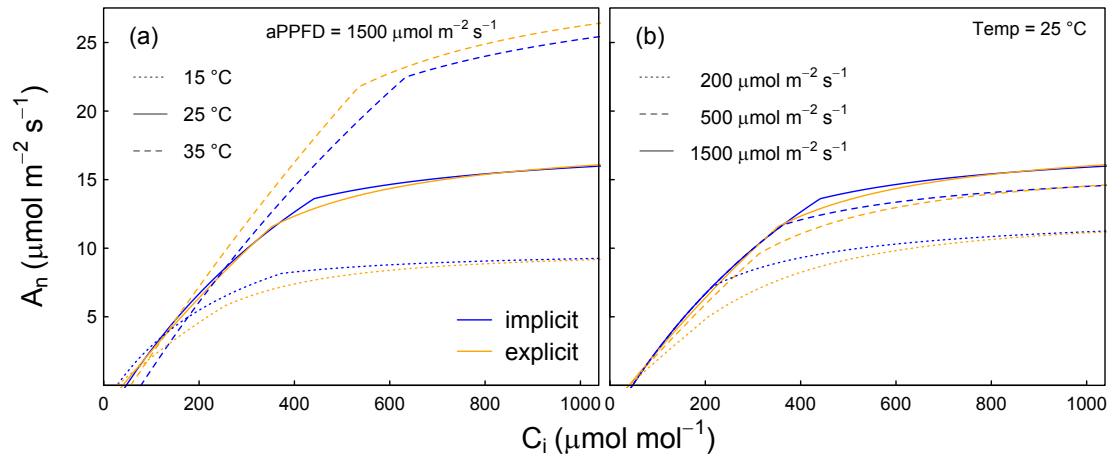
Fig. C5. Same as Fig. 5.2a,b, but for the *ExpL* model version (g_m assumed to respond to absorbed photosynthetic photon flux density (aPPFD) according to Eq. 5.6)
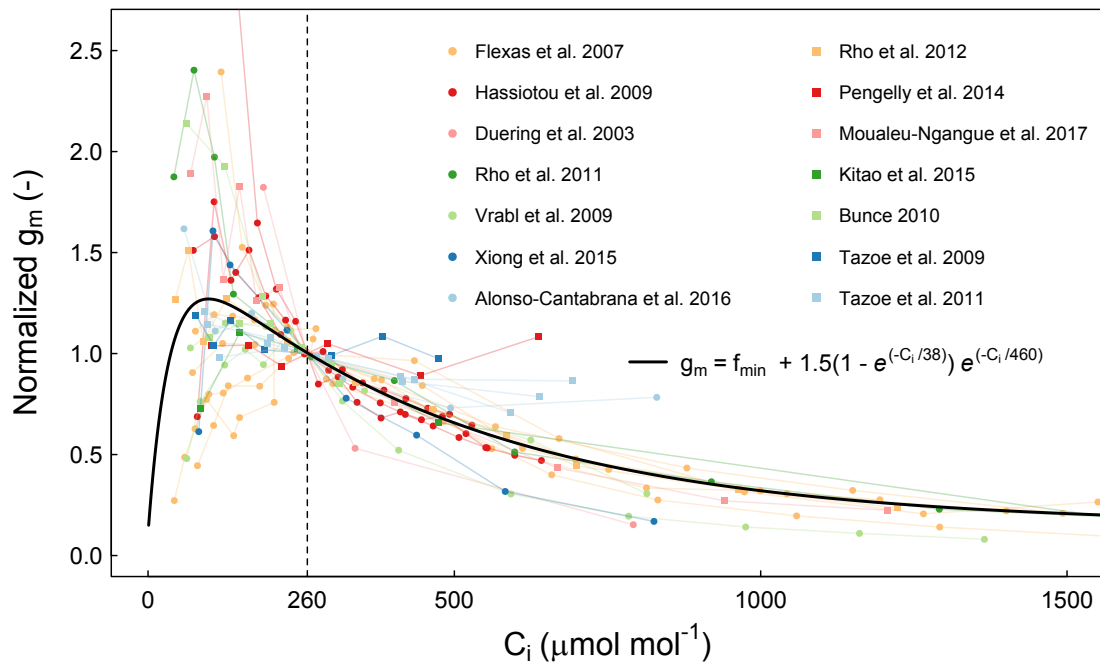
Fig. C6. Compilation of published c_i (intercellular CO_2 concentration) responses of g_m. g_m was normalized to a value of 1 at c_i of 260 µmol mol^{-1}. The bold black line illustrates the function as implemented in the model (Eq. 5.5) with $f_{min} = 0.15$.
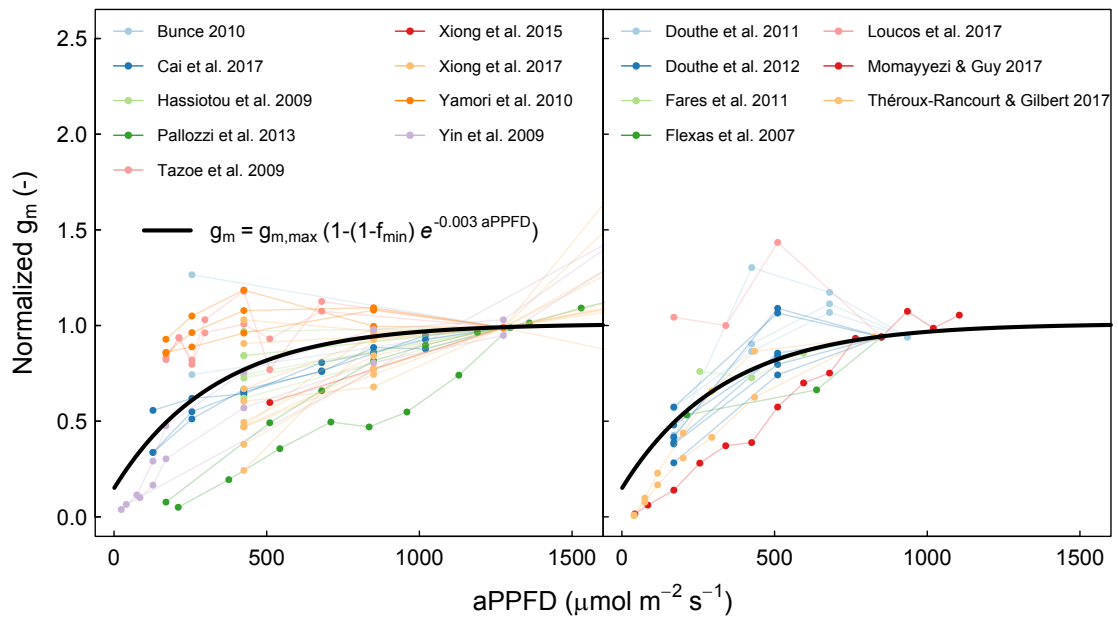
Fig. C7. Compilation of published light responses of g_m. g_m was normalized to aPPFD (absorbed photosynthetic photon flux density) of 1250 µmol m^{-2} s^{-1} (left) and 850 µmol m^{-2} s^{-1} (right). aPPFD was assumed to equal 0.85 PPFD. The bold black line illustrates the function (Eq. 5.6) as implemented in the g_m model of this study (Eq. 5.1).
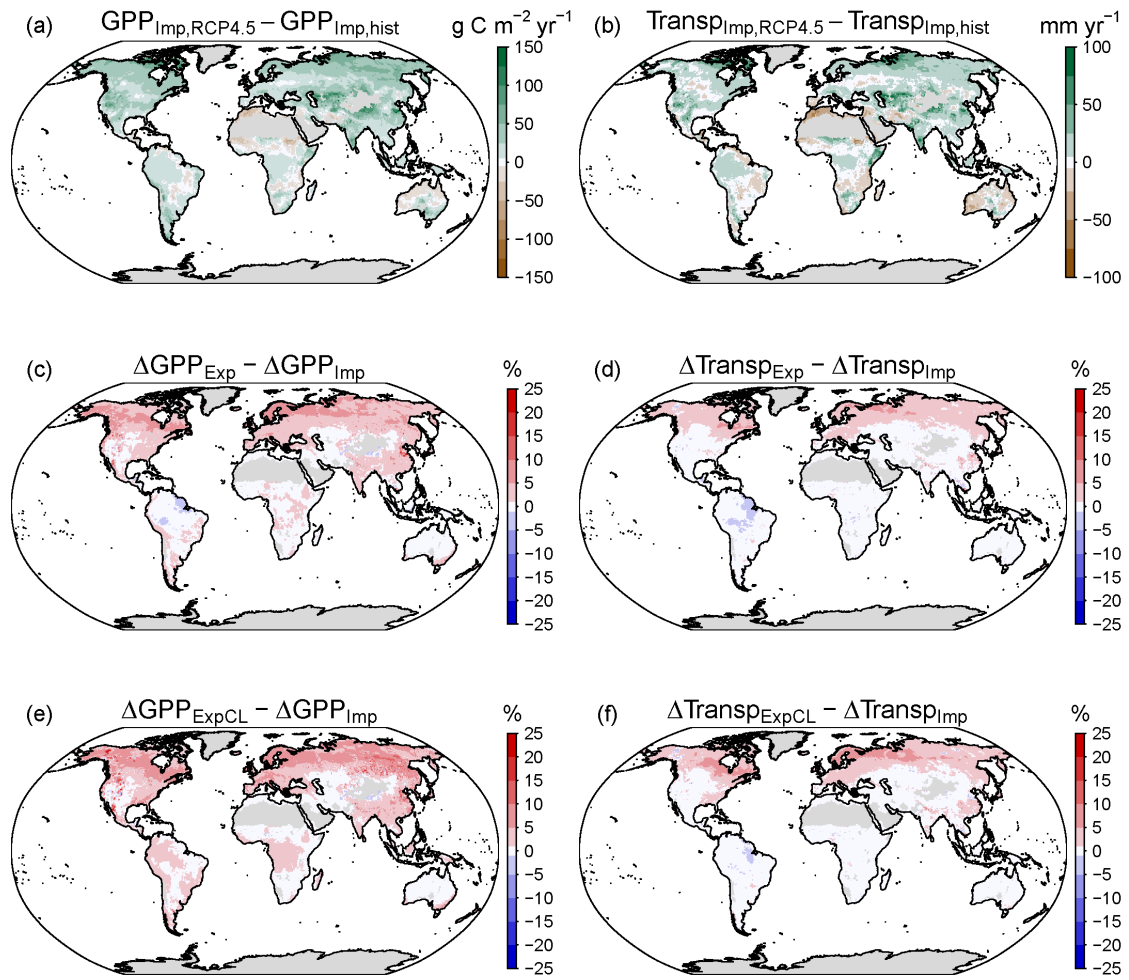
Fig. C8. Same as Fig. 5.6, but for the RCP4.5 scenario.
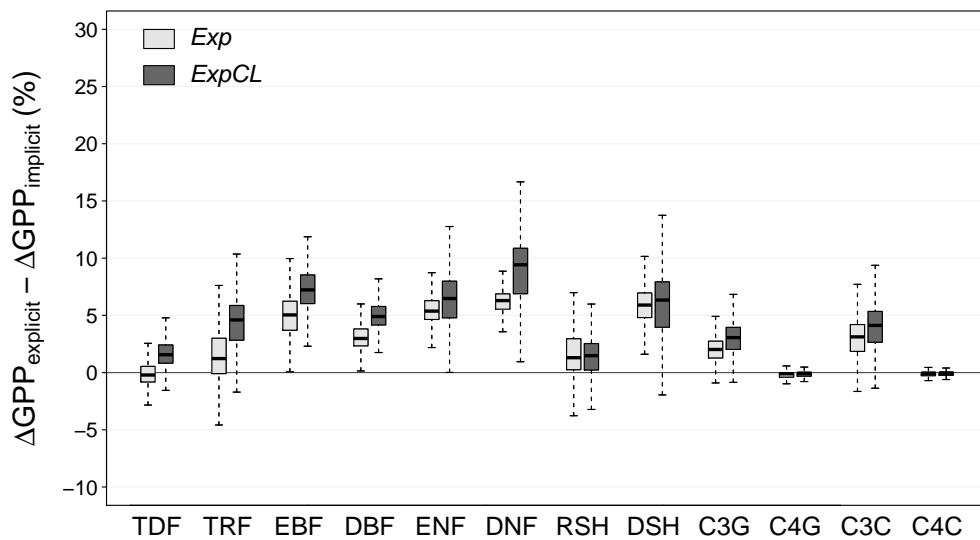
Fig. C9. Same as Fig. 5.7, but for the RCP4.5 scenario.
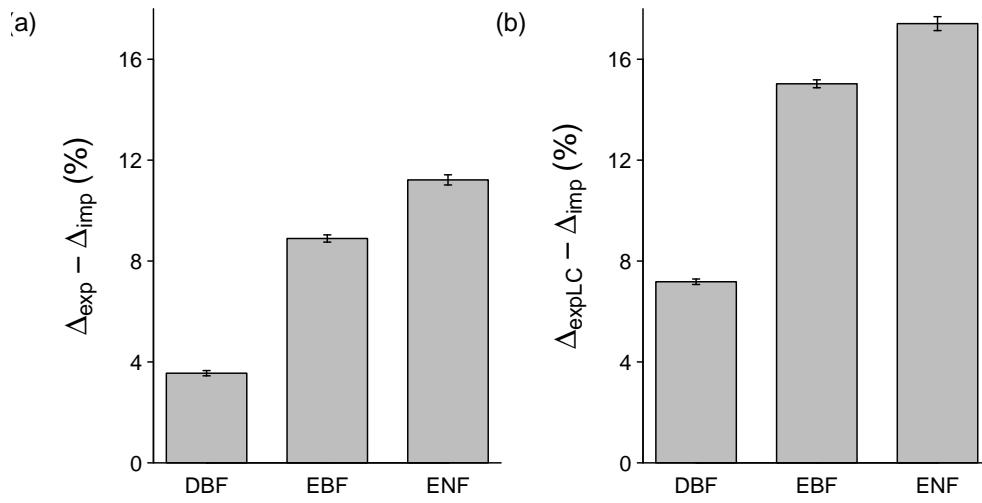
Fig. C10. Same as Fig. 5.7, but for the three co-occurring (i.e. > 5% fractional cover in the same grid cell) plant functional types deciduous broadleaf trees (DBF), evergreen broadleaf trees (EBF), and evergreen needle-leaf trees (ENF) only.
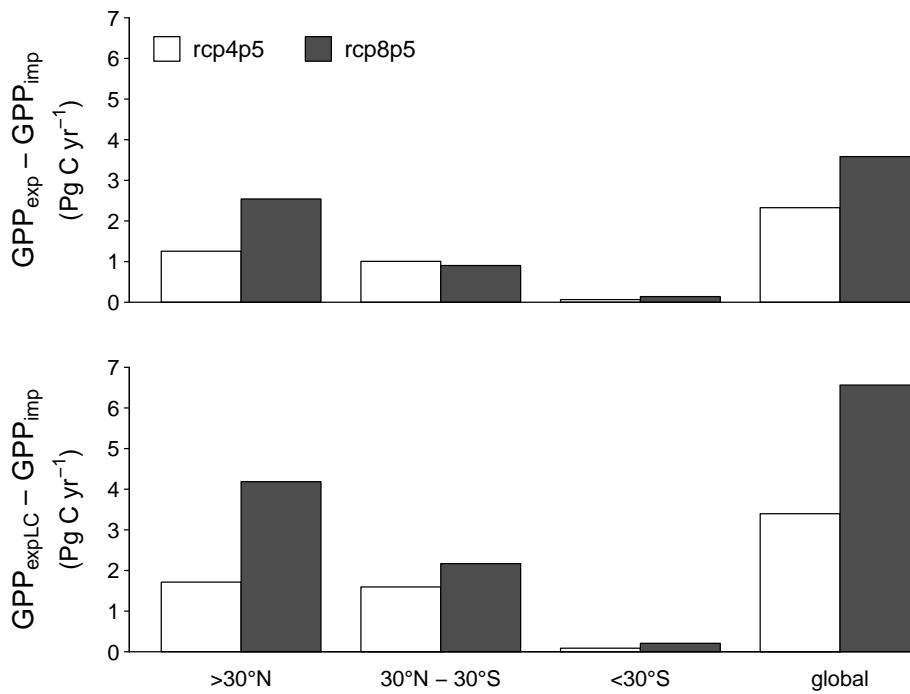
Fig. C11. Differences in mean annual GPP for different latitudinal bands and globally.
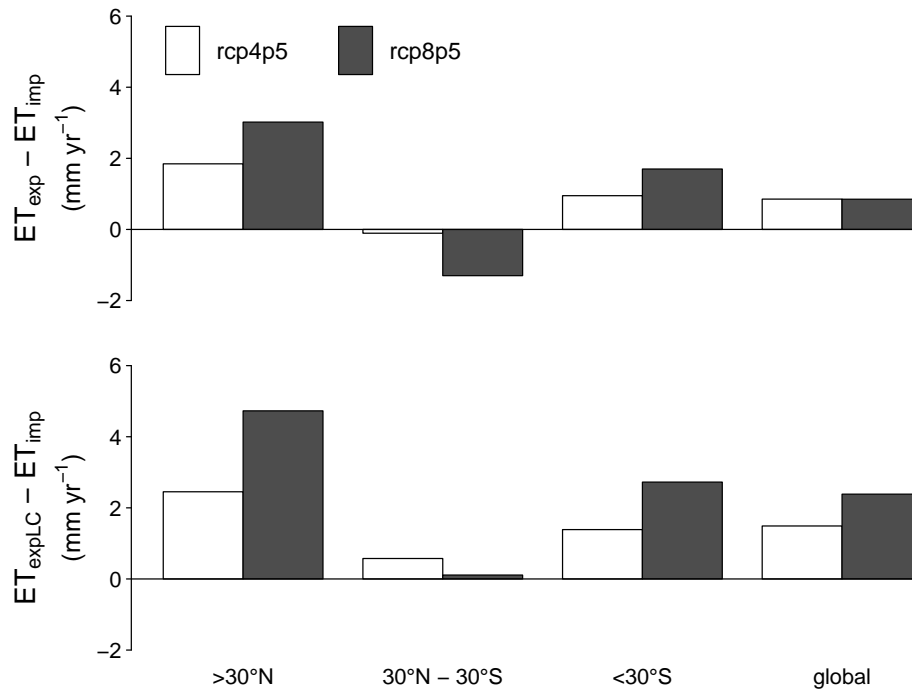
Fig. C12. Differences in mean annual evapotranspiration (ET) for different latitudinal bands and globally
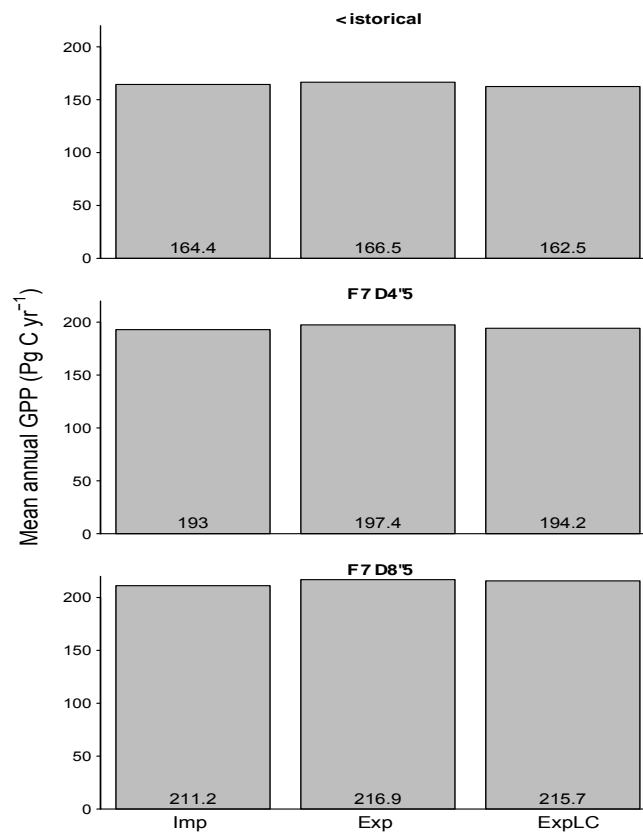
Fig. C13. Global mean annual GPP for the different model versions and scenarios

References

Ainsworth, E. A. and Long, S. P. (2005). What have we learned from 15 years of free-air CO_2 enrichment (FACE)? A meta-analytic review of the responses of photosynthesis, canopy properties and plant production to rising CO_2. *New Phytologist* 165, 351–372.

Ainsworth, E. A. and Rogers, A. (2007). The response of photosynthesis and stomatal conductance to rising $[CO_2]$: mechanisms and environmental interactions. *Plant, Cell & Environment* 30, 258–270.

Anderson, M. C., Kustas, W. P., and Norman, J. M. (2003). Upscaling and downscaling—A regional view of the soil–plant–atmosphere continuum. *Agronomy Journal* 95, 1408–1423.

Andrews, T., Doutriaux-Boucher, M., Boucher, O., and Forster, P. M. (2011). A regional and global analysis of carbon dioxide physiological forcing and its impact on climate. *Climate Dynamics* 36, 783–792.

Aphalo, P. and Jarvis, P. (1991). Do stomata respond to relative humidity? *Plant, Cell & Environment* 14, 127–132.

Atkin, O. K., Westbeek, M. H., Cambridge, M. L., Lambers, H., and Pons, T. L. (1997). Leaf respiration in light and darkness (a comparison of slow-and fast-growing *Poa* species). *Plant Physiology* 113, 961–965.

Aubinet, M., Grelle, A., Ibrom, A., Rannik, Moncrieff, J, Foken, T., Kowalski, A., Martin, P., Berbigier, P, Bernhofer, C., et al. (1999). Estimates of the annual net carbon and water exchange of forests: the EUROFLUX methodology. *Advances in Ecological Research* 30, 113–175.

Aubinet, M., Heinesch, B., and Longdoz, B. (2002). Estimation of the carbon sequestration by a heterogeneous forest: Night flux corrections, heterogeneity of the site and inter-annual variability. *Global Change Biology* 8, 1053–1071.

Bahar, N. H., Hayes, L., Scafaro, A. P., Atkin, O. K., and Evans, J. R. (2018). Mesophyll conductance does not contribute to greater photosynthetic rate per unit nitrogen in temperate compared with tropical evergreen wet-forest tree leaves. *New Phytologist* 218, 492–505.

Baldocchi, D. and Harley, P. (1995). Scaling carbon dioxide and water vapour exchange from leaf to canopy in a deciduous forest. II. Model testing and application. *Plant, Cell & Environment* 18, 1157–1173.

Baldocchi, D. (2008). Turner Review No. 15. 'Breathing'of the terrestrial biosphere: lessons learned from a global network of carbon dioxide flux measurement systems. *Australian Journal of Botany* 56, 1–26.

Baldocchi, D. and Ma, S. (2013). How will land use affect air temperature in the surface boundary layer? Lessons learned from a comparative study on the energy balance of an oak savanna and annual grassland in California, USA. *Tellus B: Chemical and Physical Meteorology* 65, 19994.

Baldocchi, D., Falge, E., Gu, L., Olson, R., Hollinger, D., Running, S., Anthoni, P., Bernhofer, C., Davis, K., Evans, R., et al. (2001). FLUXNET: A new tool to study the temporal and spatial variability of ecosystem-scale carbon dioxide, water vapor, and energy flux densities. *Bulletin of the American Meteorological Society* 82, 2415–2434.

Baldocchi, D. D., Vogel, C. A., and Hall, B. (1997). Seasonal variation of energy and water vapor exchange rates above and below a boreal jack pine forest canopy. *Journal of Geophysical Research: Atmospheres (1984–2012)* 102, 28939–28951.

Ball, J. T., Woodrow, I. E., and Berry, J. A. (1987). A model predicting stomatal conductance and its contribution to the control of photosynthesis under different environmental conditions. In:

Progress in photosynthesis research. Ed. by J Biggins. Martinus Nijhoff Publishers, Dordrecht, Netherlands, 221–224.

Barbour, M. M., Evans, J. R., Simonin, K. A., and Caemmerer, S. (2016). Online CO_2 and H2O oxygen isotope fractionation allows estimation of mesophyll conductance in C4 plants, and reveals that mesophyll conductance decreases as leaves age in both C4 and C3 plants. *New Phytologist* 210, 875–889.

Barnard, D. and Bauerle, W. (2013). The implications of minimum stomatal conductance on modeling water flux in forest canopies. *Journal of Geophysical Research: Biogeosciences* 118, 1322–1333.

Barr, A., Morgenstern, K., Black, T., McCaughey, J., and Nesic, Z. (2006). Surface energy balance closure by the eddy-covariance method above three boreal forest stands and implications for the measurement of the CO_2 flux. *Agricultural and Forest Meteorology* 140, 322–337.

Battipaglia, G., Saurer, M., Cherubini, P., Calfapietra, C., McCarthy, H. R., Norby, R. J., and Francesca Cotrufo, M (2013). Elevated CO_2 increases tree-level intrinsic water use efficiency: insights from carbon and oxygen isotope analyses in tree rings across three forest FACE sites. *New Phytologist* 197, 544–554.

Beer, C, Ciais, P, Reichstein, M, Baldocchi, D, Law, B., Papale, D, Soussana, J.-F., Ammann, C, Buchmann, N, Frank, D, et al. (2009). Temporal and among-site variability of inherent water use efficiency at the ecosystem level. *Global Biogeochemical Cycles* 23.

Belmecheri, S., Maxwell, R. S., Taylor, A. H., Davis, K. J., Freeman, K. H., and Munger, W. J. (2014). Tree-ring $\delta^{13}C$ tracks flux tower ecosystem productivity estimates in a NE temperate forest. *Environmental Research Letters* 9, 074011.

Benyon, R. and Doody, T. (2015). Comparison of interception, forest floor evaporation and transpiration in *Pinus radiata* and *Eucalyptus globulus* plantations. *Hydrological Processes* 29, 1173–1187.

Berbigier, P., Bonnefond, J.-M., and Mellmann, P. (2001). CO_2 and water vapour fluxes for 2 years above Euroflux forest site. *Agricultural and Forest Meteorology* 108, 183–197.

Beringer, J., McHugh, I., Hutley, L. B., Isaac, P., and Kljun, N. (2017). Dynamic INtegrated Gap-filling and partitioning for OzFlux (DINGO). *Biogeosciences* 14, 1457.

Berkelhammer, M, Noone, D., Wong, T., Burns, S., Knowles, J., Kaushik, A, Blanken, P., and Williams, M. (2016). Convergent approaches to determine an ecosystem's transpiration fraction. *Global Biogeochemical Cycles* 30, 933–951.

Bernacchi, C. J., Portis, A. R., Nakano, H., von Caemmerer, S., and Long, S. P. (2002). Temperature response of mesophyll conductance. Implications for the determination of Rubisco enzyme kinetics and for limitations to photosynthesis in vivo. *Plant Physiology* 130, 1992–1998.

Bernacchi, C., Singsaas, E., Pimentel, C, Portis Jr, A., and Long, S. (2001). Improved temperature response functions for models of Rubisco-limited photosynthesis. *Plant, Cell & Environment* 24, 253–259.

Bernacchi, C., Pimentel, C, and Long, S. (2003). In vivo temperature response functions of parameters required to model RuBP-limited photosynthesis. *Plant, Cell & Environment* 26, 1419–1430.

Berry, J. A., Beerling, D. J., and Franks, P. J. (2010). Stomata: key players in the earth system, past and present. *Current Opinion in Plant Biology* 13, 232–239.

Betts, R. A., Boucher, O., Collins, M., Cox, P. M., Falloon, P. D., Gedney, N., Hemming, D. L., Huntingford, C., Jones, C. D., Sexton, D. M., et al. (2007). Projected increase in continental runoff due to plant responses to increasing carbon dioxide. *Nature* 448, 1037–1041.

Biemans, H, Hutjes, R., Kabat, P, Strengers, B., Gerten, D, and Rost, S (2009). Effects of precipitation uncertainty on discharge calculations for main river basins. *Journal of Hydrometeorology* 10, 1011–1025.

Blanken, P. and Black, T. (2004). The canopy conductance of a boreal aspen forest, Prince Albert National Park, Canada. *Hydrological Processes* 18, 1561–1578.

Blanken, P., Black, T., Yang, P., Neumann, H., Nesic, Z, Staebler, R, den Hartog, G, Novak, M., and Lee, X (1997). Energy balance and canopy conductance of a boreal aspen forest: Partitioning overstory and understory components. *Journal of Geophysical Research* 102, 28–915.

Boden, T., Marland, G, and Andres, R. (2013). Global, regional, and national fossil-fuel CO_2 emissions. *Carbon Dioxide Information Analysis Center, Oak Ridge National Laboratory, U.S. Department of Energy, Oak Ridge, TN, U.S.A.*

Boettger, T., Haupt, M., Knöller, K., Weise, S. M., Waterhouse, J. S., Rinne, K. T., Loader, N. J., Sonninen, E., Jungner, H., Masson-Delmotte, V., et al. (2007). Wood cellulose preparation methods and mass spectrometric analyses of $\delta^{13}C$, $\delta^{18}O$, and nonexchangeable δ^2H values in cellulose, sugar, and starch: an interlaboratory comparison. *Analytical Chemistry* 79, 4603–4612.

Bonal, D., Bosc, A., Ponton, S., Goret, J.-Y., Burban, B., Gross, P., Bonnefond, J, Elbers, J., Longdoz, B., Epron, D., et al. (2008). Impact of severe dry season on net ecosystem exchange in the Neotropical rainforest of French Guiana. *Global Change Biology* 14, 1917–1933.

Bonan, G. B. (2008). Forests and climate change: forcings, feedbacks, and the climate benefits of forests. *Science* 320, 1444–1449.

Bonan, G. B. and Doney, S. C. (2018). Climate, ecosystems, and planetary futures: The challenge to predict life in Earth system models. *Science* 359, eaam8328.

Bonan, G. B., Levis, S., Sitch, S., Vertenstein, M., and Oleson, K. W. (2003). A dynamic global vegetation model for use with climate models: concepts and description of simulated vegetation dynamics. *Global Change Biology* 9, 1543–1566.

Bonan, G. B., Lawrence, P. J., Oleson, K. W., Levis, S., Jung, M., Reichstein, M., Lawrence, D. M., and Swenson, S. C. (2011). Improving canopy processes in the Community Land Model version 4 (CLM4) using global flux fields empirically inferred from FLUXNET data. *Journal of Geophysical Research: Biogeosciences* 116.

Booth, B. B., Jones, C. D., Collins, M., Totterdell, I. J., Cox, P. M., Sitch, S., Huntingford, C., Betts, R. A., Harris, G. R., and Lloyd, J. (2012). High sensitivity of future global warming to land carbon cycle processes. *Environmental Research Letters* 7, 024002.

Boucher, O., Jones, A., and Betts, R. A. (2009). Climate response to the physiological impact of carbon dioxide on plants in the Met Office Unified Model HadCM3. *Climate Dynamics* 32, 237–249.

Bounoua, L, Hall, F., Sellers, P., Kumar, A, Collatz, G., Tucker, C., and Imhoff, M. (2010). Quantifying the negative feedback of vegetation to greenhouse warming: A modeling approach. *Geophysical Research Letters* 37.

Brooks, A and Farquhar, G. (1985). Effect of temperature on the CO_2/O_2 specificity of ribulose-1, 5-bisphosphate carboxylase/oxygenase and the rate of respiration in the light. *Planta* 165, 397–406.

Brovkin, V., Sitch, S., Von Bloh, W., Claussen, M., Bauer, E., and Cramer, W. (2004). Role of land cover changes for atmospheric CO_2 increase and climate change during the last 150 years. *Global Change Biology* 10, 1253–1266.

Brovkin, V., Raddatz, T., Reick, C. H., Claussen, M., and Gayler, V. (2009). Global biogeophysical interactions between forest and climate. *Geophysical Research Letters* 36.

Brugnoli, E., Hubick, K. T., von Caemmerer, S., Wong, S. C., and Farquhar, G. D. (1988). Correlation between the carbon isotope discrimination in leaf starch and sugars of C3 plants and the ratio of intercellular and atmospheric partial pressures of carbon dioxide. *Plant physiology* 88, 1418–1424.

Buckley, T. N. and Mott, K. A. (2013). Modelling stomatal conductance in response to environmental factors. *Plant, Cell & Environment* 36, 1691–1699.

Businger, J. A., Wyngaard, J. C., Izumi, Y, and Bradley, E. F. (1971). Flux-profile relationships in the atmospheric surface layer. *Journal of the Atmospheric Sciences* 28, 181–189.

Cai, Y.-F., Yang, Q.-Y., Li, S.-F., Wang, J.-H., and Huang, W. (2017). The water-water cycle is a major electron sink in Camellia species when CO_2 assimilation is restricted. *Journal of Photochemistry and Photobiology B: Biology* 168, 59–66.

Cano, F., Sánchez-Gómez, D, Gascó, A, Rodríguez-Calcerrada, J, Gil, L, Warren, C., and Aranda, I (2011). Light acclimation at the end of the growing season in two broadleaved oak species. *Photosynthetica* 49, 581–592.

Cao, L., Bala, G., Caldeira, K., Nemani, R., and Ban-Weiss, G. (2010). Importance of carbon dioxide physiological forcing to future climate change. *Proceedings of the National Academy of Sciences* 107, 9513–9518.

Carrara, A., Janssens, I. A., Curiel Yuste, J., and Ceulemans, R. (2004). Seasonal changes in photosynthesis, respiration and NEE of a mixed temperate forest. *Agricultural and Forest Meteorology* 126, 15–31.

Casals, P., Gimeno, C., Carrara, A., Lopez-Sangil, L., and Sanz, M. (2009). Soil CO_2 efflux and extractable organic carbon fractions under simulated precipitation events in a Mediterranean Dehesa. *Soil Biology and Biochemistry* 41, 1915–1922.

Cernusak, L. A., Ubierna, N., Winter, K., Holtum, J. A., Marshall, J. D., and Farquhar, G. D. (2013). Environmental and physiological determinants of carbon isotope discrimination in terrestrial plants. *New Phytologist* 200, 950–965.

Chazdon, R. L. (1988). Sunflecks and their importance to forest understorey plants. *Advances in Ecological Research* 18, 1–63.

Choudhury, B. and Monteith, J. (1988). A four-layer model for the heat budget of homogeneous land surfaces. *Quarterly Journal of the Royal Meteorological Society* 114, 373–398.

Ciais, P., Reichstein, M, Viovy, N., Granier, A, Ogée, J., Allard, V, Aubinet, M., Buchmann, N, Bernhofer, C., Carrara, A, et al. (2005a). Europe-wide reduction in primary productivity caused by the heat and drought in 2003. *Nature* 437, 529–533.

Ciais, P., Cuntz, M., Scholze, M., Mouillot, F., Peylin, P., and Gitz, V. (2005b). Remarks on the use of ^{13}C and ^{18}O isotopes in atmospheric CO_2 to quantify biospheric carbon fluxes. *Stable Isotopes and Biosphere–Atmosphere Interactions: Processes and Biological Controls (eds Flanagan LB, Ehleringer JR, Pataki DE, Mooney HA)*, 235–267.

Collatz, G. J., Ribas-Carbo, M, and Berry, J. (1992). Coupled photosynthesis-stomatal conductance model for leaves of C4 plants. *Functional Plant Biology* 19, 519–538.

Cook, B. I., Smerdon, J. E., Seager, R., and Coats, S. (2014). Global warming and 21st century drying. *Climate Dynamics* 43, 2607–2627.

Cook, B. D., Davis, K. J., Wang, W., Desai, A., Berger, B. W., Teclaw, R. M., Martin, J. G., Bolstad, P. V., Bakwin, P. S., Yi, C., et al. (2004). Carbon exchange and venting anomalies in

an upland deciduous forest in northern Wisconsin, USA. *Agricultural and Forest Meteorology* 126, 271–295.

Cowan, I. and Farquhar, G. (1977). Stomatal function in relation to leaf metabolism and environment. In: *Symposia of the Society for Experimental Biology*. Vol. 31, 471–505.

Cowling, S. A. and Field, C. B. (2003). Environmental control of leaf area production: implications for vegetation and land-surface modeling. *Global Biogeochemical Cycles* 17, 7–1.

Cox, P. M., Betts, R. A., Jones, C. D., Spall, S. A., and Totterdell, I. J. (2000). Acceleration of global warming due to carbon-cycle feedbacks in a coupled climate model. *Nature* 408, 184–187.

Dai, A., Qian, T., Trenberth, K. E., and Milliman, J. D. (2009). Changes in continental freshwater discharge from 1948 to 2004. *Journal of Climate* 22, 2773–2792.

Damour, G., Simonneau, T., Cochard, H., and Urban, L. (2010). An overview of models of stomatal conductance at the leaf level. *Plant, Cell & Environment* 33, 1419–1438.

de Arellano, J. V.-G., van Heerwaarden, C. C., and Lelieveld, J. (2012). Modelled suppression of boundary-layer clouds by plants in a CO_2-rich atmosphere. *Nature Geoscience* 5, 701–704.

de Jong, R., de Bruin, S., de Wit, A., Schaepman, M. E., and Dent, D. L. (2011). Analysis of monotonic greening and browning trends from global NDVI time-series. *Remote Sensing of Environment* 115, 692–702.

De Boeck, H. J., Lemmens, C., Bossuyt, H., Malchair, S., Carnol, M., Merckx, R., Nijs, I., and Ceulemans, R. (2006). How do climate warming and plant species richness affect water use in experimental grasslands? *Plant and Soil* 288, 249–261.

De Bruin, H. (1983). A model for the Priestley-Taylor parameter α. *Journal of Climate and Applied Meteorology* 22, 572–578.

De Kauwe, M. G., Medlyn, B. E., Zaehle, S., Walker, A. P., Dietze, M. C., Hickler, T., Jain, A. K., Luo, Y., Parton, W. J., Prentice, I. C., et al. (2013). Forest water use and water use efficiency at elevated CO_2: a model-data intercomparison at two contrasting temperate forest FACE sites. *Global Change Biology* 19, 1759–1779.

De Kauwe, M. G., Medlyn, B. E., Knauer, J., and Williams, C. A. (2017). Ideas and perspectives: how coupled is the vegetation to the boundary layer? *Biogeosciences* 14, 4435–4453.

De Pury, D. and Farquhar, G. (1997). Simple scaling of photosynthesis from leaves to canopies without the errors of big-leaf models. *Plant, Cell & Environment* 20, 537–557.

Dekker, S. C., Groenendijk, M., Booth, B. B., Huntingford, C., and Cox, P. M. (2016). Spatial and temporal variations in plant water use efficiency inferred from tree-ring, eddy covariance and atmospheric observations. *Earth System Dynamics Discussions* 7, 525–533.

Denmead, O., Dunin, F., Wong, S., and Greenwood, E. (1993). Measuring water use efficiency of Eucalypt trees with chambers and micrometeorological techniques. *Journal of Hydrology* 150, 649–664.

Desai, A. R., Richardson, A. D., Moffat, A. M., Kattge, J., Hollinger, D. Y., Barr, A., Falge, E., Noormets, A., Papale, D., Reichstein, M., et al. (2008). Cross-site evaluation of eddy covariance GPP and RE decomposition techniques. *Agricultural and Forest Meteorology* 148, 821–838.

Diefendorf, A. F., Mueller, K. E., Wing, S. L., Koch, P. L., and Freeman, K. H. (2010). Global patterns in leaf ^{13}C discrimination and implications for studies of past and future climate. *Proceedings of the National Academy of Sciences* 107, 5738–5743.

Dolman, A., Moors, E., and Elbers, J. (2002). The carbon uptake of a mid latitude pine forest growing on sandy soil. *Agricultural and Forest Meteorology* 111, 157–170.

Domingues, T. F., Martinelli, L. A., and Ehleringer, J. R. (2007). Ecophysiological traits of plant functional groups in forest and pasture ecosystems from eastern Amazonia, Brazil. *Plant Ecology* 193, 101–112.

Donohue, R. J., Roderick, M. L., McVicar, T. R., and Farquhar, G. D. (2013). Impact of CO_2 fertilization on maximum foliage cover across the globe's warm, arid environments. *Geophysical Research Letters* 40, 3031–3035.

Dorman, J. and Sellers, P. J. (1989). A global climatology of albedo, roughness length and stomatal resistance for atmospheric general circulation models as represented by the simple biosphere model (SiB). *Journal of Applied Meteorology* 28, 833–855.

Douthe, C., Dreyer, E., Brendel, O., and Warren, C. R. (2012). Is mesophyll conductance to CO_2 in leaves of three Eucalyptus species sensitive to short-term changes of irradiance under ambient as well as low O_2? *Functional Plant Biology* 39, 435–448.

Doutriaux-Boucher, M, Webb, M., Gregory, J. M., and Boucher, O (2009). Carbon dioxide induced stomatal closure increases radiative forcing via a rapid reduction in low cloud. *Geophysical Research Letters* 36.

Dubbert, M., Piayda, A., Cuntz, M., Correia, A. C., Costa e Silva, F., Pereira, J. S., and Werner, C. (2014). Stable oxygen isotope and flux partitioning demonstrates understory of an oak savanna contributes up to half of ecosystem carbon and water exchange. *Frontiers in Plant Science* 5, 530.

Dunn, A. L., Barford, C. C., Wofsy, S. C., Goulden, M. L., and Daube, B. C. (2007). A long-term record of carbon exchange in a boreal black spruce forest: Means, responses to interannual variability, and decadal trends. *Global Change Biology* 13, 577–590.

Dyer, A. and Hicks, B. (1970). Flux-gradient relationships in the constant flux layer. *Quarterly Journal of the Royal Meteorological Society* 96, 715–721.

Egea, G., González-Real, M. M., Baille, A., Nortes, P. A., and Diaz.-Espejo, A. (2011a). Disentangling the contributions of ontogeny and water stress to photosynthetic limitations in almond trees. *Plant, Cell & Environment* 34, 962–979.

Egea, G., Verhoef, A., and Vidale, P. L. (2011b). Towards an improved and more flexible representation of water stress in coupled photosynthesis–stomatal conductance models. *Agricultural and Forest Meteorology* 151, 1370–1384.

Ehleringer, J. R. and Cerling, T. E. (1995). Atmospheric CO_2 and the ratio of intercellular to ambient CO_2 concentrations in plants. *Tree Physiology* 15, 105–111.

Ehleringer, J., Hall, A., and Farquhar, G. (1993). Stable Isotopes and Plant Carbon-Water Relations. Ed. by J. Ehleringer, A. Hall, and G. Farquhar. San Diego: Academic Press.

Ethier, G. and Livingston, N. (2004). On the need to incorporate sensitivity to CO_2 transfer conductance into the Farquhar–von Caemmerer–Berry leaf photosynthesis model. *Plant, Cell & Environment* 27, 137–153.

Evans, J. R. and Von Caemmerer, S. (2013). Temperature response of carbon isotope discrimination and mesophyll conductance in tobacco. *Plant, Cell & Environment* 36, 745–756.

Evans, J. R., Caemmerer, S., Setchell, B. A., and Hudson, G. S. (1994). The relationship between CO_2 transfer conductance and leaf anatomy in transgenic tobacco with a reduced content of Rubisco. *Functional Plant Biology* 21, 475–495.

Evans, J. R., Kaldenhoff, R., Genty, B., and Terashima, I. (2009). Resistances along the CO_2 diffusion pathway inside leaves. *Journal of Experimental Botany* 60, 2235–2248.

Falge, E., Baldocchi, D., Olson, R., Anthoni, P., Aubinet, M., Bernhofer, C., Burba, G., Ceulemans, R., Clement, R., Dolman, H., et al. (2001). Gap filling strategies for defensible annual sums of net ecosystem exchange. *Agricultural and Forest Meteorology* 107, 43–69.

Farquhar, G., von Caemmerer, S. v., and Berry, J. (1980). A biochemical model of photosynthetic CO_2 assimilation in leaves of C3 species. *Planta* 149, 78–90.

Farquhar, G., Hubick, K., Condon, A., and Richards, R. (1989). Carbon isotope fractionation and plant water-use efficiency. In: *Stable Isotopes in Ecological Research*. Springer, 21–40.

Farquhar, G. D. and Busch, F. A. (2017). Changes in the chloroplastic CO_2 concentration explain much of the observed Kok effect: a model. *New Phytologist* 214, 570–584.

Farquhar, G. D., O'leary, M., and Berry, J. (1982). On the relationship between carbon isotope discrimination and the intercellular carbon dioxide concentration in leaves. *Functional Plant Biology* 9, 121–137.

Feng, X. (1999). Trends in intrinsic water-use efficiency of natural trees for the past 100–200 years: a response to atmospheric CO_2 concentration. *Geochimica et Cosmochimica Acta* 63, 1891–1903.

Field, C., Jackson, R., and Mooney, H. (1995). Stomatal responses to increased CO_2: implications from the plant to the global scale. *Plant, Cell & Environment* 18, 1214–1225.

Finnigan, J. (2008). An introduction to flux measurements in difficult conditions. *Ecological Applications* 18, 1340–1350.

Fisher, J. B., Baldocchi, D. D., Misson, L., Dawson, T. E., and Goldstein, A. H. (2007). What the towers don't see at night: nocturnal sap flow in trees and shrubs at two AmeriFlux sites in California. *Tree Physiology* 27, 597–610.

Fisher, J. B., Huntzinger, D. N., Schwalm, C. R., and Sitch, S. (2014). Modeling the terrestrial biosphere. *Annual Review of Environment and Resources* 39, 91–123.

Flexas, J., Díaz-Espejo, A., Galmés, J., Kaldenhoff, R., Medrano, H., and Ribas-Carbo, M. (2007). Rapid variations of mesophyll conductance in response to changes in CO_2 concentration around leaves. *Plant, Cell & Environment* 30, 1284–1298.

Flexas, J., Ribas-Carbo, M., Díaz-Espejo, A., Galmés, J., and Medrano, H. (2008). Mesophyll conductance to CO_2: current knowledge and future prospects. *Plant, Cell & Environment* 31, 602–621.

Flexas, J., Barbour, M. M., Brendel, O., Cabrera, H. M., Carriquí, M., Díaz-Espejo, A., Douthe, C., Dreyer, E., Ferrio, J. P., Gago, J., et al. (2012). Mesophyll diffusion conductance to CO_2: An unappreciated central player in photosynthesis. *Plant Science* 193, 70–84.

Flexas, J., Díaz-Espejo, A., Conesa, M., Coopman, R., Douthe, C, Gago, J, Gallé, A, Galmés, J, Medrano, H, Ribas-Carbo, M, et al. (2016). Mesophyll conductance to CO_2 and Rubisco as targets for improving intrinsic water use efficiency in C3 plants. *Plant, Cell & Environment* 39, 965–982.

Foken, T. and Wichura, B. (1996). Tools for quality assessment of surface-based flux measurements. *Agricultural and Forest Meteorology* 78, 83–105.

Foken, T. (2008). The energy balance closure problem: an overview. *Ecological Applications* 18, 1351–1367.

Forkel, M., Carvalhais, N., Rödenbeck, C., Keeling, R., Heimann, M., Thonicke, K., Zaehle, S., and Reichstein, M. (2016). Enhanced seasonal CO_2 exchange caused by amplified plant productivity in northern ecosystems. *Science* 351, 696–699.

Frank, D., Poulter, B, Saurer, M, Esper, J, Huntingford, C, Helle, G, Treydte, K, Zimmermann, N., Schleser, G., Ahlström, A., et al. (2015). Water-use efficiency and transpiration across European forests during the Anthropocene. *Nature Climate Change* 5, 579–583.

Frankenberg, C., O'Dell, C., Berry, J., Guanter, L., Joiner, J., Köhler, P., Pollock, R., and Taylor, T. E. (2014). Prospects for chlorophyll fluorescence remote sensing from the Orbiting Carbon Observatory-2. *Remote Sensing of Environment* 147, 1–12.

Franks, P. J., Adams, M. A., Amthor, J. S., Barbour, M. M., Berry, J. A., Ellsworth, D. S., Farquhar, G. D., Ghannoum, O., Lloyd, J., McDowell, N., et al. (2013). Sensitivity of plants to changing atmospheric CO_2 concentration: from the geological past to the next century. *New Phytologist* 197, 1077–1094.

Franks, P. J., Bonan, G. B., Berry, J. A., Lombardozzi, D. L., Holbrook, N. M., Herold, N., and Oleson, K. W. (2018). Comparing optimal and empirical stomatal conductance models for application in Earth system models. *Global Change Biology.*

Fratini, G and Mauder, M (2014). Towards a consistent eddy-covariance processing: an intercomparison of EddyPro and TK3. *Atmospheric Measurement Techniques* 7, 2273–2281.

Friedlingstein, P., Meinshausen, M., Arora, V. K., Jones, C. D., Anav, A., Liddicoat, S. K., and Knutti, R. (2014). Uncertainties in CMIP5 climate projections due to carbon cycle feedbacks. *Journal of Climate* 27, 511–526.

Frieler, K., Lange, S., Piontek, F., Reyer, C. P., Schewe, J., Warszawski, L., Zhao, F., Chini, L., Denvil, S., Emanuel, K., et al. (2017). Assessing the impacts of 1.5°C global warming–simulation protocol of the Inter-Sectoral Impact Model Intercomparison Project (ISIMIP2b). *Geoscientific Model Development* 10, 4321–4345.

Friend, A. D. and Kiang, N. Y. (2005). Land Surface Model Development for the GISS GCM: Effects of Improved Canopy Physiology on Simulated Climate. *Journal of Climate* 18, 2883–2902.

Gagen, M., Finsinger, W., Wagner-Cremer, F., McCarroll, D., Loader, N. J., Robertson, I., Jalkanen, R., Young, G., and Kirchhefer, A. (2011). Evidence of changing intrinsic water-use efficiency under rising atmospheric CO_2 concentrations in Boreal Fennoscandia from subfossil leaves and tree ring $\delta^{13}C$ ratios. *Global Change Biology* 17, 1064–1072.

Galmés, J., Medrano, H., and Flexas, J. (2007). Photosynthetic limitations in response to water stress and recovery in Mediterranean plants with different growth forms. *New Phytologist* 175, 81–93.

Garratt, J. and Hicks, B. (1973). Momentum, heat and water vapour transfer to and from natural and artificial surfaces. *Quarterly Journal of the Royal Meteorological Society* 99, 680–687.

Gedney, N., Cox, P., Betts, R., Boucher, O, Huntingford, C, and Stott, P. (2006). Detection of a direct carbon dioxide effect in continental river runoff records. *Nature* 439, 835–838.

Gerten, D., Rost, S., von Bloh, W., and Lucht, W. (2008). Causes of change in 20th century global river discharge. *Geophysical Research Letters* 35.

Gerten, D., Betts, R, and Döll, P (2014). Active Role of Vegetation in Altering Water Flows under Climate Change. *Climate Change.*

Giorgetta, M. A., Jungclaus, J., Reick, C. H., Legutke, S., Bader, J., Böttinger, M., Brovkin, V., Crueger, T., Esch, M., Fieg, K., et al. (2013). Climate and carbon cycle changes from 1850 to 2100 in MPI-ESM simulations for the Coupled Model Intercomparison Project phase 5. *Journal of Advances in Modeling Earth Systems* 5, 572–597.

Goldberg, V and Bernhofer, C (2008). Testing different decoupling coefficients with measurements and models of contrasting canopies and soil water conditions. *Annales Geophysicae* 26, 1977–1992.

Goudriaan, J. (1977). Crop micrometeorology: a simulation study. Pudoc, Center for Agricultural Publishing and Documentation.

Granier, A, Ceschia, E, Damesin, C, Dufrêne, E, Epron, D, Gross, P, Lebaube, S, Le Dantec, V, Le Goff, N, Lemoine, D., et al. (2000). The carbon balance of a young beech forest. *Functional Ecology* 14, 312–325.

Grantz, D. and Meinzer, F. (1990). Stomatal response to humidity in a sugarcane field: simultaneous porometric and micrometeorological measurements. *Plant, Cell & Environment* 13, 27–37.

Graven, H., Keeling, R., Piper, S., Patra, P., Stephens, B., Wofsy, S., Welp, L., Sweeney, C, Tans, P., Kelley, J., et al. (2013). Enhanced seasonal exchange of CO_2 by northern ecosystems since 1960. *Science* 341, 1085–1089.

Grelle, A, Lundberg, A, Lindroth, A, Moren, A.-S., and Cienciala, E (1997). Evaporation components of a boreal forest: variations during the growing season. *Journal of Hydrology* 197, 70–87.

Grünwald, T. and Bernhofer, C. (2007). A decade of carbon, water and energy flux measurements of an old spruce forest at the Anchor Station Tharandt. *Tellus B* 59, 387–396.

Groenendijk, M, Dolman, A., Ammann, C, Arneth, A., Cescatti, A, Dragoni, D, Gash, J., Gianelle, D, Gioli, B, Kiely, G, et al. (2011). Seasonal variation of photosynthetic model parameters and leaf area index from global Fluxnet eddy covariance data. *Journal of Geophysical Research: Biogeosciences* 116.

Gu, L. and Sun, Y. (2014). Artefactual responses of mesophyll conductance to CO_2 and irradiance estimated with the variable J and online isotope discrimination methods. *Plant, Cell & Environment* 37, 1231–1249.

Gu, L., Pallardy, S. G., Tu, K., Law, B. E., and Wullschleger, S. D. (2010). Reliable estimation of biochemical parameters from C3 leaf photosynthesis–intercellular carbon dioxide response curves. *Plant, Cell & Environment* 33, 1852–1874.

Guanter, L., Zhang, Y., Jung, M., Joiner, J., Voigt, M., Berry, J. A., Frankenberg, C., Huete, A. R., Zarco-Tejada, P., Lee, J.-E., et al. (2014). Global and time-resolved monitoring of crop photosynthesis with chlorophyll fluorescence. *Proceedings of the National Academy of Sciences*, 201320008.

Gunderson, C., Sholtis, J., Wullschleger, S., Tissue, D., Hanson, P., and Norby, R. (2002). Environmental and stomatal control of photosynthetic enhancement in the canopy of a sweetgum (*Liquidambar styraciflua* L.) plantation during 3 years of CO_2 enrichment. *Plant, Cell & Environment* 25, 379–393.

Hadley, J. L. and Schedlbauer, J. L. (2002). Carbon exchange of an old-growth eastern hemlock (*Tsuga canadensis*) forest in central New England. *Tree Physiology* 22, 1079–1092.

Hadley, J. L., Kuzeja, P. S., Daley, M. J., Phillips, N. G., Mulcahy, T., and Singh, S. (2008). Water use and carbon exchange of red oak-and eastern hemlock-dominated forests in the northeastern USA: implications for ecosystem-level effects of hemlock woolly adelgid. *Tree Physiology* 28, 615–627.

Hagemann, S and Dümenil, L (1998). A parametrization of the lateral waterflow for the global scale. *Climate Dynamics* 14, 17–31.

Hagemann, S. and Stacke, T. (2014). Impact of the soil hydrology scheme on simulated soil moisture memory. *Climate Dynamics*, 1–20.

Han, Q., Iio, A., Naramoto, M., and Kakubari, Y. (2010). Response of internal conductance to soil drought in sun and shade leaves of adult Fagus crenata. *Acta Silvatica et Lignaira Hungarica* 6, 123–133.

Hanba, Y., Kogami, H, and Terashima, I (2002). The effect of growth irradiance on leaf anatomy and photosynthesis in Acer species differing in light demand. *Plant, Cell & Environment* 25, 1021–1030.

Harley, P. C. and Sharkey, T. D. (1991). An improved model of C3 photosynthesis at high CO_2: reversed O_2 sensitivity explained by lack of glycerate reentry into the chloroplast. *Photosynthesis Research* 27, 169–178.

Hassiotou, F., Ludwig, M., Renton, M., Veneklaas, E. J., and Evans, J. R. (2009). Influence of leaf dry mass per area, CO_2, and irradiance on mesophyll conductance in sclerophylls. *Journal of Experimental Botany* 60, 2303–2314.

Haverd, V., Cuntz, M., Leuning, R., and Keith, H. (2007). Air and biomass heat storage fluxes in a forest canopy: calculation within a soil vegetation atmosphere transfer model. *Agricultural and Forest Meteorology* 147, 125–139.

Hempel, S., Frieler, K., Warszawski, L., Schewe, J., and Piontek, F. (2013). A trend-preserving bias correction–the ISI-MIP approach. *Earth System Dynamics* 4, 219–236.

Hicks, B., Baldocchi, D., Meyers, T., Hosker Jr, R., and Matt, D. (1987). A preliminary multiple resistance routine for deriving dry deposition velocities from measured quantities. *Water, Air, and Soil Pollution* 36, 311–330.

Hollinger, D. and Richardson, A. (2005). Uncertainty in eddy covariance measurements and its application to physiological models. *Tree Physiology* 25, 873–885.

Hollinger, D., Aber, J, Dail, B, Davidson, E., Goltz, S., Hughes, H, Leclerc, M., Lee, J., Richardson, A., Rodrigues, C, et al. (2004). Spatial and temporal variability in forest–atmosphere CO_2 exchange. *Global Change Biology* 10, 1689–1706.

Holtum, J. A. and Winter, K. (2010). Elevated [CO_2] and forest vegetation: more a water issue than a carbon issue? *Functional Plant Biology* 37, 694–702.

Hong, J, Kim, J, and Byun, Y. (2012). Uncertainty in carbon exchange modelling in a forest canopy due to kB^{-1} parametrizations. *Quarterly Journal of the Royal Meteorological Society* 138, 699–706.

Houborg, R., McCabe, M., Cescatti, A., Gao, F., Schull, M., and Gitelson, A. (2015). Joint leaf chlorophyll content and leaf area index retrieval from Landsat data using a regularized model inversion system (REGFLEC). *Remote Sensing of Environment* 159, 203–221.

Hu, Z., Yu, G., Fu, Y., Sun, X., Li, Y., Shi, P., Wang, Y., and Zheng, Z. (2008). Effects of vegetation control on ecosystem water use efficiency within and among four grassland ecosystems in China. *Global Change Biology* 14, 1609–1619.

Huang, W., Hu, H., and Zhang, S.-B. (2015). Photorespiration plays an important role in the regulation of photosynthetic electron flow under fluctuating light in tobacco plants grown under full sunlight. *Frontiers in Plant Science* 6, 1–9.

Hungate, B., Reichstein, M, Dijkstra, P, Johnson, D, Hymus, G, Tenhunen, J., Hinkle, C., and Drake, B. (2002). Evapotranspiration and soil water content in a scrub-oak woodland under carbon dioxide enrichment. *Global Change Biology* 8, 289–298.

Ito, A. and Inatomi, M. (2012). Water-use efficiency of the terrestrial biosphere: a model analysis focusing on interactions between the global carbon and water cycles. *Journal of Hydrometeorology* 13, 681–694.

Jacobs, A. F., Heusinkveld, B. G., Wichink Kruit, R. J., and Berkowicz, S. M. (2006). Contribution of dew to the water budget of a grassland area in the Netherlands. *Water Resources Research* 42, 1–8.

Jacobs, A. F., Heusinkveld, B. G., and Holtslag, A. A. (2008). Towards closing the surface energy budget of a mid-latitude grassland. *Boundary-Layer Meteorology* 126, 125–136.

Janssens, I., Lankreijer, H, Matteucci, G, Kowalski, A., Buchmann, N, Epron, D, Pilegaard, K, Kutsch, W, Longdoz, B, Grünwald, T, et al. (2001). Productivity overshadows temperature in determining soil and ecosystem respiration across European forests. *Global Change Biology* 7, 269–278.

Jarvis, P. G. and McNaughton, K. (1986). Stomatal control of transpiration: scaling up from leaf to region. *Advances in Ecological Research* 15, 1–49.

Jarvis, P. (1986). Coupling of carbon and water interactions in forest stands. *Tree Physiology* 2, 347–368.

Jenkins, J., Richardson, A., Braswell, B., Ollinger, S., Hollinger, D., and Smith, M.-L. (2007). Refining light-use efficiency calculations for a deciduous forest canopy using simultaneous tower-based carbon flux and radiometric measurements. *Agricultural and Forest Meteorology* 143, 64–79.

Jiang, C., Ryu, Y., Fang, H., Myneni, R., Claverie, M., and Zhu, Z. (2017). Inconsistencies of interannual variability and trends in long-term satellite leaf area index products. *Global Change Biology* 23, 4133–4146.

Johnson, F. H., Eyring, H., and Williams, R. (1942). The nature of enzyme inhibitions in bacterial luminescence: sulfanilamide, urethane, temperature and pressure. *Journal of Cellular Physiology* 20, 247–268.

Jung, M., Henkel, K., Herold, M., and Churkina, G. (2006). Exploiting synergies of global land cover products for carbon cycle modeling. *Remote Sensing of Environment* 101, 534–553.

Kala, J., De Kauwe, M. G., Pitman, A. J., Medlyn, B. E., Wang, Y.-P., Lorenz, R., and Perkins-Kirkpatrick, S. E. (2016). Impact of the representation of stomatal conductance on model projections of heatwave intensity. *Scientific Reports* 6.

Kaminski, T., Heimann, M., and Giering, R. (1999). A coarse grid three-dimensional global inverse model of the atmospheric transport: 1. Adjoint model and Jacobian matrix. *Journal of Geophysical Research: Atmospheres (1984–2012)* 104, 18535–18553.

Kaplan, J. O., Prentice, I. C., and Buchmann, N. (2002). The stable carbon isotope composition of the terrestrial biosphere: Modeling at scales from the leaf to the globe. *Global Biogeochemical Cycles* 16, 8–1.

Kattge, J, Knorr, W, Raddatz, T, Wirth, C, et al. (2009). Quantifying photosynthetic capacity and its relationship to leaf nitrogen content for global-scale terrestrial biosphere models. *Global Change Biology* 15, 976–991.

Kattge, J., Diaz, S., Lavorel, S., Prentice, I., Leadley, P., Bönisch, G., Garnier, E., Westoby, M., Reich, P. B., Wright, I., et al. (2011). TRY—a global database of plant traits. *Global Change Biology* 17, 2905–2935.

Katul, G., Manzoni, S., Palmroth, S., and Oren, R. (2010). A stomatal optimization theory to describe the effects of atmospheric CO_2 on leaf photosynthesis and transpiration. *Annals of Botany* 105, 431–442.

Keeling, C. D. (1960). The concentration and isotopic abundances of carbon dioxide in the atmosphere. *Tellus* 12, 200–203.

Keeling, R. F., Piper, S. C., and Heimann, M. (1996). Global and hemispheric CO_2 sinks deduced from changes in atmospheric O_2 concentration. *Nature* 381, 218.

Keeling, R. F., Graven, H. D., Welp, L. R., Resplandy, L., Bi, J., Piper, S. C., Sun, Y., Bollenbacher, A., and Meijer, H. A. (2017). Atmospheric evidence for a global secular increase in carbon isotopic discrimination of land photosynthesis. *Proceedings of the National Academy of Sciences* 114, 10361–10366.

Keenan, T., Sabate, S., and Gracia, C. (2010a). Soil water stress and coupled photosynthesis–conductance models: Bridging the gap between conflicting reports on the relative roles of stomatal, mesophyll conductance and biochemical limitations to photosynthesis. *Agricultural and Forest Meteorology* 150, 443–453.

— (2010b). The importance of mesophyll conductance in regulating forest ecosystem productivity during drought periods. *Global Change Biology* 16, 1019–1034.

Keenan, T. F., Hollinger, D. Y., Bohrer, G., Dragoni, D., Munger, J. W., Schmid, H. P., and Richardson, A. D. (2013). Increase in forest water-use efficiency as atmospheric carbon dioxide concentrations rise. *Nature* 499, 324–327.

Kelliher, F., Leuning, R, Raupach, M., and Schulze, E.-D. (1995). Maximum conductances for evaporation from global vegetation types. *Agricultural and Forest Meteorology* 73, 1–16.

Kelliher, F., Lloyd, J, Arneth, A, Byers, J., McSeveny, T., Milukova, I, Grigoriev, S, Panfyorov, M, Sogatchev, A, Varlargin, A, et al. (1998). Evaporation from a central Siberian pine forest. *Journal of Hydrology* 205, 279–296.

Kergoat, L., Lafont, S., Douville, H., Berthelot, B., Dedieu, G., Planton, S., and Royer, J.-F. (2002). Impact of doubled CO_2 on global-scale leaf area index and evapotranspiration: Conflicting stomatal conductance and LAI responses. *Journal of Geophysical Research: Atmospheres (1984–2012)* 107, ACL–30.

Khatun, R., Ohta, T., Kotani, A., Asanuma, J., Gamo, M., Han, S., Hirano, T., Nakai, Y., Saigusa, N., Takagi, K., et al. (2011). Spatial variations in evapotranspiration over East Asian forest sites. I. Evapotranspiration and decoupling coefficient. *Hydrological Research Letters* 5, 83–87.

Kirschbaum, M. (1994). The sensitivity of C3 photosynthesis to increasing CO_2 concentration: a theoretical analysis of its dependence on temperature and background CO_2 concentration. *Plant, Cell & Environment* 17, 747–754.

Kleidon, A., Fraedrich, K., and Heimann, M. (2000). A green planet versus a desert world: Estimating the maximum effect of vegetation on the land surface climate. *Climatic Change* 44, 471–493.

Klein Goldewijk, K., Beusen, A., Van Drecht, G., and De Vos, M. (2011). The HYDE 3.1 spatially explicit database of human-induced global land-use change over the past 12,000 years. *Global Ecology and Biogeography* 20, 73–86.

Kljun, N, Calanca, P, Rotach, M., and Schmid, H. (2015). A simple two-dimensional parameterisation for Flux Footprint Prediction (FFP). *Geoscientific Model Development* 8, 3695.

Knauer, J., Werner, C., and Zaehle, S. (2015). Evaluating stomatal models and their atmospheric drought response in a land surface scheme: A multibiome analysis. *Journal of Geophysical Research: Biogeosciences* 120, 1894–1911.

Knauer, J., Zaehle, S., Reichstein, M., Medlyn, B. E., Forkel, M., Hagemann, S., and Werner, C. (2017). The response of ecosystem water-use efficiency to rising atmospheric CO_2 concentrations: sensitivity and large-scale biogeochemical implications. *New Phytologist* 213, 1654–1666.

Knauer, J., Zaehle, S., Medlyn, B. E., Reichstein, M., Williams, C. A., Migliavacca, M., De Kauwe, M. G., Werner, C., Keitel, C., Kolari, P., et al. (2018). Towards physiologically meaningful water-use efficiency estimates from eddy covariance data. *Global Change Biology* 24, 694–710.

Knohl, A. and Baldocchi, D. D. (2008). Effects of diffuse radiation on canopy gas exchange processes in a forest ecosystem. *Journal of Geophysical Research: Biogeosciences* 113.

Knohl, A. and Buchmann, N. (2005). Partitioning the net CO_2 flux of a deciduous forest into respiration and assimilation using stable carbon isotopes. *Global Biogeochemical Cycles* 19.

Kolbe, A. R. and Cousins, A. B. (2017). Mesophyll conductance in Zea mays responds transiently to CO_2 availability: implications for transpiration efficiency in C4 crops. *New Phytologist* 217, 1463–1474.

Kosugi, Y., Takanashi, S., Ueyama, M., Ohkubo, S., Tanaka, H., Matsumoto, K., Yoshifuji, N., Ataka, M., and Sakabe, A. (2013). Determination of the gas exchange phenology in an evergreen coniferous forest from 7 years of eddy covariance flux data using an extended big-leaf analysis. *Ecological Research* 28, 373–385.

Kuglitsch, F., Reichstein, M, Beer, C, Carrara, A, Ceulemans, R, Granier, A, Janssens, I., Koestner, B, Lindroth, A, Loustau, D, et al. (2008). Characterisation of ecosystem water-use efficiency of european forests from eddy covariance measurements. *Biogeosciences Discussions* 5, 4481–4519.

Kull, O and Kruijt, B (1998). Leaf photosynthetic light response: a mechanistic model for scaling photosynthesis to leaves and canopies. *Functional Ecology* 12, 767–777.

Kumagai, T., Saitoh, T. M., Sato, Y., Morooka, T., Manfroi, O. J., Kuraji, K., and Suzuki, M. (2004). Transpiration, canopy conductance and the decoupling coefficient of a lowland mixed dipterocarp forest in Sarawak, Borneo: dry spell effects. *Journal of Hydrology* 287, 237–251.

Kutsch, W., Aubinet, M., Buchmann, N, Smith, P, Osborne, B, Eugster, W, Wattenbach, M, Schrumpf, M, Schulze, E., Tomelleri, E, et al. (2010). The net biome production of full crop rotations in Europe. *Agriculture, Ecosystems & Environment* 139, 336–345.

Lange, O. L., Lösch, R, Schulze, E.-D., and Kappen, L (1971). Responses of stomata to changes in humidity. *Planta* 100, 76–86.

Lasslop, G., Reichstein, M., Papale, D., Richardson, A. D., Arneth, A., Barr, A., Stoy, P., and Wohlfahrt, G. (2010). Separation of net ecosystem exchange into assimilation and respiration using a light response curve approach: critical issues and global evaluation. *Global Change Biology* 16, 187–208.

Lasslop, G., Migliavacca, M., Bohrer, G, Reichstein, M., Bahn, M, Ibrom, A, Jacobs, C, Kolari, P, Papale, D, Vesala, T, et al. (2012). On the choice of the driving temperature for eddy-covariance carbon dioxide flux partitioning. *Biogeosciences* 9, 5243–5259.

Launiainen, S (2010). Seasonal and inter-annual variability of energy exchange above a boreal Scots pine forest. *Biogeosciences* 7, 3921–3940.

Launiainen, S., Katul, G. G., Kolari, P., Vesala, T., and Hari, P. (2011). Empirical and optimal stomatal controls on leaf and ecosystem level CO_2 and H_2O exchange rates. *Agricultural and Forest Meteorology* 151, 1672–1689.

Launiainen, S., Katul, G. G., Kolari, P., Lindroth, A., Lohila, A., Aurela, M., Varlagin, A., Grelle, A., and Vesala, T. (2016). Do the energy fluxes and surface conductance of boreal coniferous forests in Europe scale with leaf area? *Global Change Biology* 22, 4096–4113.

Law, B., Falge, E, Gu, L. v., Baldocchi, D., Bakwin, P, Berbigier, P, Davis, K, Dolman, A., Falk, M, Fuentes, J., et al. (2002). Environmental controls over carbon dioxide and water vapor exchange of terrestrial vegetation. *Agricultural and Forest Meteorology* 113, 97–120.

Le Quéré, C, Moriarty, R, Andrew, R., Canadell, J., Sitch, S, Korsbakken, J., Friedlingstein, P, Peters, G., Andres, R., Boden, T., et al. (2015). Global Carbon Budget 2015. *Earth System Science Data* 7, 349–396.

Leuning, R (1995). A critical appraisal of a combined stomatal-photosynthesis model for C3 plants. *Plant, Cell & Environment* 18, 339–355.

Leuning, R., Van Gorsel, E., Massman, W. J., and Isaac, P. R. (2012). Reflections on the surface energy imbalance problem. *Agricultural and Forest Meteorology* 156, 65–74.

Leuzinger, S. and Koerner, C. (2007). Water savings in mature deciduous forest trees under elevated CO_2. *Global Change Biology* 13, 2498–2508.

Li, L., Wang, Y., Arora, V. K., Eamus, D., Shi, H., Li, J., Cheng, L., Cleverly, J., Hajima, T, Ji, D., et al. (2018). Evaluating Global Land Surface Models in CMIP5: Analysis of Ecosystem Water-and Light-Use Efficiencies and Rainfall Partitioning. *Journal of Climate* 31, 2995–3008.

Liaw, A. and Wiener, M. (2002). Classification and Regression by randomForest. *R News* 2, 18–22.

Lin, Y.-S., Medlyn, B. E., Duursma, R. A., Prentice, I. C., Wang, H., Baig, S., Eamus, D., de Dios, V. R., Mitchell, P., Ellsworth, D. S., et al. (2015). Optimal stomatal behaviour around the world. *Nature Climate Change* 5, 459 –464.

Linderson, M.-L., Mikkelsen, T. N., Ibrom, A., Lindroth, A., Ro-Poulsen, H., and Pilegaard, K. (2012). Up-scaling of water use efficiency from leaf to canopy as based on leaf gas exchange relationships and the modeled in-canopy light distribution. *Agricultural and Forest Meteorology* 152, 201–211.

Lindroth, A., Klemedtsson, L., Grelle, A., Weslien, P., and Langvall, O. (2008). Measurement of Net Ecosystem Exchange, Productivity and Respiration in Three Spruce Forests in Sweden Shows Unexpectedly Large Soil Carbon Losses. *Biogeochemistry*, 43–60.

Lindroth, A., Mölder, M., and Lagergren, F. (2010). Heat storage in forest biomass improves energy balance closure. *Biogeosciences* 7, 301–313.

Lloyd, J. and Farquhar, G. D. (1994). 13C discrimination during CO_2 assimilation by the terrestrial biosphere. *Oecologia* 99, 201–215.

Lombardozzi, D. L., Zeppel, M. J., Fisher, R. A., and Tawfik, A. (2017). Representing nighttime and minimum conductance in CLM4. 5: global hydrology and carbon sensitivity analysis using observational constraints. *Geoscientific Model Development* 10, 321.

Lombardozzi, D. L., Smith, N. G., Cheng, S. J., Dukes, J. S., Sharkey, T. D., Rogers, A., Fisher, R., and Bonan, G. B. (2018). Triose phosphate limitation in photosynthesis models reduces leaf photosynthesis and global terrestrial carbon storage. *Environmental Research Letters* 13, 074025.

Long, S. and Bernacchi, C. (2003). Gas exchange measurements, what can they tell us about the underlying limitations to photosynthesis? Procedures and sources of error. *Journal of Experimental Botany* 54, 2393–2401.

Long, S., Farage, P., and Garcia, R. (1996). Measurement of leaf and canopy photosynthetic CO_2 exchange in the field. *Journal of Experimental Botany* 47, 1629–1642.

Loucos, K. E., Simonin, K. A., and Barbour, M. M. (2017). Leaf hydraulic conductance and mesophyll conductance are not closely related within a single species. *Plant, Cell & Environment* 40, 203–215.

Luo, X., Chen, J. M., Liu, J., Black, T. A., Croft, H., Staebler, R., He, L., Arain, M. A., Chen, B., Mo, G., et al. (2018). Comparison of Big-Leaf, Two-Big-Leaf, and Two-Leaf Upscaling Schemes for Evapotranspiration Estimation Using Coupled Carbon-Water Modeling. *Journal of Geophysical Research: Biogeosciences* 123, 207–225.

Lyons, T. (2002). Clouds prefer native vegetation. *Meteorology and Atmospheric Physics* 80, 131–140.

Maechler, M., Rousseeuw, P., Croux, C., Todorov, V., Ruckstuhl, A., Salibian-Barrera, M., Verbeke, T., Koller, M., Conceicao, E. L. T., and Anna di Palma, M. (2016). *robustbase: Basic Robust Statistics*. R package version 0.92-7.

Magnani, F, Leonardi, S, Tognetti, R, Grace, J, and Borghetti, M (1998). Modelling the surface conductance of a broad-leaf canopy: effects of partial decoupling from the atmosphere. *Plant, Cell & Environment* 21, 867–879.

Martin, G. et al. (2011). The HadGEM2 family of met office unified model climate configurations. *Geoscientific Model Development* 4, 723–757.

Martin, P. (1989). The significance of radiative coupling between vegetation and the atmosphere. *Agricultural and Forest Meteorology* 49, 45–53.

Martin, T., Brown, K., Kučera, J, Meinzer, F., Sprugel, D., and Hinckley, T. (2001). Control of transpiration in a 220-year-old *Abies amabilis* forest. *Forest Ecology and Management* 152, 211–224.

Massman, W. (1999). A model study of kB_H^{-1} for vegetated surfaces using 'localized near-field' Lagrangian theory. *Journal of Hydrology* 223, 27–43.

Mastrotheodoros, T., Pappas, C., Molnar, P., Burlando, P., Keenan, T. F., Gentine, P., Gough, C. M., and Fatichi, S. (2017). Linking plant functional trait plasticity and the large increase in forest water use efficiency. *Journal of Geophysical Research: Biogeosciences* 122, 2393–2408.

Maxwell, K. and Johnson, G. N. (2000). Chlorophyll fluorescence—a practical guide. *Journal of Experimental Botany* 51, 659–668.

McCarroll, D. and Loader, N. J. (2004). Stable isotopes in tree rings. *Quaternary Science Reviews* 23, 771–801.

McNaughton, K. and Black, T. A. (1973). A study of evapotranspiration from a Douglas fir forest using the energy balance approach. *Water Resources Research* 9, 1579–1590.

McNaughton, K. and Jarvis, P. (1991). Effects of spatial scale on stomatal control of transpiration. *Agricultural and Forest Meteorology* 54, 279–302.

McNaughton, K. and Van den Hurk, B. (1995). A 'Lagrangian'revision of the resistors in the two-layer model for calculating the energy budget of a plant canopy. *Boundary-Layer Meteorology* 74, 261–288.

Medlyn, B., Barton, C., Broadmeadow, M., Ceulemans, R, De Angelis, P, Forstreuter, M, Freeman, M, Jackson, S., Kellomäki, S, Laitat, E, et al. (2001). Stomatal conductance of forest species after long-term exposure to elevated CO_2 concentration: A synthesis. *New Phytologist* 149, 247–264.

Medlyn, B. E., Dreyer, E., Ellsworth, D., Forstreuter, M, Harley, P., Kirschbaum, M., Le Roux, X., Montpied, P., Strassemeyer, J, Walcroft, A, et al. (2002). Temperature response of parameters of a biochemically based model of photosynthesis. II. A review of experimental data. *Plant, Cell & Environment* 25, 1167–1179.

Medlyn, B. E., Duursma, R. A., Eamus, D., Ellsworth, D. S., Prentice, I. C., Barton, C. V., Crous, K. Y., de Angelis, P., Freeman, M., and Wingate, L. (2011). Reconciling the optimal and empirical approaches to modelling stomatal conductance. *Global Change Biology* 17, 2134–2144.

Medlyn, B. E., De Kauwe, M. G., Lin, Y.-S., Knauer, J., Duursma, R. A., Williams, C. A., Arneth, A., Clement, R., Isaac, P., Limousin, J.-M., et al. (2017). How do leaf and ecosystem measures of water-use efficiency compare? *New Phytologist* 216, 758–770.

Mercado, L. M., Bellouin, N., Sitch, S., Boucher, O., Huntingford, C., Wild, M., and Cox, P. M. (2009). Impact of changes in diffuse radiation on the global land carbon sink. *Nature* 458, 1014–1017.

Metzger, S., Durden, D., Sturtevant, C., Luo, H., Pingintha-Durden, N., Sachs, T., Serafimovich, A., Hartmann, J., Li, J., Xu, K., et al. (2017). eddy4R 0.2. 0: a DevOps model for community-extensible processing and analysis of eddy-covariance data based on R, Git, Docker, and HDF5. *Geoscientific Model Development* 10, 3189.

Meyers, T. P. and Hollinger, S. E. (2004). An assessment of storage terms in the surface energy balance of maize and soybean. *Agricultural and Forest Meteorology* 125, 105–115.

Migliavacca, M., Meroni, M., Manca, G., Matteucci, G., Montagnani, L., Grassi, G., Zenone, T., Teobaldelli, M., Goded, I., Colombo, R., et al. (2009). Seasonal and interannual patterns of carbon and water fluxes of a poplar plantation under peculiar eco-climatic conditions. *Agricultural and Forest Meteorology* 149, 1460–1476.

Milyukova, I. M., Kolle, O., Varlagin, A. V., Vygodskaya, N. N., Schulze, E.-D., and Lloyd, J. (2002). Carbon balance of a southern taiga spruce stand in European Russia. *Tellus B* 54, 429–442.

Miner, G. L., Bauerle, W. L., and Baldocchi, D. D. (2017). Estimating the sensitivity of stomatal conductance to photosynthesis: a review. *Plant, Cell & Environment* 40, 1214–1238.

Misson, L., Limousin, J., Rodriguez, R., and Letts, M. G. (2010). Leaf physiological responses to extreme droughts in Mediterranean Quercus ilex forest. *Plant, Cell & Environment* 33, 1898–1910.

Monteith, J. (1965). Evaporation and environment. In: *Symp. Soc. Exp. Biol.* Ed. by G. Fogg. Vol. 19. Cambridge University Press, 205–234.

Monteith, J. and Unsworth, M. (2008). Principles of Environmental Physics. 3rd. Academic Press.

Montpied, P., Granier, A., and Dreyer, E. (2009). Seasonal time-course of gradients of photosynthetic capacity and mesophyll conductance to CO_2 across a beech (*Fagus sylvatica* L.) canopy. *Journal of Experimental Botany* 60, 2407–2418.

Morgan, J., Pataki, D., Körner, C., Clark, H, Del Grosso, S., Grünzweig, J., Knapp, A., Mosier, A., Newton, P., Niklaus, P. A., et al. (2004). Water relations in grassland and desert ecosystems exposed to elevated atmospheric CO_2. *Oecologia* 140, 11–25.

Morison, J. I. (1987). Intercellular CO_2 concentration and stomatal response to CO_2. *Stomatal function*, 229.

Mueller, B., Hirschi, M., Jimenez, C, Ciais, P, Dirmeyer, P., Dolman, A., Fisher, J., Jung, M, Ludwig, F, Maignan, F, et al. (2013). Benchmark products for land evapotranspiration: LandFlux-EVAL multi-data set synthesis. *Hydrology & Earth System Sciences* 17, 3707–3720.

Nave, L., Gough, C., Maurer, K., Bohrer, G, Hardiman, B., Le Moine, J, Munoz, A., Nadelhoffer, K., Sparks, J., Strahm, B., et al. (2011). Disturbance and the resilience of coupled carbon and nitrogen cycling in a north temperate forest. *Journal of Geophysical Research: Biogeosciences (2005–2012)* 116.

Niinemets, l. and Keenan, T. (2014). Photosynthetic responses to stress in Mediterranean evergreens: mechanisms and models. *Environmental and Experimental Botany* 103, 24–41.

Niinemets, l., Wright, I. J., and Evans, J. R. (2009a). Leaf mesophyll diffusion conductance in 35 Australian sclerophylls covering a broad range of foliage structural and physiological variation. *Journal of Experimental Botany* 60, 2433–2449.

Niinemets, l., Díaz-Espejo, A., Flexas, J., Galmés, J., and Warren, C. R. (2009b). Role of mesophyll diffusion conductance in constraining potential photosynthetic productivity in the field. *Journal of Experimental Botany* 60, 2249–2270.

Niinemets, l., Flexas, J., and Peuelas, J. (2011). Evergreens favored by higher responsiveness to increased CO_2. *Trends in Ecology & Evolution* 26, 136–142.

Niu, S., Xing, X., Zhang, Z., Xia, J., Zhou, X., Song, B., Li, L., and Wan, S. (2011). Water-use efficiency in response to climate change: from leaf to ecosystem in a temperate steppe. *Global Change Biology* 17, 1073–1082.

Norby, R. J. and Zak, D. R. (2011). Ecological lessons from free-air CO_2 enrichment (FACE) experiments. *Annual Review of Ecology, Evolution, and Systematics* 42, 181.

Norby, R. J., Warren, J. M., Iversen, C. M., Medlyn, B. E., and McMurtrie, R. E. (2010). CO_2 enhancement of forest productivity constrained by limited nitrogen availability. *Proceedings of the National Academy of Sciences* 107, 19368–19373.

Novick, K. A., Ficklin, D. L., Stoy, P. C., Williams, C. A., Bohrer, G., Oishi, A. C., Papuga, S. A., Blanken, P. D., Noormets, A., Sulman, B. N., et al. (2016). The increasing importance of atmospheric demand for ecosystem water and carbon fluxes. *Nature Climate Change* 6, 1023–1027.

Oren, R, Sperry, J., Katul, G., Pataki, D., Ewers, B., Phillips, N, and Schäfer, K. (1999). Survey and synthesis of intra-and interspecific variation in stomatal sensitivity to vapour pressure deficit. *Plant, Cell & Environment* 22, 1515–1526.

Osmond, C., Björkman, O, and Anderson, D. (1980). Physiological Processes in Plant Ecology. Vol. 36. Berlin: Springer.

Owen, P. and Thomson, W. (1963). Heat transfer across rough surfaces. *Journal of Fluid Mechanics* 15, 321–334.

Papale, D, Reichstein, M, Aubinet, M, Canfora, E, Bernhofer, C, Kutsch, W, Longdoz, B, Rambal, S, Valentini, R, Vesala, T, et al. (2006). Towards a standardized processing of Net Ecosystem Exchange measured with eddy covariance technique: algorithms and uncertainty estimation. *Biogeosciences* 3, 571–583.

Pastorello, G., Papale, D, Chu, H, Trotta, C, Agarwal, D., Canfora, E, Baldocchi, D., and Torn, M (2017). A new data set to keep a sharper eye on land-air exchanges. *Eos, Transactions American Geophysical Union (Online)* 98.

Paulson, C. A. (1970). The mathematical representation of wind speed and temperature profiles in the unstable atmospheric surface layer. *Journal of Applied Meteorology* 9, 857–861.

Paw U, K. and Meyers, T. P (1989). Investigations with a higher-order canopy turbulence model into mean source-sink levels and bulk canopy resistances. *Agricultural and Forest Meteorology* 47, 259–271.

Perez-Martin, A., Michelazzo, C., Torres-Ruiz, J. M., Flexas, J., Fernández, J. E., Sebastiani, L., and Diaz-Espejo, A. (2014). Regulation of photosynthesis and stomatal and mesophyll conductance under water stress and recovery in olive trees: correlation with gene expression of carbonic anhydrase and aquaporins. *Journal of Experimental Botany* 65, 3143–3156.

Perez-Priego, O., El-Madany, T. S., Migliavacca, M., Kowalski, A. S., Jung, M., Carrara, A., Kolle, O., Martín, M. P., Pacheco-Labrador, J., Moreno, G., et al. (2017). Evaluation of eddy covariance latent heat fluxes with independent lysimeter and sapflow estimates in a Mediterranean savannah ecosystem. *Agricultural and Forest Meteorology* 236, 87–99.

Peñuelas, J., Canadell, J. G., and Ogaya, R. (2011). Increased water-use efficiency during the 20th century did not translate into enhanced tree growth. *Global Ecology and Biogeography* 20, 597–608.

Piao, S., Friedlingstein, P., Ciais, P., de Noblet-Ducoudré, N., Labat, D., and Zaehle, S. (2007). Changes in climate and land use have a larger direct impact than rising CO_2 on global river runoff trends. *Proceedings of the National Academy of Sciences* 104, 15242–15247.

Piel, C., Frak, E., Le Roux, X., and Genty, B. (2002). Effect of local irradiance on CO_2 transfer conductance of mesophyll in walnut. *Journal of Experimental Botany* 53, 2423–2430.

Pilegaard, K., Mikkelsen, T. N., Beier, C., Jensen, N. O., Ambus, P., and Ro-Poulsen, H. (2003). Field measurements of atmosphere-biosphere interactions in a Danish beech forest. *Boreal Environment Research* 8, 315–334.

Pitman, A. (2003). The evolution of, and revolution in, land surface schemes designed for climate models. *International Journal of Climatology* 23, 479–510.

Pongratz, J, Reick, C., Raddatz, T, and Claussen, M (2010). Biogeophysical versus biogeochemical climate response to historical anthropogenic land cover change. *Geophysical Research Letters* 37, L08702.

Pongratz, J., Reick, C., Raddatz, T., and Claussen, M. (2007). Reconstruction of global land use and land cover AD 800 to 1992.

Pons, T. L., Flexas, J., Von Caemmerer, S., Evans, J. R., Genty, B., Ribas-Carbo, M., and Brugnoli, E. (2009). Estimating mesophyll conductance to CO_2: methodology, potential errors, and recommendations. *Journal of Experimental Botany* 60, 2217–2234.

Ponton, S., Flanagan, L. B., Alstad, K. P., Johnson, B. G., Morgenstern, K., Kljun, N., Black, T. A., and Barr, A. G. (2006). Comparison of ecosystem water-use efficiency among Douglas-fir forest, aspen forest and grassland using eddy covariance and carbon isotope techniques. *Global Change Biology* 12, 294–310.

Prentice, I. C., Dong, N., Gleason, S. M., Maire, V., and Wright, I. J. (2014). Balancing the costs of carbon gain and water transport: testing a new theoretical framework for plant functional ecology. *Ecology letters* 17, 82–91.

Prentice, I. C., Liang, X, Medlyn, B. E., and Wang, Y.-P. (2015). Reliable, robust and realistic: the three R's of next-generation land-surface modelling. *Atmospheric Chemistry and Physics* 15, 5987–6005.

Priestley, C. and Taylor, R. (1972). On the assessment of surface heat flux and evaporation using large-scale parameters. *Monthly Weather Review* 100, 81–92.

R Core Team (2017). *R: A Language and Environment for Statistical Computing*. R Foundation for Statistical Computing. Vienna, Austria.

Raddatz, T., Reick, C., Knorr, W., Kattge, J., Roeckner, E, Schnur, R., Schnitzler, K.-G., Wetzel, P, and Jungclaus, J (2007). Will the tropical land biosphere dominate the climate–carbon cycle feedback during the twenty-first century? *Climate Dynamics* 29, 565–574.

Rambal, S., Ourcival, J.-M., Joffre, R., Mouillot, F., Nouvellon, Y., Reichstein, M., and Rocheteau, A. (2003). Drought controls over conductance and assimilation of a Mediterranean evergreen ecosystem: scaling from leaf to canopy. *Global Change Biology* 9, 1813–1824.

Randerson, J. T., Thompson, M. V., Conway, T. J., Fung, I. Y., and Field, C. B. (1997). The contribution of terrestrial sources and sinks to trends in the seasonal cycle of atmospheric carbon dioxide. *Global Biogeochemical Cycles* 11, 535–560.

Raupach, M. and Finnigan, J. (1988). 'Single-layer models of evaporation from plant canopies are incorrect but useful, whereas multilayer models are correct but useless': Discuss. *Functional Plant Biology* 15, 705–716.

Rayment, M., Loustau, D, and Jarvis, P. (2002). Photosynthesis and respiration of black spruce at three organizational scales: shoot, branch and canopy. *Tree Physiology* 22, 219–229.

Rödenbeck, C, Houweling, S, Gloor, M, and Heimann, M (2003). CO_2 flux history 1982–2001 inferred from atmospheric data using a global inversion of atmospheric transport. *Atmospheric Chemistry and Physics* 3, 1919–1964.

Rödenbeck, C. (2005). *Estimating CO_2 sources and sinks from atmospheric mixing ratio measurements using a global inversion of atmospheric transport*. Technical Reports. Max Planck Institute for Biogeochemistry.

Reichstein, M., Tenhunen, J., Roupsard, O., Ourcival, J.-M., Rambal, S., Miglietta, F., Peressotti, A., Pecchiari, M., Tirone, G., and Valentini, R. (2003). Inverse modeling of seasonal drought effects on canopy CO_2/H_2O exchange in three Mediterranean ecosystems. *Journal of Geophysical Research: Atmospheres* 108.

Reichstein, M., Falge, E., Baldocchi, D., Papale, D., Aubinet, M., Berbigier, P., Bernhofer, C., Buchmann, N., Gilmanov, T., Granier, A., et al. (2005). On the separation of net ecosystem exchange into assimilation and ecosystem respiration: review and improved algorithm. *Global Change Biology* 11, 1424–1439.

Reichstein, M., Bahn, M., Mahecha, M. D., Kattge, J., and Baldocchi, D. D. (2014). Linking plant and ecosystem functional biogeography. *Proceedings of the National Academy of Sciences* 111, 13697–13702.

Reick, C., Raddatz, T, Brovkin, V, and Gayler, V (2013). Representation of natural and anthropogenic land cover change in MPI-ESM. *Journal of Advances in Modeling Earth Systems* 5, 459–482.

Richardson, A. D., Aubinet, M., Barr, A. G., Hollinger, D. Y., Ibrom, A., Lasslop, G., and Reichstein, M. (2012). Uncertainty quantification. In: *Eddy Covariance*. Springer, 173–209.

Rigden, A., Li, D., and Salvucci, G. (2018a). Dependence of thermal roughness length on friction velocity across land cover types: A synthesis analysis using AmeriFlux data. *Agricultural and Forest Meteorology* 249, 512–519.

Rigden, A. J., Salvucci, G. D., Entekhabi, D., and Short Gianotti, D. J. (2018b). Partitioning evapotranspiration over the continental United States using weather station data. *Geophysical Research Letters*.

Roeckner, E et al. (2003). The atmospheric general circulation model ECHAM5. Part I: Model description. *MPI Rep., Max Planck Inst. for Meteorol., Hamburg, Germany* 349, 127.

Rogers, A., Medlyn, B. E., Dukes, J. S., Bonan, G., Caemmerer, S., Dietze, M. C., Kattge, J., Leakey, A. D., Mercado, L. M., Niinemets, l., et al. (2017). A roadmap for improving the representation of photosynthesis in Earth system models. *New Phytologist* 213, 22–42.

Sato, H., Kumagai, T., Takahashi, A., and Katul, G. G. (2015). Effects of different representations of stomatal conductance response to humidity across the African continent under warmer CO_2-enriched climate conditions. *Journal of Geophysical Research: Biogeosciences* 120, 979–988.

Saurer, M., Siegwolf, R. T., and Schweingruber, F. H. (2004). Carbon isotope discrimination indicates improving water-use efficiency of trees in northern Eurasia over the last 100 years. *Global Change Biology* 10, 2109–2120.

Saurer, M., Spahni, R., Frank, D. C., Joos, F., Leuenberger, M., Loader, N. J., McCarroll, D., Gagen, M., Poulter, B., Siegwolf, R. T., et al. (2014). Spatial variability and temporal trends in water-use efficiency of European forests. *Global Change Biology* 20, 3700–3712.

Scafaro, A. P., Von Caemmerer, S., Evans, J. R., and Atwell, B. J. (2011). Temperature response of mesophyll conductance in cultivated and wild Oryza species with contrasting mesophyll cell wall thickness. *Plant, Cell & Environment* 34, 1999–2008.

Scanlon, T. M. and Kustas, W. P. (2010). Partitioning carbon dioxide and water vapor fluxes using correlation analysis. *Agricultural and Forest Meteorology* 150, 89–99.

Schlesinger, W. H. and Jasechko, S. (2014). Transpiration in the global water cycle. *Agricultural and Forest Meteorology* 189, 115–117.

Schmid, H. P., Grimmond, C. S. B., Cropley, F., Offerle, B., and Su, H.-B. (2000). Measurements of CO_2 and energy fluxes over a mixed hardwood forest in the mid-western United States. *Agricultural and Forest Meteorology* 103, 357–374.

Scholze, M, Ciais, P, and Heimann, M (2008). Modeling terrestrial ^{13}C cycling: Climate, land use and fire. *Global Biogeochemical Cycles* 22.

Schulz, J.-P., Dümenil, L., and Polcher, J. (2001). On the land surface-atmosphere coupling and its impact in a single-column atmospheric model. *Journal of Applied Meteorology* 40, 642–663.

Schulze, E.-D. and Hall, A. (1982). Stomatal responses, water loss and CO_2 assimilation rates of plants in contrasting environments. In: *Physiological Plant Ecology II*. Springer, 181–230.

Schurgers, G., Lagergren, F., Mölder, M., and Lindroth, A. (2015). The importance of micrometeorological variations for photosynthesis and transpiration in a boreal coniferous forest. *Biogeosciences* 12, 237–256.

Scott, R. L. and Biederman, J. A. (2017). Partitioning evapotranspiration using long-term carbon dioxide and water vapor fluxes. *Geophysical Research Letters* 44, 6833–6840.

Seibt, U., Rajabi, A., Griffiths, H., and Berry, J. A. (2008). Carbon isotopes and water use efficiency: sense and sensitivity. *Oecologia* 155, 441.

Sellers, P. J. (1985). Canopy reflectance, photosynthesis and transpiration. *International Journal of Remote Sensing* 6, 1335–1372.

Sellers, P., Mintz, Y., Sud, Y. e. a., and Dalcher, A (1986). A simple biosphere model (SiB) for use within general circulation models. *Journal of the Atmospheric Sciences* 43, 505–531.

Sellers, P., Bounoua, L, Collatz, G., Randall, D., Dazlich, D., Los, S., Berry, J., Fung, I, Tucker, C., Field, C., et al. (1996). Comparison of radiative and physiological effects of doubled atmospheric CO_2 on climate. *Science* 271, 1402–1405.

Sellers, P., Dickinson, R., Randall, D., Betts, A., Hall, F., Berry, J., Collatz, G., Denning, A., Mooney, H., Nobre, C., et al. (1997). Modeling the exchanges of energy, water, and carbon between continents and the atmosphere. *Science* 275, 502–509.

Sellin, A., Eensalu, E., and Niglas, A. (2010). Is distribution of hydraulic constraints within tree crowns reflected in photosynthetic water-use efficiency? An example of Betula pendula. *Ecological Research* 25, 173–183.

Shaw, R. H. and Pereira, A. (1982). Aerodynamic roughness of a plant canopy: a numerical experiment. *Agricultural Meteorology* 26, 51–65.

Sheffield, J., Wood, E. F., and Munoz-Arriola, F. (2010). Long-term regional estimates of evapotranspiration for Mexico based on downscaled ISCCP data. *Journal of Hydrometeorology* 11, 253–275.

Shuttleworth, W. J. and Wallace, J. (1985). Evaporation from sparse crops-an energy combination theory. *Quarterly Journal of the Royal Meteorological Society* 111, 839–855.

Spitters, C. (1986). Separating the diffuse and direct component of global radiation and its implications for modeling canopy photosynthesis Part II. Calculation of canopy photosynthesis. *Agricultural and Forest Meteorology* 38, 231–242.

Stoy, P. C., Mauder, M., Foken, T., Marcolla, B., Boegh, E., Ibrom, A., Arain, M. A., Arneth, A., Aurela, M., Bernhofer, C., et al. (2013). A data-driven analysis of energy balance closure across FLUXNET research sites: The role of landscape scale heterogeneity. *Agricultural and Forest Meteorology* 171, 137–152.

Su, Z, Schmugge, T, Kustas, W., and Massman, W. (2001). An evaluation of two models for estimation of the roughness height for heat transfer between the land surface and the atmosphere. *Journal of Applied Meteorology* 40, 1933–1951.

Sud, Y., Shukla, J, and Mintz, Y. (1988). Influence of land surface roughness on atmospheric circulation and precipitation: A sensitivity study with a general circulation model. *Journal of Applied Meteorology* 27, 1036–1054.

Suits, N. S., Denning, A. S., Berry, J., Still, C., Kaduk, J., Miller, J., and Baker, I. (2005). Simulation of carbon isotope discrimination of the terrestrial biosphere. *Global Biogeochemical Cycles* 19.

Sun, Y., Gu, L., Dickinson, R. E., Pallardy, S. G., Baker, J., Cao, Y., DaMatta, F. M., Dong, X., Ellsworth, D., Van Goethem, D., et al. (2014a). Asymmetrical effects of mesophyll conductance on fundamental photosynthetic parameters and their relationships estimated from leaf gas exchange measurements. *Plant, Cell & Environment* 37, 978–994.

Sun, Y., Gu, L., Dickinson, R. E., Norby, R. J., Pallardy, S. G., and Hoffman, F. M. (Nov. 2014b). Impact of mesophyll diffusion on estimated global land CO_2 fertilization. *Proceedings of the National Academy of Sciences* 111, 15774–15779.

Tang, J., Qi, Y., Xu, M., Misson, L., and Goldstein, A. H. (2005). Forest thinning and soil respiration in a ponderosa pine plantation in the Sierra Nevada. *Tree Physiology* 25, 57–66.

Tang, X., Li, H., Desai, A. R., Nagy, Z., Luo, J., Kolb, T. E., Olioso, A., Xu, X., Yao, L., Kutsch, W., et al. (2014). How is water-use efficiency of terrestrial ecosystems distributed and changing on Earth? *Scientific Reports* 4.

Tapley, B. D., Bettadpur, S., Ries, J. C., Thompson, P. F., and Watkins, M. M. (2004). GRACE measurements of mass variability in the Earth system. *Science* 305, 503–505.

Tazoe, Y., Von Caemmerer, S., Badger, M. R., and Evans, J. R. (2009). Light and CO_2 do not affect the mesophyll conductance to CO_2 diffusion in wheat leaves. *Journal of Experimental Botany* 60, 2291–2301.

Teuling, A. J., Seneviratne, S. I., Stöckli, R., Reichstein, M., Moors, E., Ciais, P., Luyssaert, S., Van Den Hurk, B., Ammann, C., Bernhofer, C., et al. (2010). Contrasting response of European forest and grassland energy exchange to heatwaves. *Nature Geoscience* 3, 722–727.

Tholen, D. and Zhu, X.-G. (2011). The mechanistic basis of internal conductance: a theoretical analysis of mesophyll cell photosynthesis and CO_2 diffusion. *Plant Physiology* 156, 90–105.

Thom, A. (1972). Momentum, mass and heat exchange of vegetation. *Quarterly Journal of the Royal Meteorological Society* 98, 124–134.

Théroux-Rancourt, G. and Gilbert, M. E. (2017). The light response of mesophyll conductance is controlled by structure across leaf profiles. *Plant, Cell & Environment* 40, 726–740.

Thum, T., Aalto, T., Laurila, T., Aurela, M., Kolari, P., and Hari, P. (2007). Parametrization of two photosynthesis models at the canopy scale in a northern boreal Scots pine forest. *Tellus B* 59, 874–890.

Tian, H., Chen, G., Liu, M., Zhang, C., Sun, G., Lu, C., Xu, X., Ren, W., Pan, S., and Chappelka, A. (2010). Model estimates of net primary productivity, evapotranspiration, and water use efficiency in the terrestrial ecosystems of the southern United States during 1895–2007. *Forest Ecology and Management* 259, 1311–1327.

Tomás, M., Flexas, J., Copolovici, L., Galmés, J., Hallik, L., Medrano, H., Ribas-Carbó, M., Tosens, T., Vislap, V., and Niinemets, l. (2013). Importance of leaf anatomy in determining mesophyll diffusion conductance to CO_2 across species: quantitative limitations and scaling up by models. *Journal of Experimental Botany* 64, 2269–2281.

Twine, T. E., Kustas, W., Norman, J., Cook, D., Houser, P., Meyers, T., Prueger, J., Starks, P., and Wesely, M. (2000). Correcting eddy-covariance flux underestimates over a grassland. *Agricultural and Forest Meteorology* 103, 279–300.

Ubierna, N. and Farquhar, G. D. (2014). Advances in measurements and models of photosynthetic carbon isotope discrimination in C3 plants. *Plant, Cell & Environment* 37, 1494–1498.

Ubierna, N., Gandin, A., Boyd, R. A., and Cousins, A. B. (2016). Temperature response of mesophyll conductance in three C4 species calculated with two methods: ^{18}O discrimination and in vitro V_{pmax}. *New Phytologist*.

Ueyama, M., Tahara, N., Iwata, H., Euskirchen, E. S., Ikawa, H., Kobayashi, H., Nagano, H., Nakai, T., and Harazono, Y. (2016). Optimization of a biochemical model with eddy covariance measurements in black spruce forests of Alaska for estimating CO_2 fertilization effects. *Agricultural and Forest Meteorology* 222, 98–111.

Ukkola, A. M., Prentice, I. C., Keenan, T. F., van Dijk, A. I., Viney, N. R., Myneni, R. B., and Bi, J. (2016). Reduced streamflow in water-stressed climates consistent with CO_2 effects on vegetation. *Nature Climate Change* 6, 75.

Urbanski, S, Barford, C, Wofsy, S, Kucharik, C, Pyle, E, Budney, J, McKain, K, Fitzjarrald, D, Czikowsky, M, and Munger, J. (2007). Factors controlling CO_2 exchange on timescales from hourly to decadal at Harvard Forest. *Journal of Geophysical Research: Biogeosciences* 112, G02020.

van Dijk, A. I., Gash, J. H., van Gorsel, E., Blanken, P. D., Cescatti, A., Emmel, C., Gielen, B., Harman, I. N., Kiely, G., Merbold, L., et al. (2015). Rainfall interception and the coupled surface water and energy balance. *Agricultural and Forest Meteorology* 214, 402–415.

Varone, L., Ribas-Carbo, M., Cardona, C., Gallé, A., Medrano, H., Gratani, L., and Flexas, J. (2012). Stomatal and non-stomatal limitations to photosynthesis in seedlings and saplings of Mediterranean species pre-conditioned and aged in nurseries: Different response to water stress. *Environmental and Experimental Botany* 75, 235–247.

Verhoef, A, De Bruin, H., and Van Den Hurk, B. (1997). Some practical notes on the parameter kB^{-1} for sparse vegetation. *Journal of Applied Meteorology* 36, 560–572.

Verma, S. (1989). Aerodynamic resistances to transfers of heat, mass and momentum. In: *Estimation of areal evapotranspiration*. Ed. by T. Black, D. Spittlehouse, M. Novak, and D. Price. Vol. 177. International Association of Hydrological Sciences, 13–20.

Verma, S. B., Dobermann, A., Cassman, K. G., Walters, D. T., Knops, J. M., Arkebauer, T. J., Suyker, A. E., Burba, G. G., Amos, B., Yang, H., et al. (2005). Annual carbon dioxide exchange in irrigated and rainfed maize-based agroecosystems. *Agricultural and Forest Meteorology* 131, 77–96.

Vesala, T, Suni, T, Rannik, Keronen, P, Markkanen, T, Sevanto, S, Grönholm, T, Smolander, S, Kulmala, M, Ilvesniemi, H, et al. (2005). Effect of thinning on surface fluxes in a boreal forest. *Global Biogeochemical Cycles* 19.

Voelker, S. L., Brooks, J. R., Meinzer, F. C., Anderson, R., Bader, M. K.-F., Battipaglia, G., Becklin, K. M., Beerling, D., Bert, D., Betancourt, J. L., et al. (2016). A dynamic leaf gas-exchange strategy is conserved in woody plants under changing ambient CO_2: evidence from carbon isotope discrimination in paleo and CO_2 enrichment studies. *Global Change Biology* 22, 889–902.

von Caemmerer, S and Evans, J. (1991). Determination of the average partial pressure of CO_2 in chloroplasts from leaves of several C3 plants. *Functional Plant Biology* 18, 287–305.

von Caemmerer, S and Farquhar, G. (1981). Some relationships between the biochemistry of photosynthesis and the gas exchange of leaves. *Planta* 153, 376–387.

von Caemmerer, S. (2000). Biochemical models of leaf photosynthesis. Techniques in plant sciences; no. 2. CSIRO Publishing.

von Caemmerer, S. and Evans, J. R. (2015). Temperature responses of mesophyll conductance differ greatly between species. *Plant, Cell & Environment* 38, 629–637.

von Caemmerer, S. and Furbank, R. T. (1999). Modeling C4 photosynthesis. In: *C4 Plant Biology*. Ed. by R. F. Sage and R. K. Monson. Academic Press Toronto, ON, Canada. Chap. 6, 173–211.

Walker, A. P., Hanson, P. J., De Kauwe, M. G., Medlyn, B. E., Zaehle, S., Asao, S., Dietze, M., Hickler, T., Huntingford, C., Iversen, C. M., et al. (2014). Comprehensive ecosystem model-data synthesis using multiple data sets at two temperate forest free-air CO_2 enrichment experiments: Model performance at ambient CO_2 concentration. *Journal of Geophysical Research: Biogeosciences* 119, 937–964.

Walker, B., Ariza, L. S., Kaines, S., Badger, M. R., and Cousins, A. B. (2013). Temperature response of in vivo Rubisco kinetics and mesophyll conductance in *Arabidopsis thaliana*: comparisons to *Nicotiana tabacum*. *Plant, Cell & Environment* 36, 2108–2119.

Walker, X. J., Mack, M. C., and Johnstone, J. F. (2015). Stable carbon isotope analysis reveals widespread drought stress in boreal black spruce forests. *Global Change Biology* 21, 3102–3113.

Wang, W., Liang, S., and Meyers, T. (2008). Validating MODIS land surface temperature products using long-term nighttime ground measurements. *Remote Sensing of Environment* 112, 623–635.

Wang, Y.-P. and Leuning, R (1998). A two-leaf model for canopy conductance, photosynthesis and partitioning of available energy I: Model description and comparison with a multi-layered model. *Agricultural and Forest Meteorology* 91, 89–111.

Wang, Y. P. (2003). A comparison of three different canopy radiation models commonly used in plant modelling. *Functional Plant Biology* 30, 143–152.

Warren, C. R. (2008). Stand aside stomata, another actor deserves centre stage: the forgotten role of the internal conductance to CO_2 transfer. *Journal of Experimental Botany* 59, 1475–1487.

Warren, C., Löw, M, Matyssek, R, and Tausz, M (2007). Internal conductance to CO_2 transfer of adult *Fagus sylvatica*: Variation between sun and shade leaves and due to free-air ozone fumigation. *Environmental and Experimental Botany* 59, 130–138.

Waterhouse, J. S., Switsur, V., Barker, A., Carter, A., Hemming, D., Loader, N. J., and Robertson, I (2004). Northern European trees show a progressively diminishing response to increasing atmospheric carbon dioxide concentrations. *Quaternary Science Reviews* 23, 803–810.

Weedon, G. P., Balsamo, G., Bellouin, N., Gomes, S., Best, M. J., and Viterbo, P. (2014). The WFDEI meteorological forcing data set: WATCH Forcing Data methodology applied to ERA-Interim reanalysis data. *Water Resources Research* 50, 7505–7514.

Wehr, R, Munger, J., McManus, J., Nelson, D., Zahniser, M., Davidson, E., Wofsy, S., and Saleska, S. (2016). Seasonality of temperate forest photosynthesis and daytime respiration. *Nature* 534, 680–683.

Wei, Z., Yoshimura, K., Wang, L., Miralles, D. G., Jasechko, S., and Lee, X. (2017). Revisiting the contribution of transpiration to global terrestrial evapotranspiration. *Geophysical Research Letters* 44, 2792–2801.

Wieder, W. R., Cleveland, C. C., Smith, W. K., and Todd-Brown, K. (2015). Future productivity and carbon storage limited by terrestrial nutrient availability. *Nature Geoscience* 8, 441.

Williams, C. A., Reichstein, M., Buchmann, N., Baldocchi, D., Beer, C., Schwalm, C., Wohlfahrt, G., Hasler, N., Bernhofer, C., Foken, T., et al. (2012). Climate and vegetation controls on the surface water balance: Synthesis of evapotranspiration measured across a global network of flux towers. *Water Resources Research* 48.

Wilson, K., Carlson, T., Bunce, J. A., et al. (1999). Feedback significantly influences the simulated effect of CO_2 on seasonal evapotranspiration from two agricultural species. *Global Change Biology* 5, 903–917.

Wilson, K., Goldstein, A., Falge, E., Aubinet, M., Baldocchi, D., Berbigier, P., Bernhofer, C., Ceulemans, R., Dolman, H., Field, C., et al. (2002a). Energy balance closure at FLUXNET sites. *Agricultural and Forest Meteorology* 113, 223–243.

Wilson, K. B., Baldocchi, D. D., Aubinet, M., Berbigier, P., Bernhofer, C., Dolman, H., Falge, E., Field, C., Goldstein, A., Granier, A., et al. (2002b). Energy partitioning between latent and sensible heat flux during the warm season at FLUXNET sites. *Water Resources Research* 38.

Wohlfahrt, G. and Gu, L. (2015). The many meanings of gross photosynthesis and their implication for photosynthesis research from leaf to globe. *Plant, Cell & Environment* 38, 2500–2507.

Wohlfahrt, G., Bahn, M., Haslwanter, A., Newesely, C., and Cernusca, A. (2005). Estimation of daytime ecosystem respiration to determine gross primary production of a mountain meadow. *Agricultural and Forest Meteorology* 130, 13–25.

Wohlfahrt, G., Hammerle, A., Haslwanter, A., Bahn, M., Tappeiner, U., and Cernusca, A. (2008). Seasonal and inter-annual variability of the net ecosystem CO_2 exchange of a temperate mountain grassland: Effects of weather and management. *Journal of Geophysical Research: Atmospheres* 113.

Wohlfahrt, G., Haslwanter, A., Hörtnagl, L., Jasoni, R. L., Fenstermaker, L. F., Arnone, J. A., and Hammerle, A. (2009). On the consequences of the energy imbalance for calculating surface conductance to water vapour. *Agricultural and Forest Meteorology* 149, 1556–1559.

Wohlfahrt, G., Brilli, F., Hörtnagl, L., Xu, X., Bingemer, H., Hansel, A., and Loreto, F. (2012). Carbonyl sulfide (COS) as a tracer for canopy photosynthesis, transpiration and stomatal conductance: potential and limitations. *Plant, Cell & Environment* 35, 657–667.

Wolf, A., Akshalov, K., Saliendra, N., Johnson, D. A., and Laca, E. A. (2006). Inverse estimation of Vcmax, leaf area index, and the Ball-Berry parameter from carbon and energy fluxes. *Journal of Geophysical Research: Atmospheres* 111.

Wolz, K. J., Wertin, T. M., Abordo, M., Wang, D., and Leakey, A. D. (2017). Diversity in stomatal function is integral to modelling plant carbon and water fluxes. *Nature Ecology & Evolution* 1, 1292.

Wong, S., Cowan, I., and Farquhar, G. (1979). Stomatal conductance correlates with photosynthetic capacity. *Nature* 282, 424–426.

Wullschleger, S. D., Wilson, K. B., and Hanson, P. J. (2000). Environmental control of whole-plant transpiration, canopy conductance and estimates of the decoupling coefficient for large red maple trees. *Agricultural and Forest Meteorology* 104, 157–168.

Wullschleger, S. D., Gunderson, C., Hanson, P., Wilson, K., and Norby, R. (2002). Sensitivity of stomatal and canopy conductance to elevated CO_2 concentration–interacting variables and perspectives of scale. *New Phytologist* 153, 485–496.

Wutzler, T., Lucas-Moffat, A., Migliavacca, M., Knauer, J., Sickel, K., Šigut, L., Menzer, O., and Reichstein, M. (2018). Basic and extensible post-processing of eddy covariance flux data with REddyProc. *Biogeosciences* 15, 5015–5030.

Xiong, D., Liu, X., Liu, L., Douthe, C., Li, Y., Peng, S., and Huang, J. (2015). Rapid responses of mesophyll conductance to changes of CO_2 concentration, temperature and irradiance are affected by N supplements in rice. *Plant, Cell & Environment* 38, 2541–2550.

Xu, K., Metzger, S., and Desai, A. R. (2018). Surface-atmosphere exchange in a box: Space-time resolved storage and net vertical fluxes from tower-based eddy covariance. *Agricultural and Forest Meteorology* 255, 81–91.

Xue, W., Ko, J., Werner, C., and Tenhunen, J. (2017). A spatially hierarchical integration of close-range remote sensing, leaf structure and physiology assists in diagnosing spatiotemporal dimensions of field-scale ecosystem photosynthetic productivity. *Agricultural and Forest Meteorology* 247, 503–519.

Yamori, W., Evans, J. R., and Von Caemmerer, S. (2010). Effects of growth and measurement light intensities on temperature dependence of CO_2 assimilation rate in tobacco leaves. *Plant, Cell & Environment* 33, 332–343.

Yamori, W., Nagai, T., and Makino, A. (2011). The rate-limiting step for CO_2 assimilation at different temperatures is influenced by the leaf nitrogen content in several C3 crop species. *Plant, Cell & Environment* 34, 764–777.

Yin, X., Struik, P. C., Romero, P., Harbinson, J., Evers, J. B., Van Der Putten, P. E., and Vos, J. (2009). Using combined measurements of gas exchange and chlorophyll fluorescence to estimate parameters of a biochemical C3 photosynthesis model: a critical appraisal and a new integrated approach applied to leaves in a wheat (*Triticum aestivum*) canopy. *Plant, Cell & Environment* 32, 448–464.

Yu, G., Song, X., Wang, Q., Liu, Y., Guan, D., Yan, J., Sun, X., Zhang, L., and Wen, X. (2008). Water-use efficiency of forest ecosystems in eastern China and its relations to climatic variables. *New Phytologist* 177, 927–937.

Zaehle, S and Friend, A. (2010). Carbon and nitrogen cycle dynamics in the O-CN land surface model: 1. Model description, site-scale evaluation, and sensitivity to parameter estimates. *Global Biogeochemical Cycles* 24.

Zaehle, S., Medlyn, B. E., De Kauwe, M. G., Walker, A. P., Dietze, M. C., Hickler, T., Luo, Y., Wang, Y.-P., El-Masri, B., Thornton, P., et al. (2014). Evaluation of 11 terrestrial carbon-nitrogen cycle models against observations from two temperate Free-Air CO_2 Enrichment studies. *New Phytologist* 202, 803–822.

Zeng, N., Zhao, F., Collatz, G. J., Kalnay, E., Salawitch, R. J., West, T. O., and Guanter, L. (2014). Agricultural Green Revolution as a driver of increasing atmospheric CO_2 seasonal amplitude. *Nature* 515, 394–397.

Zhang, F., Ju, W., Shen, S., Wang, S., Yu, G., and Han, S. (2014). How recent climate change influences water use efficiency in East Asia. *Theoretical and Applied Climatology* 116, 359–370.

Zhang, S.-B., Yin, L.-X., et al. (2012). Plasticity in photosynthesis and functional leaf traits of *Meconopsis horridula* var. *racemosa* in response to growth irradiance. *Botanical Studies* 53, 335–343.

Zhao, M., Pitman, A., and Chase, T. (2001). The impact of land cover change on the atmospheric circulation. *Climate Dynamics* 17, 467–477.

Zhou, S., Yu, B., Huang, Y., and Wang, G. (2014). The effect of vapor pressure deficit on water use efficiency at the subdaily time scale. *Geophysical Research Letters* 41.

Zhou, S., Yu, B., Zhang, Y., Huang, Y., and Wang, G. (2016). Partitioning evapotranspiration based on the concept of underlying water use efficiency. *Water Resources Research*.

Zhou, S., Yu, B., Schwalm, C. R., Ciais, P., Zhang, Y., Fisher, J. B., Michalak, A. M., Wang, W., Poulter, B., Huntzinger, D. N., et al. (2017). Response of water use efficiency to global environmental change based on output from terrestrial biosphere models. *Global Biogeochemical Cycles* 31, 1639–1655.

Zhou, S., Yu, B., Zhang, Y., Huang, Y., and Wang, G. (2018). Water use efficiency and evapotranspiration partitioning for three typical ecosystems in the Heihe River Basin, northwestern China. *Agricultural and Forest Meteorology* 253, 261–273.

Zhu, Q., Jiang, H., Peng, C., Liu, J., Wei, X., Fang, X., Liu, S., Zhou, G., and Yu, S. (2011). Evaluating the effects of future climate change and elevated CO_2 on the water use efficiency in terrestrial ecosystems of China. *Ecological Modelling* 222, 2414–2429.

Author contributions to the manuscripts

Erklärung zu den Eigenanteilen des Promovenden sowie der weiteren Doktoranden/Doktorandinnen als Koautoren an den Publikationen und Zweitpublikationsrechten bei einer kumulativen Dissertation.

Für alle in dieser kumulativen Dissertation verwendeten Manuskripte liegen die notwendigen Genehmigungen der Verlage ("Reprint permissions") für die Zweitpublikation vor.

Die Co-Autoren der in dieser kumulativen Dissertation verwendeten Manuskripte sind sowohl über die Nutzung, als auch über die oben angegebenen Eigenanteile der weiteren Doktoranden/Doktorandinnen als Koautoren an den Publikationen und Zweitpublikationsrechten bei einer kumulativen Disseratation informiert und stimmen dem zu.

Die Anteile des Promovenden sowie der weiteren Doktoranden/Doktorandinnen als Koautoren an den Publikationen und Zweitpublikationsrechten bei einer kumulativen Dissertation sind in der Anlage aufgeführt.

Name des Promovenden   Datum   Ort   Unterschrift

Ich bin mit der Abfassung der Dissertation als publikationsbasiert, d.h. kumulativ, einverstanden und bestätige die vorstehenden Angaben. Eine entsprechend begründete Befürwortung mit Angabe des wissenschaftlichen Anteils des Doktoranden an den verwendeten Publikationen werde ich parallel an den Rat der Fakultät der Chemisch-Geowissenschaftlichen Fakultät richten.

Name Erstbetreuerin   Datum   Ort   Unterschrift

Anlage Erklärung zu den Eigenanteilen des Promovenden sowie der weiteren Doktoranden/Doktorandinnen als Koautoren an den Publikationen und Zweitpublikationsrechten bei einer kumulativen Dissertation.

Publikation 1: Knauer, J., Zaehle, S., Reichstein, M., Medlyn, B.E., Forkel, M., Hagemann, S., Werner, C. (2017). The response of ecosystem water-use efficiency to rising atmospheric CO_2 concentrations: sensitivity and large-scale biogeochemical implications. *New Phytologist* 213, 1654-1666, doi: 10.1111/nph.14288.							
Beteiligt an:							
	Jürgen Knauer	Sönke Zaehle	Markus Reich-stein	Belinda E. Medlyn	Matthias Forkel	Stefan Hage-mann	Christiane Werner
Konzeption des Forschungsansatzes	x	x					
Planung der Untersuchungen	x						
Datenerhebung	x						
Datenanalyse und -interpretation	x	x	x		x		x
Schreiben des Manuskripts	x	x	x	x	x	x	x
Vorschlag Anrechnung Publikationsäquivalente	100%						

Publikation 2: Knauer, J., Zaehle, S., Medlyn, B.E., Reichstein, M., Williams, C.A., Migliavacca, M., De Kauwe, M.G., Werner, C., Keitel, C., Kolari, P., Limousin, J-M., Linderson, M-L. (2018). Towards physiologically meaningful water-use efficiency estimates from eddy covariance data. *Global Change Biology* 24, 694-710, doi: 10.1111/gcb.13893.						
Beteiligt an (Teil 1):						
	Jürgen Knauer	Sönke Zaehle	Belinda E. Medlyn	Markus Reichstein	Christopher A. Williams	Mirco Migliavacca
Konzeption des Forschungsansatzes	x	x	x	x		
Planung der Untersuchungen	x		x		x	
Datenerhebung						
Datenanalyse und -interpretation	x			x		x
Schreiben des Manuskripts	x	x	x	x	x	x
Vorschlag Anrechnung Publikationsäquivalente	100%					

Publikation 2: Knauer, J., Zaehle, S., Medlyn, B.E., Reichstein, M., Williams, C.A., Migliavacca, M., De Kauwe, M.G., Werner, C., Keitel, C., Kolari, P., Limousin, J-M., Linderson, M-L. (2018). Towards physiologically meaningful water-use efficiency estimates from eddy covariance data. *Global Change Biology* 24, 694-710, doi: 10.1111/gcb.13893.						
Beteiligt an (Teil 2):						
	Martin G. De Kauwe	Christiane Werner	Claudia Keitel	Pasi Kolari	Jean-Marc Limousin	Maj-Lena Linderson
Konzeption des Forschungsansatzes						
Planung der Untersuchungen						
Datenerhebung			x	x	x	x
Datenanalyse und -interpretation		x				
Schreiben des Manuskripts	x	x	x	x	x	x
Vorschlag Anrechnung Publikationsäquivalente						

Publikation 3: Knauer, J., El-Madany, T.S., Zaehle, S., Migliavacca, M. (2018). Bigleaf – An R package for the calculation of physical and physiological ecosystem properties from eddy covariance data. *PLoS ONE* 13, e0201114, doi:10.1371/journal.pone.0201114.				
Beteiligt an:				
	Jürgen Knauer	Tarek S. El-Madany	Sönke Zaehle	Mirco Migliavacca
Konzeption des Forschungsansatzes	x		x	x
Planung der Untersuchungen	x	x		
Datenerhebung	x	x		
Datenanalyse und - interpretation	x	x		
Schreiben des Manuskripts	x	x	x	x
Vorschlag Anrechnung Publikationsäquivalente	100%			

Manuskript 4: Knauer, J., Zaehle, S., De Kauwe, M.G., Bahar, N.H.A., Evans, J.R., Medlyn, B.E., Reichstein, M., Werner, C. Effects of mesophyll conductance on vegetation responses to elevated CO_2 concentrations in a land surface model. Submitted to *Global Change Biology* on 07 September 2018.								
Beteiligt an:								
	Jürgen Knauer	Sönke Zaehle	Martin G. De Kauwe	Nur H.A. Bahar	John R. Evans	Belinda E. Medlyn	Markus Reich-stein	Christiane Werner
Konzeption des Forschungsansatzes	x							
Planung der Untersuchungen	x	x						x
Datenerhebung	x			x				
Datenanalyse und - interpretation	x							
Schreiben des Manuskripts	x	x	x	x	x	x	x	x
Vorschlag Anrechnung Publikationsäquivalente	100%							

Curriculum Vitae

Personal Information

Name:	Jürgen Knauer
Place of birth:	Eggenfelden, Germany
Date of birth:	30.11.1989
Nationality:	German
Address:	Am Anger 16
	07743 Jena, Germany
Telephone:	+49 3641 576234
E-Mail:	jknauer@bgc-jena.mpg.de

Education

11/2014 – 10/2018

PhD student at the **Max Planck Institute for Biogeochemistry**, Jena and the **Friedrich Schiller University Jena**, Germany.

Thesis title: "Integrating observations and models to understand ecophysiological controls on terrestrial water-carbon coupling"

10/2012 – 09/2014

Master of Science in **Global Change Ecology** at the **University of Bayreuth**, Germany.

Master Thesis: "Modeling the response of water and carbon fluxes to atmospheric humidity in the land surface model JSBACH: A case study evaluating alternative process representations using multi-biome eddy covariance data."

10/2009 - 09/2012

Bachelor of Science in **Geography** and **Biology** (minor subject) at the **Ludwig-Maximilians-University (LMU) Munich**.

Bachelor Thesis: "Analysis of the spatial and temporal LAI-modeling with SWAT in comparison with MODIS remote sensing data."

06/2009

Abitur (Higher education entrance qualification) at Tassilo-Gymnasium Simbach am Inn

Professional Experience

10/2013 – 03/2014	**Student assistant** at the Chair of Biogeography at the **University of Bayreuth**: Modeling USUV Virus transmission in dependence of environmental factors. **Tutor** in the courses "Introduction to R" and "Statistical Modeling with R" of the graduate program (M.Sc.) Global Change Ecology.
08/2013 – 09/2013	**Research internship** at the **Max Planck Institute for Biogeochemistry, Jena, Germany**: Evaluation of site-level simulations of a land surface scheme with eddy covariance data; Simulations and parameter estimation for a simple diagnostic ecosystem model.
04/2012 – 07/2012	**Student assistant** at the research and teaching unit "Physical Geography and Remote Sensing" of the **Department of Geography** at the LMU Munich.
02/2012 - 04/2012	**Research internship** at the **Helmholtz Centre for Environmental Research** in Leipzig, Germany. Department of Computational Landscape Ecology: Sensitivity of crop rotations on simulated hydrology, crop yield, and nutrient dynamics in the Soil and Water Assessment Tool (SWAT).
11/2011- 03/2012	**Working student** at **ENVIRON Germany GmbH** (environmental consulting company): GIS-based spatial analyses in 2-D and 3-D (e.g. contour maps of groundwater table, volume calculations)
08/2011 - 10/2011	**Research internship** at the **Centre for Mined Land Rehabilitation (CMLR)** at the **University of Queensland**, Brisbane, Australia: Germination experiments on native plant communities of the Brigalow Belt in Australia. Design, implementation, and monitoring of the experiments and statistical analysis of the results.

Science Schools

06/2015	Alpine Summer School "**Land-Atmosphere Interactions**", Valsavarenche, Italy
08/2013	Summer School on **Alpine Field Ecology**. Alpine Research Centre Obergurgl, Austria
03/2013	UFZ - Winter School **Ecological Modelling**. Centre for Environmental Research in Leipzig, Germany
02/2013	Science School "La Palma 2013 – **Island biogeography** revisited". Department of Biogeography and Disturbance Ecology, University of Bayreuth

Awards

03/2011	DAAD-scholarship within the framework of the RISE worldwide program: research project at the University of Queensland, Brisbane, Australia
10/2009	e-fellows.net online scholarship
06/2009	"Bio Zukunfts Preis" 2009

Computer Skills

Programming languages: R, Fortran, Unix Shell, C++

Version control: git, svn

Word processing: MS Word, Latex

Geographic Information Systems: ArcGIS 9.3/10

Language Skills

German: native

English: fluent (C1; IELTS: 8.0)

French: good (B2)

Spanish: basic (B1)

Publications

Peer-reviewed Journal Articles

Knauer, J., El-Madany, T.S., Zaehle, S., Migliavacca, M. (2018): Bigleaf—An R package for the calculation of physical and physiological ecosystem properties from eddy covariance data. *PLOS ONE*, 13(8), e0201114. doi:10.1371/journal.pone.0201114

Wutzler, T., Lucas-Moffat, A., Migliavacca, M., **Knauer, J.**, Sickel, K., Šigut, L., Menzer, O., Reichstein, M. (2018): Basic and extensible post-processing of eddy covariance flux data with REddyProc. *Biogeosciences*, 15, 5015-5030. doi:10.5194/bg-15-5015-2018

Schaphoff, S., von Bloh, W., Rammig, A., Thonicke, K., Biemans, H., Forkel, M., Gerten, D., Heinke, J., Jägermeyr, J., **Knauer, J.**, Langerwisch, F., Lucht, W., Müller, C., Rolinski, S., Waha, K. (2018): LPJmL4 – a dynamic global vegetation model with managed land – Part 1: Model description. *Geoscientific Model Development*, 11, 1343-1375. doi:10.5194/gmd-11-1343-2018.

Schaphoff, S., Forkel, M., Müller, C., **Knauer, J.**, von Bloh, W., Gerten, D., Jägermeyr, J., Lucht, W., Rammig, A., Thonicke, K., Waha, K. (2018): LPJmL4 – a dynamic global vegetation model with managed land – Part 2: Model evaluation. *Geoscientific Model Development*, 11, 1377-1403. doi:10.5194/gmd-11-1377-2018.

Knauer, J., Zaehle, S., Medlyn, B.E., Reichstein, M., Williams, C.A., Migliavacca, M., De Kauwe, M.G., Werner, C., Keitel, C., Kolari, P., Limousin, J-M., Linderson, M-L. (2018): Towards physiologically meaningful water-use efficiency estimates from eddy covariance data. *Global Change Biology*, 24, 694–710. doi:10.1111/gcb.13893.

De Kauwe, M.G., Medlyn, B.E., **Knauer, J.**, Williams, C.A. (2017): Ideas and perspectives: How coupled is the vegetation to the boundary layer? *Biogeosciences*, 14, 4435–4453. doi:10.5194/bg-14-4435-2017.

Medlyn, B.E., De Kauwe, M.G., Lin, Y-S., **Knauer, J.**, Duursma, R.A., Williams, C.A., Arneth, A., Clement, R., Isaac, P., Limousin, J-M., Linderson, M-L., Meir, P., Martin-StPaul, N., Wingate, L. (2017): How do leaf and ecosystem measures of water-use efficiency compare? *New Phytologist*, 216, 758-770. doi:10.1111/nph.14626.

Knauer, J., Zaehle, S., Reichstein, M., Medlyn, B.E., Forkel, M., Hagemann, S., Werner, C. (2017): The response of ecosystem water-use efficiency to rising atmospheric CO_2 concentrations: sensitivity and large-scale biogeochemical implications. *New Phytologist*, 213, 1654–1666. doi:10.1111/nph.14288.

Knauer, J., Werner C., Zaehle, S. (2015): Evaluating stomatal models and their atmospheric drought response in a land surface scheme: A multibiome analysis. *Journal of Geophysical Research: Biogeosciences*, 120, 1894–1911. doi:10.1002/2015JG003114.

Arnold, S., Kailichova, Y., **Knauer, J.**, Ruthsatz, A. D., Baumgartl, T. (2014): Effects of soil water potential on germination of co-dominant Brigalow species: Implications for rehabilitation of water-limited ecosystems in the Brigalow Belt bioregion. *Ecological Engineering*, 70, 35-42. doi:10.1016/j.ecoleng.2014.04.015.

Poster Presentations

Mäkelä, J., Susiluoto, J., **Knauer, J.**, Aurela, M., Lohila, A., Mammarella, I., Black, A., Margolis, H., Suzuki, R., Heimann, M., Varlagin, A., Markkanen, T., Thum, T., Zaehle, S., Aalto, T. (2017): Multimodel parameter optimization of JSBACH canopy conductance, GPP and ET formulations against micrometeorological flux data at boreal sites. *10th International Carbon Dioxide Conference*, Interlaken, Switzerland

Knauer, J., Zaehle, S., Medlyn, B.E., Reichstein, M., Williams, C.A., Migliavacca, M., De Kauwe, M.G., Werner, C., Keitel, C., Kolari, P., Limousin, J-M., Linderson, M-L. (2017): Deriving Physiologically Meaningful Stomatal Parameters from Eddy Covariance Data. *FLUXNET Conference 2017,* Berkeley, USA

Wutzler, T., Moffat, A., Migliavacca, M., **Knauer, J.**, Menzer, O., Sickel, K., Reichstein, M. (2017): REddyProc: Enabling researchers to process Eddy-Covariance data. Geophysical Research Abstracts, *EGU General Assembly 2017*, Vol. 19, EGU2017-12954

Mäkelä, J., Susiluoto, J., **Knauer J.**, Aurela, M., Mammarella, I., Markkanen, T., Thum, T., Zaehle, S., Aalto, T. (2017): Multimodel parameter optimization with adaptive population importance sampler (APIS), Geophysical Research Abstracts, *EGU General Assembly 2017*, Vol. 19, EGU2017-704

Mäkelä, J., **Knauer, J.**, Markkanen, T., Susiluoto, J., Thum, T., Aalto, T. (2016): The effect of different stomatal conductance formulations on the parametrization of JSBACH. *2nd ICOS Science Conference*, Helsinki, Finland

Arnold**,** S., **Knauer, J.**, Baiquni, H., and Baumgartl, T. (2012). Effect of water potential on germination of seeds in ecosystem restoration, Brigalow Belt, Queensland, Australia. *5th Joint Australian and New Zealand Soil Science Conference 2012,* Hobart, Australia

Oral Presentations

Knauer, J., De Kauwe, M. G., Lin, Y. S., Duursma, R., Williams, C. A., Arneth, A., Clement, R., Isaac, P. R., Linderson, M. L., Limousin, J. M., Meir, P., Martin-StPaul, N. K., Wingate, L., Medlyn, B. E. (2016): Discrepancies between leaf and ecosystem measures of water-use efficiency. *AGU Fall General Assembly 2016*, Abstract ID: B14B-04.

Software

Knauer, J. (2018): bigleaf: Physical and Physiological Ecosystem Properties from Eddy Covariance Data. R package version 0.6.5. https://bitbucket.org/juergenknauer/bigleaf

Jena, 30. October 2018

Jürgen Knauer

Selbstständigkeitserklärung

Ich erkläre, dass ich die vorliegende Arbeit selbstständig und unter Verwendung der angegebenen Hilfsmittel, persönlichen Mitteilungen und Quellen angefertigt habe.

Jena, 30. Oktober 2018

_____
Jürgen Knauer